
# Harmonic Emissions in Electric Vehicle Smart Charging

PhD Thesis

Murat Senol

Department of Electronic and Electrical Engineering

University of Strathclyde, Glasgow

October 2025

This thesis is the result of the author's original research. It has been composed by the author and has not been previously submitted for examination which has led to the award of a degree.

# Abstract

Smart charging for Electric Vehicles (EVs) is increasingly recognized as a pivotal strategy for managing the challenges posed by large-scale EV adoption. It offers significant economic and operational benefits by mitigating grid congestion, deferring infrastructure upgrades, and enabling off-peak charging. Governments worldwide have responded by mandating smart charging capabilities in EV infrastructure, underlining its critical role in advancing sustainable energy systems. However, while extensive research has addressed the benefits of smart charging in load management and voltage regulation, its power quality implications, particularly the generation of harmonic emissions, remain relatively underexplored. As EV penetration increases, understanding and managing the harmonic impacts of smart charging on the power system is vital to maintaining grid stability and power quality.

This thesis adopts a comprehensive approach encompassing four main stages: measurement, analysis, quantification, and solution development. First, in the measurement phase, a detailed experimental setup is conducted to capture harmonic emissions from eight commercially available EV models. Each vehicle is charged using smart chargers across a range of current levels, measured in 1 A increments from the minimum to the maximum permissible charging current. Harmonic amplitudes and phase angles are recorded for both single and multi-EV charging setups, providing a high-resolution dataset suitable for further analysis.

Next, the analysis phase statistically examines current total harmonic distortion ($THD_I$), dominant harmonic orders, and phase angle interactions. A consistent inverse relationship is observed between charging current and harmonic emissions, where lower

charging rates led to higher $THD_I$. Multi-EV scenarios demonstrate partial harmonic cancellation due to phase diversity, though worst-case configurations still reach $THD_I$ levels exceeding 25%, with half of the tested EVs violating individual harmonic order limits. These findings suggest that similar $THD_I$ values can hide significant differences in individual harmonic order profiles, highlighting the limitations of $THD_I$ as a sole compliance metric.

In the quantification phase, a Monte Carlo simulation framework is developed to evaluate the probabilistic nature of harmonic emissions resulting from simultaneous multiple EV charging events. This allows the assessment of standard compliance risks under varying EV combinations and charging rates, incorporating uncertainties in real-world operating conditions. The assessment also incorporates a comparison of harmonic emissions from both single and multiple EV charging scenarios against the thresholds for $THD_I$ and individual harmonic orders as defined in international power quality standards(e.g. IEC 61000 and IEEE 519).

Additionally, the impact of harmonic-rich loading on the aging of distribution transformers is quantified. A thermal-electrical model based on IEEE C57.91 and IEEE C57.110 standards is applied to a 160 kVA distribution transformer evaluated under full-load conditions, which are achieved by varying the number of simultaneously charging EVs at fixed current levels. Results reveal that harmonic-induced losses significantly elevate hot-spot temperatures and aging acceleration factors, particularly at low charging currents, potentially reducing transformer lifespan to under 10 years in worst-case conditions. Based on these findings, a rule-based harmonics-averse EV charging strategy is proposed to guide system operators in prioritizing charging rates, such as 13 A, that balance transformer longevity and connection capacity. This strategy provides an actionable guideline for transformer protection in heavily loaded scenarios without requiring additional infrastructure.

Finally, in addition to proposing a rule-based EV charging management strategy for heavily loaded networks to mitigate transformer aging, the solution phase also introduces a harmonics-aware smart charging optimization framework specifically designed for partially loaded networks, aiming to ensure power quality compliance while

meeting energy delivery requirements. A Particle Swarm Optimization (PSO) algorithm is combined with a Water Filling mechanism to generate charging schedules that meet user demand while maintaining $THD_I$ below regulatory limits. Regression models linking charging power to $THD_I$ enable tractable, real-time enforcement of harmonic constraints. Results reveal that this strategy maintains compliance without compromising energy delivery and avoids the need for costly hardware interventions, such as active filters.

This thesis contributes to the state of knowledge by bridging a critical gap between smart charging design and harmonic-aware grid operation. Through experimental evidence, probabilistic modelling, and rule-based and optimization-based control, it offers actionable insights into balancing charging demand, power quality, and asset longevity. The work also highlights shortcomings in existing harmonic standards when applied to smart, controllable loads. It recommends revising compliance protocols to accommodate the dynamic behaviour of smart charging and offers practical guidance to support utilities, regulators, and researchers in enabling scalable and reliable EV integration.

# Acknowledgements

I would like to express my deepest gratitude to my supervisors, Dr. Safak Bayram and Prof. Stuart Galloway, for their constant guidance, support, and encouragement throughout my doctoral journey. Their expertise and mentorship have been invaluable in shaping both my research and academic development.

I am also thankful to the ERIGrid 2.0 Project for providing me with the opportunity to conduct electric vehicle (EV) charging experiments at the Technical University of Denmark (DTU). I would like to extend my sincere appreciation to the outstanding DTU team for their collaboration and support during my time at the DTU Risø Campus.

Special thanks go to the Ministry of National Education of the Republic of Türkiye for its financial support over the past four years through the YLSY scholarship program. I also want to express my gratitude to the Turkish Consulate General Education Attaché Office in Edinburgh for its dedication to supporting students like myself. Without their tireless efforts, countless students would not have the chance to study at prestigious institutions, advance their academic careers, and broaden their horizons.

To my friends in Glasgow and around the world, and my colleagues at the Technology Innovation Centre (TIC), thank you for your friendship and the many moments of shared learning and laughter. Your companionship made the challenging days of research more bearable and enjoyable.

I also want to acknowledge the Student Experience and Wellbeing Service at the University of Strathclyde. Working alongside you has been a privilege, and I am grateful for the kindness and understanding you have shown during this journey.

A heartfelt thank you to Strathclyde Sport, my gym and second home in Glasgow, for helping me maintain both my physical and mental health throughout the most stressful phases of my PhD.

Finally, I wish to thank myself for enduring and overcoming the many challenges encountered throughout this journey. To my family, despite the distance that has separated us, your constant love and support have always been with me. Your encouragement has been a source of strength and resilience during this process. For all of this, I am deeply grateful.

# Table of Contents

**Abstract** **iv**

**Acknowledgements** **vi**

**List of Figures** **xii**

**List of Tables** **xv**

**List of Abbreviations** **xviii**

**1 Introduction** **1**

1.1 Motivation . . . . . 1

1.2 Research Gap . . . . . 5

1.3 Research Questions . . . . . 7

1.4 Research Contributions . . . . . 8

1.5 Associated Publications . . . . . 9

1.5.1 Journals . . . . . 9

1.5.2 Conferences (Full Paper) . . . . . 10

1.5.3 Symposiums . . . . . 11

1.6 Thesis Outline . . . . . 11

**2 Literature Review** **15**

2.1 EV Smart Charging . . . . . 16

2.1.1 Smart Charging Strategies . . . . . 19

2.1.1.1 Peak Shaving (System Level / Wholesale) . . . . . 20

2.1.1.2 Ancillary Services (System and Local Levels / Transmission and Distribution System Operators) . . . . . 22
2.1.1.3 Behind-the-Meter Optimization and Backup Power (Local Level / Consumers and Prosumers) . . . . . 23
2.1.2 Functions of Smart Charging . . . . . 24
2.1.2.1 Modulation . . . . . 24
2.1.2.2 Scheduling . . . . . 25
2.1.2.3 Shifting . . . . . 25
2.1.2.4 Phase Curtailment . . . . . 26
2.1.2.5 Deployment Readiness of Smart Charging Functions . . 27
2.1.3 Practical Implementation and Technical Constraints of Smart Charging . . . . . 28
2.1.3.1 EV Manufacturer Support and Electrical Configurations 28
2.1.3.2 Charging Stations Support for Smart Charging . . . . . 29
2.1.3.3 Harmonic Considerations in VGI Operation Modes . . . 29
2.1.4 On-board and Off-board Chargers . . . . . 30
2.1.5 EV Charging Power Levels and Impacts on Smart Charging . . . 31
2.2 Impacts of EV Charging on Power Networks . . . . . 33
2.2.1 Power Quality Issues in Distribution Networks . . . . . 35
2.2.1.1 Overloading . . . . . 36
2.2.1.2 Voltage Drop . . . . . 36
2.2.1.3 Phase Balance (Unbalanced Voltage) . . . . . 37
2.3 Bulk Power System . . . . . 37
2.3.1 Peak Demand . . . . . 38
2.3.2 Grid Security and Reliability . . . . . 39
2.4 Harmonics . . . . . 40
2.4.1 Amplitude and Phase Angle . . . . . 42
2.4.2 Voltage versus Current Harmonic Distortion . . . . . 46
2.4.3 Harmonic Indices . . . . . 48
2.4.4 Harmonic Phase Sequences . . . . . 49

2.4.5 Harmonic Sources . . . . . 50
2.4.6 Impacts of Harmonics . . . . . 51
2.5 Harmonic Impact Assessment of EV Charging . . . . . 55
2.5.1 Impacts of Constant Current and Constant Voltage Charging on Harmonic Distortion . . . . . 56
2.5.2 Impacts of Low Temperatures EV Charging on Harmonic Distortion 60
2.6 Industry Standards for Harmonic Limitation . . . . . 61
2.7 Regulatory Frameworks, Market Incentives, and Stakeholder Alignment 65
2.8 Chapter Summary . . . . . 67

**3 Data Collection 70**
3.1 Motivation for Dedicated EV Harmonic Data Collection . . . . . 70
3.1.1 Existing EV Harmonic Measurement Studies . . . . . 71
3.1.2 Lack of Phase Angle Information and Harmonic Summation . . . 73
3.1.3 Implications for EV Harmonic Assessment . . . . . 74
3.1.4 Comparison of Existing EV Harmonic Studies . . . . . 75
3.2 Experimental Set-up . . . . . 76
3.2.1 EV Chargers . . . . . 78
3.2.1.1 Fronius Wattpilot . . . . . 79
3.2.1.2 Zaptec Pro . . . . . 79
3.2.1.3 Keba KeContact P30 . . . . . 79
3.2.2 Power Quality Analyzers . . . . . 79
3.2.2.1 Yokogawa WT500 . . . . . 79
3.2.2.2 Fluke 437 Series II . . . . . 80
3.3 Harmonics Measurement . . . . . 80
3.4 Chapter Summary . . . . . 83

**4 Statistical Harmonics Data Analysis 85**
4.1 THD Analysis . . . . . 85
4.2 Amplitude Analysis . . . . . 95
4.3 Phase Angle Analysis . . . . . 100

4.4 Chapter Summary . . . . . 103

**5 Power Quality Assessment of EV Smart charging 104**

5.1 Power Quality Assessment-Single EV Charging . . . . . 104

5.2 Power Quality Assessment-Multiple EV Charging . . . . . 110

5.2.1 Lab Measurements Case Study . . . . . 110

5.2.2 Background of Monte Carlo Simulation . . . . . 113

5.2.3 Implementation of Monte Carlo Simulation for Multiple EV Charging . . . . . 113

5.3 Chapter Summary . . . . . 122

**6 Transformer Aging Under Harmonic Emissions from EV Smart Charging 124**

6.1 Modelling Distribution Transformer Losses for Harmonic Analysis . . . 125

6.1.1 Transformer Temperature Rise Modeling . . . . . 129

6.1.2 Transformer Lifetime Modelling . . . . . 130

6.2 Monte Carlo Simulation for Transformer Aging . . . . . 131

6.3 Case Study - I: Full Load Conditions . . . . . 133

6.3.1 Transformer Lifetime Analysis . . . . . 134

6.3.2 Rule-based EV Charging Management . . . . . 136

6.4 Case Study - II: Overloading Conditions . . . . . 139

6.5 Chapter Summary . . . . . 140

**7 Harmonics-Aware Smart Charging 143**

7.1 Smart Charging Harmonic Emissions . . . . . 144

7.2 Harmonics Modelling . . . . . 147

7.3 Harmonics-Aware Smart Charging . . . . . 149

7.3.1 Optimization Problem I: Smart Charging without THD Constraints 151

7.3.2 Optimization Problem II: Smart Charging with THD constraints 151

7.4 Particle Swarm Optimization . . . . . 152

7.5 Water Filling Algorithm . . . . . 154

7.6 Case-Study: Large-scale EV Parking Lots . . . . . 157
7.7 Chapter Summary . . . . . 162

**8 Conclusions and Future Work** **164**
8.1 Conclusions . . . . . 164
8.2 Limitations of Research . . . . . 168
8.3 Future Work . . . . . 169

**A Harmonic Data: Amplitudes and Phase Angles of Individual Harmonic Orders Across EV-Specific Charging Levels** **172**

**Bibliography** **202**

# List of Figures


1.1 Greenhouse gas emissions by sectors (%) in the UK in 2024. . . . . 2
1.2 Overview of the thesis structure. . . . . 12

2.1 Capabilities that EVs can offer to the power grid. . . . . 21
2.2 Peak shaving and load shifting in EV charging. . . . . 22
2.3 Example of on-board and off-board EV charger. . . . . 30
2.4 Fourier series representation of a distorted waveform. . . . . 41
2.5 Example of the distorted signal. . . . . 42
2.6 Example for harmonic vector summation of 3rd, 5th and 7th harmonic orders for multiple EVs charging. . . . . 46
2.7 Harmonic currents flowing through the system impedance generate harmonic voltage distortions at the load. . . . . 47
2.8 Block Diagram of EV charging . . . . . 51
2.9 Three-phase bidirectional AC-DC converter topology. . . . . 52
2.10 Current behaviour during CC and CV charging phase. . . . . 57
2.11 Current waveform during CC and CV charging phase. . . . . 58
2.12 $THD_I$ during CC and CV charging phase. . . . . 59
2.13 Various harmonic power quality standards. . . . . 62

3.1 Overview of the experimental set-up and laboratory environment. . . . . 78
3.2 Arrangement for an experiment involving smart chargers and power quality analyzers. . . . . 82

List of Figures

4.1 $THD_I$ (%) versus charging rate for all tested EVs. . . . . 90
4.2 Correlation between $I_{charge}/I_{max}$ and $THD_I$ (%). . . . . 91
4.3 75th percentiles of $THD_V$ (%) for all EVs during smart charging. . . . . 93
4.4 $THD_V$ assessment before and during charging. . . . . 94
4.5 Individual current harmonic amplitudes (A) across different charging rates for all tested EVs. . . . . 99
4.6 Phase angles of (in degrees) 3rd, 5th and 7th harmonic orders for all EVs.101

5.1 Violation of individual current harmonics against the IEC 61000-3-2 standard for all tested EVs. . . . . 109
5.2 3 EVs (Tesla Y Long Range, Renault Zoe R90 and Peugeot e-2008) charging simultaneously. . . . . 111
5.3 Measurement results of three EVs charging simultaneously. . . . . 112
5.4 Monte Carlo number of iterations decision considering Case Study 1 and 5 EVs charging simultaneously in accordance to 5% $THD_I$ limits. . . . . 117
5.5 Simulation results of multiple simultaneous EV charging for Case Study-1.118
5.6 Simulation results of multiple simultaneous EV charging for Case Study-2.119
5.7 Exceeding individual harmonic current limits for two case studies based on the IEC 61000-3-12 power quality standard. . . . . 120

6.1 Transformer losses diagram. . . . . 125
6.2 Flowchart illustrating the transformer aging assessment framework. . . . 132
6.3 Overview of the transformer aging metrics under full load conditions. . . 135
6.4 Comparison of transformer aging under harmonic distorted and non-harmonic distorted conditions. . . . . 137
6.5 Rule-based EV charging management for new connection requests during peak hours. . . . . 138
6.6 Overview of transformer aging metrics under 25% transformer overloading allowance. . . . . 139

7.1 Relationship between EV charging power and THD (per phase). . . . . 146

7.2 Vector summation versus arithmetic mean comparison of THD with 3 EVs charging . . . . . 148
7.3 Step-by-step illustration of the Water Filling Algorithm for dynamic slot allocation. . . . . 156
7.4 Arrival/departure times and the number of active EVs at the charging station. . . . . 159
7.5 Hourly electrical power usage for Optimization Problems I (no THD limit) and II (with THD limit). . . . . 159
7.6 THD comparison for both optimization cases. . . . . 160
7.7 Example of THD-aware smart charging for Peugeot e-2008. . . . . 160
7.8 Demand completion rates for 200 EVs under both optimization frameworks. . . . . 161

# List of Tables


2.1 AC charging levels according to IEC 61851 and SAE J1772. . . . . 32
2.2 Power system stability issues due to EV charging. . . . . 40
2.3 Example for harmonic cancellation of multiple EVs charging. ($A$ denotes amplitude and $\theta$ denotes phase angle in degrees). . . . . 44
2.4 Harmonics and Symmetrical Components . . . . . 49
2.5 Current total harmonic distortion and corresponding currents for different temperatures. . . . . 60
2.6 Impacts of temperature on fast charging current. (T represents the battery temperature). . . . . 61
2.7 Restrictions for current harmonics in IEC 61000-3-2. . . . . 63
2.8 Restrictions for current harmonics in IEC 61000-3-12. . . . . 63
2.9 Restrictions for voltage harmonics in IEC 61000-2-4. . . . . 64
2.10 Restrictions for current harmonics between 120 V and 69 kV in IEEE 519-2014. . . . . 64
2.11 Restrictions for voltage harmonics in IEEE 519-2014. . . . . 64

3.1 Comparison of Key EV Harmonic Distortion Studies (AC: AC Charging, DC: DC Charging, Smart: Smart Charging, Single EV: Single EV Charging, Multiple EV: Multiple Simultaneous EV Charging, P. Angle: Phase Angle) . . . . . 75
3.2 Overview of technical specifications for EVs used in the experiments. . . 77
3.3 Measured Electrical Parameters and Their Units. . . . . 81

List of Tables

4.1 Correlation coefficient ($r$) and quadratic polynomial parameters ($f(x) = p_1x^2 + p_2x + p_3$) between $I_{Charge}/I_{Max}$ and $THD_I(\%)$. $R^2$ denotes the R-squared statistics. . . . . 92
4.2 Circular descriptive statistics for phase angles (in degrees). . . . . 102

5.1 Charging currents for Tesla Model Y Long Range, Renault Zoe R90, and Peugeot e-2008 charging simultaneously. . . . . 111

6.1 Overview of Technical Specifications of Distribution Transformer . . . . 134

7.1 Quadratic polynomial fitting parameters for THD as a function of charging power. . . . . 145

A.1 Renault Zoe R90 — Harmonic Orders $h_2$ to $h_9$ . . . . . 173
A.2 Renault Zoe R90 — Harmonic Orders $h_{10}$ to $h_{16}$ . . . . . 174
A.3 Renault Zoe R90 — Harmonic Orders $h_{17}$ to $h_{24}$ . . . . . 175
A.4 Renault Zoe R90 — Harmonic Orders $h_{25}$ to $h_{31}$ . . . . . 176
A.5 Peugeot e-208 — Harmonic Orders $h_2$ to $h_9$ . . . . . 177
A.6 Peugeot e-208 — Harmonic Orders $h_{10}$ to $h_{16}$ . . . . . 177
A.7 Peugeot e-208 — Harmonic Orders $h_{17}$ to $h_{24}$ . . . . . 178
A.8 Peugeot e-208 — Harmonic Orders $h_{25}$ to $h_{31}$ . . . . . 178
A.9 Nissan Leaf e+ — Harmonic Orders $h_2$ to $h_9$ . . . . . 179
A.10 Nissan Leaf e+ — Harmonic Orders $h_{10}$ to $h_{17}$ . . . . . 180
A.11 Nissan Leaf e+ — Harmonic Orders $h_{18}$ to $h_{25}$ . . . . . 181
A.12 Nissan Leaf e+ — Harmonic Orders $h_{26}$ to $h_{33}$ . . . . . 182
A.13 Nissan Leaf e+ — Harmonic Orders $h_{34}$ to $h_{41}$ . . . . . 183
A.14 Nissan Leaf e+ — Harmonic Orders $h_{42}$ to $h_{49}$ . . . . . 184
A.15 VW ID.3 Pro — Harmonic Orders $h_2$ to $h_9$ . . . . . 185
A.16 VW ID.3 Pro — Harmonic Orders $h_{10}$ to $h_{16}$ . . . . . 185
A.17 VW ID.3 Pro — Harmonic Orders $h_{17}$ to $h_{24}$ . . . . . 186
A.18 VW ID.3 Pro — Harmonic Orders $h_{25}$ to $h_{31}$ . . . . . 186
A.19 Renault Zoe ZE50 — Harmonic Orders $h_2$ to $h_9$ . . . . . 187

A.20 Renault Zoe ZE50 — Harmonic Orders $h_{10}$ to $h_{17}$ . . . . . 188
A.21 Renault Zoe ZE50 — Harmonic Orders $h_{18}$ to $h_{25}$ . . . . . 189
A.22 Renault Zoe ZE50 — Harmonic Orders $h_{26}$ to $h_{33}$ . . . . . 190
A.23 Renault Zoe ZE50 — Harmonic Orders $h_{34}$ to $h_{41}$ . . . . . 191
A.24 Renault Zoe ZE50 — Harmonic Orders $h_{42}$ to $h_{49}$ . . . . . 192
A.25 VW ID.4 Pro — Harmonic Orders $h_2$ to $h_9$ . . . . . 193
A.26 VW ID.4 Pro — Harmonic Orders $h_{10}$ to $h_{17}$ . . . . . 193
A.27 VW ID.4 Pro — Harmonic Orders $h_{18}$ to $h_{25}$ . . . . . 194
A.28 VW ID.4 Pro — Harmonic Orders $h_{26}$ to $h_{33}$ . . . . . 194
A.29 VW ID.4 Pro — Harmonic Orders $h_{34}$ to $h_{41}$ . . . . . 195
A.30 VW ID.4 Pro — Harmonic Orders $h_{42}$ to $h_{49}$ . . . . . 195
A.31 Tesla Model Y LR — Harmonic Orders $h_2$ to $h_9$ . . . . . 196
A.32 Tesla Model Y LR — Harmonic Orders $h_{10}$ to $h_{17}$ . . . . . 196
A.33 Tesla Model Y LR — Harmonic Orders $h_{18}$ to $h_{25}$ . . . . . 197
A.34 Tesla Model Y LR — Harmonic Orders $h_{26}$ to $h_{33}$ . . . . . 197
A.35 Tesla Model Y LR — Harmonic Orders $h_{34}$ to $h_{41}$ . . . . . 198
A.36 Tesla Model Y LR — Harmonic Orders $h_{42}$ to $h_{49}$ . . . . . 198
A.37 Peugeot e-2008 — Harmonic Orders $h_2$ to $h_9$ . . . . . 199
A.38 Peugeot e-2008 — Harmonic Orders $h_{10}$ to $h_{17}$ . . . . . 199
A.39 Peugeot e-2008 — Harmonic Orders $h_{18}$ to $h_{25}$ . . . . . 200
A.40 Peugeot e-2008 — Harmonic Orders $h_{26}$ to $h_{33}$ . . . . . 200
A.41 Peugeot e-2008 — Harmonic Orders $h_{34}$ to $h_{41}$ . . . . . 201
A.42 Peugeot e-2008 — Harmonic Orders $h_{42}$ to $h_{49}$ . . . . . 201

# List of Abbreviations

**Acronyms**

| | |
|---|---|
| AC | Alternating Current |
| AFIR | Alternative Fuels Infrastructure Regulation |
| BEV | Battery Electric Vehicle |
| BMS | Battery Management System |
| CC | Constant Current |
| CENELEC | European Committee for Electrotechnical Standardization |
| CV | Constant Voltage |
| DC | Direct Current |
| DER | Distributed Energy Resources |
| DNO | Distribution Network Operator |
| DSM | Demand-Side Management |
| EMI | Electromagnetic Interference |
| EN | European Norm |
| EN 50160 | European Standard for Voltage Characteristics in Public Distribution Systems |

List of Abbreviations

| | |
|---|---|
| EV | Electric Vehicle |
| EVSE | Electric Vehicle Supply Equipment |
| Fluke 437 | Fluke 437 Series II Power Quality Analyzer |
| HST | Hot-Spot Temperature |
| IEC | International Electrotechnical Commission |
| IEEE | Institute of Electrical and Electronics Engineers |
| IGBT | Insulated-Gate Bipolar Transistor |
| K-Factor | Transformer Harmonic Rating Factor |
| LV | Low Voltage |
| MV | Medium Voltage |
| PCC | Point of Common Coupling |
| PSO | Particle Swarm Optimization |
| PV | Photovoltaic |
| PWM | Pulse Width Modulation |
| RCSE | Short-Circuit Ratio |
| RMS | Root Mean Square |
| SMPS | Switched-Mode Power Supply |
| SoC | State of Charge |
| SYSLAB | Energy System Integration Lab |
| TDD | Total Demand Distortion |
| THC | Total Harmonic Current |

| | |
|---|---|
| THD | Total Harmonic Distortion |
| $\text{THD}_\text{I}$ | Total Harmonic Distortion of Current |
| $\text{THD}_\text{V}$ | Total Harmonic Distortion of Voltage |
| TOT | Top-Oil Temperature |
| TSO | Transmission System Operator |
| UPS | Uninterruptible Power Supply |
| V2G | Vehicle-to-Grid |
| VGI | Vehicle-Grid Integration |
| VRE | Variable Renewable Energy |
| WT500 | Yokogawa WT500 Power Analyzer |

**Transformer Modelling Variables**

| | |
|---|---|
| $\Delta\theta_{HS}$ | Hot-spot rise over top-oil (°C) |
| $\Delta\theta^r_{HS}$ | Rated hot-spot temperature rise (°C) |
| $\Delta\theta_{TO}$ | Top-oil temperature rise over ambient (°C) |
| $\Delta\theta^r_{TO}$ | Rated top-oil temperature rise (°C) |
| $\text{Life}_\text{norm}$ | Transformer lifetime under rated conditions |
| $\text{Life}_\text{real}$ | Estimated transformer lifetime under harmonic loading |
| $\theta_A$ | Ambient temperature (°C) |
| $\theta_{HS}$ | Hot-spot temperature (°C) |
| $\theta_{TO}$ | Top-oil temperature (°C) |
| $F_{AA}$ | Aging acceleration factor |

| | |
|---|---|
| $F_{HL}^{ec}$ | Harmonic loss factor for eddy currents |
| $F_{HL}^{os}$ | Harmonic loss factor for other stray losses |
| $h$ | Harmonic order |
| $h_{\max}$ | Maximum harmonic order considered |
| $I_h$ | RMS current at harmonic order $h$ |
| $I_L^h$ | RMS load current under harmonic conditions |
| $I_L^r$ | RMS rated load current |
| $I_{L,pu}$ | Per-unit load current |
| $P_{CL}$ | Copper losses (W) |
| $P_{CL}^r$ | Rated copper losses (W) |
| $P_{ECL}$ | Winding eddy-current losses (W) |
| $P_{ECL}^r$ | Rated eddy-current losses (W) |
| $P_{LL}$ | Load losses (W) |
| $P_{NL}$ | No-load losses (W) |
| $P_{OSL}$ | Other stray losses (W) |
| $P_{OSL}^r$ | Rated other stray losses (W) |
| $P_{SL}$ | Stray losses (W) |
| $P_{TL}$ | Total transformer losses (W) |

**Optimization and PSO Variables**

| | |
|---|---|
| $\bar{T}$ | Set of time slots with THD violations |
| $\mathrm{THD}(x^t, k^t)$ | Estimated THD at time $t$ |

| | |
|---|---|
| $\omega$ | Penalty weight for THD violation in optimisation |
| $a_i$ | Arrival time of EV $i$ |
| $C$ | System-wide per-phase charging-capacity limit (kW) |
| $c_1$ | Cognitive coefficient (self-influence) |
| $c_2$ | Social coefficient (swarm influence) |
| $c_{\max}$ | Maximum allowable charging power (3.68 kW) |
| $c_{\min}$ | Minimum allowable charging power (1.38 kW) |
| $D_i$ | Energy demand of EV $i$ (kWh) |
| $d_i$ | Departure time of EV $i$ |
| $D_{\min}$ | Minimum required percentage of energy to be delivered |
| $G$ | Global best position found by the swarm |
| $h_{\lim}$ | Maximum permissible THD level |
| $i$ | Index of electric vehicles (EVs) |
| $K$ | Total number of EV types |
| $k$ | Index of EV types |
| $k^t$ | Vector of EV types active at time $t$ |
| $M$ | Minimum required connection duration (time slots) |
| $N$ | Total number of electric vehicles |
| $P$ | Total number of particles in the swarm |
| $P_p$ | Personal best position found by particle $p$ |
| $r_1$, $r_2$ | Random numbers $\sim \mathcal{U}(0, 1)$ |

| | |
|---|---|
| $T$ | Total number of time slots in the optimisation horizon |
| $t$ | Index of discrete time slots |
| $V_p$ | Current velocity vector of particle $p$ |
| $w$ | Inertia weight |
| $x^t$ | Charging powers of all EVs at time slot $t$ |
| $x_i$ | Charging schedule vector for EV $i$ |
| $x_i(t)$ | Charging power assigned to EV $i$ at time $t$ (kW) |
| $X_p$ | Current position (charging schedule) of particle $p$ |

# Chapter 1

# Introduction

## 1.1 Motivation

Climate neutrality has become a global priority, with governments worldwide committed to ambitious greenhouse gas (GHG) emission reduction targets [1]. The 2015 Paris Agreement established a legally binding international framework to limit global warming to well below 2°C, preferably 1.5°C, compared to pre-industrial levels [2]. To achieve this target, signatory countries have committed to reducing GHG emissions by at least 90% from 1990 levels by 2050 [3]. Several nations, including the United Kingdom (UK), France, and Norway, have reinforced these commitments through national net-zero targets and supporting legislation [4, 5].

A key component of these decarbonization efforts is the transformation of the transportation sector, which remains a major contributor to GHG emissions [6]. Globally, transport contributes nearly one-quarter of GHG emissions, with road vehicles responsible for about 75% of that total [7]. In the UK, for instance, domestic transport accounts for 30% of national emissions, making it the largest emitting sector as of 2024 [8]. By comparison, the buildings and product use sector accounted for 21%, followed by industry at 13%, agriculture at 12%, and electricity supply at 10%. The percentage of emissions contributed by all sectors in the UK is shown in Figure 1.1. In this thesis, the discussion of transport-related emissions and electrification challenges focuses primarily on domestic road transport and EV charging, which account for the dominant

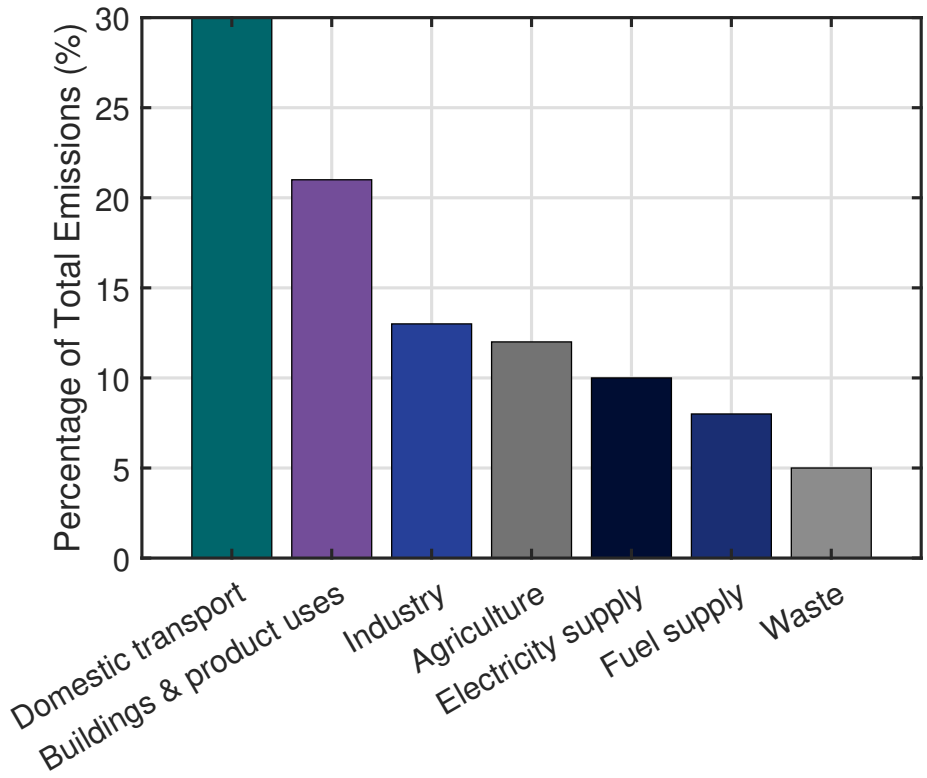


Figure 1.1: Greenhouse gas emissions by sectors (%) in the UK in 2024 [8].

share of transport-sector emissions and directly interact with low-voltage distribution networks.

As part of its strategy to decarbonize transport, the UK has announced a ban on the sale of new petrol and diesel cars by 2030, with all new vehicles required to be fully zero-emission by 2035 [9]. These policy measures have led to a rapid increase in electric vehicle (EV) adoption, with more than 1.4 million battery-electric vehicles (BEVs) on the UK roads as of early 2025 [10]. Projections suggest EVs will account for 60% of global new car sales by 2030 and nearly all new car sales by 2040 [11].

The transition to electric mobility introduces significant operational challenges for power systems. As EV adoption increases, there is a pressing need to integrate an aging distribution grid with a rapidly expanding network of charging infrastructure. Achieving this integration requires timely grid upgrades, strategic placement of charging stations, and coordinated regulatory policies that can support both widespread elec-

trification and the long-term reliability of the power system [12]. Without coordinated control, uncontrolled EV charging could lead to significant issues such as transformer overloading, voltage drops, and increased infrastructure costs [13, 14]. These costs are primarily driven by simultaneous charging behaviour, which raises peak demand at the distribution level, accelerates asset aging, and forces premature reinforcement or replacement of network components dimensioned for peak load rather than annual energy demand.

Evidence from distribution network studies and field measurements indicates that high EV penetration can exacerbate peak demand, voltage deviations, and power quality issues, particularly under concurrent charging conditions, thereby stressing low-voltage networks that were not initially designed for large engagements of power-electronic loads [15]. From a grid planning perspective, distribution networks are usually designed for long-term forecasts, typically over a 20-year horizon, and include built-in capacity margins. However, at high levels of EV penetration, uncontrolled EV charging can push peak demand beyond initial planning assumptions, necessitating infrastructure upgrades sooner than expected. Such upgrades often involve multiple stakeholders and lengthy approval processes; for instance, the typical timelines in the UK are discussed in [16]. To address these challenges, smart charging has emerged as a critical EV load management strategy. By leveraging the flexibility between when EVs are plugged in and when they actually need to be charged, smart charging enables peak demand reduction, load shifting, and improved infrastructure utilization [17–19]. For instance, a vehicle connected overnight (7 pm to 7 am) may require only a few hours to fully recharge, enabling the remaining hours to be used for grid-friendly charging schedules [20]. Smart charging strategies are also implemented in parking facilities equipped with EV chargers to mitigate peak demand and lower infrastructure expenses [21]. In this thesis, smart charging is considered as a control-based approach that aims to meet EV user energy delivery requirements while simultaneously ensuring compliance with power quality constraints, particularly maintaining current harmonic levels within the limits defined by existing IEEE and IEC standards.

In recognition of the potential benefits of smart charging, governments have begun

to mandate smart charging capabilities. Since July 2019, the UK EV infrastructure grant schemes have only supported chargers with smart functionality [22], and the 2021 Electric Vehicle Smart Charge Points Regulations require that all new residential and workplace EV chargers incorporate built-in smart charging features [23]. Similar regulatory frameworks are in place across Europe under the Alternative Fuels Infrastructure Regulation (AFIR) [24]. These policies underscore the growing role of smart charging in the future electricity ecosystem.

Numerous studies have demonstrated the benefits of smart charging in reducing peak loads, balancing phases, and minimizing transformer stress in both residential and commercial charging [19,25,26]. Financial incentives also encourage consumers to shift charging to off-peak periods with lower electricity prices [27]. Despite these advantages, increasing attention is being directed toward the interaction between smart charging and the performance of on-board EV chargers [28]. In AC charging scenarios, the load profile is primarily determined by the on-board charger [29], which is crucial for maintaining grid stability and protecting infrastructure through performance indicators such as power factor, efficiency, and harmonic distortion. Although power factor and efficiency have been thoroughly investigated in [30], which assessed over 35 EV models, the impact of smart charging on harmonic distortion remains underexplored.

Harmonic emissions are a growing concern in power systems, primarily due to the non-linear behaviour of on-board EV chargers operating at different power levels. This non-linear behaviour occurs because the AC–DC rectification and high-frequency switching stages within on-board chargers draw current in accordance with internal conduction and control states rather than a linear voltage–current relationship, resulting in non-sinusoidal input currents even under sinusoidal supply voltages. The literature review indicates that at low ambient temperatures, increases battery internal resistance leads the Battery Management System (BMS) to reduce charging current in order to prevent overvoltage. Under these conditions, EVs tend to produce higher levels of current harmonic distortion [28, 29, 31]. This observation forms a key motivation for the thesis, as it suggests that the dynamic current adjustments in smart charging may produce harmonic distortion patterns similar to those observed under temperature-induced

current limitations.

The presence of harmonics introduces several power quality issues, including transformer overheating, insulation degradation, increased cable losses, and electromagnetic interference [32–35]. These effects are particularly problematic when multiple EVs charge simultaneously at low current levels, as partial harmonic cancellation becomes more challenging to predict. Despite the growing penetration of smart charging and the existence of well-established harmonic standards, industry standards such as IEC 61000-3-2 and IEC 61000-3-12 primarily evaluate harmonic emissions at rated charging conditions, and therefore do not explicitly address the dynamically varying current levels and operating behaviours introduced by smart charging.

While smart charging offers clear benefits in mitigating peak demand and infrastructure stress, its broader implications for power quality, particularly harmonic distortion under realistic operating conditions, remain insufficiently understood. Given these limitations, this thesis aims to investigate the harmonic performance of on-board chargers across a wide range of smart charging current setpoints. It also evaluates the adequacy of existing harmonic emission standards, particularly under realistic smart charging conditions. The study further assesses the impact of harmonics on transformer aging using probabilistic modelling techniques. Finally, it proposes rule-based EV charging management and harmonics-aware charging strategies that account for both thermal and power quality constraints. By addressing these interconnected challenges, this work contributes to the development of resilient, standards-compliant, and harmonics-aware EV integration strategies for future distribution networks.

## 1.2 Research Gap

EVs are crucial to reducing GHG emissions and transitioning to sustainable energy systems. Since EVs are connected to the power grid via power electronics-based on-board chargers, they introduce challenges to power quality and grid stability [36]. Among these challenges, harmonic distortion is a critical issue. Harmonics are generated during the AC to DC conversion process within on-board chargers, and their impact becomes

more prominent in scenarios involving smart charging.

Smart charging is widely recognized as a solution to alleviate grid stress by optimizing charging schedules and improving voltage profiles. However, its impact on harmonic emissions has not been sufficiently studied [30]. Unlike traditional harmonic sources, EV chargers operating under smart charging conditions exhibit variable power levels. This variability, driven by dynamic charging rates and schedules, alters the harmonic behaviour of on-board chargers in ways not adequately captured by current harmonic standards [37]. These standards are typically designed for power electronic devices operating at fixed points, such as rated power, and do not account for the dynamic operating conditions introduced by smart charging [38]. This creates a significant knowledge gap, as smart charging introduces new harmonic patterns and interactions that could adversely affect power quality.

Furthermore, the literature reveals a lack of comprehensive datasets documenting EV chargers' harmonic behaviour under varying smart charging conditions. While some studies provide insights into harmonic magnitudes, few consider the phase angles of harmonic currents, which are crucial for accurate harmonic summation analysis in multi-vehicle charging scenarios. Such datasets are vital for understanding the cumulative harmonic impact of multiple EVs charging simultaneously on power grid infrastructure. Without this understanding, the integration of EVs into power systems risks exacerbating issues such as voltage distortion, increased thermal stress on transformers, and accelerated aging of critical grid components.

This research addresses these gaps by investigating the relationship between smart charging currents and the resulting harmonic emissions. By developing comprehensive datasets that include both harmonic magnitudes and phase angles across various smart charging rates, this study aims to enhance the understanding of how single and multiple EV charging scenarios affect power grid infrastructure. The findings will contribute to improving harmonic standards, developing mitigation strategies, and ensuring the sustainable integration of EVs into modern power systems.

## 1.3 Research Questions

This thesis addresses key research gaps related to the harmonic impacts of EV smart charging on power distribution networks. The research is guided by the following questions, organized into three thematic categories:

### 1. Harmonic Profiling of EVs under Smart Charging Conditions and Aggregation Effects

RQ1: How do different EV models behave in terms of harmonic emissions across varying smart charging current levels, and what is the relationship between charging rate and harmonic distortion?

RQ2: What is the cumulative harmonic impact of multiple EVs charging simultaneously, and how do phase angle variations influence harmonic cancellation effects at the point of common coupling (PCC)?

### 2. Power Quality Standards Compliance and Power Grid Impact

RQ3: To what extent do current harmonic emission standards (e.g., IEC 61000-3-2, IEC 61000-3-12) adequately capture the dynamic and variable conditions introduced by smart charging?

RQ4: How do harmonic-rich load conditions affect transformer performance, particularly in terms of thermal stress, aging acceleration, and estimated lifetime, under different loading scenarios?

### 3. Harmonics-Aware Charging Strategies for Considering Power Quality and Demand Management

RQ5: How can harmonics-aware smart charging strategies be developed and optimized to comply with power quality standards, minimize transformer aging, and ensure adequate energy delivery?

RQ6: What trade-offs emerge between minimizing harmonic emissions and meeting user energy demand, and how can these be addressed through smart charging control mechanisms?

## 1.4 Research Contributions

The key contributions of this thesis are summarized as follows:

1. A comprehensive dataset is developed through experimental measurements of eight commercially available EVs, captured across varying smart charging current levels. The dataset includes harmonic amplitudes and phase angles from both individual EVs and multi-EV charging scenarios, using three smart chargers and two power quality analysers. *(Chapter 3)*

2. A statistical analysis is performed to examine the relationship between charging current and harmonic emissions, with a focus on current total harmonic distortion ($THD_I$), dominant harmonic orders, and phase angle dispersion. The results confirm inverse correlations between $THD_I$ and charging current, and reveal harmonic cancellation effects during multiple simultaneous EV charging. *(Chapter 4)*

3. The magnitude of individual harmonics is evaluated against IEC 61000-3-2 limits to identify compliance issues and benchmark EV on-board charger performance. The analysis reveals that some EVs exceed limits despite having a moderate $THD_I$, highlighting the limitations of aggregate distortion metrics. *(Chapter 5)*

4. A Monte Carlo-based probabilistic simulation framework is introduced to assess harmonic emissions from multiple EVs charging simultaneously. The simulation quantifies the likelihood of standard limit violations and demonstrates how harmonic distortion varies with EV model and charging current diversity. *(Chapter 5)*

5. A thermal-electrical transformer model is developed to evaluate aging under harmonic-rich loading. Harmonic loss coefficients were integrated into a top-oil

and hot-spot temperature model, allowing for the estimation of aging acceleration factors and transformer lifetime following IEEE C57.91 and IEEE C57.110 standards. *(Chapter 6)*

6. A rule-based charging management strategy is proposed for heavily-loaded transformers, recommending optimal charging current levels (e.g., 13 A) to balance transformer aging and connection capacity. The strategy identifies suboptimal charging ranges and provides practical guidelines for peak-period EV charging. *(Chapter 6)*

7. A harmonics-aware smart charging optimization framework is formulated for partially loaded networks. Second-order regression models are used to approximate $THD_I$ as a function of charging power, enabling the enforcement of harmonic limits within the optimization process. A Particle Swarm Optimization (PSO) algorithm, integrated with a Water Filling repair mechanism, is implemented to solve the smart charging optimization problem. This approach ensures compliance with power quality constraints, minimum energy delivery, and charger current limitations. *(Chapter 7)*

8. Limitations in existing harmonic compliance standards (e.g., IEC 61000-3-2 and IEC 61000-3-12) are identified. The thesis recommends the adoption of dynamic compliance testing for EVs across varying charging rates to better reflect the operational characteristics of smart-charging-enabled vehicles. Recommendations are provided to improve standardisation practices and enhance harmonic mitigation strategies. *(Chapters 2, 5, and 8)*

## 1.5 Associated Publications

### 1.5.1 Journals

- **M. Senol** and I. S. Bayram, "Impact Assessment and Mitigation of Electric Vehicle Smart Charging Harmonics", *IEEE Access*, vol. 13, pp. 207412-207432, 2025, doi (IF: 3.9).

- **M. Senol**, I. S. Bayram, L. Hunter, K. Sevdari, C. McGarry, D. Campos-Gaona, O. Gehrke and S. Galloway, "Harmonics Measurement, Analysis, and Impact Assessment of Electric Vehicle Smart Charging", *IEEE Open Journal of Vehicular Technology*, vol. 6, pp. 109-127, 2024, doi (IF: 6.4).

- **M. Senol**, I. S. Bayram, Y. Naderi and S. Galloway, "Electric Vehicles Under Low Temperatures: A Review on Battery Performance, Charging Needs, and Power Grid Impacts", *IEEE Access*, vol. 11, pp. 39879-39912, 2023, doi (IF: 3.9).

### 1.5.2 Conferences (Full Paper)

- **M. Senol**, I. S. Bayram, D. Campos-Gaona, K. Sevdari, O. Gehrke, B. Pepper, and S. Galloway, "Measurement-based harmonic analysis of electric vehicle smart charging", *2024 IEEE Transportation Electrification Conference & Expo, (ITEC)*, Chicago, IL, USA, 2024 (**Best Paper Award**), doi.

- **M. Senol**, I. S. Bayram and S. Galloway, "Probabilistic Harmonic Impact Assessment of Multiple Electric Vehicle Fast Charging", *2024 IEEE Transportation Electrification Conference & Expo, (ITEC)*, Chicago, IL, USA, 2024, doi.

- I. S. Bayram, L. Hunter, **M. Senol**, and K. Sevdari, "Analyzing Phase Imbalance in Smart Charging of Multiple EVs: An Experimental Approach", *8th E-Mobility Power System Integration Symposium (EMOB 2024)*, Helsinki, Finland, 2024, doi.

- **M. Senol**, I. S. Bayram and X. Shi, "Transformer Aging Under Harmonic Emissions from Electric Vehicle Smart Charging", *2025 IEEE Transportation Electrification Conference & Expo + Electric Aircraft Technologies Symposium, (ITEC)*, Anaheim, CA, USA, 2025, doi.

- I. S. Bayram, **M. Senol**, R. Jovanovic and X.Shi, "Harmonics-aware Smart Charging of Electric Vehicles", *2025 IEEE Transportation Electrification Conference & Expo + Electric Aircraft Technologies Symposium, (ITEC)*, Anaheim,

CA, USA, 2025, doi.

### 1.5.3 Symposiums

- **M. Senol**, I. S. Bayram and S. Galloway, "Electric Vehicles Under Low Temperatures: A Review on Battery Performance, Charging Needs, and Power Grid Impacts", *Manchester Energy and Electrical Power Systems (MEEPS) Symposium*, Manchester, the UK, 2022 (poster presentation).

## 1.6 Thesis Outline

This thesis is structured into eight chapters, as shown in Figure 1.2, each building upon the previous to comprehensively explore harmonics in EV smart charging and their impacts on power distribution systems. The progression of chapters reflects the research's logical flow from background and experimental measurements to advanced modelling, simulation, and optimization. A brief overview of each chapter is provided below to guide the reader through the thesis:

- Chapter 2 presents an extensive literature review covering EV smart charging strategies, vehicle-grid integration, and the technical and regulatory challenges associated with large-scale EV deployment. It explores the impacts of EVs on distribution network planning, voltage quality, harmonic emissions, and transformer aging. Special attention is given to harmonic decomposition techniques, harmonic summation, and power quality standards such as IEEE 519 and IEC 61000. The chapter also reviews existing harmonic datasets and identifies research gaps, particularly the limited availability of phase angle data and the lack of harmonics-aware smart charging assessments.

- Chapter 3 outlines the experimental setup used to measure harmonic emissions from various EVs. It defines the tested EVs, smart chargers, power quality analyzers, and data acquisition methodology. The resulting dataset provides the empirical basis for the analyses and simulations in the following chapters.

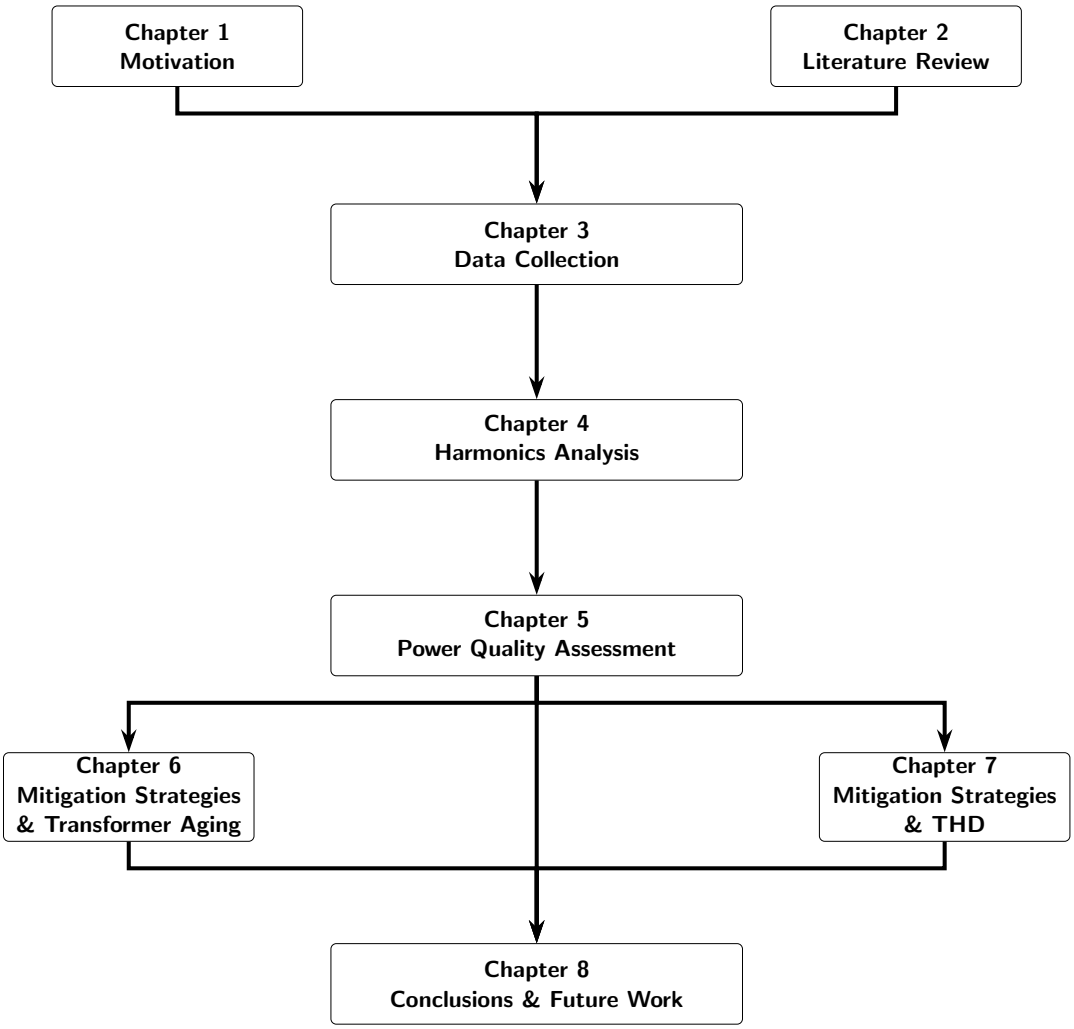


Figure 1.2: Overview of the thesis structure.

- Chapter 4 presents a statistical analysis of harmonic emissions from EV charging, focusing on $THD_I$ and the behaviour of individual harmonic components. It introduces key concepts such as amplitude variations, phase angles, and harmonic interactions. These findings provide valuable insights into the impacts of power quality and inform the modelling approaches in later chapters.

- Chapter 5 evaluates the impacts of EV charging on power quality by analyzing both single and multiple EV scenarios. It compares measured harmonic emissions with industry standards and introduces a Monte Carlo simulation to model

various charging combinations. The chapter also presents a case study to explore harmonic behaviour in real-world scenes and highlights how charging strategies can influence overall power quality performance.

- Chapter 6 introduces a comprehensive modelling framework to evaluate the impact of harmonic distortion on distribution transformer aging in heavily loaded networks. It develops a thermal-electrical loss model that accounts for copper, eddy-current, and stray losses under harmonic conditions. The chapter incorporates hot-spot temperature and aging acceleration factor calculations, linking them to transformer lifetime. A Monte Carlo simulation is employed to assess the cumulative effects of multiple EVs charging at different current levels. Based on these insights, a rule-based, harmonics-averse charging strategy is proposed to extend transformer lifespan and maintain grid reliability under high EV penetration.

- Chapter 7 investigates harmonic mitigation strategies in partially-loaded distribution networks, where thermal stress is minimal but power quality concerns persist. It introduces a harmonics-aware smart charging framework that integrates $\mathrm{THD_I}$ constraints into the scheduling process. The chapter develops a scalable optimization model using polynomial-based harmonic modelling, approximated aggregation methods, and a PSO-based algorithm with a water-filling repair strategy. A large-scale EV parking lot case study demonstrates the framework's ability to ensure compliance with harmonic distortion limits while delivering high energy fulfilment rates. The findings highlight the potential of control-based solutions for improving power quality without requiring additional harmonic filtering infrastructure.

- Chapter 8 concludes the thesis by summarizing key findings and outlining future research directions. It consolidates the results across experimental, simulation, and optimization-based studies, demonstrating how harmonic distortion from EV charging affects transformer aging and power quality. The chapter highlights the effectiveness of harmonics-aware strategies, including rule-based management and

optimization with $THD_I$ constraints, in preserving grid reliability. It also identifies research limitations related to ambient temperature, transformer diversity, harmonic modelling, and dataset scope. Finally, the chapter proposes future work to extend transformer aging models, enhance harmonic aggregation techniques, broaden EV testing, and integrate advanced simulation tools, paving the way for improved standards and grid planning under high EV penetration.

# Chapter 2

# Literature Review

This chapter reviews the existing literature on key aspects of EV charging and its impacts on power networks. The discussion begins with EV smart charging, emphasizing its role in mitigating grid congestion, reducing peak demand, and integrating renewable energy sources. Various factors influencing distribution grid investments, such as congestion levels, coincidence factors, and load characteristics, are examined in detail. Additionally, the role of vehicle-grid integration (VGI) technologies in providing ancillary services, peak shaving, and supporting grid stability is discussed, along with real-world implementations and regulatory measures from different regions.

The chapter then explores the impacts of EV charging on power networks, distinguishing between distribution-level concerns, including voltage drops, transformer overloading, and phase imbalance, and bulk power system challenges, such as peak demand fluctuations and grid security risks. A significant focus is placed on harmonic distortion, a key issue in EV charging due to the widespread use of power electronics-based chargers. The principles of harmonic decomposition using Fourier analysis are presented, followed by a detailed examination of harmonic summation effects, phase cancellation, and their implications for power system components. The review also includes an assessment of existing harmonic measurement studies, highlighting data limitations, particularly the absence of phase angle information, and the need for improved modelling of harmonic interactions in large-scale EV charging scenarios.

The chapter concludes with an overview of industry standards for harmonic limi-

tations, including IEEE 519 and IEC 61000, which define permissible harmonic distortion levels in electrical networks. By synthesizing these findings, this chapter provides a comprehensive understanding of the technical and regulatory challenges associated with EV charging, forming the foundation for the subsequent analytical framework in this thesis.

## 2.1 EV Smart Charging

The large-scale adoption of EVs introduces challenges and opportunities for power systems, particularly in efficiently managing charging demand [39]. Uncontrolled charging could lead to grid congestion, peak demand spikes, and power quality issues [40]. However, smart charging strategies offer a viable solution by dynamically adjusting charging schedules based on grid conditions, electricity prices, and renewable energy availability [41]. As the integration of renewable energy sources, such as solar and wind, continues to grow, there is an increasing opportunity to align EV charging with periods of high renewable energy generation [42]. This enables EV charging to be powered by cleaner and more sustainable energy sources, enhancing both environmental and grid benefits [43]. Furthermore, by leveraging VGI technologies, EVs can not only optimize their charging patterns but also provide ancillary services such as load balancing and frequency regulation, thereby enhancing overall grid stability [44].

Unlike conventional demand-side management (DSM) techniques, such as time-of-use pricing, direct load control, and demand response programs, smart charging capitalizes on the inherent flexibility of EV charging behaviour [45]. Given that vehicles remain parked for extended periods, charging can be shifted away from peak hours or synchronized with renewable generation, thereby reducing strain on the grid and improving system efficiency [43]. Unlocking the full potential of EV smart charging requires coordinated efforts in technology development, regulatory frameworks, and business models to ensure an ideal integration into power networks while maximizing economic and environmental benefits [46].

Without effective control mechanisms, the simultaneous charging of EVs could sig-

nificantly increase peak demand, potentially overloading distribution networks and necessitating costly infrastructure reinforcements [47, 48]. The additional demand might also require adjustments in electricity generation capacity or modifications to production cost structures [49, 50]. The extent of these impacts depends on factors such as the power system's generation mix, grid topology, and EV penetration levels. Numerous global studies have highlighted how these effects vary across different power system configurations, reinforcing the need for proactive grid management strategies [15, 51–54].

EV charging will influence investment requirements for distribution grids, particularly regarding cable and transformer upgrades. The extent of these investments at a given location depends on several key parameters:

- **Congestion**: The required level of infrastructure reinforcement largely depends on the existing congestion within the local distribution network prior to EV deployment. In areas already experiencing high load density or operating near maximum capacity limits, the addition of EV charging loads can quickly exceed network capacity, leading to transformer overloads, cable overheating, and accelerated infrastructure degradation. This situation necessitates immediate reinforcement and more extensive upgrades to maintain reliability and safety. Conversely, areas with relatively low existing load levels may initially accommodate EV charging with minimal upgrades, delaying or reducing overall investment needs. Therefore, accurately assessing pre-existing network congestion is essential in forecasting necessary grid enhancements for widespread EV adoption [55, 56].

- **Coincidence Factor**: This coefficient, which varies according to the size and characteristics of each distribution grid, quantifies the likelihood that multiple devices or loads will operate simultaneously, thereby determining the aggregate peak demand on the network. In the context of EV charging, the coincidence factor is particularly important, as the simultaneous charging of multiple vehicles, such as during peak evening hours after commuters return home, can substantially increase load levels. Different distribution network operators (DNOs) employ varying coincidence factors in their planning processes, often based on empirical

data, historical consumption patterns, and anticipated behavioural changes related to EV adoption. A higher coincidence factor indicates a greater probability of simultaneous operation, necessitating more robust network reinforcements such as transformer upgrades or enhanced feeder capacities. Therefore, accurately estimating coincidence factors is critical for efficient, cost-effective grid expansion and reinforcement strategies, especially in regions expected to experience rapid EV growth [57–59].

- **Load Characteristics**: Uncontrolled EV charging can considerably impact areas characterized by high electric heating loads, especially during winter peaks, due to the concurrent increase in electricity demand from both heating systems and EVs. In such regions, the simultaneous operation of electric heaters and the uncontrolled charging of EVs can quickly push local distribution networks toward or beyond their designed capacity, exacerbating issues like transformer overload, cable overheating, voltage drops, and increased energy losses. Consequently, these areas typically require more substantial and costly grid reinforcements to handle the compounded load [25].

- **Low-Voltage Generation Assets**: In regions with high penetration of solar photovoltaic (PV) systems at the low-voltage distribution level, smart charging can enhance the integration of renewable generation by timing EV charging sessions to match peak solar production periods. This increases local renewable energy utilization, mitigates voltage rise issues, and reduces stress on the transformer and feeder. Conversely, widespread EV adoption may intensify peak loads in areas lacking significant solar PV capacity, thereby increasing strain on distribution grids [60, 61].

- **Grid Code Limits and Regulatory Constraints**: National grid codes establish technical constraints on acceptable voltage and frequency variations that DNOs must adhere to to ensure system stability and reliability. These regulations define operational limits, including permissible voltage deviations, frequency boundaries, and power quality requirements. Increased EV penetration could

challenge compliance with these established parameters due to potential voltage drops, voltage imbalances, and increased harmonic distortions. As a result, additional grid reinforcements, such as upgrading transformers, enhancing voltage regulation equipment, or improving distribution feeders, may become necessary to accommodate EV-induced load dynamics and ensure continued compliance with regulatory standards, thus maintaining overall system stability and power quality [62, 63].

These factors collectively determine the scale and nature of distribution grid investments required to support the adoption of large-scale EVs. However, smart charging strategies can effectively mitigate these negative impacts. By intelligently scheduling or modulating EV charging sessions, smart charging can shift EV demand away from peak hours or periods of high overall electricity demand. This optimizes grid capacity utilization, potentially reducing or deferring the need for expensive infrastructure upgrades. Additionally, smart charging can leverage renewable energy peaks or off-peak electricity tariffs, simultaneously benefiting the grid, consumers, and network operators by maintaining power quality, stabilizing local voltage profiles, and managing congestion more efficiently [48, 64, 65].

### 2.1.1 Smart Charging Strategies

Smart charging, enabled by VGI technologies, is a key strategy for managing EV loads and optimizing power system operation. Unlike uncontrolled charging, which can strain the grid by increasing peak demand, smart charging strategically adjusts charging times and power levels based on real-time grid conditions, user preferences, and market signals. Three primary mechanisms enable smart charging:

i) Customer-driven responses to price signals [66],

ii) Automated control by electric vehicle supply equipment (EVSE) in reaction to grid and market conditions [67],

iii) A hybrid approach that balances both while ensuring vehicle availability [68].

Smart charging is time-shifting charging periods or modulating charging power in line with varying constraints such as connection capacity, user demand, and real-time local energy availability. As a result, it optimizes the charging process by aligning it with distribution grid limitations, renewable energy availability, and the preferences of both drivers and EVSE site operators [47].

When integrated with smart charging strategies, EVs can mitigate rather than exacerbate stress on the local grid while simultaneously providing flexibility services at both the local and system levels. By strategically adjusting charging and discharging patterns, EVs can help reduce variable renewable energy (VRE) curtailment, enhance local self-consumption of VRE generation, and minimize the need for peak generation capacity investments [69, 70]. Additionally, smart charging can alleviate grid reinforcement requirements, ensuring a more efficient and balanced power system [46].

Smart charging not only reduces EV-induced demand peaks but also smooths the load curve, facilitating the seamless integration of VRE at both the system-wide and local levels, particularly over shorter time scales. By strategically adjusting charging patterns considering that most vehicles remain parked and idle for 90–95% of the time [71].

The following sections explore specific implementation strategies and real-world applications of smart charging. Smart charging enables EVs to provide various flexibility services across different levels of the power system, including wholesale markets, transmission system operations, distribution networks, and behind-the-meter applications, as illustrated in Figure 2.1 [72].

#### 2.1.1.1 Peak Shaving (System Level / Wholesale)

Smart charging helps flatten peak demand and fill demand valleys by incentivizing late-morning and afternoon charging in regions with high solar penetration and nighttime charging aligned with wind generation. Given that vehicles remain parked longer than required for a full charge, charging can be deferred from early evening peaks to avoid additional grid stress [73].

Peak shaving and load shifting techniques are commonly employed to optimize

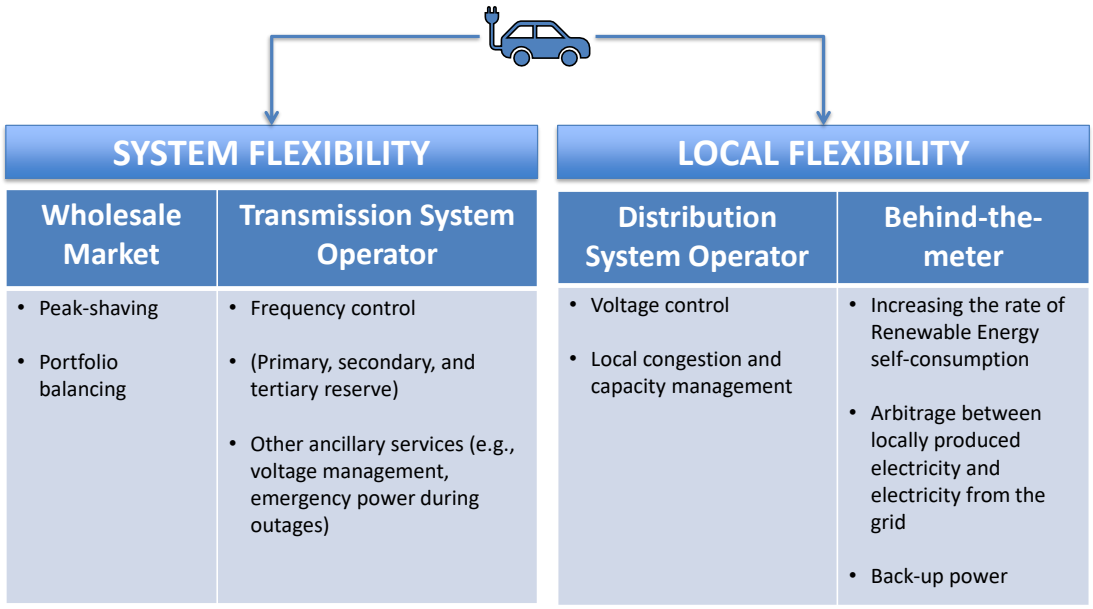


Figure 2.1: Capabilities that EVs can offer to the power grid [72].

energy demand in EV charging. These demand management strategies are illustrated in Figure 2.2. Peak shaving reduces the maximum power demand by limiting charging during peak hours, thereby preventing grid overloads. Load shifting, on the other hand, redistributes charging loads to off-peak periods, thereby better aligning with grid capacity and reducing electricity costs.

In the UK, the Electric Vehicles (Smart Charge Points) Regulations 2021 require that all private EV charge points sold and installed from June 30, 2022, incorporate smart functionality. These smart charge points are designed to optimize energy consumption by encouraging charging during periods of lower grid demand or higher renewable energy generation. To reduce strain on the national grid, the regulations mandate default off-peak charging schedules, restricting charging during peak hours, 8 am to 11 am and 4 pm to 10 pm on weekdays. This measure aims to mitigate excessive demand during high-load periods while still allowing users to override the settings based on individual needs [74].

In the Netherlands, the regional grid operator Stedin has introduced measures to mitigate grid congestion during peak demand periods. One proposed strategy involves temporarily disabling public EV charging stations between 4 pm and 9 pm, aligning

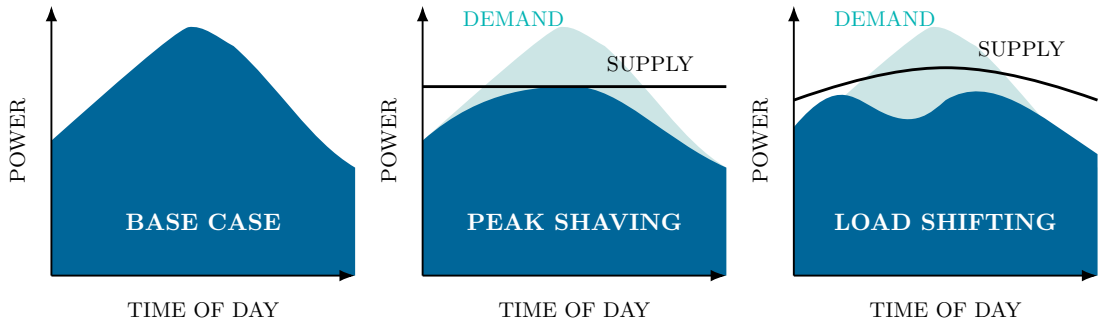


Figure 2.2: Peak shaving and load shifting in EV charging.

with peak electricity consumption from residential and commercial sectors. This approach seeks to prevent network overloads and enhance grid stability as EV adoption expands [75].

Octopus Energy offers specialized EV charging tariffs in the UK, encouraging off-peak charging to reduce costs and support grid stability. Octopus Go provides a reduced electricity rate of 9p/kWh during a fixed five-hour window (12:30 am – 5:30 am), while the daytime rate is 29p/kWh. Intelligent Octopus Go extends this flexibility by dynamically scheduling charging sessions within a six-hour off-peak period (11:30 pm – 5:30 am) at a lower rate of 7.5p/kWh. An exclusive Intelligent Octopus Go - EV Saver plan further reduces costs for Octopus EV customers, offering 5p/kWh off-peak charging rate. These tariffs leverage smart charging to optimize energy consumption, minimize peak demand, and align EV charging with higher renewable energy availability periods [76].

#### 2.1.1.2 Ancillary Services (System and Local Levels / Transmission and Distribution System Operators)

Smart charging supports real-time grid balancing by adjusting EV charging levels to maintain stable voltage and frequency. While transmission system operators (TSOs) have well-established flexibility mechanisms, DNOs have yet to integrate flexibility from distributed energy resources (DERs). Despite numerous demonstration projects and ongoing regulatory discussions, particularly in Europe and the US, DNOs still face challenges in leveraging EV flexibility for grid operations [41].

Aggregators are pivotal in integrating EV flexibility into power systems by coordinating charging schedules to provide grid services. In the UK, platforms like Piclo facilitate the participation of EVs in flexibility markets, enabling them to respond to real-time grid needs by modulating charging demand [77]. Similarly, Denmark has explored smart charging technologies, with companies like Nuvve collaborating on projects to harness EV flexibility for grid support [78]. A notable initiative in Scotland, the Local Constraint Market, aims to manage grid constraints by enabling flexible resources, including EVs, to absorb excess wind generation, thereby preventing curtailment and enhancing grid stability [79]. Additionally, Axle Energy has developed software platforms that connect distributed assets, such as EV chargers, to flexibility markets, optimizing charging patterns based on real-time market signals and renewable energy availability [80]. These developments underscore the growing importance of EVs in ancillary services, ensuring both local and system-wide grid stability.

#### 2.1.1.3 Behind-the-Meter Optimization and Backup Power (Local Level / Consumers and Prosumers)

Smart charging enhances the self-consumption of locally generated renewable energy (e.g. PV), reducing reliance on the grid and optimizing electricity costs. By charging at off-peak hours when electricity prices are lower, EV owners can store energy and use it during peak tariff periods, lowering their energy bills and increasing grid independence [48].

Smart pricing strategies for EV charging have been implemented in various countries to incentivize off-peak charging and enhance grid flexibility. In Spain, for instance, Endesa's Tempo Zero tariff offers EV drivers free charging during predefined nighttime hours, specifically between 1 am and 7 am, for the first 200 kWh each month [81]. This approach encourages load shifting to periods of lower electricity demand.

In the UK, the Octopus Agile tariff integrates with the half-hourly day-ahead market, adjusting prices based on real-time grid conditions to promote the use of renewable energy and provide flexibility. This dynamic pricing model incentivizes EV owners to charge during periods of lower demand and higher renewable generation [82].

Similarly, in Denmark, the Radius network operator applies a time-of-use network pricing scheme that includes higher charges during winter peak hours, specifically from 5 pm to 8 pm. This strategy aims to manage seasonal demand fluctuations by encouraging consumers to shift their electricity usage, including EV charging, to off-peak periods [83]. These pricing mechanisms demonstrate how dynamic electricity tariffs can be leveraged to optimize EV charging behaviour, reduce peak demand, and facilitate the integration of renewable energy sources.

### 2.1.2 Functions of Smart Charging

The smart charging of EVs is essential for managing the growing demand for EV charging within an already constrained power network [84]. By leveraging the inherent flexibility of EV loads, smart charging can be implemented through the following key approaches [30].

#### 2.1.2.1 Modulation

Modulation in smart charging refers to the dynamic adjustment of an EV's charging current within the minimum and maximum allowable limits to enhance grid stability and efficiency. This approach allows for the fine-tuning of charging rates in response to real-time grid conditions, thereby optimizing energy distribution and minimizing peak demand.

A study conducted by the Lawrence Berkeley National Laboratory demonstrated the practical benefits of modulation-based smart charging. The research implemented smart charging control strategies for public EVs, resulting in a 26.7% reduction in peak demand without compromising the mobility needs of EV users. This was achieved by adjusting the charging power of EVs during periods of high demand, effectively distributing the load more evenly across the grid [85].

Further research highlights the role of modulation in integrating renewable energy sources. By aligning EV charging times with high renewable energy generation periods, modulation strategies can absorb excess energy, reducing curtailment and promoting a more sustainable energy ecosystem. This supports grid stability and enhances the

economic viability of renewable energy investments [86].

#### 2.1.2.2 Scheduling

Smart charging scheduling enables controlled activation and deactivation of the charger to align charging sessions with grid conditions and energy availability. By determining optimal charging times, this approach helps balance the load on the electrical grid, reduce peak demand, and enhance the integration of renewable energy sources.

An optimal EV charge scheduling algorithm that considers power grid stability and operational constraints is introduced in [87]. The algorithm directs users to appropriate charging stations, effectively distributing the charging demand and maintaining grid stability. This method ensures that EV charging does not compromise the reliability of the power system.

In [88], intelligently managing EV charging schedules can prevent transformer overloading and defer the need for grid infrastructure upgrades. By optimizing the allocation of available capacity among EVs, grid operators can mitigate peak loads and maintain system reliability.

#### 2.1.2.3 Shifting

Shifting in the context of smart charging involves altering the phase connection of EV chargers within a three-phase electrical system to achieve optimal load distribution across all phases. This practice is essential for maintaining grid stability, enhancing power delivery efficiency, and preventing phase overloading.

In three-phase power systems, imbalances can occur when the electrical load is not evenly distributed among the three phases. Such imbalances may lead to increased losses, voltage fluctuations, and reduced equipment lifespan. By strategically assigning EV chargers to different phases, a process known as phase shifting, utilities and charging infrastructure operators can more effectively balance the load. This ensures that no single phase is disproportionately burdened, thereby enhancing the overall reliability and performance of the electrical network.

A study in [89] delves into the challenges of phase optimization for EV charging.

The researchers formulated the problem as a non-convex mixed-integer programming task aimed at minimizing charging losses. They introduced the PXA algorithm, which, under certain conditions, converges to the global optimum solution. The study demonstrated that, compared to empirical phase balancing strategies, the PXA algorithm significantly improves charging performance by maximizing energy delivery, minimizing costs, and aiding in future energy planning. These findings underscore the importance of intelligent phase shifting in achieving balanced and efficient EV charging networks.

Implementing phase shifting requires advanced smart charging systems capable of real-time monitoring and control. These systems assess the current load on each phase and dynamically adjust the phase allocation of EV chargers to maintain balance. Such adaptive strategies are crucial as the penetration of EVs increases, ensuring that the existing electrical infrastructure can accommodate the additional load without extensive upgrades.

#### 2.1.2.4 Phase Curtailment

Phase Curtailment in EV charging refers to the strategic reduction of charging operations from three-phase to single-phase modes. This approach aims to enhance overall charging efficiency and prevent imbalances within the electrical grid.

Maintaining a balanced load across all phases is crucial for grid stability and efficient power distribution in three-phase electrical systems. Imbalances can lead to increased losses, voltage fluctuations, and undue stress on infrastructure. By curtailing EV charging from three-phase to single-phase operation during periods of high demand or when imbalances are detected, utilities can mitigate these challenges.

A study in [90] explores the potential of using EVs' charging spots to reduce grid imbalances. The research indicates that managing single-phase EV charging can effectively contribute to phase balancing, thereby enhancing the stability and reliability of the power system. This strategy involves dynamically allocating EV charging loads to specific phases based on real-time grid conditions, ensuring an even distribution of power demand.

Implementing phase curtailment requires advanced smart charging infrastructure

capable of real-time monitoring and control. Such systems can assess the load on each phase and adjust charging operations accordingly, switching between three-phase and single-phase modes as needed. This dynamic approach prevents grid imbalances and optimizes the utilization of existing electrical infrastructure, potentially deferring the need for costly upgrades.

These strategies ensure that EV charging remains grid-friendly, reducing stress on the power network while maximizing the integration of renewable energy sources.

#### 2.1.2.5 Deployment Readiness of Smart Charging Functions

While modulation, scheduling, phase shifting, and phase curtailment are all well-established control concepts in the literature, their practical deployment is constrained by the capabilities of today's grid infrastructure, EVSE, and communication systems.

Among the four approaches, modulation and scheduling are the most readily deployable under current conditions. Both functions primarily rely on adjusting charging current or start times via IEC 61851-compliant EVSE and existing communication back-ends. They do not require any modification of the physical phase connection or wiring of the charging point. They can be implemented using today's smart chargers, cloud platforms, and price- or signal-based control schemes. As a result, these two functions already form the backbone of most commercial smart charging deployments.

In contrast, phase shifting and phase curtailment place stronger requirements on the electrical interface between the EVSE and the distribution network. Phase shifting requires either multi-phase chargers with controllable phase allocation or reconfigurable switchgear at the charging point, which is not yet standard in most residential or public installations. Phase curtailment further assumes that the charger and on-board electronics can dynamically transition between three-phase and single-phase operation without violating charging or power quality constraints. These capabilities are technically feasible but are only available in a limited subset of advanced charging systems and are rarely integrated into current distribution network management systems.

From a near-term deployment perspective, modulation and scheduling therefore represent the most scalable and infrastructure-ready smart charging functions, while

phase shifting and phase curtailment are best viewed as medium- to long-term solutions that will become more relevant as three-phase EVSE, advanced metering, and distribution-level control platforms become more widely deployed. This distinction is important when assessing the practical impact of smart charging on grid performance, as the achievable flexibility is fundamentally limited by the physical and digital interfaces available in the field.

### 2.1.3 Practical Implementation and Technical Constraints of Smart Charging

The real-world effectiveness of smart charging depends on the technical capabilities of EVs and the charging infrastructure that interfaces with the power grid. Although smart charging is often framed as an optimization or control problem, its deployment is fundamentally constrained by vehicle-side electrical configurations, charger capabilities, and power quality considerations [46].

#### 2.1.3.1 EV Manufacturer Support and Electrical Configurations

Most modern EVs support smart charging through standardized AC charging interfaces, primarily defined by IEC 61851-1, which enable external modulation of charging current without requiring proprietary vehicle-side control logic. As a result, smart charging functionality is implemented mainly at the EVSE level, while the EV responds passively to current setpoints imposed by the charging station [91, 92].

For Level 2 AC charging, commonly supported current ranges are approximately 6 A to 32 A, corresponding to power levels of 1.4 kW to 7.4 kW under single-phase operation. In three-phase systems, typically found in European distribution networks, charging power can reach up to 22 kW at 32 A [93]. In residential environments, single-phase charging remains dominant, whereas public and workplace infrastructure increasingly supports three-phase connections.

The supported number of phases is determined by the design of the on-board charger. While single-phase charging is common for residential applications, most contemporary EV platforms are designed to operate across multiple electrical con-

figurations, ensuring compatibility with smart charging schemes across different grid environments [36].

#### 2.1.3.2 Charging Stations Support for Smart Charging

Smart charging is primarily implemented through EVSE connected to centralized or cloud-based control platforms. These systems enable charging power modulation, scheduling, and coordinated control across multiple charging points [47, 48]. From a grid operation perspective, smart EVSE can mitigate transformer overloading, feeder congestion, and phase imbalance by employing strategies such as dynamic load balancing, peak shaving, and phase-aware charging [21, 64]. These approaches distribute available capacity among connected vehicles while respecting local grid constraints. However, practical limitations may endure because upgrading existing installations to support higher currents or three-phase connections can be costly, particularly in residential buildings with legacy electrical infrastructure. Smart charging addresses these constraints by operating within existing capacity limits rather than requiring immediate reinforcement [56]. In addition, charging power modulation is constrained by battery thermal limits and charger design, reinforcing the need for coordinated consideration of grid constraints and vehicle charging behaviour.

#### 2.1.3.3 Harmonic Considerations in VGI Operation Modes

Vehicle–grid integration (VGI), encompassing both unidirectional smart charging and bidirectional vehicle-to-grid (V2G) operation, introduces additional power quality challenges. EV chargers rely on power electronic converters for AC–DC conversion, which are inherently nonlinear and generate harmonic emissions [94,95]. Harmonic behaviour differs between grid-to-vehicle (G2V) and vehicle-to-grid (V2G) modes due to changes in converter operating points, switching behaviour, and control strategies. While some studies indicate that bidirectional chargers may provide limited harmonic mitigation through reactive power control or active filtering, other work highlights the potential for resonance phenomena and increased distortion, particularly at higher frequencies [38, 96].

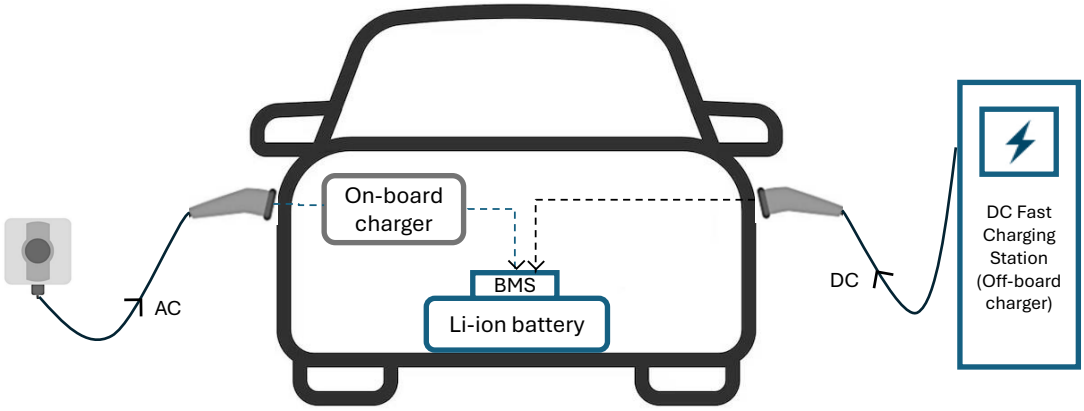


Figure 2.3: Example of on-board and off-board EV charger.

Harmonic performance in smart charging and VGI systems is typically evaluated using standardised measurement frameworks such as IEC 61000-4-7 and IEC 61000-4-30, employing indicators such as THD and individual harmonic orders. However, most existing analyses focus on rated operating conditions or single-EV scenarios and do not fully capture harmonic interactions under coordinated smart charging of multiple EVs [97, 98]. This limitation directly motivates the harmonic-aware experimental and probabilistic analysis framework adopted in this thesis.

### 2.1.4 On-board and Off-board Chargers

The charging infrastructure is a key factor influencing the availability of EV flexibility. While AC power is supplied through the electric distribution grid, EV batteries operate on DC power, necessitating an AC/DC conversion for charging. This converter can be integrated either into the charging station ("off-board charger") or within the vehicle itself ("on-board charger") [92], as shown in Figure 2.3. The selection between on-board and off-board charging involves a trade-off:

On-board chargers are more cost-effective for charging infrastructure, as they rely on widely available AC power from standard sockets. However, the integrated converter increases the vehicle's weight and cost [99].

Off-board chargers, in contrast, accommodate the conversion equipment within the charging station, reducing the vehicle's weight and potentially lowering its manufac-

turing cost. However, this approach increases the complexity and expense of charging infrastructure [100]. Due to the widespread availability of AC charging in many locations, on-board chargers have become a popular option, balancing considerations of cost and accessibility [36]. Since smart charging is primarily used with slow-charging AC chargers, the remainder of this study will focus on on-board chargers.

### 2.1.5 EV Charging Power Levels and Impacts on Smart Charging

The classification of EV charging power levels varies by region, with North America and Europe using distinct terminologies. In North America, the widely adopted classification follows the Society of Automotive Engineers (SAE) standard, specifically SAE J1772 [101], which categorizes EVSE into three levels [102]:

- **Level 1 (AC $\leq$ 3.7 kW):** Typically installed in private households and reliant on standard electrical outlets; these are not necessarily dedicated EV charging solutions.
- **Level 2 (AC $>$ 3.7 kW and $\leq$ 22 kW):** More powerful systems commonly found in public or semi-public locations such as parking garages or workplaces.
- **Level 3 (AC or DC $>$ 22 kW):** High-power fast chargers typically deployed along highways or at commercial fleet depots.

In European terminology, Levels 1 and 2 are generally referred to as "slow chargers," while Level 3 corresponds to "fast charging." Despite this general classification, the boundary between AC and DC fast charging continues to evolve, with manufacturers offering various on-board and off-board solutions depending on vehicle class and infrastructure requirements.

Reflecting the distinct types of charging technology and typical operating conditions in Europe, the power levels are grouped as follows [93]:

- **Low AC ($<$ 2.3 kW):** Socket charging without dedicated charging equipment, typically using a standard 230 V outlet with a maximum current of 10 A.

Table 2.1: AC charging levels according to IEC 61851 and SAE J1772 [91].

| Standard | Type | Connection | Power (kW) | Max current (A) |
|---|---|---|---|---|
| IEC 61851 (European) | Mode 1 | 1 phase | 3.68 | 16 |
| | Mode 2 | 1 or 3 phase | 22 | 32 |
| | Mode 3 | 3 phase | >22 | >32 |
| SAE J1772 (US) | Level 1 | 1 phase | 3.3 | 12 |
| | Level 2 | 1 or 3 phase | 14.4 | 32 |

- **Medium AC (3.7 – 7.4 kW):** Single-phase AC charging using dedicated equipment, typically operating at 230 V with current ratings of 16–32 A.
- **High AC (11 – 22 kW):** Three-phase AC charging equipment operating at 230 V with 3 × 16–32 A configurations, suitable for both residential and public installations.
- **DC Fast Charging (≥ 50 kW):** High-power DC charging infrastructure commonly used in public networks, commercial applications, and heavy-duty EVs. These systems typically rely on off-board AC/DC conversion to reduce on-board charger complexity and enable rapid charging.

Table 2.1 provides an overview of AC charging levels as defined by the IEC 61851 standard (commonly used in Europe) and the SAE J1772 standard (prevalent in North America). The classifications differ in naming conventions, power ranges, and connection types, reflecting regional variations in EVSE design and grid compatibility [91]. These power levels are closely linked to the potential grid impacts and suitability of different charging strategies, particularly smart charging.

While fast and ultra-fast charging, typically corresponding to the higher power levels, are prioritized for mobility and user convenience, they can impose substantial strain on local distribution networks. These high-power charging modes can significantly increase peak demand, often necessitating grid reinforcements to accommodate the elevated power requirements [103].

Conversely, slow and moderate AC charging levels are generally more compatible with smart charging strategies. Their lower power demand allows for more flexi-

ble scheduling and integration with grid constraints and renewable energy availability, making them better suited for demand-side management programs [104].

Currently, only a limited number of residential and public charging stations are equipped with smart grid capabilities [105], and relatively few EV models currently support vehicle-to-grid (V2G) functionality. As the number of EVs on the road continues to increase, the deployment of standardized and interoperable charging infrastructure becomes increasingly important. Achieving interoperability is vital to ensure seamless operation across various charging platforms and grid environments, enabling cost-effective and efficient integration of EVs. Standardization will facilitate reliable communication between EVs, charging stations, and distribution networks, supporting the evolution of more intelligent and flexible power systems.

## 2.2 Impacts of EV Charging on Power Networks

An expanding body of research examines the impacts of EV charging on electrical power grids, with existing studies generally categorized into two main areas. The first category focuses on the distribution-level impacts of EV charging, primarily assessing power quality concerns such as harmonics, substation overloading, voltage drops, and phase imbalances [106–109]. These power quality issues are particularly critical in electric networks with high EV penetration, as both the high power demand and non-linear characteristics of EV charging stations contribute to grid disturbances [106]. The consequences of these disturbances manifest in load profiles and equipment performance, leading to transformer, cable, and motor overheating, malfunctions in smart metering and sensitive control devices, mechanical stress on electrical motors, and degraded performance of monitoring and control instruments. Given these challenges, it is crucial to analyze how EVSE affects the power quality of distribution networks, particularly in low-voltage (LV) systems [110].

The second category of studies examines the regional and national-level impacts of EV charging on power grid reliability, stability, and peak generation requirements [49, 111]. Grid reliability and stability concerns primarily stem from the instantaneous

connection or disconnection of large-scale EVSEs, which can significantly influence grid frequency fluctuations and overall system stability. In contrast, studies on peak generation and load forecasting analyze various EVSE penetration scenarios to estimate the additional electrical demand required to support widespread EV adoption at a regional or national level.

Although large-scale EV adoption can influence both transmission and distribution systems, the nature of the impacts differs substantially across voltage levels. At the transmission level, EV electrification primarily affects aggregate demand patterns, generation dispatch, and power flows, particularly by increasing evening peak loads and altering load profiles at the system scale. These effects are typically addressed through generation planning, market-based dispatch, and reinforcement of the high-voltage network. In contrast, distribution networks are directly exposed to the electrical behaviour of EV chargers, including simultaneous charging, phase imbalance, voltage drops, and harmonic distortion, because EVs are connected at low- and medium-voltage levels. Consequently, while transmission-level impacts are mainly driven by aggregated energy demand, distribution-level impacts are driven by both demand magnitude and power quality. For this reason, this thesis focuses on distribution networks, where the interaction between EV charging behaviour, harmonic emissions, and asset loading most strongly affects local grid performance and infrastructure lifetime.

While harmonic distortion is a key concern for this thesis, EV charging also introduces other challenges to power grids, including overloading, voltage drops, phase imbalance (unbalanced voltage), peak demand, and grid security and reliability. Collectively, these factors impact the stability and efficiency of the electrical network, requiring coordinated management strategies to mitigate their effects.

As EVs become more prevalent, their impact on residential distribution networks is becoming increasingly significant, particularly in densely populated areas with high penetration rates of EVs. Unregulated charging can impose substantial stress on distribution infrastructure, leading to increased demand, voltage imbalance, power quality deterioration, and potential overloading of network components [112]. While three-phase charging enables faster replenishment of battery capacity, most residential EV

charging relies on single-phase connections, placing additional strain on low-voltage distribution systems [113]. Given these challenges, understanding the effects of EV charging on distribution networks is crucial. The following sections provide an overview of key impacts associated with EV integration into distribution grids.

### 2.2.1 Power Quality Issues in Distribution Networks

Power quality refers to the capability of an electrical system to deliver current and voltage waveforms that closely approximate a perfect sinusoidal shape at the rated magnitude and frequency [114]. It is influenced by the interaction between the electricity network and its users, as well as by the characteristics of the equipment and facilities connected to the grid. Ensuring adequate power quality is the responsibility of distribution network operators, typically governed by industry standards such as IEC and IEEE. Power quality disturbances arise when deviations occur in voltage or current waveform shape, magnitude, or frequency, leading to potential disruptions in grid performance. Since power quality encompasses both current and voltage characteristics, disturbances in either parameter can harm the grid and its components [115].

Power quality in the presence of EVs is influenced by the type of EV charger, its rated capacity, and the proportion of its operational capacity within the power network. Since EVSE relies on power electronics-based devices to draw electricity from the grid, utility companies are increasingly concerned about potentially violating LV network hosting capacity [116]. The hosting capacity of a given network determines the maximum number of EVs that can be charged while maintaining power quality within acceptable limits [110, 117, 118]. For instance, transformers may become overloaded in urban areas with high load density due to the rising demand for EV charging. Conversely, in rural regions, additional EV load can cause undervoltage issues due to the extended length of feeders and the smaller cross-sections of distribution cables. Furthermore, unbalanced phase loading in distribution networks leads to increased energy losses and excessive heating of network equipment. A particularly significant power quality challenge arises from voltage and current harmonics resulting from the AC/DC conversion process of EV chargers. As the number of power electronic devices con-

nected to the grid increases, harmonic emissions in the system intensify. Consequently, the erratic charging behaviour of EV users introduces power quality concerns related to harmonics, voltage deviations, and phase imbalances [107, 110, 119]. Special emphasis is placed on harmonic distortions, as the analysis in the next section highlights that harmonics are a primary concern for EV charging, primarily due to smart charging.

#### 2.2.1.1 Overloading

EV charging during peak hours significantly impacts the sub-transmission grid, often leading to network overloading when the hosting capacity is insufficient. Overloading caused by the widespread adoption of EVs is typically addressed at the low-voltage level [120,121]. However, the increasing penetration of EVs can also serve as a balancing mechanism for mitigating load fluctuations and grid challenges associated with rising wind and solar energy generation [122].

Apart from periods of overload, there are several hours when the electricity supply exceeds EV charging demand. Without appropriate electricity tariff incentives and control strategies, uncontrolled EV charging can lead to higher peak demand, straining both sub-transmission lines and distribution networks. To alleviate overloading issues, various demand response strategies such as coordinated load shifting, peak shaving, and valley filling can be employed to optimize EV charging patterns and enhance grid stability [66, 123].

#### 2.2.1.2 Voltage Drop

The increasing presence of EVs in distribution networks leads to voltage drops due to rising demand [124]. According to EN 50160 [125], voltage levels should remain within 90% to 110% of the rated value. Overvoltage occurs above 110%, while undervoltage is below 90%. High electricity demand, especially during peak hours, contributes to undervoltage, with voltage dips occurring when the voltage falls below 90% for up to one minute [115].

Studies show that EV penetration between 20% and 80% can cause voltage drops of 13% to 43% [126]. Even a 1% to 2% rise in EV integration impacts system voltage [127].

Research in the UK and Portugal indicates that 50% EV load penetration exceeds voltage limits even with slow charging [119, 128]. To maintain voltage stability, a threshold for EV penetration is necessary.

Traditional mitigation methods include shortening feeder lengths and adding transformers [129]. Reactive power control is sometimes proposed but may worsen conditions in low-voltage networks [115]. EV charging also causes voltage fluctuations, leading to light flicker due to rapid load current variations [109, 110]. Flicker is more prominent in high-voltage networks due to reactive components, while in low-voltage networks, active components are the main contributors [54, 110].

#### 2.2.1.3 Phase Balance (Unbalanced Voltage)

The growth of EVs and slow chargers can lead to voltage unbalance in three-phase distribution systems when single-phase loads exceed others, increasing neutral current and power losses [130]. Voltage unbalance occurs when the three-phase voltages have different RMS values [115], with EN 50160 and IEC 61000-2-5 setting the limit at 2%, or 3% in certain cases [125, 131].

Studies show that uncontrolled EV charging can exceed voltage unbalance limits at 50% EV penetration, whereas tariff-based charging helps keep unbalance within acceptable levels [132]. A study on a suburban residential feeder in Dublin found that single-phase EV charging significantly affects voltage stability, with phase-specific voltage drops occurring as EV penetration increases [15].

Beyond EVs, single-phase solar PV systems also contribute to voltage unbalance, making coordinated management of EV and PV systems essential [133]. Mitigation strategies such as energy storage, voltage regulators, and feeder capacitors can improve power quality [130, 134].

## 2.3 Bulk Power System

As the integration of EVs into the power grid continues to grow, battery capacity and charging station speeds are accelerating to extend driving range and minimize charging

durations. However, uncoordinated charging can pose significant risks to the stability and security of the overall power system. Although EVs are primarily connected to the distribution network, their increasing penetration and higher power demand, along with rapid fluctuations in charging loads, can considerably strain the high-voltage transmission system. This can lead to elevated peak demand, increased operational uncertainty, more frequent grid congestion, and potential violations of system constraints, all of which may compromise grid reliability. The following subsections further examine these challenges and their implications for power system stability.

### 2.3.1 Peak Demand

The widespread adoption of EVs is expected to strain power systems, particularly during peak demand periods. Estimating this increased load is typically performed using scenario-based probabilistic models. According to the National Grid's 2021 Future Energy Scenario [135], EV sales have continued to rise despite the challenges posed by the pandemic. However, further acceleration is necessary to meet the net-zero carbon emissions target by 2050.

In the slowest decarbonization scenario ("Steady Progression"), the UK is projected to have 4.7 million EVs by 2030, whereas in the most ambitious scenario ("Leading the Way"), this figure is expected to reach 11 million. By 2040, the estimated number of EVs on the road will rise to 23 million and 31 million, respectively. Electrification of the transport sector is anticipated to drive total annual road transport energy demand to approximately 100 TWh in both scenarios. Additionally, peak electricity demand is expected to rise due to the increased electricity generation for heating and transport. Under the most aggressive EV adoption scenario, charging demand could add as much as 19 GW to typical daytime electricity loads by 2050.

As EV adoption grows, smart charging and V2G technologies will be crucial in mitigating peak demand [136]. The flexibility offered by these approaches could enable peak shaving of up to 32 GW under the mid-range "Consumer Transformation" scenario. A study by [137] projects that the UK will have over 7 million ultra-low emission vehicles by 2030. Similarly, Deloitte's forecast [138] anticipates 31.1 million

EVs on roads worldwide by the same year.

The rising demand for EVs will also substantially increase charging infrastructure. Expanding fast-charging networks could contribute to peak demand as multiple EVs charge simultaneously at high power levels [139]. Additionally, advancements in battery technology are expected to result in higher-capacity batteries, further increasing electricity demand during charging sessions [11].

### 2.3.2 Grid Security and Reliability

The generation and consumption of electrical energy must remain in real-time equilibrium to maintain grid stability. Any imbalance between supply and demand causes fluctuations in the system frequency, which ideally remains at either 50 Hz or 60 Hz, depending on the region. However, minor variations occur due to fluctuations in electricity generation and demand. An acceptable frequency range in a 50 Hz system is typically between 49.5 and 50.5 Hz [115]. When EV charging demand rises, additional electricity generation is required to keep the frequency within this range [140].

The unpredictable nature of EV charging, including variations in charging start times and durations, introduces further uncertainty in power system demand [141]. Table 2.2 highlights key stability challenges associated with EV charging. The first two concerns, step changes and ramping effects, arise when large numbers of EV chargers switch on or off simultaneously within short intervals. Such abrupt changes in load can strain power system operations and cause frequency deviations, potentially threatening overall system stability. Additional risks stem from the uncontrolled activation of chargers following major outages or system restorations.

Conversely, smart charging strategies and V2G technology can support frequency regulation by adjusting charging behavior to grid conditions [142]. Techniques such as load shaping and DSM offer viable solutions to mitigate frequency instability by optimizing the timing and distribution of EV charging demand [143].

Table 2.2: Power system stability issues due to EV charging.

| **Issue** | **Reason** |
|---|---|
| Step (demand jump) | Too many chargers switching on or off simultaneously. |
| Ramp (demand increase) | Too many chargers switching on and off within minutes. |
| Oscillations | A group of chargers repeatedly switching on and off. |
| Restoration | The restoration process is hindered by erratic behavior after a restart. |

## 2.4 Harmonics

Harmonic distortion is among the most prevalent electromagnetic disturbances in power systems. It refers to the steady-state deviation of voltage and current waveforms from an ideal sine wave [144]. Periodic distortions in voltage and current are typically analyzed using the Fourier transform, which decomposes the distorted signals into a linear combination of pure sinusoidal components:

$$x(t) = c_0 + \sum_{k=1}^{\infty} c_k \cdot \sin\big(2\pi \cdot f_k \cdot t + \theta_k\big) \tag{2.1}$$

where $c_0$ represents the DC component, while $c_k$ and $\theta_k$ denote the amplitude and phase angle of the spectral component of order $k$ with a frequency of $f_k = (k/N) \times f_{h1}$. Here, $f_{h1}$ refers to the fundamental frequency, typically 50 Hz or 60 Hz in most power systems, and $N$ represents the number of fundamental periods within the window width. According to IEC 61000-4-7 [145], $N = 10$ for 50 Hz systems and $N = 12$ for 60 Hz systems. In this study, all quantities are referenced to a 50 Hz system.

Figure 2.4 illustrates that any periodic, distorted waveform can be represented as a sum of sinusoidal components. When a waveform remains identical across successive cycles, it can be decomposed into a series of pure sine waves, where each sinusoidal component has a frequency that is an integer multiple of the fundamental frequency of the distorted waveform. These integer multiples are called harmonics of the fundamental frequency, giving rise to harmonic distortion. The mathematical representation of a waveform as a sum of sinusoids is known as a Fourier series, named after the mathematician Jean-Baptiste Joseph Fourier, who pioneered this analytical approach.

Using the Fourier transform, the total waveform distortion can be decomposed into

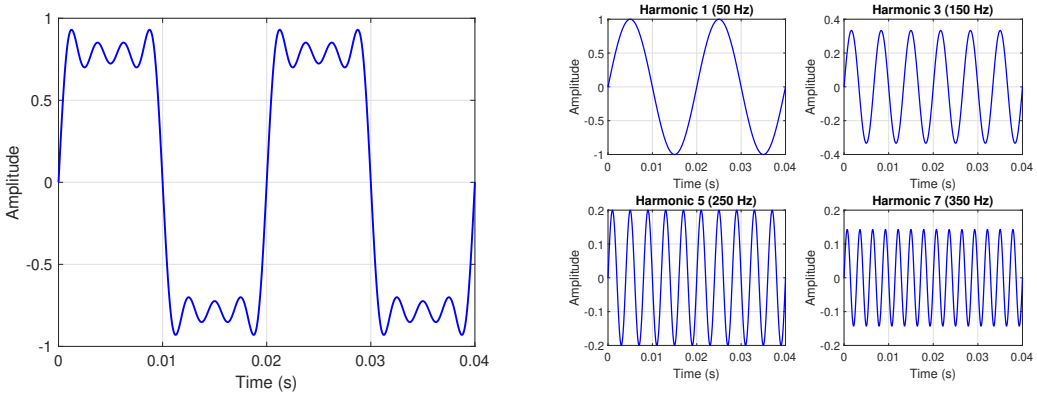


(a) Total Distorted Waveform (b) Individual Harmonics

Figure 2.4: Fourier series representation of a distorted waveform.

the following components:

- **Harmonics**: Spectral components with frequencies that are integer multiples of the fundamental frequency. These components are referred to as harmonic components. For example, the 20th harmonic component corresponds to the $f_{h1} = 20 \times 50Hz = 1000Hz$.
- **Interharmonics**: Components with frequencies that are non-integer multiples of the fundamental frequency. For example, $f_{35} = 3.5 \times 50$ Hz $= 175$ Hz if $N = 10$ and $f_{h1} = 50$ Hz. Interharmonics with frequencies below the fundamental frequency ($k = 1, 2, ..., 9$) are specifically known as *subharmonics*.
- **Supraharmonics**: Spectral components in the frequency range between 2 kHz and 150 kHz.
- **DC-offset**: The constant component $c_0$, representing the non-sinusoidal component of the waveform.

Figure 2.5 presents an example of a distorted signal with a fundamental frequency of 50 Hz, composed of a DC-offset, a subharmonic component at 25 Hz, and two harmonic components at 100 Hz (second harmonic) and 150 Hz (third harmonic), as described

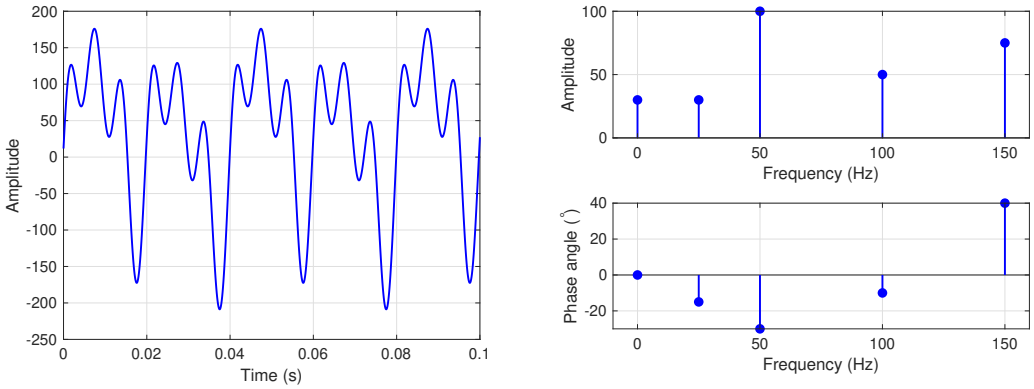


(a) Time-domain signal (b) Frequency-domain signal

Figure 2.5: Example of the distorted signal.

below:

$$x(t) = 30 + 30 \cdot \sin(2\pi \cdot 25 \cdot t - 15^\circ) + 100 \cdot \sin(2\pi \cdot 50 \cdot t - 30^\circ)$$
$$+ 50 \cdot \sin(2\pi \cdot 100 \cdot t - 10^\circ) + 75 \cdot \sin(2\pi \cdot 150 \cdot t + 40^\circ)$$

In most public power networks, DC-offset, interharmonics, and supraharmonics are typically minimal and challenging to measure or analyze. Consequently, research has primarily focused on low-order harmonics (harmonics with frequencies below 2 kHz), as their prevalence has increased due to the growing number of harmonic-emitting sources in power networks. Understanding their effects on network components has become increasingly important for maintaining power quality and grid stability. Therefore, the scope of this thesis is restricted to the analysis of low-order harmonics, which are below 2.5 kHz, since the literature has generally considered low-order harmonics until that frequency [98, 146].

### 2.4.1 Amplitude and Phase Angle

Previously measured harmonic data from the literature were examined as potential input data for this study. Specifically, [97] provides harmonic measurements for slow charging using 23 different EVs, while [98] presents a simulation-based evaluation of

harmonic impacts for fast charging with two EVs. Despite their relevance, both datasets exhibit inconsistencies that limit their applicability. In [97], mean harmonic current distortions are reported as a percentage of the fundamental current. However, an inconsistency is observed where the 3rd harmonic order exceeds the reported total harmonic distortion (THD), which is theoretically impossible since THD should always be greater than any individual harmonic order. Additionally, the dataset lacks phase angle information, making harmonic summation infeasible.

Similarly, anomalies were identified in [98]. While this dataset provides phase angle data along with odd harmonic orders and THD, it presents its harmonic values as percentages of an unspecified fundamental current, making it impossible to perform harmonic aggregation. Moreover, discrepancies exist between the reported THD and the THD calculated from the individual harmonic orders. The fact that THD increases despite a reduction in individual harmonic orders further raises concerns about data reliability and accuracy. These inconsistencies highlight the challenges in relying on existing datasets and reinforce the need for more comprehensive and accurately recorded harmonic measurements to support harmonic summation and power quality analysis.

The amplitude and phase angle of individual harmonics play a crucial role in determining their impact on the power system. While the amplitude quantifies the magnitude of a given harmonic component, the phase angle determines its alignment relative to the fundamental frequency. Each harmonic order contributes to harmonic distortion, influencing overall power quality at the point of common coupling (PCC).

When multiple EVs are charged simultaneously, their individual harmonic components interact with one another, leading to constructive or destructive interference depending on their phase relationships. This phenomenon, known as harmonic cancellation, can significantly reduce the current total harmonic distortion ($\mathrm{THD_I}$) at the PCC. To analyze this effect, each harmonic order is represented as a phasor in the polar form:

$$\text{Phasor} = A \cdot e^{j\theta}$$

Table 2.3: Example for harmonic cancellation of multiple EVs charging. ($A$ denotes amplitude and $\theta$ denotes phase angle in degrees).

| | Harmonic Orders (1st minute) | | | | | |
|---|---|---|---|---|---|---|
| | 3 | | 5 | | 7 | |
| | $A$ | $\theta$ | $A$ | $\theta$ | $A$ | $\theta$ |
| Tesla Model Y LR | 0.24 | -83.6 | 0.09 | -60.0 | 0.45 | -73.5 |
| Renault Zoe R90 | 0.23 | 152.1 | 4.08 | 0.98 | 10.56 | 87.3 |
| Peugeot e-2008 | 3.35 | 47.3 | 7.92 | -67.0 | 21.43 | 40.7 |
| PCC | 3.14 | 48.1 | 10.27 | -45.3 | 29.42 | 54.9 |

where $A$ is the amplitude of the harmonic component, $\theta$ is the phase angle in degrees, and $j$ is the imaginary unit ($j = \sqrt{-1}$). However, for mathematical summation, these phasors must be converted into rectangular form, which consists of real and imaginary components:

$$\text{Rectangular Form} = A \cdot (\cos(\theta) + j \sin(\theta))$$

Table 2.3 presents a snapshot of our measured harmonic amplitudes and phase angles for the 3rd, 5th, and 7th harmonic orders, recorded from three EVs—Tesla Model Y Long Range, Renault Zoe R90, and Peugeot e-2008—along with the corresponding values at the PCC. Harmonic measurements were logged every second throughout the charging process.

For example, considering the 3rd harmonic order, the measured amplitudes ($A$) and phase angles ($\theta$) for each EV are as follows:

$$A_{\text{Tesla Model Y LR}} = 0.24, \quad \theta_{\text{Tesla Model Y LR}} = -83.6^\circ$$

$$A_{\text{Renault Zoe R90}} = 0.23, \quad \theta_{\text{Renault Zoe R90}} = 152.1^\circ$$

$$A_{\text{Peugeot e-2008}} = 3.35, \quad \theta_{\text{Peugeot e-2008}} = 47.3^\circ$$

Each harmonic component is converted into rectangular form as:

$$\text{Tesla Model Y LR:} \quad 0.24 \cdot (\cos(-83.6^\circ) + j\sin(-83.6^\circ))$$

$$\text{Renault Zoe R90:} \quad 0.23 \cdot (\cos(152.1^\circ) + j\sin(152.1^\circ))$$

$$\text{Peugeot e-2008:} \quad 3.35 \cdot (\cos(47.3^\circ) + j\sin(47.3^\circ))$$

The total harmonic contribution at the PCC is then determined by summing the real and imaginary components of these phasors:

$$\text{Total Phasor} = \sum_{\text{EVs}} \text{Rectangular Form of each EV}$$

The resultant phasor is then converted back to polar form to obtain the overall amplitude and phase angle:

$$A_{\text{PCC}} = \sqrt{(\text{Real Part})^2 + (\text{Imaginary Part})^2}$$

$$\theta_{\text{PCC}} = \tan^{-1}\left(\frac{\text{Imaginary Part}}{\text{Real Part}}\right)$$

For this case, the summation of the three EVs' harmonics results in:

$$\text{Real part} = 2.097, \quad \text{Imaginary part} = 2.337$$

$$A_{\text{PCC}} = 3.14, \quad \theta_{\text{PCC}} = 48.1^\circ$$

Without harmonic cancellation, the amplitude at the PCC would be the simple arithmetic sum of the individual amplitudes:

$$A_{\text{PCC, no cancellation}} = 0.24 + 0.23 + 3.35 = 3.82$$

However, $A_{PCC} = 3.14$. This comparison highlights the significant role of phase angle interactions in determining the overall harmonic contribution at the PCC. Harmonic cancellation effects vary depending on the harmonic order, the number of contributing loads, and their relative phase angles. Understanding and accurately modelling these effects is crucial for maintaining power quality and ensuring compliance with industry

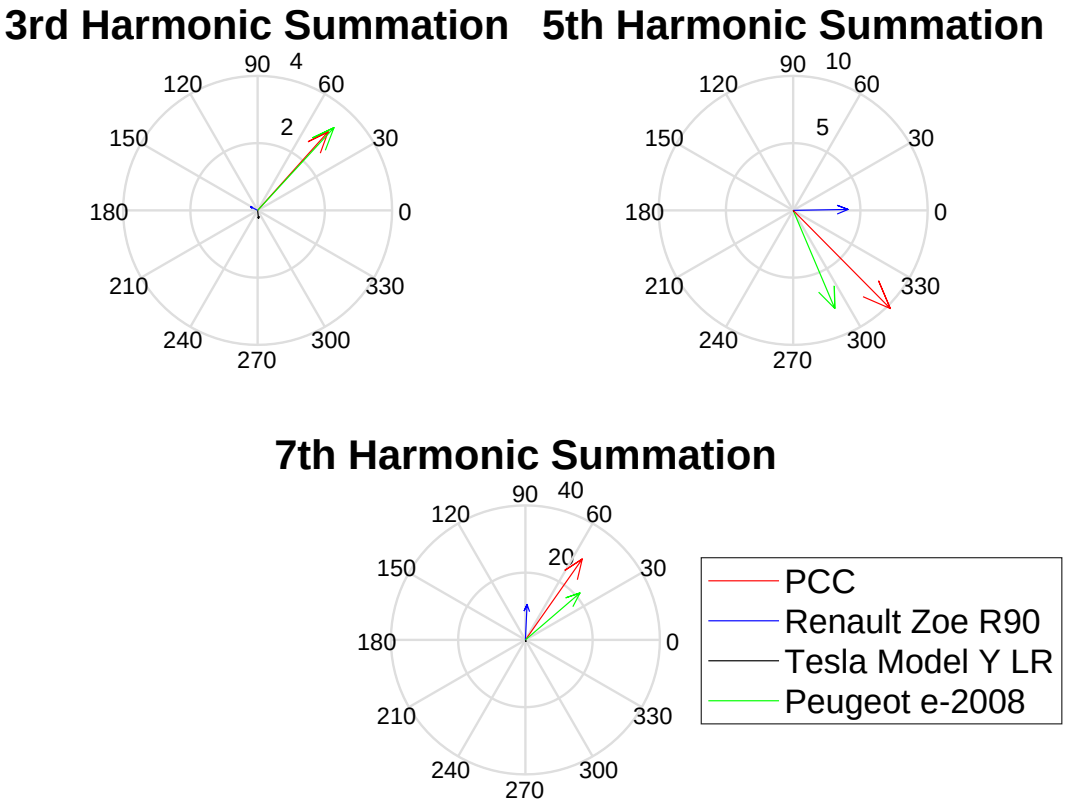


Figure 2.6: Example for harmonic vector summation of 3rd, 5th and 7th harmonic orders for multiple EVs charging.

harmonic standards.

The mathematical representation of the summation of the 3rd harmonics, along with the vector summation of the 3rd, 5th, and 7th harmonics, is depicted in Figure 2.6. While the PCC shows a higher amplitude for the combined 5th and 7th harmonics compared to the individual EV contributions, the 3rd harmonic amplitude of the Peugeot e-2008 exceeds that at the PCC. This highlights the crucial role of both amplitude magnitude and phase angle positioning in determining the harmonic aggregation in the system.

### 2.4.2 Voltage versus Current Harmonic Distortion

The term "harmonics" is often used without further qualification, although it can refer to issues with voltage or current distortion. For example, operational issues in

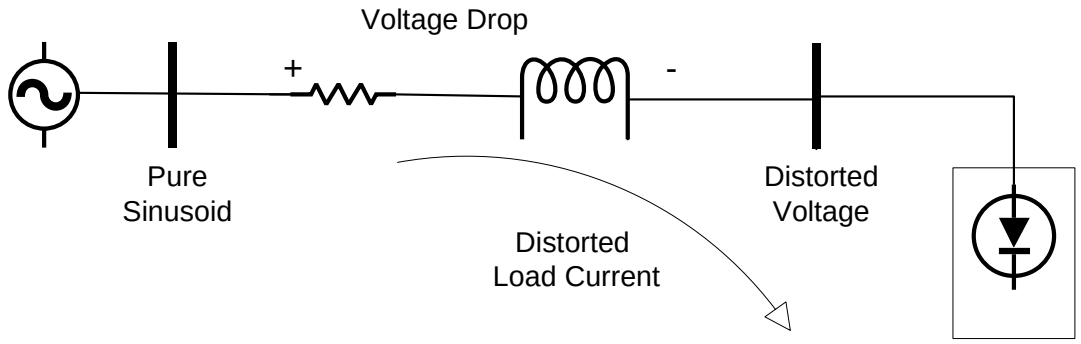


Figure 2.7: Harmonic currents flowing through the system impedance generate harmonic voltage distortions at the load.

equipment such as adjustable-speed drives or induction furnaces are often attributed to harmonics. However, this could refer to several distinct phenomena: (1) elevated harmonic voltages disrupting the control of firing angles, (2) excessive harmonic currents exceeding the capacity of system components, such as transformers, or (3) harmonic currents generating excessive harmonic voltages due to system impedance. These variations underscore the importance of using precise terminology when discussing harmonic effects, as both the sources and the consequences must be clearly identified.

Nonlinear loads act as sources of harmonic currents, injecting distortions into the power system. As illustrated in Figure 2.7, voltage distortion arises when these distorted currents pass through the system's series impedance, leading to voltage harmonics at the load bus. The extent of distortion depends on both system impedance and current magnitude. While load-generated harmonics contribute to voltage distortion, the load has no control over the resulting voltage quality, which varies depending on grid conditions at different locations.

Standards such as IEEE 519-2014 establish guidelines for harmonic control and assign responsibility accordingly. End-use applications are responsible for limiting harmonic current injection, while system operators, typically utilities, manage voltage distortion by controlling system impedance. To ensure clarity, the term harmonics should always be specified, as it can refer to either harmonic currents, typically associated with loads, or harmonic voltages, which are more relevant to the utility system.

### 2.4.3 Harmonic Indices

THD is a key metric used to quantify the degree of distortion in current or voltage waveforms relative to an ideal sinusoidal signal. It represents the proportion of signal energy present at frequencies other than the fundamental frequency, indicating the extent of harmonic contamination.

THD for current harmonics is mathematically defined as:

$$THD_I = \frac{\sqrt{\sum_{n=2}^{\infty} I_n^2}}{I_1}, \tag{2.2}$$

where $I_{n\in\{2,3,4...\}}$ denotes the root mean square (RMS) value of the $n$ th harmonic component, and $I_1$ represents the RMS value of the fundamental frequency component of the current.

Similarly, THD for voltage harmonics is defined as:

$$THD_V = \frac{\sqrt{\sum_{n=2}^{\infty} V_n^2}}{V_1}, \tag{2.3}$$

where $V_{n\in\{2,3,4...\}}$ is the RMS value of the $n$ th harmonic component, and $V_1$ represents the RMS value of the fundamental frequency component of the voltage.

It is important to note that the RMS value of a harmonically distorted signal differs from that of its fundamental component. For a distorted current, the total RMS value is obtained by the quadratic sum of the RMS values of all harmonic components, including the fundamental.

$$I_{RMS} = \sqrt{\sum_{h=1}^{\infty} I_h^2}, \tag{2.4}$$

To quantify the portion of the total RMS current attributed to harmonics, the total harmonic current (THC) can be defined. It is calculated as the quadratic sum of the RMS values of each harmonic component and is expressed as:

$$THC = \sqrt{\sum_{h=2}^{\infty} I_h^2} \tag{2.5}$$

Table 2.4: Harmonics and Symmetrical Components [147]

| **Harmonic Order** | 1 | 2 | 3 | 4 | 5 | 6 | 7 | 8 | 9 | 10 | 11 | 12 | 13 | 14 | 15 |
|---|---|---|---|---|---|---|---|---|---|---|---|---|---|---|---|
| **Positive Sequence** | + | | | + | | | + | | | + | | | + | | |
| **Negative Sequence** | | - | | | - | | | - | | | - | | | - | |
| **Zero Sequence** | | | 0 | | | 0 | | | 0 | | | 0 | | | 0 |

where $I_h$ represents the RMS value of the $h$th harmonic component of the current. Finally, with these definitions, the RMS value of the current is given by:

$$I_{RMS} = \sqrt{I_1^2 + THC^2} = \sqrt{I_1^2(1 + THD^2)} \tag{2.6}$$

This equation shows that the higher the THD, the greater the RMS current, leading to increased heating in electrical equipment.

### 2.4.4 Harmonic Phase Sequences

Symmetrical components are traditionally used in three-phase power system analysis, simplifying complex unbalanced conditions by transforming them into three balanced single-phase systems. This method can also be applied to harmonic current analysis, provided its fundamental assumptions remain valid [147].

Any unbalanced set of phase currents or voltages can be decomposed into three balanced components:

- *Positive-sequence* components follow the A-B-C phase rotation (e.g., $0°, -120°, 120°$).
- *Negative-sequence* components follow the A-C-B rotation (e.g., $0°, 120°, -120°$).
- *Zero-sequence* components are in phase $(0°, 0°, 0°)$.

In a balanced three-phase system, the harmonic phase sequence is determined by multiplying the harmonic order ($h$) by the fundamental phase rotation. For instance, the second harmonic ($h = 2$) produces a negative sequence, while the third harmonic ($h = 3$) results in a zero-sequence component. Each harmonic frequency corresponds to a specific sequence in a balanced system, as shown in Table 2.4.

Since power system waveforms primarily contain odd harmonics, only odd-harmonic phase sequences are typically considered in most studies. Zero-sequence harmonics also require special consideration due to their propagation characteristics within the system: In a three-phase system, zero-sequence harmonics sum in the neutral conductor, potentially leading to neutral overheating. These harmonics circulate within the delta windings of transformers, preventing them from propagating beyond the transformer. As a result, any 3rd harmonic distortion is generated locally and does not transfer through the transformer [147].

### 2.4.5 Harmonic Sources

Harmonic distortion arises from nonlinear devices, which draw current waveforms that are not directly proportional to the applied voltage. Many electrical devices exhibit nonlinear behaviour. For instance, power transformers and generators operate with ferromagnetic materials near their nonlinear region, leading to nonsinusoidal magnetizing currents even when supplied with a purely sinusoidal voltage [148].

However, electronic devices used across industrial, commercial, and residential sectors primarily contribute to harmonic distortion in power systems. Industrial equipment such as three-phase power converters and arc welders generate significant harmonic currents. In public low-voltage networks, the primary sources of harmonics are household and commercial electronic appliances, including energy-efficient lighting (CFLs and LEDs), computers, televisions, and battery chargers [96].

Power electronic devices, such as rectifiers, inverters, and switched-mode power supplies (SMPS), are key contributors to harmonic distortion due to their non-linear switching behaviour [149]. These devices are widely used in motor drives, uninterruptible power supplies (UPS), and renewable energy systems. For instance, single-phase diode bridge rectifiers, commonly found in consumer electronics like battery chargers and LED drivers, introduce significant harmonic currents into the grid by drawing current in short pulses rather than as a continuous waveform. Similarly, pulse-width modulation (PWM) inverters, used in variable-speed motor drives and solar PV inverters, generate high-frequency harmonics that can affect power quality [95].

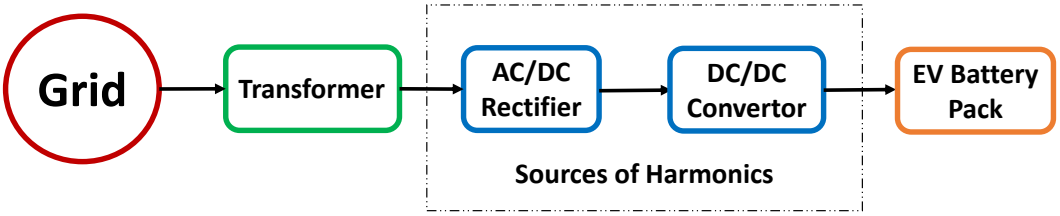


Figure 2.8: Block Diagram of EV charging

Power electronic devices utilized in EV charging introduce current and voltage harmonics into the power system due to their non-linear switching behaviour during the AC-to-DC conversion process [94]. Figure 2.8 presents a block diagram illustrating the EV charging process. Depending on the charging configuration, this AC/DC conversion can occur either within the EVSE or through the vehicle's onboard charger.

Figure 2.9 shows the topology of a three-phase bidirectional AC-DC converter, which facilitates power transfer between a three-phase AC supply and a DC voltage bus [150]. This converter consists of six IGBT-diode switches $S_1$–$S_6$, which are connected to the three-phase AC supply through series filter inductance $L_s$ and resistance $R_s$. To maintain a stable DC bus voltage $V_{dc}$, a DC capacitor $C_{dc}$ is placed across the voltage bus.

The bidirectional AC-DC converter operates in two distinct modes. It functions as a front-end rectifier in rectifier mode, enabling power transfer from the three-phase AC supply to the DC voltage bus. In inverter mode, power flows in the opposite direction from the DC bus to the three-phase AC supply, where the converter operates as a voltage source inverter. However, this AC-DC conversion process, relying on power electronics, introduces harmonic distortion into the supply network due to the non-linear switching behaviour of semiconductor devices.

### 2.4.6 Impacts of Harmonics

This section provides a general overview of the impacts of harmonic distortion on various power system components, serving as a foundational background for EV-specific analysis presented later. Harmonic currents generated by nonlinear loads are fed back

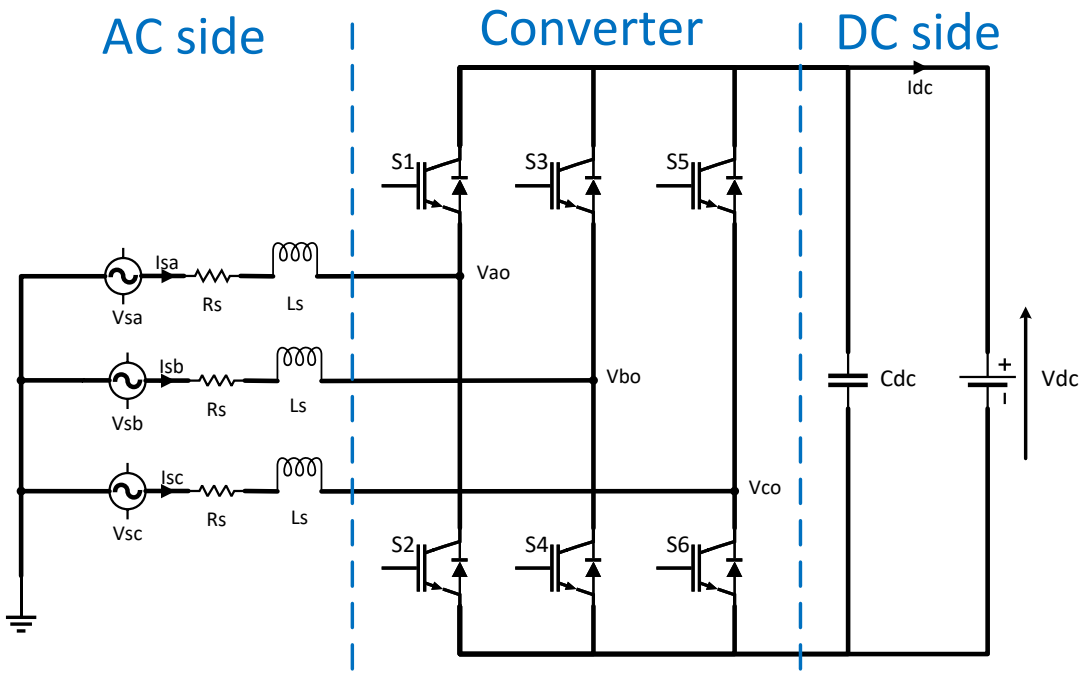


Figure 2.9: Three-phase bidirectional AC-DC converter topology.

into the supply system, where they can negatively affect various power system components. These currents can lead to increased losses, overheating, and overloading in equipment such as capacitors, transformers, and motors [31]. Additionally, harmonics may interfere with telecommunication lines and introduce errors in power metering [151]. This section examines the specific impacts of harmonic distortion on different power system elements:

- **Transformers**: Transformers are designed to supply power to connected loads with minimal losses at the fundamental frequency. However, harmonic distortion leads to additional heating and efficiency losses, particularly in current [152]. To accommodate higher frequencies, transformer designs may include continuously transposed cables instead of solid conductors and additional cooling ducts. A transformer experiencing current distortion above 5% typically requires derating to account for the additional thermal stress caused by harmonics [147].

  Harmonics increase transformer heating through three main effects. First, RMS current: Harmonic currents can raise the total RMS current beyond the trans-

former's rated capacity, increasing conductor losses. Second, eddy current losses: Harmonic-induced eddy currents circulate in the windings, core, and surrounding conductive parts, generating additional heat. These losses increase with the square of the harmonic frequency. Third, core losses: Harmonics affect the voltage waveform, potentially increasing eddy currents in the core laminations. The impact depends on the core's material and lamination thickness, though core losses are generally less critical than conductor and eddy current losses [32].

- **Capacitors**: Capacitor banks are often the first components to exhibit problems related to harmonic distortion. Resonance occurs when the inductive reactance of the system matches the capacitive reactance, leading to excessive voltage and current amplification at specific harmonic frequencies [153]. During resonance, capacitors experience high voltage distortion and excessive harmonic currents. These currents, particularly monotonic harmonics, can significantly exceed the capacitor's rated RMS current. For instance, when resonance occurs at the 11th harmonic, the resulting current waveform consists of the 11th harmonic superimposed on the fundamental frequency. Such conditions indicate a resonant state involving capacitor banks. High-frequency harmonic currents can also lead to overheating, fuse failures, and potential damage to capacitors if not properly mitigated [115].

- **Motors**: Harmonic voltage distortion at motor terminals generates harmonic fluxes that do not contribute to torque but induce high-frequency currents in the rotor. Similar to negative-sequence currents, this effect leads to increased losses, reducing efficiency and causing overheating, vibration, and high-pitched noise [154]. At harmonic frequencies, motors behave as a blocked rotor reactance across the supply. Lower-order harmonics are particularly significant, as their higher magnitudes and lower motor impedance make them more impactful. Generally, motors do not require derating if voltage distortion remains within IEEE Standard 519-2014 limits of 5% THD and 3% for any individual harmonic. However, excessive heating issues arise when distortion exceeds 8–10%, necessitating

corrective measures to ensure motor longevity [144].

- **Telecommunications**: Harmonic currents can interfere with communication lines that run parallel to power conductors, especially in the 540–1200 Hz voice frequency range. Triplen harmonics (e.g., 3rd, 9th) are particularly problematic in four-wire systems, as they sum in the neutral and increase coupling risk. Although shielded twisted-pair cables reduce inductive interference, high shield currents can still cause voltage imbalances. Proper grounding and shielding remain essential to minimize harmonic-induced disruptions in telecom systems [144].

- **Energy and Demand Metering**: Harmonic currents from nonlinear loads can affect the accuracy of watthour and demand meters, leading to measurement errors [155]. Traditional induction-based meters tend to under-register energy at harmonic frequencies, while modern electronic meters are more accurate but may still be configured to measure only fundamental power. The most significant errors occur in demand metering, where harmonic distortion can cause an underestimation of kVA demand by up to 10–15%. While these errors are usually small at the plant level, they can be more pronounced in facilities dominated by PWM drives or other high-harmonic loads [148].

- **Cables and Lines**: Harmonic currents cause additional heating in cables and transmission lines, though the effect is less severe than in transformers. High-frequency harmonics increase the risk of hot spots forming at cable joints, leading to insulation degradation and potential failures over time [156].

- **Neutral Conductors**: The neutral conductor typically carries minimal current in a three-phase system. However, triple harmonics from phase conductors accumulate in the neutral, sometimes exceeding the phase current. This can lead to overheating of the neutral conductor, posing a risk of insulation damage or failure, as overload protection may not detect and mitigate the issue [115].

- **Electronic Equipment**: Waveform distortion can cause zero-crossing shifts or multiple zero-crossings, affecting devices that rely on voltage zero-crossing for

phase-angle detection. Additionally, high-frequency distortion can couple through the power supply circuit, leading to malfunctions in sensitive electronic equipment [115].

## 2.5 Harmonic Impact Assessment of EV Charging

Building on the general impacts of harmonics, this section examines the specific impacts of EV charging, reviewing key datasets and studies that assess EV-induced harmonic distortion under various charging conditions. As non-linear loads, EV chargers generate harmonics due to the power electronics used in AC-DC conversion, which inject current and voltage harmonics into the power grid [94]. With the increasing number of EV charging sessions, harmonic distortion can significantly degrade power quality. If the total harmonic content exceeds the limits defined by industry standards, it may pose challenges to grid stability and reliability [157].

Harmonic distortion caused by EV charging can adversely affect distribution network components, including cables, transformers, switchgear, and customer equipment [158]. In cables, harmonics increase resistive losses, leading to overheating and insulation degradation, which can shorten their operational lifespan if not adequately rated [31, 159]. Transformers are particularly vulnerable to harmonics due to higher eddy current losses and core saturation, which result in excessive heating and reduced efficiency. This can contribute to voltage irregularities and premature failure [32]. Additionally, harmonics distort the magnetic flux, further exacerbating core saturation, reducing transformer lifespan, and increasing the likelihood of network voltage fluctuations [33]. The K-value is a crucial index for evaluating a transformer's ability to withstand harmonic currents. A higher K-value correlates with more significant thermal stress, which can potentially reduce the transformer's lifespan. This relationship follows a quadratic correlation that links harmonic order and magnitude to the K-value [160]. The methodology for quantifying transformer loss of life due to harmonic effects is defined in IEEE Standard C57.91 [161].

Switchgear components, such as circuit breakers, are susceptible to harmonic dis-

tortion, thermal stress, and nuisance tripping, which can reduce their operational lifespan [162]. For customer equipment, EV-induced harmonics contribute to overheating, voltage irregularities, and electromagnetic interference (EMI), leading to malfunctions, reduced efficiency, and potential damage to sensitive electronics. Additionally, increased EMI from harmonic distortion presents a significant risk to on-board vehicle systems, potentially disrupting their functionality [163]. Harmonic distortion can weaken insulation, accelerate component aging, and compromise overall system reliability if not properly managed.

In the evolving field of electric mobility, on-board EV chargers have seen significant advancements since the late 2000s. Early chargers primarily performed basic AC-to-DC conversion, whereas modern designs offer higher efficiency, increased charging power, bi-directional capability, and smart charging features [164].

While these advances improve efficiency and flexibility, they also modify harmonic emission patterns and increase the complexity of harmonic interactions in modern EV-dominated networks. Consequently, understanding how harmonics propagate and aggregate in present-day EV charging environments requires data and models that reflect current charger technology rather than early-generation designs.

### 2.5.1 Impacts of Constant Current and Constant Voltage Charging on Harmonic Distortion

Constant current (CC) and constant voltage (CV) charging, the standard methodology employed in fast charging, directly influence harmonic levels. In CC-CV charging, the battery undergoes two distinct stages, dictated by its state of charge (SoC), to complete the charging cycle. During the CC phase, the battery is charged at a constant current irrespective of its voltage, continuing until it reaches a predefined SoC threshold. This phase represents the primary charging period, typically covering the range from 0 to 80% SoC. Conversely, the CV phase maintains a fixed voltage while the charging current gradually decreases as the battery approaches full capacity. Once the SoC surpasses the level charged in the CC stage, the CV phase is employed until the battery reaches full charge [165]. Figure 2.10 illustrates the relationship between charging current and

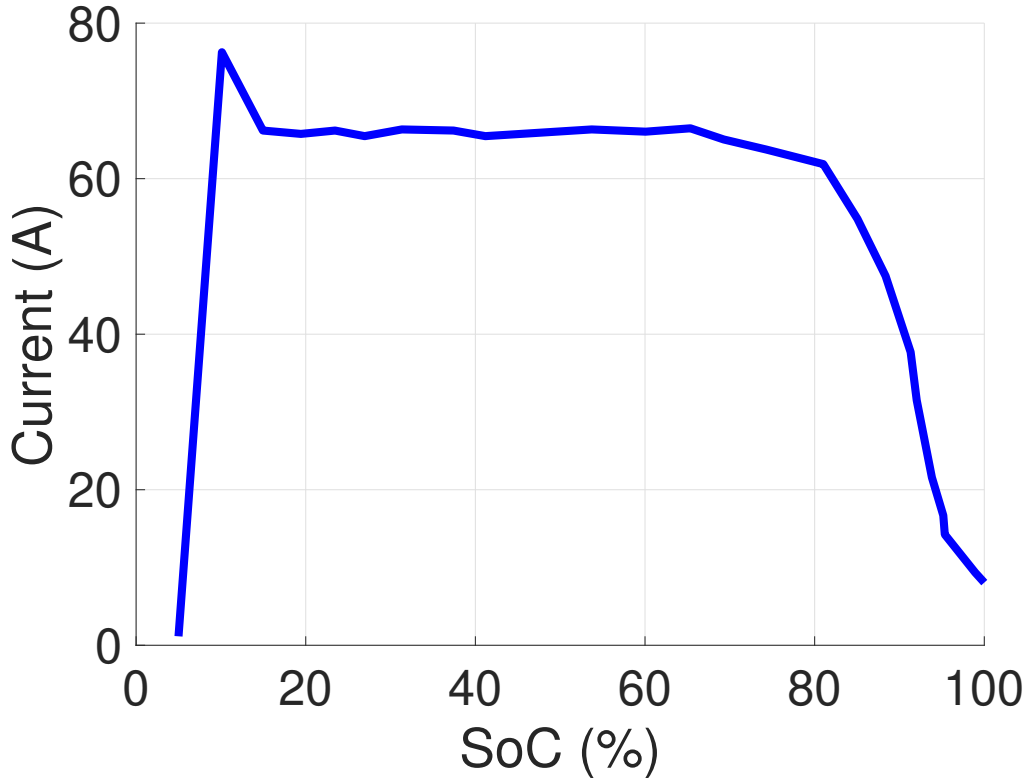


Figure 2.10: Current behaviour during CC and CV charging phase [98].

SoC throughout the CC and CV phases.

CC charging techniques encompass various methods, including fast, trickle, and pulse. Fast charging delivers a high current to rapidly charge a battery, whereas trickle charging applies a low current to sustain a fully charged battery over an extended period. Pulse charging, on the other hand, employs intermittent bursts of high current, followed by rest periods, to enhance battery performance and longevity. In contrast, CV charging methods primarily consist of float and taper charging [166]. Float charging maintains the battery at full charge by supplying a constant voltage, while taper charging gradually reduces the charging current as the battery nears full capacity to prevent overcharging and potential battery degradation.

Different battery chemistries require tailored charging techniques to optimize performance and longevity. Nickel-metal hydride (NiMH) batteries typically utilize constant current (CC) and trickle charging, whereas lithium-ion (Li-ion) batteries employ

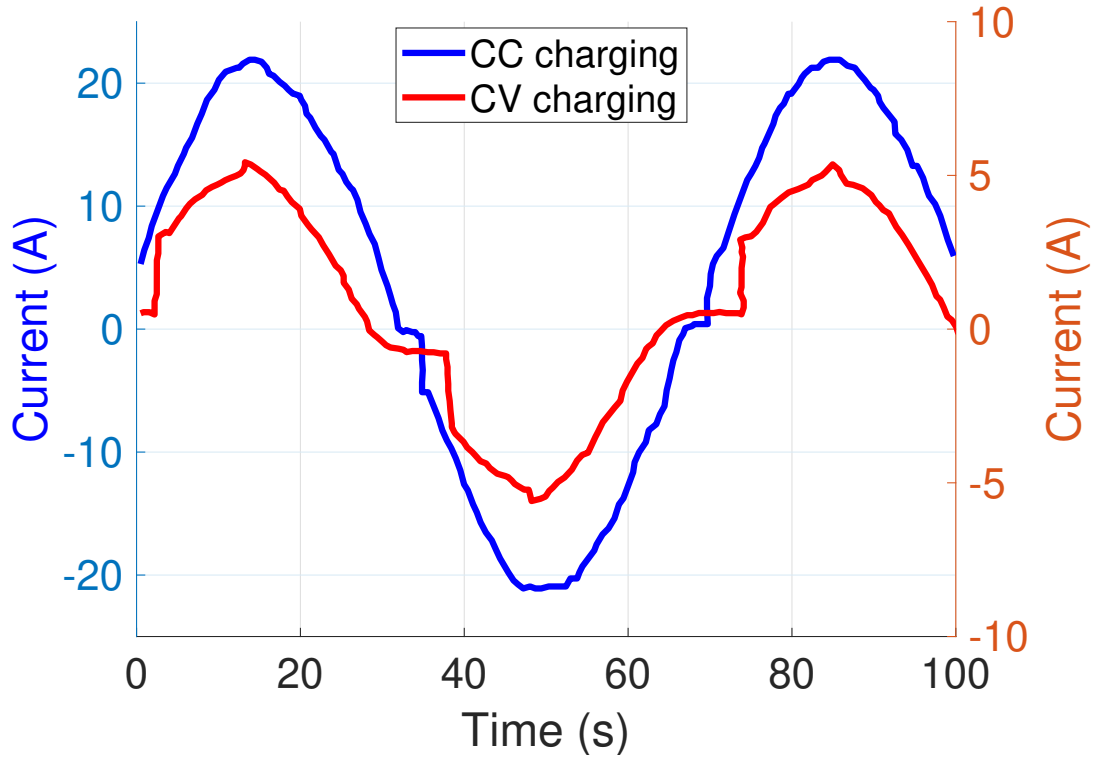


Figure 2.11: Current waveform during CC and CV charging phase [168].

a combination of CC, CV, and trickle charging methods. Temperature plays a critical role in charging efficiency, as both battery types exhibit reduced performance under extreme thermal conditions. In cold climates, trickle charging is often used to preheat the battery, ensuring its temperature reaches an optimal range of 20–25°C before initiating standard charging. Additionally, to prevent overcharging and extend battery lifespan, Li-ion battery charging is automatically terminated once it approaches full capacity [167].

From a harmonics perspective, EV chargers exhibit distinct characteristics during different charging stages. During the CC phase, the current waveform remains relatively undistorted, whereas harmonic distortion increases significantly in the CV phase. This behavior is illustrated in Figure 2.11, which depicts the current waveform variations in both charging phases.

The trends in THD throughout the CC and CV phases are further analyzed in

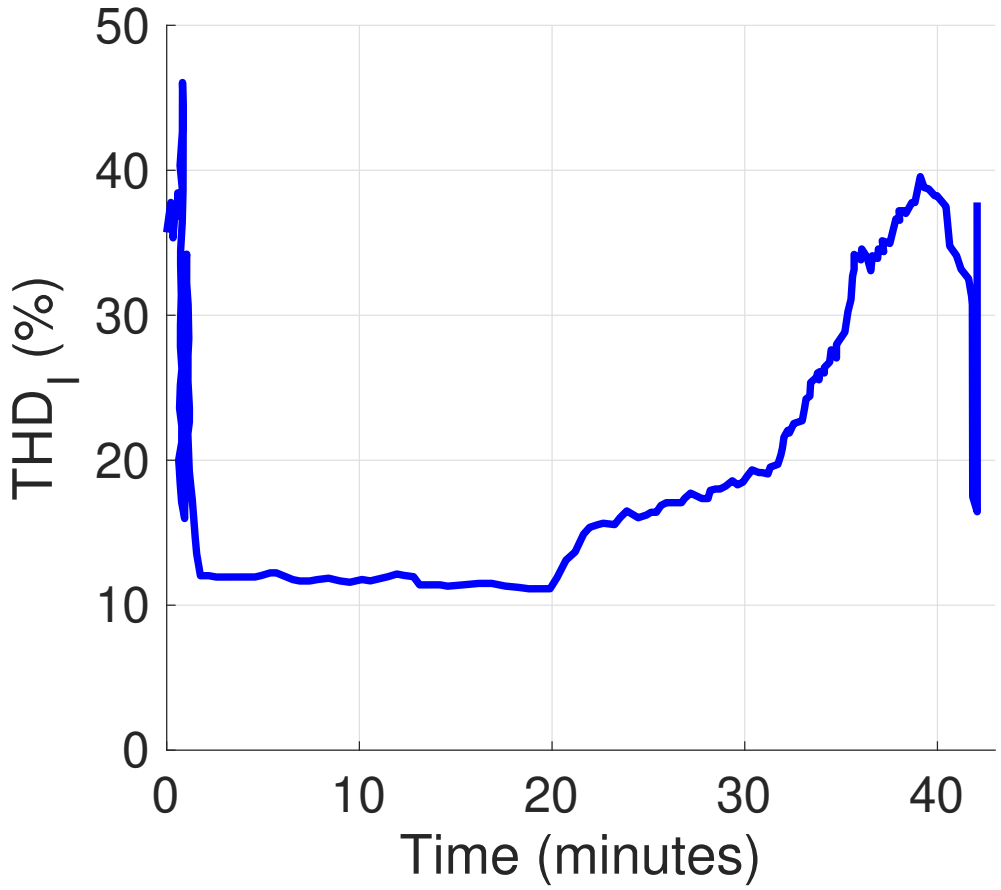


Figure 2.12: $THD_I$ during CC and CV charging phase [98].

Figure 2.12. Both Figure 2.10 and Figure 2.12 represent approximately 40 minutes of fast charging, highlighting three distinct stages. Initially, at the start of charging, THD reaches its peak before gradually decreasing as the current increases. In the second stage, corresponding to the CC phase, THD stabilizes at approximately 12%, maintaining relatively low distortion levels. As charging transitions to the CV phase, spanning from 77% to 100% SoC, the current gradually decreases over a 15-minute period. During this stage, THD rises steadily, peaking towards the end of charging. These variations underscore the nonlinear behavior of EV chargers and their impact on power quality during different stages of the charging cycle.

Table 2.5: Current total harmonic distortion and corresponding currents for different temperatures [146].

| Charger | Units | Temperature Levels | | | |
|---|---|---|---|---|---|
| | | -25 °C | -15 °C | 20 °C | 40 °C |
| A | $THD_I$ (%) | 15.06 | 13.37 | 6.43 | 8.23 |
| 120 kW DC | $I_L$ (A) | 17.6 | 28.53 | 82 | 81 |
| B | $THD_I$ (%) | 37.63 | 24.67 | 10.63 | 11.03 |
| up to 50 kW DC | $I_L$ (A) | 9.13 | 24.47 | 79.2 | 77.03 |
| C | $THD_I$ (%) | Failed to | 8.33 | 8.6 | 6.37 |
| from 20 to 44 kW DC | $I_L$ (A) | charge | 37.1 | 68.3 | 67.13 |
| D | $THD_I$ (%) | Failed to | 11.07 | 7.97 | 8.33 |
| Max power 50 kW DC | $I_L$ (A) | charge | 31.73 | 61.8 | 80.83 |
| E | $THD_I$ (%) | Failed to | 8 | 4.4 | 4.1 |
| Max power 50 kW DC | $I_L$ (A) | charge | 29.07 | 75.67 | 75.5 |
| F | $THD_I$ (%) | 23.9 | 15.67 | 11.77 | 8.53 |
| Max power 60 kW DC | $I_L$ (A) | 15.87 | 43.3 | 80.33 | 83.03 |

### 2.5.2 Impacts of Low Temperatures EV Charging on Harmonic Distortion

Previous studies have examined the effects of EV charging on power distribution networks from multiple perspectives. However, most of this research assumes optimal temperature conditions, typically equating them with ambient temperature, without explicitly accounting for the influence of low temperatures. As a result, the specific effects of reduced temperatures on EV charging behaviour and associated power quality issues have not been thoroughly explored. In particular, harmonic distortion tends to become more pronounced under low-temperature conditions [31].

Experimental results from [169] reveal that low ambient temperatures significantly influence fast chargers' charging behaviour and harmonic emissions. In the study, an ABB Terra 53 CJ 50 kW DC fast charger was used to charge a 2015 Nissan Leaf, and the harmonic profile was analyzed under varying temperature conditions. The findings indicate an inverse relationship between ambient temperature and harmonic distortion: as temperatures decrease, the charging power output is reduced, leading to increased

Table 2.6: Impacts of temperature on fast charging current. (T represents the battery temperature) [170].

| | $T < 10°C$ | $10°C \leq T \leq 20°C$ | $T > 20°C$ |
|---|---|---|---|
| Charging current (A) | 25 | 50 | 125 (rated) |

harmonic emissions. In contrast, the charger delivers higher power when the temperature approaches optimal levels and the associated harmonic distortion decreases. Under subzero conditions, THD exceeded the limits defined by existing standards, highlighting the sensitivity of harmonic performance to environmental conditions.

In [146], a Nissan Leaf with a 24 kWh battery was fully charged at four ambient temperatures ($-25°C$, $-15°C$, $20°C$, and $40°C$) using six different commercial fast chargers. The results, summarized in Table 2.5, present the average $THD_I$ and load current ($I_L$) across all three phases. The findings indicate that $THD_I$ levels generally increased as ambient temperature decreased. Moreover, certain chargers were unable to initiate charging at extremely low temperatures.

The study in [170] examined how ambient and battery temperatures, along with the SoC, affect the performance of an ABB fast charger. When charging from an initial SoC of 10% to 80%, a warm battery completed the process in 25 minutes, while a cold battery required 62 minutes. The results, summarized in Table 2.6, indicate that lower battery temperatures lead to a noticeable reduction in charging current.

## 2.6 Industry Standards for Harmonic Limitation

The International Electrotechnical Commission (IEC), the European Committee for Electrotechnical Standardization (CENELEC), and the Institute of Electrical and Electronics Engineers (IEEE) establish widely accepted power quality standards. These standards define permissible levels of harmonic distortion in electrical networks to ensure power quality and grid stability. The key standards relevant to this analysis are outlined below and summarized in Figure 2.13.

- IEC 61000 defines various types of power quality disturbances, along with their

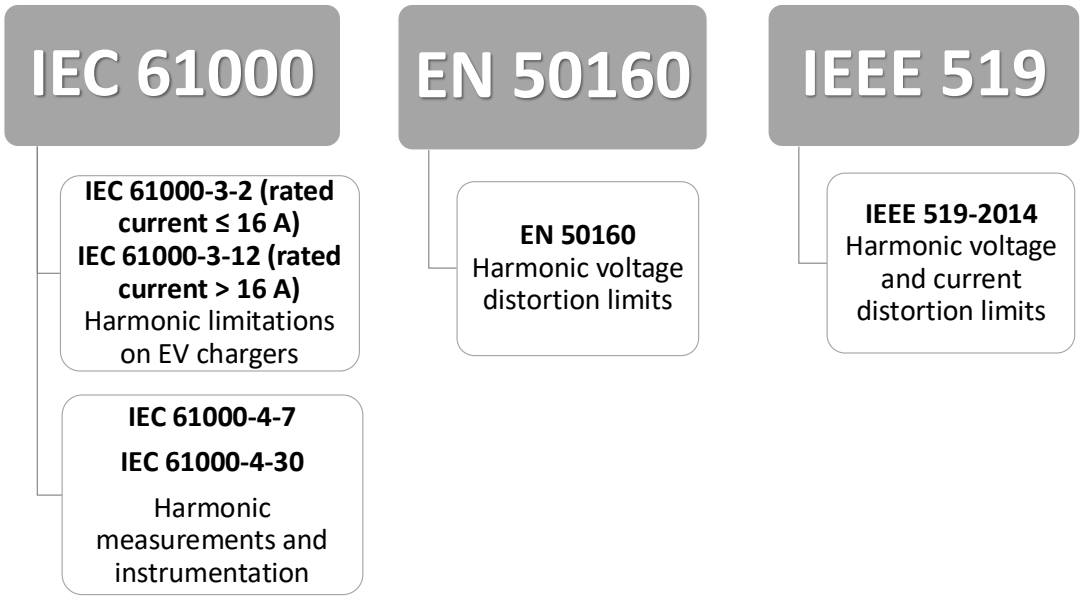


Figure 2.13: Various harmonic power quality standards.

characteristics and measurement methodologies. EV chargers must comply with the IEC 61000 series standards for electromagnetic compatibility, which set limits on harmonic emissions such as current harmonics, voltage harmonics, and power factor requirements. Specifically, IEC 61000-3-2 [171] (for devices rated at $\leq$ 16A) and IEC 61000-3-12 [172] (for devices rated above 16A) regulate the harmonic current emissions from EV chargers, as summarized in Table 2.7 and Table 2.8. Meanwhile, IEC 61000-2-2 [173] and IEC 61000-2-4 [174] establish voltage harmonic limits for public and industrial power networks, respectively, as detailed in Table 2.9. Standards IEC 61000-4-7 [145] and IEC 61000-4-30 [175] provide guidelines for harmonic measurement techniques and instrumentation.

- European Norm (EN) 50160 [125], developed by CENELEC, sets voltage quality limits for LV and MV distribution networks, defining the acceptable range of voltage parameters at the PCC. This standard specifies the voltage distortion levels that distribution network operators must comply with.

- IEEE 519-2014 [176] provides recommendations on voltage and current distortion limits for both network operators and end-users. The current harmonic restric-

Table 2.7: Restrictions for current harmonics in IEC 61000-3-2.

| Harmonic order (n) | Maximum permissible harmonic current (A) |
|---|---|
| Odd Harmonics | |
| 3 | 2.30 |
| 5 | 1.14 |
| 7 | 0.77 |
| 9 | 0.40 |
| 11 | 0.33 |
| 13 | 0.21 |
| $15 \leq n \leq 39$ | 0.15 x (15/n) |
| Even Harmonics | |
| 2 | 1.08 |
| 4 | 0.43 |
| 6 | 0.30 |
| $8 \leq n \leq 40$ | 0.23 x (8/n) |

Table 2.8: Restrictions for current harmonics in IEC 61000-3-12.

| Minimum RCSE | Admissible individual harmonic current $I_h/I_{ref}$ (%) | | | | Admissible harmonic parameters (%) | |
|---|---|---|---|---|---|---|
| | $I_5$ | $I_7$ | $I_{11}$ | $I_{13}$ | $THC/I_{ref}$ | $PWHC/I_{ref}$ |
| 33 | 10.7 | 7.2 | 3.1 | 2 | 13 | 22 |
| 66 | 14 | 9 | 5 | 3 | 16 | 25 |
| 120 | 19 | 12 | 7 | 4 | 22 | 28 |
| 250 | 31 | 20 | 12 | 7 | 37 | 38 |
| 350+ | 40 | 25 | 15 | 10 | 48 | 46 |

RSCE - Short-circuit ratio; $I_h$ - Harmonic current component;
$I_{ref}$ - Reference current; THC - Total Harmonic Current;
PWHC - Partial Weighted Harmonic Current

tions outlined in IEEE 519-2014 for voltage levels between 120 V and 69 kV are summarized in Table 2.10. Additionally, voltage harmonic limits based on bus voltage levels are detailed in Table 2.11.

These standards provide essential guidelines for assessing and mitigating the impact of harmonic distortion on power systems. Their widespread adoption in industry

Table 2.9: Restrictions for voltage harmonics in IEC 61000-2-4.

| Harmonic order n (Non multiples of 3) | Class 1 Harmonic V. (%) | Class 2 Harmonic V. (%) | Class 3 Harmonic V. (%) |
|---|---|---|---|
| 5 | 3 | 6 | 8 |
| 7 | 3 | 5 | 7 |
| 11 | 3 | 3.5 | 5 |
| 13 | 3 | 3 | 4.5 |
| 17 | 2 | 2 | 4 |
| $THD_V$ | 5 | 8 | 10 |

Class 1: Compatibility level lower than public (protected supplies).
Class 2: Compatibility level equals the public (industrial networks).
Class 3: Compatibility level higher than public (dedicated or heavy industry networks)

Table 2.10: Restrictions for current harmonics between 120 V and 69 kV in IEEE 519-2014.

| Maximum harmonic current distortion in percent of $I_L$ | | | | | | |
|---|---|---|---|---|---|---|
| | Individual harmonic order (odd harmonics) | | | | | |
| $I_{SC}$ / $I_L$ | $3 \leq h < 11$ | $11 \leq h < 17$ | $17 \leq h < 23$ | $23 \leq h < 35$ | $35 \leq h \leq 50$ | TDD |
| $[0, 20)$ | 4.0 | 2.0 | 1.5 | 0.6 | 0.3 | 5.0 |
| $[20, 50)$ | 7.0 | 3.5 | 2.5 | 1.0 | 0.5 | 8.0 |
| $[50, 100)$ | 10.0 | 4.5 | 4.0 | 1.5 | 0.7 | 12.0 |
| $[100, 1000)$ | 12.0 | 5.5 | 5.0 | 2.0 | 1.0 | 15.0 |
| $[1000, -)$ | 15.0 | 7.0 | 6.0 | 2.5 | 1.4 | 20.0 |

Table 2.11: Restrictions for voltage harmonics in IEEE 519-2014.

| Bus Voltage V at PCC | Individual Harmonic Voltage Distortion (%) | Total Harmonic Voltage Distortion ($THD_V$) (%) |
|---|---|---|
| $V \leq 1$ kV | 5.0 | 8.0 |
| 1 kV $< V \leq$ 69 kV | 3.0 | 5.0 |
| 69 kV $< V \leq$ 161 kV | 1.5 | 2.5 |
| $V >$ 161 kV | 1.0 | 1.5 |

and academia ensures consistency in monitoring, comparing, and managing harmonic emissions across different systems and geographies. In line with these established frameworks, this study focuses specifically on THD and individual harmonic orders, which are among the most recognized and validated indicators in the literature for quantifying harmonic-related disturbances and ensuring compliance with regulatory thresholds.

## 2.7 Regulatory Frameworks, Market Incentives, and Stakeholder Alignment

The technical constraints defined by harmonic, voltage, and current standards do not operate in isolation. Their practical relevance is realised through regulatory frameworks and electricity market mechanisms that determine how EV charging infrastructure is deployed and how charging behaviour is shaped in real power systems. While IEC 61000, IEEE 519, and EN 50160 specify permissible limits on harmonic distortion and voltage quality, compliance with these limits is enforced through grid codes, distribution network connection agreements, and market-based incentives that affect both EV owners and charging infrastructure operators. Consequently, the ability of smart charging to mitigate power quality and loading problems depends not only on control algorithms, but also on how regulatory and commercial structures translate technical requirements into operational behaviour.

From a distribution system operator (DSO) perspective, EV charging represents a new class of highly variable and spatially concentrated load. DSOs are responsible for ensuring that voltage levels, thermal limits, and power quality indices at the PCC remain within statutory limits. Exceeding these limits leads to regulatory non-compliance, accelerated asset aging, and in some cases, penalties or mandatory network reinforcements. Smart charging, therefore, provides DSOs with a non-wires alternative for managing congestion, voltage deviations, and harmonic stress by shaping EV charging profiles instead of physically upgrading cables and transformers. In this sense, smart charging is directly aligned with regulatory objectives for cost-effective grid operation and long-term asset protection.

At the transmission system level, the primary concern is not local voltage or harmonics but the aggregate impact of EV charging on system-wide demand, frequency stability, and generation dispatch. Large-scale electrification of transport increases evening peak demand and amplifies the variability introduced by renewable energy sources. Market-based flexibility mechanisms allow aggregators and retailers to coordinate EV charging in response to wholesale price signals and ancillary service markets,

thereby supporting system balancing and renewable integration. Although individual EVs are connected at low voltage, their collective behaviour influences high-voltage network loading and generation requirements, linking distribution-level charging decisions to transmission-level system stability.

EV users and charging service providers respond primarily to economic incentives. Time-of-use tariffs, dynamic pricing, and flexibility payments create financial incentives to shift or modulate charging away from peak periods and toward periods of high renewable availability. Regulatory frameworks increasingly require new charging points to support smart functionality and external control, ensuring that these price signals translate into actual charging behaviour. In this way, regulatory mandates and market incentives work together to align consumer behaviour with grid constraints, while preserving user mobility requirements through override and minimum-charge guarantees.

Importantly, these regulatory and market mechanisms also shape the power-quality outcomes that are central to this thesis. When smart charging shifts or modulates the EV load, it changes not only the active power demand but also the operating point of the power electronic converters within chargers. As demonstrated earlier in this chapter, charging current level, phase configuration, and charging stage (CC or CV) strongly influence harmonic emissions. Market-driven charging strategies, therefore, indirectly affect harmonic distortion at the distribution level by altering the timing and operation of EV chargers. This establishes a direct link between economic incentives, regulatory compliance, and harmonic performance.

In this context, the distribution network is the most critical layer for evaluating the impacts of smart charging. Transmission systems experience EV charging primarily as aggregated demand, which is managed through generation scheduling and wholesale markets. Distribution networks, by contrast, are exposed to coincident charging, phase imbalance, voltage drops, and harmonic injection at the point of connection. These phenomena determine transformer loading, insulation aging, and compliance with power quality standards. For this reason, although EV electrification influences both transmission and distribution systems, the most immediate and technically complex impacts arise at the distribution level, where EV chargers physically interface with the grid.

This thesis, therefore, focuses on distribution networks, where regulatory limits, market-driven charging behaviour, and power-electronic characteristics intersect most strongly. By analysing harmonic emissions, loading, and thermal stress under smart charging scenarios, the work directly addresses the network layer that is both most constrained and most affected by the large-scale deployment of EVs.

Although standards such as IEC 61000 and IEEE 519 define acceptable harmonic limits, their practical enforcement depends on the availability of detailed, phase-resolved harmonic data under realistic charging conditions. Existing studies do not provide datasets that capture the combined effects of smart charging, multiple EVs, and harmonic phase angle interactions. This gap prevents both network operators and market actors from quantitatively assessing whether flexibility-based charging strategies remain compliant with power quality constraints. For this reason, a dedicated experimental data collection campaign was required, which is described in Chapter 3.

## 2.8 Chapter Summary

This chapter provided a comprehensive review of the technical, regulatory, and power quality considerations associated with EV charging, with a focus on its integration into power systems and the resulting harmonic distortion. It began by examining smart charging strategies, which were shown to be essential for mitigating peak demand, enhancing grid flexibility, and supporting renewable energy integration. The review distinguished smart charging from traditional demand-side management and emphasized the role of VGI technologies in delivering flexible services at the system, local, and consumer levels. Various implementation strategies, including modulation, scheduling, shifting, and phase curtailment, were discussed, highlighting their implications for grid stability and power quality.

The chapter then analyzed key drivers for distribution network investment, including congestion levels, coincidence factors, and local load characteristics. It was shown that smart charging could reduce the need for costly infrastructure upgrades by aligning charging behaviour with local energy conditions such as heating demand and photo-

voltaic output. Regulatory developments in countries such as the UK, the Netherlands, Spain, and Denmark were referenced to demonstrate how real-world policies and tariffs influenced smart charging deployment.

A classification of EV charging equipment and power levels followed, differentiating between on-board and off-board charging systems, and discussing the respective roles of slow and fast charging in enabling smart charging applications. Although fast charging was recognized for its user convenience, the analysis emphasized that slow charging was more compatible with flexibility services and grid stability objectives.

Subsequently, the chapter explored the impacts of EV charging on power networks, distinguishing between local distribution-level issues, such as transformer overloading, voltage drops, and phase imbalances, and system-wide challenges, including peak demand escalation and frequency instability. Particular attention was paid to the role of EVs in affecting power quality, especially through the generation of harmonic distortion. The chapter presented the mathematical foundation for harmonic decomposition using Fourier analysis, explaining the relevance of amplitude, phase angle, and harmonic summation.

Special emphasis was placed on harmonic cancellation phenomena, where phase angle diversity among multiple EVs could reduce aggregate THD at the PCC. Real measurement examples were used to illustrate how both amplitude and phase angle interactions shaped the resulting harmonic content and highlighted the limitations of simple arithmetic summation methods in accurately assessing harmonics.

The chapter further distinguished between current and voltage harmonic distortion, clarifying how nonlinear loads injected current harmonics that were then amplified by grid impedance. The concept of THD was explained in both contexts, along with supporting indices such as total harmonic current, and their implications for increased RMS values and thermal stress on equipment.

The analysis extended to harmonic phase sequences using symmetrical components, categorizing positive-, negative-, and zero-sequence harmonics and discussing their implications for transformer loading and neutral conductor stress. Triple harmonics in four-wire systems were identified as particularly problematic.

The sources and impacts of harmonic distortion were then reviewed, with a focus on nonlinear loads such as EV chargers, variable-speed drives, and other power electronic devices. The consequences for power system components, including transformers, capacitors, motors, telecommunications equipment, meters, cables, and sensitive electronics, were outlined, emphasizing issues such as thermal stress, resonance conditions, metering inaccuracies, and electromagnetic interference.

A critical evaluation of existing harmonic measurement studies revealed significant limitations in data accuracy, standardization, and particularly the availability of phase angle data. Most prior studies lacked detailed analysis of multiple EVs charging simultaneously, and none adequately addressed harmonic behaviour under smart charging conditions. This gap underscored the need for probabilistic modelling approaches and comprehensive harmonic datasets to enable more accurate impact assessments.

The chapter also discussed harmonic variations observed during the CC and CV phases of charging, showing that THD levels changed significantly between these phases. These findings highlighted the importance of SoC-dependent harmonic analysis, especially when modelling fast-charging behaviour.

Finally, the chapter summarized harmonic limits defined by industry standards such as IEC 61000, EN 50160, and IEEE 519. These standards established permissible harmonic levels and clarified the responsibilities of end-users and system operators for maintaining compliance. A set of summary tables presented allowable current and voltage distortion limits by equipment class, voltage level, and harmonic order.

Overall, this chapter provided a solid technical background for understanding the complex implications of EV charging on power quality and distribution grid infrastructure. It integrated insights from literature, industry standards, and measurement challenges, forming the foundation for the experimental and simulation-based analyses developed in the following chapters.

# Chapter 3

# Data Collection

This chapter presents data collection to bridge existing literature gaps, serving as a foundation for data analysis and as input for the thesis's advanced modelling and simulation studies. The section will describe the experimental setup, including the EVs tested, the charging devices, and the power quality analyzer used for measurements. Furthermore, the methodology for data acquisition will be outlined, specifying the key parameters recorded, such as current, voltage, and individual harmonic orders. This collected data will be crucial for assessing the impact of EV charging on power quality and validating simulation models.

## 3.1 Motivation for Dedicated EV Harmonic Data Collection

While the literature has clearly established that EV chargers are major sources of harmonic distortion, the quantitative assessment of their impact under realistic smart charging conditions remains fundamentally constrained by the availability and quality of measurement data. Most existing datasets were collected for isolated vehicles, fixed charging currents, or early-generation chargers, and therefore do not capture the diversity of converter technologies, phase-angle interactions, and coordinated charging behaviours that now characterize modern EV fleets. As a result, the ability to evaluate harmonic aggregation, cancellation effects, and compliance with IEC and IEEE limits

under multi-EV smart charging scenarios is severely limited.

This chapter shifts from reviewing impacts to explaining why a dedicated experimental measurement campaign is required. By critically examining existing EV harmonic datasets, it demonstrates that current data are insufficient for probabilistic harmonic summation, transformer aging assessment, and grid-level power-quality modelling. This gap provides the technical motivation for the laboratory measurements, high-resolution harmonic recordings, and controlled charging experiments presented in the following sections, which form the empirical foundation of this thesis.

### 3.1.1 Existing EV Harmonic Measurement Studies

One of the early harmonic measurement studies [98] recorded EV harmonic time series across various initial and final state-of-charge values. The study introduced a probabilistic methodology to evaluate the harmonic effects of two EVs charging simultaneously. Findings indicate that during the second phase of the constant current–constant voltage (CC-CV) charging profile, harmonic content increases significantly as charging current decreases, leading to a rise in $THD_I$. However, only odd harmonic magnitudes were reported at selected operating points, and fundamental and even harmonics were omitted.

The study in [177] conducted harmonic testing on 18 EV models (pre-2016) using AC Level 2 chargers, primarily with single-phase on-board chargers. The $THD_I$ of tested EVs varied between 1.7% and 11.9%, indicating a lack of standardization in harmonic emissions. The study also examined the 3rd, 5th, and 7th harmonics, along with their phase angles, to enable limited assessment of harmonic cancellation. Given advancements in EV technology, the data do not reflect modern charger designs.

The work in [97] presents harmonic measurements from 23 different EVs using slow AC chargers with power ratings between 2.3 and 7.2 kW. Only the magnitude of individual harmonics was measured. Phase angle information was not recorded, and harmonic summation was estimated using IEC statistical summation laws rather than direct phasor aggregation. The study introduces a probabilistic simulation technique to estimate the harmonic hosting capacity of rural and urban power networks in the

UK.

In [178] investigates harmonic emissions during DC charging and bi-directional discharging of a Nissan Leaf at 2, 5, and 10 kW charging rates. Harmonics were evaluated against IEEE 519 limits, but only for a single EV, without coordinated charging scenarios [176].

A recent study [179] presents EV charging profile measurements for 12 different EVs, including both pure electric and plug-in hybrid vehicles. The dataset includes active power (kW), reactive power (kVAR), apparent power (kVA), voltage (V rms), current (A rms), and both voltage and current harmonics. Each EV was charged for several hours using Level 2 chargers rated at 6.6 kW. The findings indicate that, in most cases, $THD_I$ remain within industry limits. However, smart charging was not used, and phase angles were not recorded.

The study in [180] examines voltage and current harmonic measurements at the PCC of an EV charging station. The analysis primarily focuses on the third harmonic, which exhibits the highest harmonic content. Findings suggest that current harmonics pose a greater concern than voltage harmonics. Despite the station's peak active power reaching approximately 60 kW, the total demand distortion exceeds 10%. Because the analysis is based on a single monitoring location, it does not include detailed information on individual EV types or their charging levels. Moreover, phase relationships are also unavailable.

The study in [180] analysed harmonics at the PCC of a charging station supplying multiple EVs, reporting total demand distortion above 10%. However, individual EV contributions and phase relationships were not available.

In [38], the study investigates supra-harmonics (frequencies above 2 kHz) under varying charging currents. The findings confirm that EV chargers contribute to supra-harmonic emissions, highlighting the need for standardization efforts to mitigate related power quality issues. However, low-order harmonic aggregation was not addressed.

### 3.1.2 Lack of Phase Angle Information and Harmonic Summation

Until recently, most harmonic studies have not recorded phase angles due to limitations in measurement technology. To compensate for the absence of phase angle data, the IEC introduced a summation law that estimates harmonic summation without phase angle considerations [181]. The summation effect of harmonic currents is expressed as follows [182]:

$$(I)_{h,\Sigma}^{\alpha} = \sum_{i}^{N_d} (I)_{h,i}^{\alpha},$$

where $\alpha$ is the summation coefficient for harmonic order $h$, $I_{h,i}^{\alpha}$ is the 95% non-exceeding value of the $h$th harmonic current of load $i$, and $N_d$ is the total number of loads (which corresponds to the number of EVs in the case of smart charging).

The IEC 61000-3-6 standard [182] defines the summation coefficients ($\alpha$) based on the harmonic order $h$ as follows:

- For harmonic orders less than five ($h < 5$), $\alpha = 1$, reflecting minimal phase-angle dispersion and strong correlation among lower-order harmonics.
- For harmonic orders between five and ten ($5 \leq h \leq 10$), $\alpha = 1.4$, capturing moderate diversity in phase angles and partial cancellation effects.
- For harmonic orders greater than ten ($h > 10$), $\alpha = 2$, accounting for greater randomness and dispersion in higher-order harmonic phase angles.

These coefficients aim to capture statistical phase diversity but do not capture the true phasor-based harmonic interactions that arise when EVs with different converters operate simultaneously.

Beyond EV applications, [183] demonstrates that summation coefficients, derived from data across multiple arc furnace sites, are sensitive to the probability threshold and calculation interval, both of which influence the degree of random variation in harmonic voltages and currents. In [184], summation coefficients up to the 20th harmonic order were calculated for a railway rectifier, with values ranging between 1.8 and 2.0.

Additionally, [185] highlights that wind farm topology and assumptions about magnitude and phase angle distributions can significantly impact summation coefficients.

### 3.1.3 Implications for EV Harmonic Assessment

The harmonic cancellation effect of multiple loads has been studied in [186], which showed that measured harmonic sums differ substantially from arithmetic aggregation. Using EV charging data from [187], [186] demonstrated that EV harmonic cancellation exhibits greater variability than LED lighting loads due to the diverse converter designs used in vehicles.

These findings reveal that existing EV harmonic datasets lack the resolution required for accurate harmonic aggregation. Most datasets do not include phase angle information, smart charging conditions, or coordinated multi-EV operation. As a result, it is not possible to evaluate probabilistically whether future smart-charging scenarios will violate IEC or IEEE harmonic limits using existing data alone.

In practice, distribution network compliance is assessed against percentile-based harmonic limits, such as the 95% non-exceedance values defined in IEC 61000 and IEEE 519. Evaluating these limits requires not only average harmonic magnitudes but also statistical distributions of harmonic currents across time, charging states, and vehicle combinations. Datasets that report only mean or steady-state harmonic values are insufficient for grid-planning and asset-rating purposes because they cannot represent the tails of the distribution where regulatory violations and accelerated aging are most likely to occur.

Furthermore, smart charging fundamentally alters the operating point of on-board converters by continuously varying charging current and phase configuration. As shown in earlier sections, harmonic distortion depends strongly on these operating conditions, particularly during low-current and CV phases. Without time-synchronised harmonic measurements across multiple EVs under controlled smart charging actions, it is impossible to capture how coordinated control strategies influence harmonic summation and cancellation. This limitation directly motivates the controlled experimental framework and high-resolution harmonic dataset developed in this thesis.

Table 3.1: Comparison of Key EV Harmonic Distortion Studies
(AC: AC Charging, DC: DC Charging, Smart: Smart Charging, Single EV: Single EV Charging, Multiple EV: Multiple Simultaneous EV Charging, P. Angle: Phase Angle)

| Study | AC | DC | Smart | Single EV | Multiple EV | P. Angle |
|---|---|---|---|---|---|---|
| This study | **Y** | **Y** | **Y** | **Y** | **Y** | **Y** |
| [98] | Y | N | **N** | Y | Y | N |
| [177] | Y | N | **N** | Y | N | Y |
| [97] | Y | N | **N** | Y | N | N |
| [178] | N | Y | **N** | Y | N | N |
| [179] | Y | N | **N** | Y | N | N |
| [180] | N | Y | **N** | N | Y | N |
| [38] | Y | N | **N** | Y | N | N |

### 3.1.4 Comparison of Existing EV Harmonic Studies

In real-world distribution networks, the harmonic impact of EV charging depends not only on the number of connected vehicles but also on their charger types, charging currents, and the phase-angle relationships between their harmonic currents. Since EVs can operate over a wide range of charging rates (e.g., 6–16 A in residential smart charging), the number of possible charging combinations grows rapidly with fleet size. Under such conditions, deterministic worst-case analysis becomes impractical, and a probabilistic simulation framework is required to evaluate the likelihood of exceeding IEC and IEEE harmonic limits. Such an approach requires detailed harmonic datasets that capture magnitude, phase angle, and operating-point dependence for individual EVs.

Table 3.1 provides a comparative overview of key EV harmonic measurement studies, highlighting the scope and methodology used in each study. The table categorizes the studies based on several parameters, including whether they analyze AC charging, DC charging, and smart charging, as well as whether they examine single EV or multiple EVs charging simultaneously. Additionally, it indicates whether phase angle data was recorded, a crucial factor in accurately assessing harmonic aggregations.

The comparison reveals a systematic gap in existing datasets. Although many studies report harmonic magnitudes for AC charging of single EVs, almost none examine coordinated or smart charging, despite this being the dominant operational mode in

modern charging infrastructure. Only a limited subset considers multiple EVs charging simultaneously, and even fewer provide harmonic phase angle data, which is essential for physically correct harmonic summation and cancellation analysis.

More importantly, none of the reviewed datasets simultaneously include variable charging currents, multi-EV interactions, and full harmonic phasor information. As a result, existing studies cannot support probabilistic assessment of harmonic limit violations, transformer thermal stress, or power-quality compliance under realistic smart charging scenarios. This gap directly motivates the experimental measurement campaign and probabilistic harmonic modelling framework developed in this thesis.

## 3.2 Experimental Set-up

The EV smart charging experiments presented in this study were conducted at the Energy System Integration Lab (SYSLAB) at the Technical University of Denmark (DTU) [188]. A total of eight different battery electric vehicles (BEVs) were tested, including Renault Zoe R90, Peugeot e-208, Nissan Leaf e+, VW ID.3 Pro, Renault Zoe ZE50, VW ID.4 Pro, Tesla Model Y Long Range, and Peugeot e-2008. These EV models were selected to reflect the diversity in market share, model year, battery capacity, and onboard charging technologies, ensuring a comprehensive analysis of current EVs.

The technical specifications of the tested vehicles are summarized in Table 3.2, highlighting differences in battery sizes and charging capabilities. At the time of testing, the average vehicle age was less than two years, meaning most of the EVs assessed had larger battery capacities than those examined in previous studies (see Section 2.5). This is particularly relevant, as newer EVs tend to have improved efficiency, higher power ratings, and more advanced charging characteristics.

The charging power for each EV model is calculated using the formula:

$$\begin{aligned}\text{Charging Power (kW)} = \text{Charging Current (A)} \times \text{Single-phase Voltage (V)} \\ \times \text{Number of Phases}\end{aligned} \tag{3.1}$$

For example, the Peugeot e-208, with a practical charging current range of 6.01

Table 3.2: Overview of technical specifications for EVs used in the experiments.

| EV Model | Model Year | Nominal Battery Capacity (kWh) | Practical Charging Current Range (A) | Charging Type (AC) | Practical Charging Power Range (kW) |
|---|---|---|---|---|---|
| Renault Zoe R90 | 2018 | 44.1 | 5.91 to 31.10 | 3-$\phi$ | 0.00 to 21.46 |
| Peugeot e-208 | 2021 | 50 | 6.01 to 14.66 | 3-$\phi$ | 4.15 to 10.12 |
| Nissan Leaf e+ | 2022 | 62 | 5.90 to 28.39 | 1-$\phi$ | 1.36 to 6.530 |
| VW ID.3 Pro | 2023 | 62 | 6.09 to 15.86 | 3-$\phi$ | 4.20 to 10.94 |
| Renault Zoe ZE50 | 2022 | 54.7 | 6.68 to 30.32 | 3-$\phi$ | 3.08 to 20.92 |
| VW ID.4 Pro | 2024 | 82 | 6.06 to 15.67 | 3-$\phi$ | 4.18 to 10.81 |
| Tesla Model Y Long Range | 2022 | 78.1 | 6.09 to 16.15 | 3-$\phi$ | 4.20 to 11.14 |
| Peugeot e-2008 | 2022 | 50 | 5.83 to 15.23 | 3-$\phi$ | 4.02 to 10.51 |

to 14.66 A and a three-phase configuration, has a charging power range calculated as follows:

- **Minimum Charging Power:**

$$6.01\,\mathrm{A} \times 230\,\mathrm{V} \times 3 \approx 4.15\,\mathrm{kW}$$

- **Maximum Charging Power:**

$$14.66\,\mathrm{A} \times 230\,\mathrm{V} \times 3 \approx 10.12\,\mathrm{kW}$$

Regarding the Renault Zoe R90, when charged at a current of 6 A, it operates at a purely reactive power level, resulting in no active power consumption. This means that the energy drawn from the grid does not perform any real work but instead oscillates between the source and the load, which can affect the efficiency and power quality of the electrical system [189].

Figure 3.1 illustrates the experimental setup for a single EV and multiple EV charging sessions. The study also describes the charging infrastructure and measurement equipment, including EV chargers and power quality analysers, to accurately capture charging profiles, power fluctuations, and harmonic emissions.

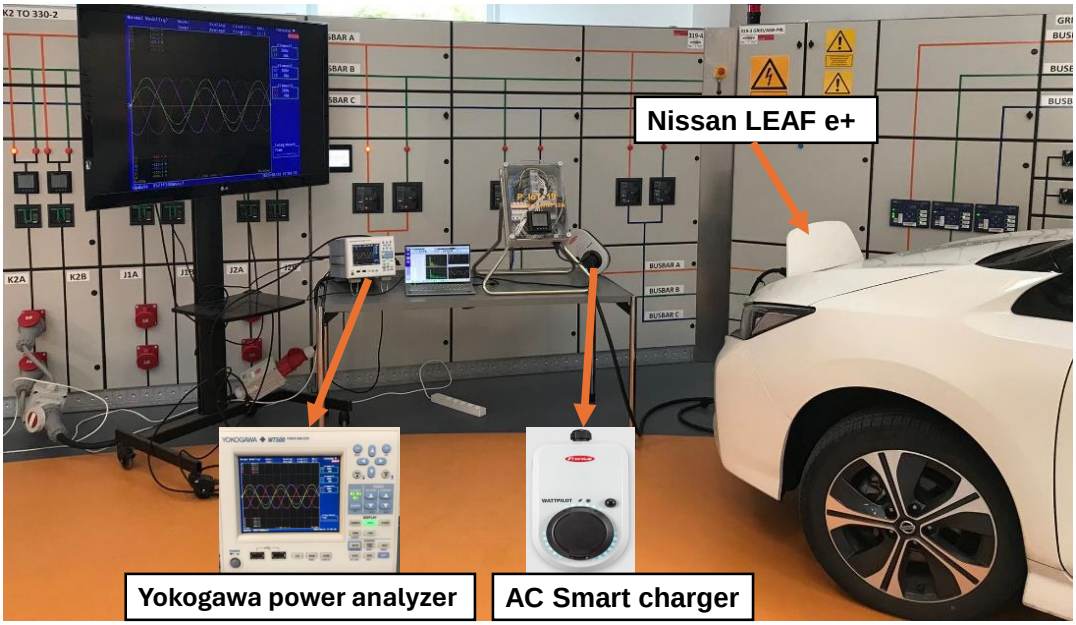


(a) Single EV Charging Setup

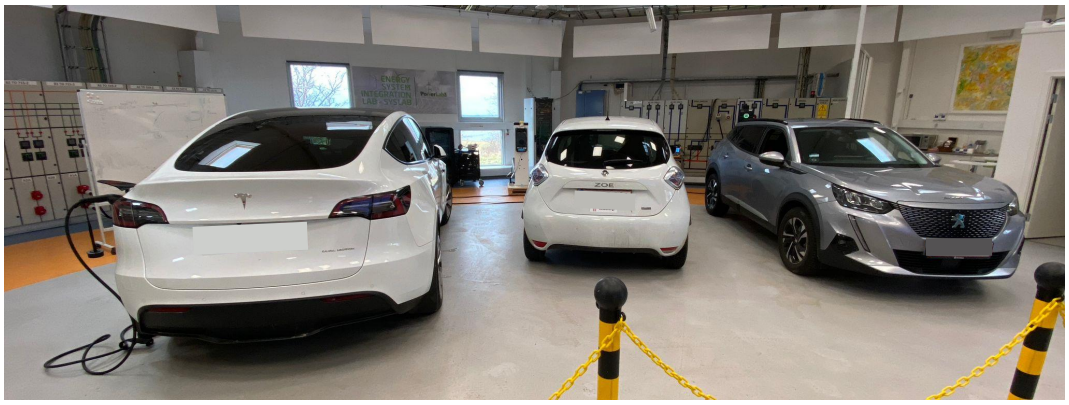

(b) Multiple EVs Charging Setup

Figure 3.1: Overview of the experimental set-up and laboratory environment.

### 3.2.1 EV Chargers

We employed advanced AC smart chargers and precision power quality analyzers in these experiments to assess the harmonic impacts of EV charging. AC smart chargers, namely Fronius Wattpilot, Zaptec Pro and Keba KeContact P30, were used in the experiments.

#### 3.2.1.1 Fronius Wattpilot

This three-phase charger delivers up to 32 A per phase, supporting a maximum charging power of 11 kW 11 kW [190]. It offers scheduling and modulation capabilities, allowing users to optimize charging times and power levels. Control is facilitated through the Solar.wattpilot mobile application provides an intuitive interface for real-time adjustments.

#### 3.2.1.2 Zaptec Pro

The Zaptec Pro is a three-phase charger capable of delivering up to 22 kW of power at 32 A per phase, designed for robust performance [191]. It features advanced scheduling and modulation functions, enabling efficient energy management. Users can access and control the charger via a dedicated web-based portal, offering flexibility and ease of use.

#### 3.2.1.3 Keba KeContact P30

This versatile charger supports both single-phase (up to 7.4 kW) and three-phase (up to 22 kW) charging, with adjustable current settings ranging to 32 A [192]. It includes scheduling and modulation features to align charging sessions with energy availability and grid demands. The Keba eMobility App provides a user-friendly platform for monitoring and controlling charging activities.

### 3.2.2 Power Quality Analyzers

We employed Yokogawa WT500 and Fluke 437 Series II power quality analyzers to measure related harmonic emission data from EV charging.

#### 3.2.2.1 Yokogawa WT500

This mid-range power analyzer offers an essential power accuracy of 0.1%, with voltage measurement capabilities up to 1000 V and current measurements up to 40 A [193]. It features a measurement bandwidth from DC to 100 kHz, enabling comprehensive

analysis of power parameters, including harmonic components up to the 50th order. The device's high-speed data updating (100 ms) and simultaneous measurement of voltage, current, power, and harmonics make it ideal for dynamic assessments.

#### 3.2.2.2 Fluke 437 Series II

This Class A-compliant three-phase power quality and energy analyzer is designed to capture and analyze power quality issues in single-phase and three-phase power distribution systems [194]. It offers advanced features such as an energy loss calculator, PowerWave data capture, and waveform capture capabilities. The analyzer can measure harmonic components up to the 50th order, providing detailed insights into power quality and energy losses.

## 3.3 Harmonics Measurement

The vehicles were charged at 1A increments within their respective minimum and maximum charging current ranges to replicate realistic smart charging scenarios. As specified by the IEC 61851-1 standard [195], EVs are not permitted to charge below 6A. The maximum allowable charging current is governed by both the IEC 61851-1 standard and the technical constraints imposed by the vehicle's battery management system (BMS) and onboard charger [30]. While actual charging currents may fluctuate based on network conditions and vehicle settings, the upper nominal charging limit is typically either 16A or 32A, as shown in Table 3.2.

Charging data were systematically recorded using a power analyzer, capturing key electrical parameters essential for power quality assessment. These parameters include the root mean square (RMS) charging current (A), the RMS voltage (V) at the charging outlet, and both the fundamental current and voltage components. Additionally, detailed harmonic analysis was performed by measuring individual harmonic orders, each characterized by their respective amplitude and phase angle (in degrees) for both current and voltage. Harmonic orders were mostly measured up to the 49th, depending on the device's functionality, with some cases limited to the 31st. To ensure high-resolution

Table 3.3: Measured Electrical Parameters and Their Units.

| **Parameter** | **Symbol** | **Unit** |
|---|---|---|
| RMS Voltage | $V$ | Volt (V) |
| RMS Current | $I$ | Ampere (A) |
| Fundamental Voltage | $V_1$ | Volt (V) |
| Fundamental Current | $I_1$ | Ampere (A) |
| Amplitudes of individual voltage harmonics | $V_2$ to $V_{49}$ | Volt (V) |
| Amplitudes of individual current harmonics | $I_2$ to $I_{49}$ | Ampere (A) |
| Phase angles of individual voltage harmonics | $\phi_{V2}$ to $\phi_{V49}$ | Degrees (°) |
| Phase angles of individual current harmonics | $\phi_{I2}$ to $\phi_{I49}$ | Degrees (°) |
| Total harmonic distortion of the voltage waveform | $\mathrm{THD_v}$ | % |
| Total harmonic distortion of the current waveform | $\mathrm{THD_i}$ | % |

data acquisition, measurements were taken at one-second intervals.

The measured data for each EV is given in Table 3.3. This real-time data collection was enabled through a direct connection between the power quality analyzer and a dedicated workstation computer, allowing for continuous monitoring and analysis of EV charging behaviour. Such a setup accurately represents transient variations in harmonic emissions, making it possible to investigate dynamic charging characteristics and their impact on grid stability.

To ensure the accuracy and reliability of the collected data, all measurement devices were recently calibrated and certified prior to the experiments. The Yokogawa WT500 was utilized for measurements requiring up to 40 A, while the Fluke 437 Series II was configured to handle higher currents, accommodating measurements up to 100 A at the PCC. This strategic deployment of equipment allowed for precise monitoring and analysis of harmonic distortions across various charging scenarios. Figure 3.2 illustrates the experimental setup, detailing the integration of smart chargers and power quality analyzers to assess EV charging harmonics.

The measurements were performed using a dedicated distribution transformer at DTU SYSLAB, as shown in Figure 3.2, with the only connected loads during the experiments being the EVs under test. Harmonic measurements at the PCC were taken on the secondary side of this transformer, allowing the aggregated impact of the simultaneously charging EVs to be captured without interference from background

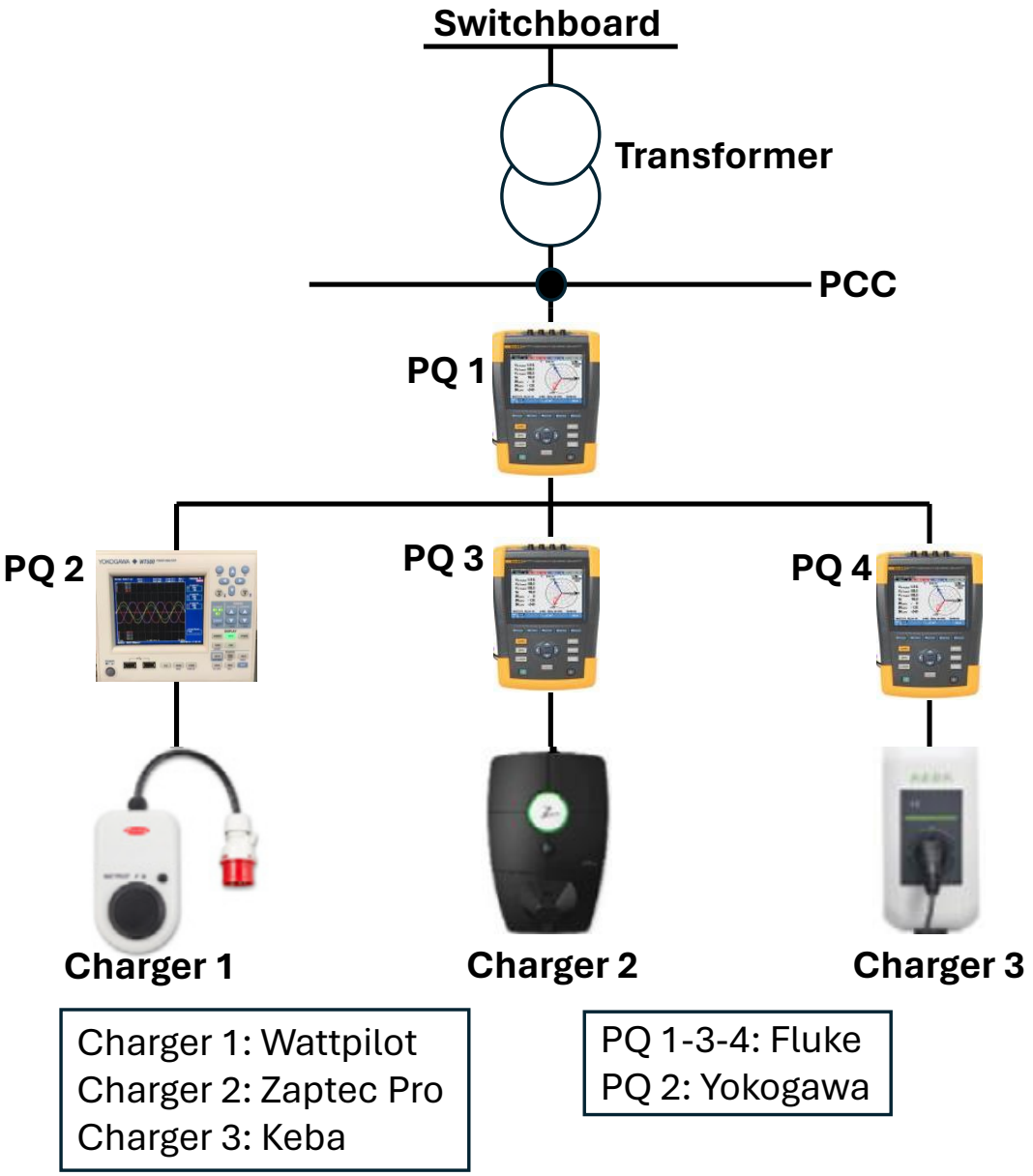


Figure 3.2: Arrangement for an experiment involving smart chargers and power quality analyzers.

loads. This configuration ensured that the recorded voltage and current harmonics directly reflected EV charging behaviour under controlled smart charging conditions.

Two distinct measurement approaches were employed to assess the harmonic emissions associated with different charging scenarios. The first set of experiments focused on characterizing the harmonic profile of individual EVs. Charger 1 (Wattpilot) was

selected in this configuration due to its ease of configurability and was used to charge each vehicle separately. Harmonic measurements were recorded across the full range of charging currents at 1A granularity, from the minimum allowable level up to the vehicle's maximum charging capability.

The second set of experiments aimed to evaluate harmonic behaviour in a multi-EV charging scenario. In this case, all three chargers (Wattpilot, Zaptec Pro, and Keba KeContact P30) were simultaneously connected to different EVs (Tesla Model Y, Renault Zoe R90, and Peugeot e-2008), and harmonics were measured at both the individual-vehicle level and at the PCC. These vehicles were charged concurrently under four representative current setpoints to emulate realistic smart charging scenarios between their allowable minimum and maximum charging current, corresponding to simultaneous charging at 6–6–6 A, 9–9–9 A, 12–12–12 A, and 15–15–15 A, across the three EVs. This controlled variation of the charging current enabled a systematic assessment of how harmonic emissions and cancellation effects evolve with the operating point under coordinated multi-EV charging.

In accordance with EU Horizon's data protection and management policies, all raw datasets collected during the experimental measurement were securely uploaded to the University of Strathclyde's secure online data repository. The collected data was processed (e.g. removing blank entries or unintended data collection) in the weeks following data acquisition to ensure the accuracy and usability of the dataset. Sample processed datasets for each vehicle, including harmonic magnitudes and phase angle measurements, are provided in Appendix A.

## 3.4 Chapter Summary

This chapter presented the experimental setup and methodology used to collect high-resolution data on EV charging and its impact on power quality. Eight EVs were tested at DTU's SYSLAB and were selected to reflect a broad range of battery sizes, charging technologies, and market relevance.

Charging was conducted using three smart AC chargers—Fronius Wattpilot, Zaptec

Pro, and Keba KeContact P30—while harmonic emissions and electrical parameters were recorded with Yokogawa WT500 and Fluke 437 Series II power quality analyzers. Measurements included current, voltage, harmonic amplitudes, and phase angles, captured at one-second intervals.

Experiments covered both single-EV and multi-EV charging scenarios, which enabled analysis of individual harmonic profiles and combined effects at the PCC. Charging currents were varied in 1 A increments to simulate realistic smart charging conditions within each vehicle's allowable range.

The resulting dataset formed a critical foundation for harmonic impact assessment and served as validated input for further simulation and modelling work in this thesis.

# Chapter 4

# Statistical Harmonics Data Analysis

As EV charging introduces harmonics into the power grid, understanding their statistical behaviour is crucial for assessing their impact on power quality. This chapter provides a comprehensive analysis of harmonic distortions, focusing on the amplitude variations and phase angle distributions observed in the experimental dataset. This analysis aims to offer insights into the dominant harmonic orders and their cumulative effects on power systems by statistically evaluating harmonic trends.

## 4.1 THD Analysis

Total Harmonic Distortion (THD) is a crucial parameter in assessing the impact of EV charging on power quality. It quantifies the degree of waveform distortion by comparing the cumulative contribution of harmonic components to the fundamental frequency. In this section, the total harmonic distortion of both current and voltage waveforms ($THD_I$ and $THD_V$) is analysed across various EV charging scenarios. The variation of THD concerning charging current levels, EV models, and charging configurations is examined to assess how smart charging strategies affect harmonic emissions. Understanding these trends is essential for ensuring compliance with industry standards and mitigating adverse effects on the electrical grid.

THD is used to measure the extent of distortion in current or voltage waveforms relative to their ideal sinusoidal shape. It represents the proportion of signal energy present at harmonic frequencies beyond the fundamental component [196]. $THD_I$ and $THD_V$ are calculated using the equations provided in 2.2 and 2.3, respectively.

To emulate smart charging scenarios, each EV was charged incrementally within its minimum and maximum charging current range, with intervals of 1 A. However, the VW ID.3 Pro was tested using intervals of 2 A owing to limited availability during the experimental period. The time series measurements of $THD_I$ during smart charging for all eight EV models are illustrated in Figure 4.1. It is important to note that the minimum charging current for all tested vehicles was uniformly set at 6 A, in accordance with the IEC 61851-1 standard [195]. Among the tested models, the Renault Zoe R90, Nissan Leaf e+, and Renault Zoe ZE50 were capable of charging at currents up to 32 A, whereas the other vehicles were limited to a maximum of 16 A, as shown in Figure 4.1. It should also be noted that, in practice, the actual maximum charging current may fall below the nominal value due to system and connection losses.

Single-EV charging measurements were systematically conducted using a Yokogawa WT500 power quality analyser, enabling high-resolution, phase-resolved measurements of voltage and current harmonics. To ensure consistency across all tested vehicles, harmonic measurements were performed on a single phase, even for EVs capable of three-phase charging. This approach allows the voltage range and harmonic distortion produced by an individual on-board charger to be isolated and accurately quantified. Notably, the Nissan Leaf e+ supports only single-phase charging among the selected EVs, making single-phase measurement not only methodologically consistent but also technically representative of real-world operation for this vehicle. The resulting single-phase harmonic datasets serve as the fundamental input for the statistical aggregation and multi-EV harmonic modelling developed in the subsequent chapters, in which phase interactions and network-level effects are reconstructed analytically. Several key observations can be made from these results:

1. The lowest $THD_I$ values occur when EVs charge at their maximum allowable rate, suggesting that on-board chargers are optimized to function most efficiently

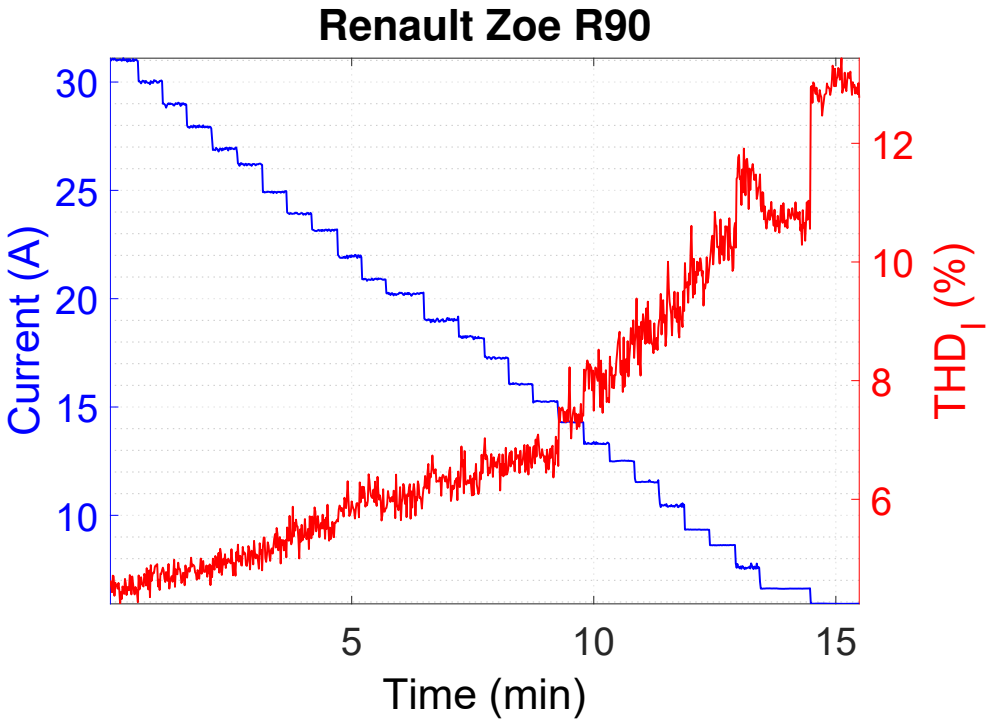


(a) Renault Zoe R90

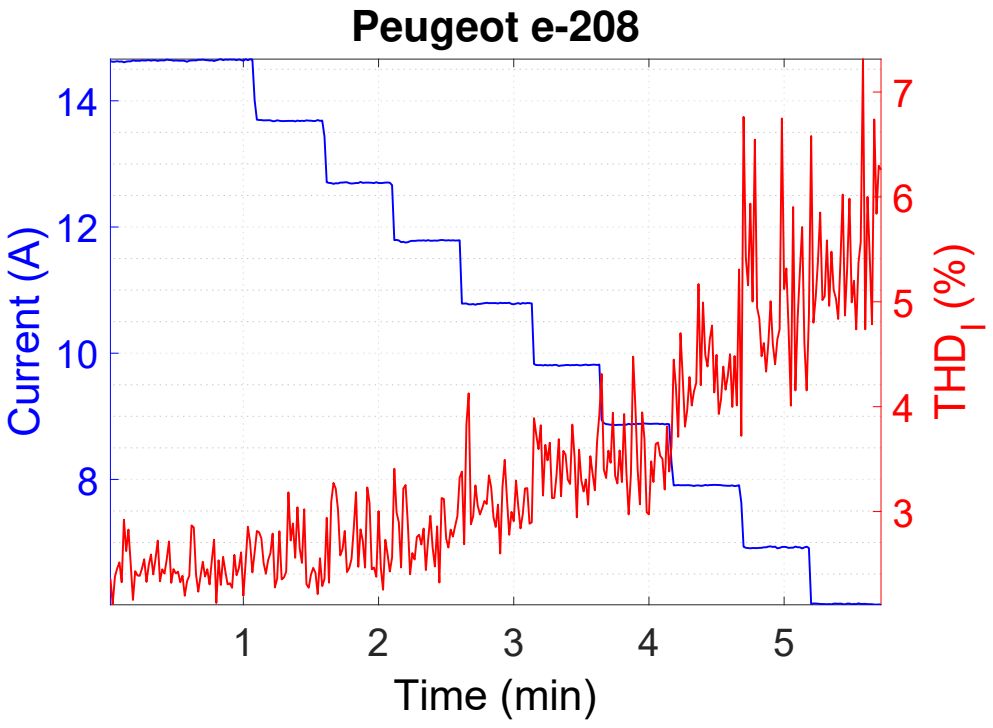


(b) Peugeot e-208

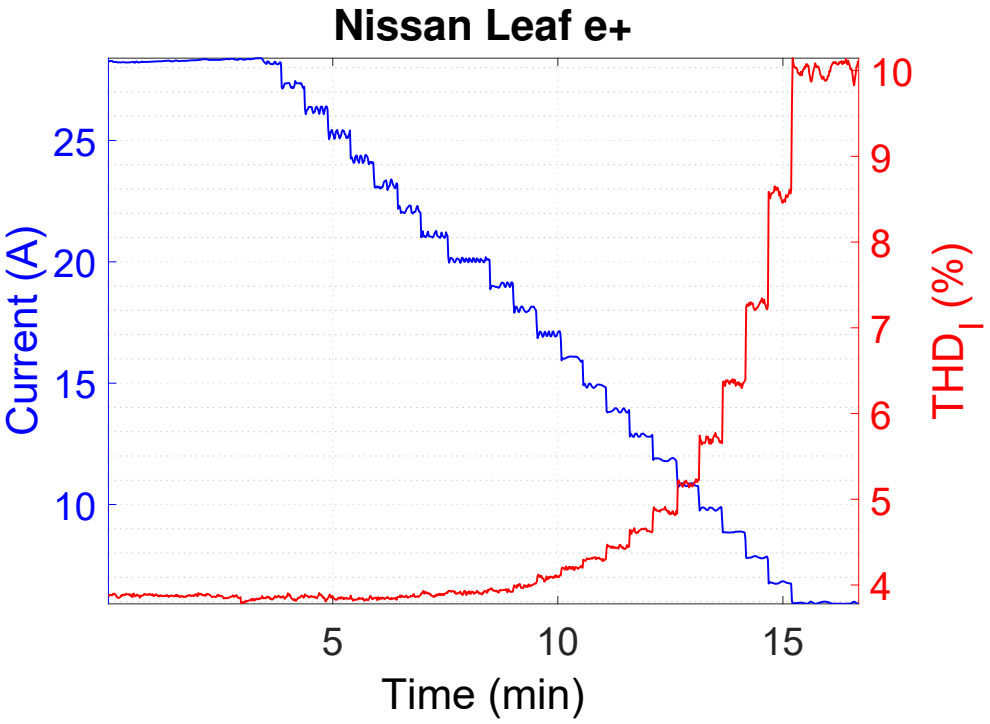


(c) Nissan Leaf e+

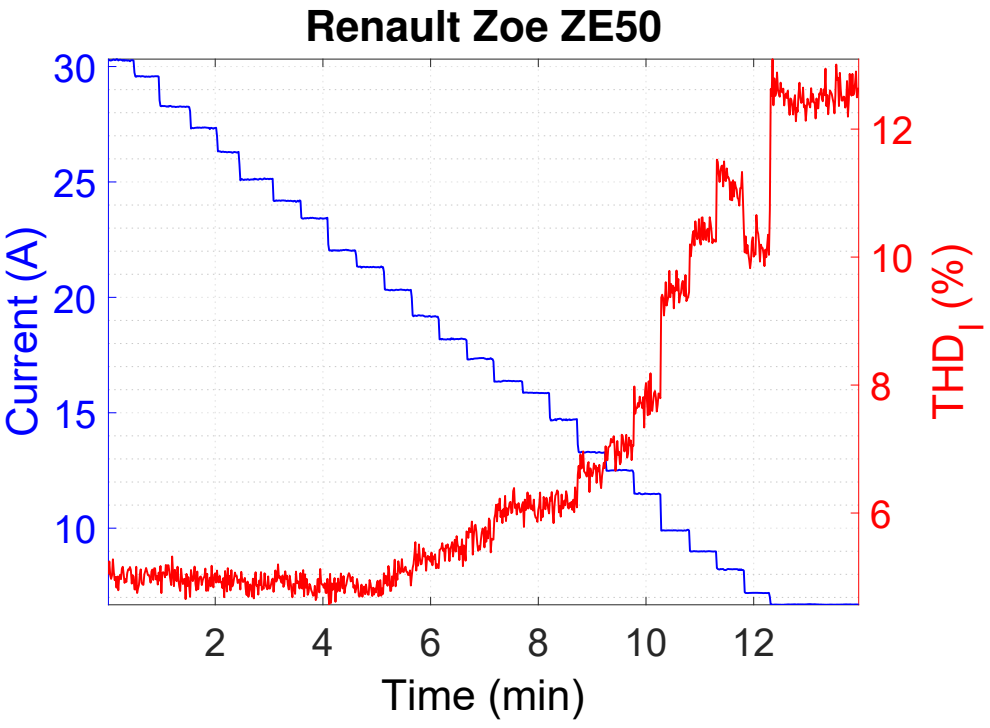


(d) Renault Zoe ZE50

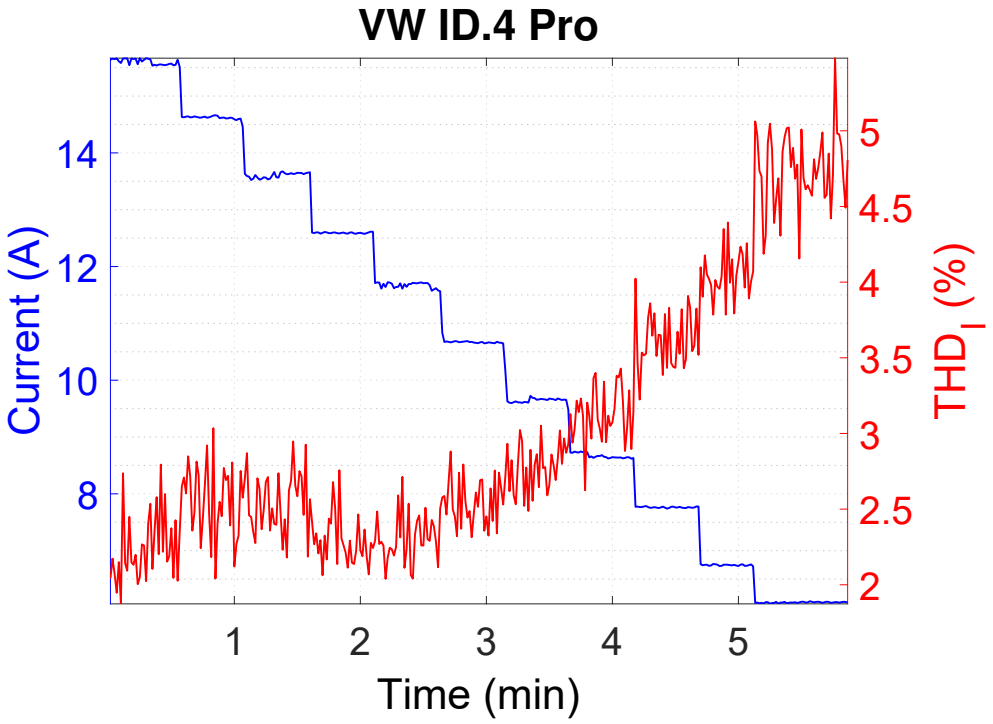


(e) VW ID.4 Pro

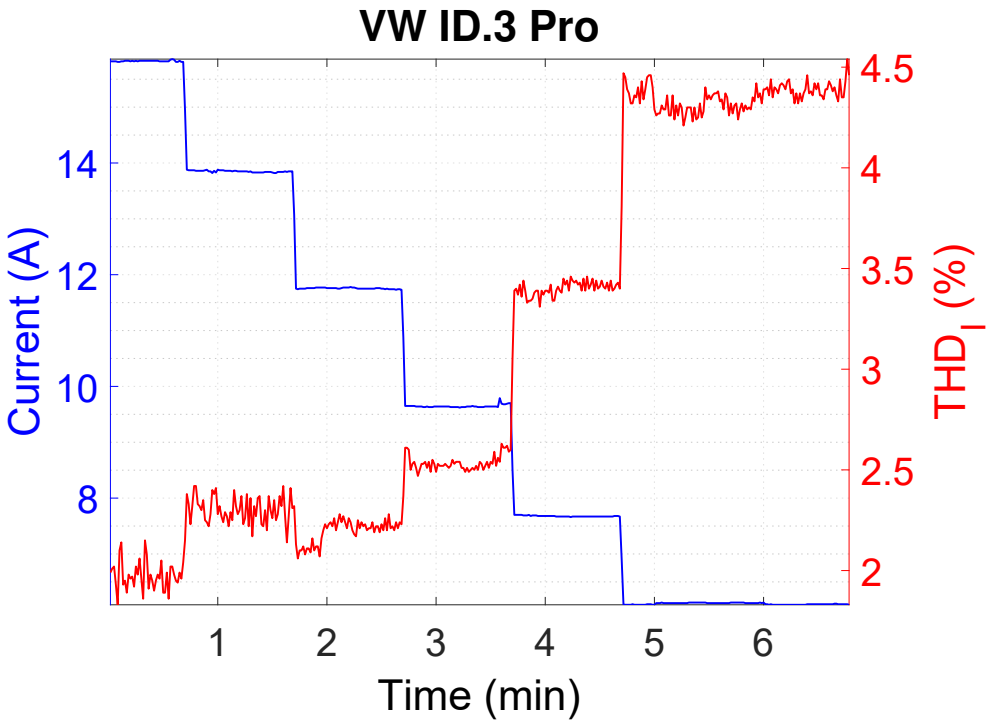


(f) VW ID.3 Pro

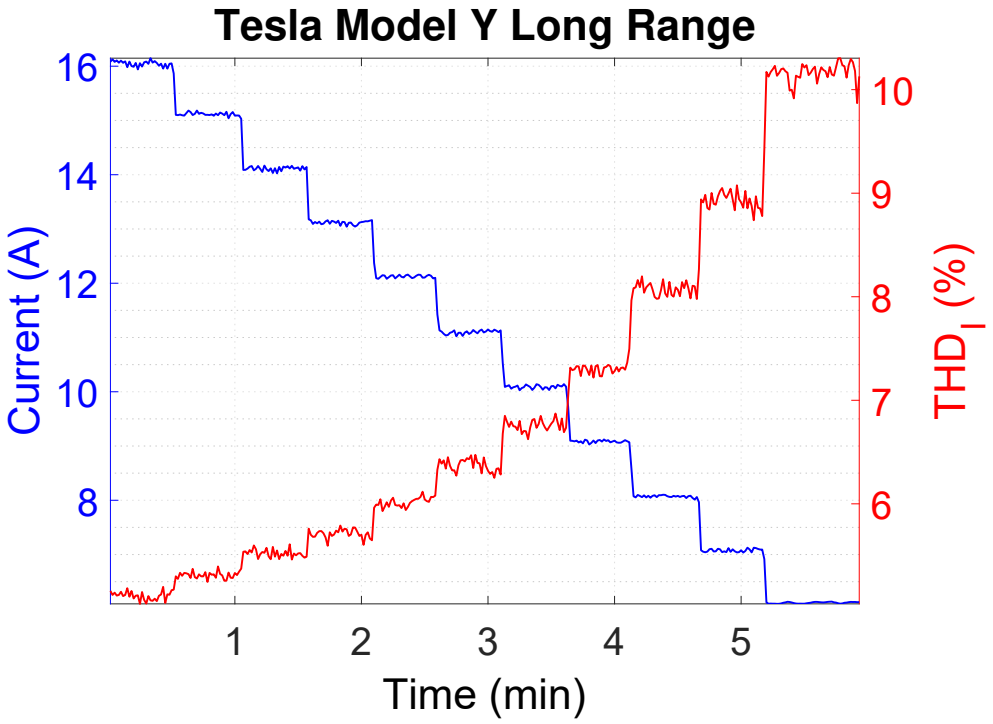


(g) Tesla Model Y Long Range

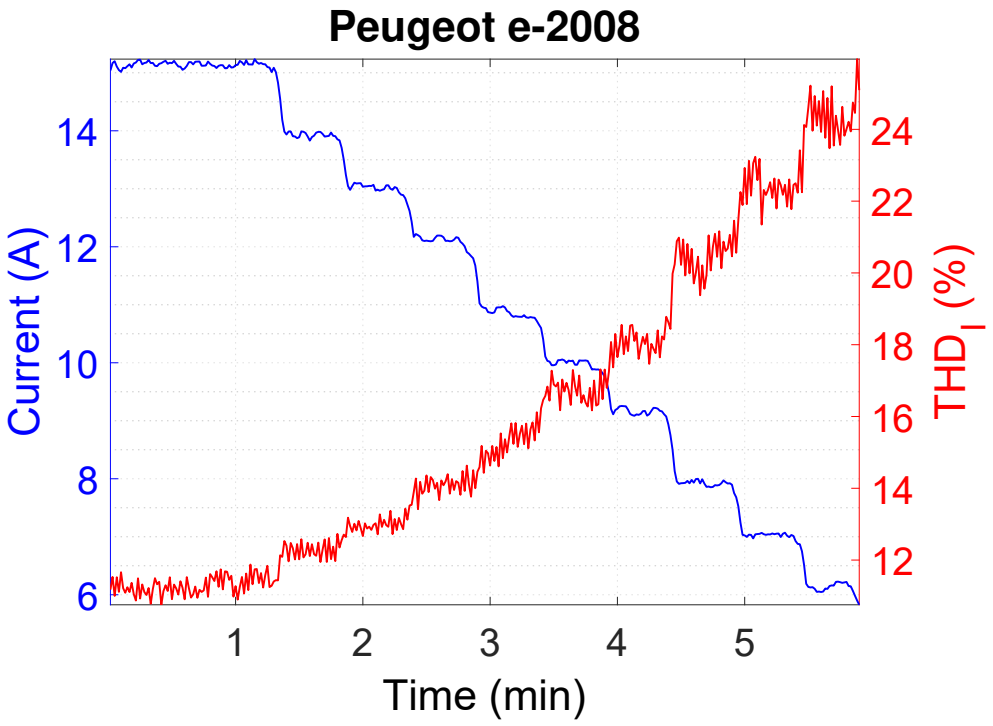


(h) Peugeot e-2008

Figure 4.1: $THD_I$ (%) versus charging rate for all tested EVs.

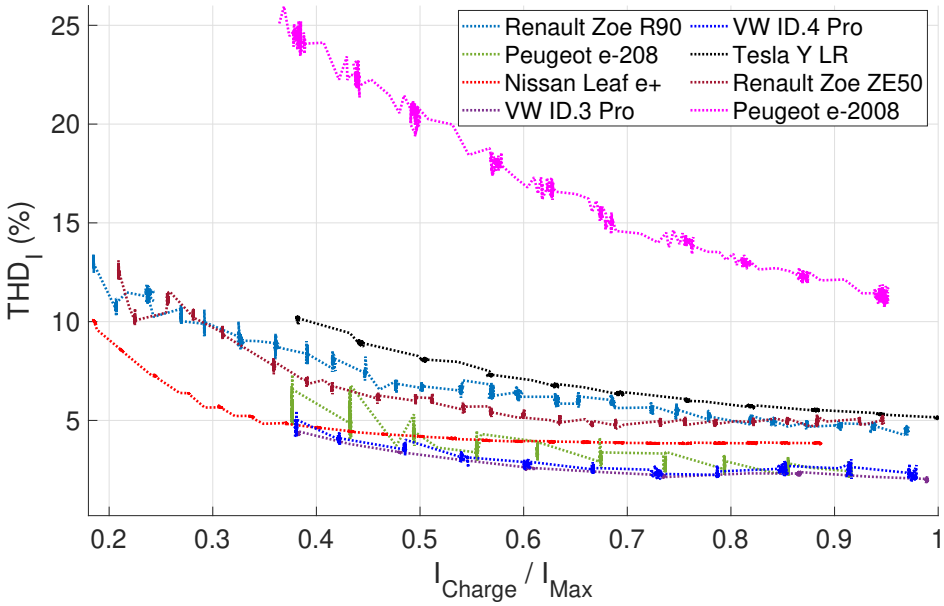


Figure 4.2: Correlation between $I_{charge}/I_{max}$ and $THD_I$ (%).

at their rated capacity.

2. $THD_I$ and charging current exhibit an inverse relationship. As the charging rate decreases, $THD_I$ increases substantially, often by more than three times in most tested vehicles.

3. The response time of EVs to changing charging rates varies. As shown in Figure 4.1, some vehicles, such as the Peugeot e-208 and VW ID.3 Pro, quickly adjust to fluctuations in charging current, whereas others, like the Peugeot e-2008, exhibit a more delayed response. Although this variance has minimal impact on harmonic emissions, response times play a crucial role in V2G applications [189].

Let $I_{\text{Charge}}$ represent the per-phase charging current of an EV and $I_{\text{Max}}$ denote its maximum charging rate (refer to the charging rate column in Table 3.2). Since the maximum charging rates fall into two distinct categories, approximately 16 A and 32 A, the charging current for each vehicle is normalized as $I_{\text{Charge}}/I_{\text{Max}}$ and plotted against $THD_I$ (%) in Figure 4.2. Among the tested vehicles, only the VW ID.3 Pro and VW ID.4 Pro exhibit harmonic distortion levels consistently below 5% across all charging

Table 4.1: Correlation coefficient ($r$) and quadratic polynomial parameters ($f(x) = p_1x^2 + p_2x + p_3$) between $I_{Charge}/I_{Max}$ and $THD_I(\%)$. $R^2$ denotes the R-squared statistics.

| EV Model | $r$ | $p_1$ | $p_2$ | $p_3$ | $R^2$ |
|---|---|---|---|---|---|
| Renault Zoe R90 | -0.94 | 13.91 | -25.08 | 16.14 | 0.97 |
| Peugeot e-208 | -0.89 | 11.06 | -19.85 | 11.42 | 0.86 |
| Nissan Leaf e+ | -0.79 | 22.01 | -30.63 | 13.98 | 0.92 |
| VW ID.3 Pro | -0.92 | 9.889 | -17.03 | 9.363 | 0.97 |
| Renault Zoe ZE50 | -0.87 | 26.05 | -38.71 | 18.92 | 0.97 |
| VW ID.4 Pro | -0.85 | 11.68 | -19.36 | 10.28 | 0.92 |
| Tesla Model Y LR | -0.95 | 13.6 | -26.37 | 18.07 | 0.99 |
| Peugeot e-2008 | -0.98 | 26.25 | -58.01 | 42.74 | 0.99 |

currents. In contrast, the Peugeot e-2008 demonstrates the highest harmonic emissions, while the remaining EVs maintain $THD_I$ values ranging between 5% and 14%.

To further examine the relationship between $THD_I$ and the charging current, correlation coefficients have been calculated and summarized in Table 4.1. The correlation coefficient quantifies the strength and direction of a linear relationship between two variables, ranging from -1 to +1. A value of +1 indicates a perfect positive correlation, whereas -1 represents a perfect negative correlation, and 0 implies no linear correlation between the variables [197].

The findings reveal a strong negative correlation, with seven out of eight EVs exhibiting correlation coefficients between -0.85 and -0.99. The Nissan Leaf e+ has a slightly weaker correlation at -0.79, attributed to the relatively stable $THD_I$ (%) observed up to a charging current of 10 A, as depicted in Figure 4.1. Given the high correlation observed, quadratic regression ($f(x) = p_1x^2 + p_2x + p_3$) has been applied across all EV models. The resulting polynomial coefficients, along with R-squared statistics, are presented in Table 4.1.

This polynomial regression approach could serve as a valuable tool in future studies to model $THD_I$ as a function of charging current. It could also be integrated as a constraint in optimization models for individual EV charging strategies. Additionally, the derived polynomial values may provide reliable estimations for non-integer charging rates, enhancing the accuracy of predictive modelling in smart charging applications.

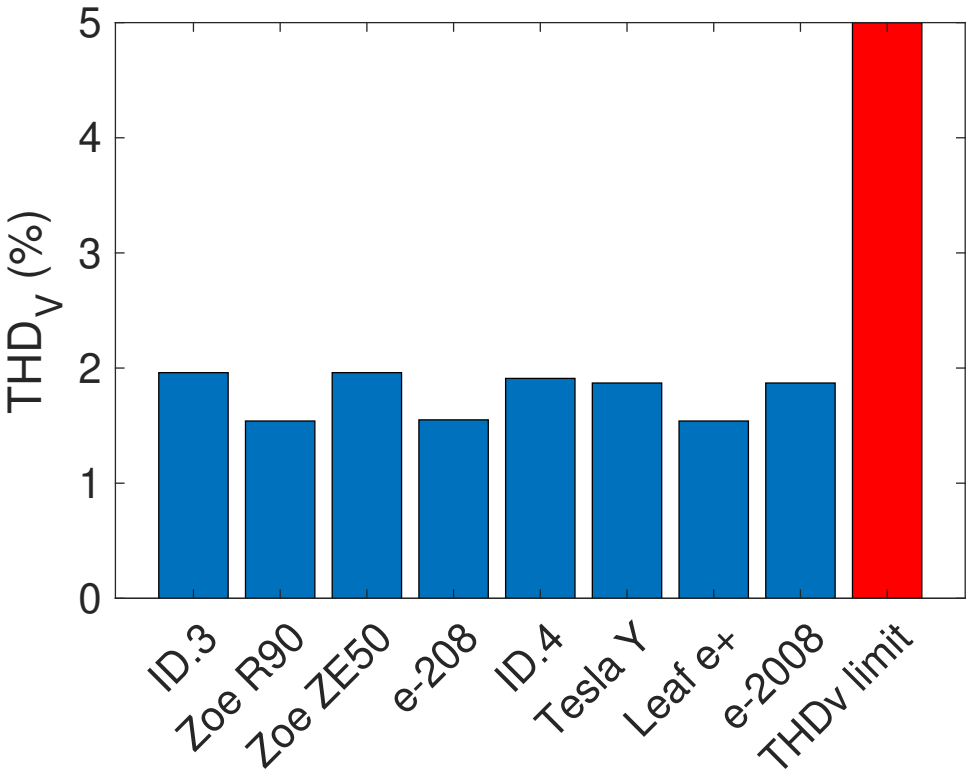


Figure 4.3: 75th percentiles of $\mathrm{THD_V}$ (%) for all EVs during smart charging.

For example, if Renault Zoe R90 operates at a charging current of 7.5 A, the corresponding $\mathrm{THD_I}$ (%) can be estimated using the quadratic regression model:

$$f\left(\frac{7.5}{31.10}\right) = 13.91 \times \left(\frac{7.5}{31.10}\right)^2 - 25.08 \times \left(\frac{7.5}{31.10}\right) + 16.14 = 10.9\%.$$

In this calculation, the charging current is $I_{\mathrm{Charge}} = 7.5\mathrm{A}$, while the maximum charging current for this vehicle is $I_{\mathrm{Max}} = 31.10\mathrm{A}$.

The analysis now shifts to examining the $\mathrm{THD_V}$ during smart charging. As part of the same smart charging measurement campaign used to characterise current harmonics and $\mathrm{THD_I}$, voltage harmonics and the $\mathrm{THD_V}$ were also systematically recorded. This parallel measurement ensures a consistent and comprehensive assessment of both current- and voltage-based power-quality indices under identical operating and charging conditions. Figure 4.3 presents the 75th percentile values of $\mathrm{THD_V}$ (%) across all

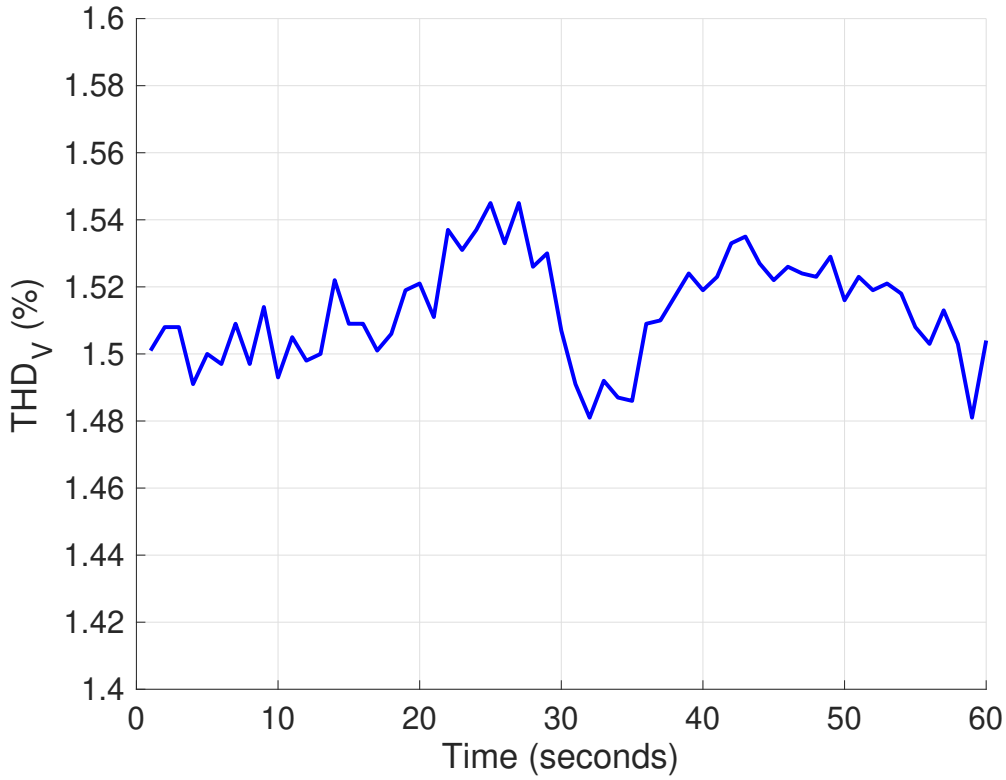


Figure 4.4: $THD_V$ assessment before and during charging.

EVs, alongside the corresponding regulatory limits. In contrast to $THD_I$, the 75th percentile values of $THD_V$ remain relatively stable, ranging narrowly between 1.5% and 2%, regardless of the charging current level. Notably, $THD_V$ remains well within the permissible limits established by IEC 61000-2-4 [174], which sets a 5% threshold for Class 1 protected supplies, and IEEE 519-2014 [176], which enforces an 8% limit for low-voltage systems (below 1 kV).

Beyond evaluating voltage harmonics during EV charging, their influence was further examined by comparing measurements taken before and during the charging process. Figure 4.4 presents the $THD_V$ values for a Renault Zoe R90 under both conditions, with charging started at the $19^{th}$ second. The results indicate no significant correlation between EV charging and $THD_V$, suggesting that voltage harmonics primarily originate from the supply side rather than the load. This implies that the observed voltage harmonics are attributable to background distortion originating from the supply side,

rather than being induced by the EV load. Consequently, the subsequent analysis in this study focuses on current harmonics, which more accurately reflect the distortion introduced by EV charging.

## 4.2 Amplitude Analysis

Harmonic amplitudes represent the magnitude of distortions introduced at different harmonic orders. This section examines the statistical distribution of harmonic amplitudes for individual and aggregated EV charging sessions. The analysis considers variations in amplitude across different charging currents, vehicle models, and operational conditions. Furthermore, it compares the amplitude contributions of dominant harmonic orders and their compliance with power quality standards.

The amplitudes of individual harmonics are essential for calculating $THD_I$ and ensuring compliance with power quality standards. These measurements were recorded as a time series at one-second intervals and then averaged over one-minute intervals. Figure 4.5 presents a heatmap illustrating the amplitudes of individual harmonic orders across all tested EVs.

While the previous section established a negative correlation between charging current and $THD_I$, the relationship between individual harmonic orders and charging current does not follow a uniform trend, as shown in Figure 4.5. Some harmonics exhibit an increase in amplitude as the charging current rises (e.g., the 2nd harmonic in VW ID.3 Pro and VW ID.4 Pro), whereas others show a decreasing trend (e.g., the 17th harmonic in Renault Zoe R90). Additionally, certain harmonics display no clear pattern with variations in charging current, highlighting the complexity of harmonic behaviour in EV charging scenarios.

When analyzing different harmonic orders within the same vehicle, the 7th harmonic consistently exhibits the highest magnitude, irrespective of the charging current. Alongside the 7th harmonic, the 3rd and 5th harmonics also display significantly larger amplitudes compared to other harmonic orders. As highlighted in Section 2.5, prior studies have primarily focused on the 3rd, 5th, and 7th harmonics due to their substan-

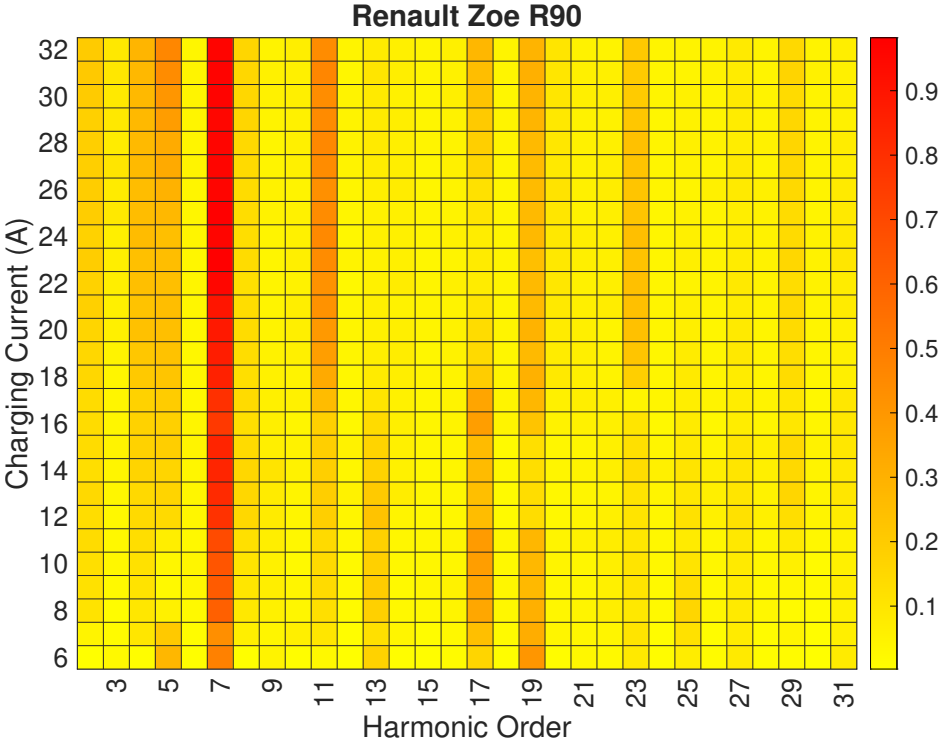


(a) Renault Zoe R90

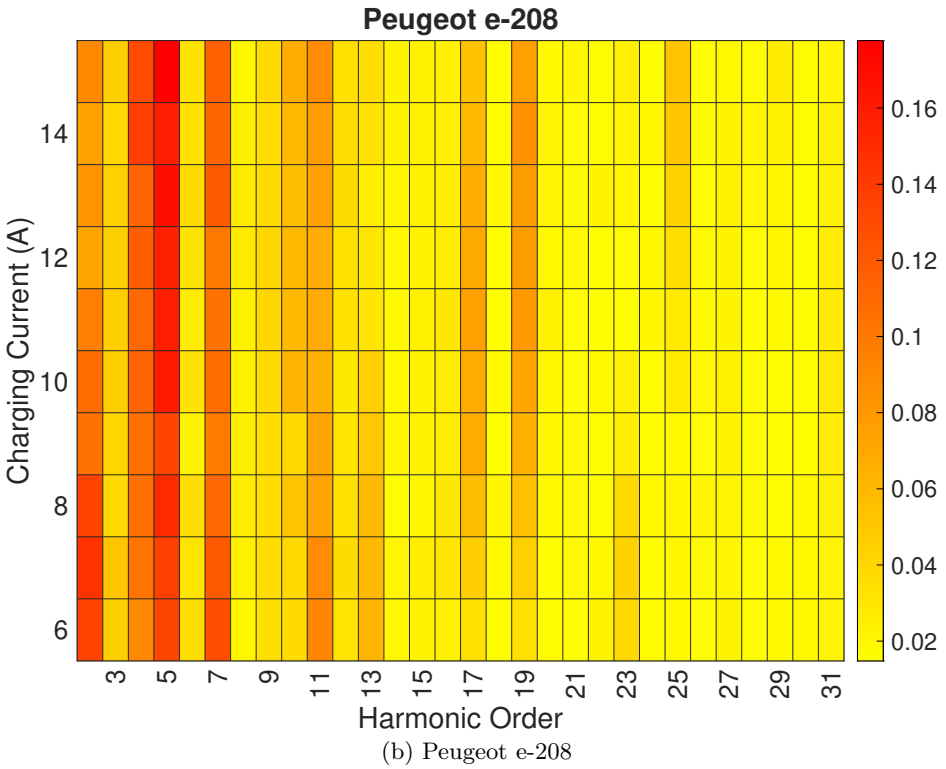


(b) Peugeot e-208

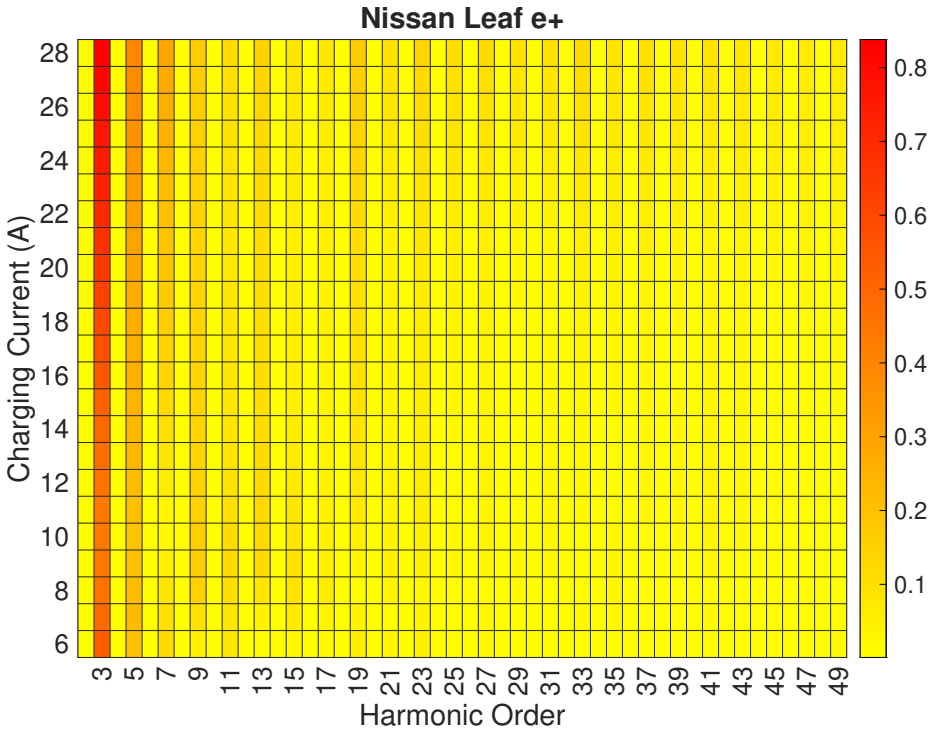


(c) Nissan Leaf e+

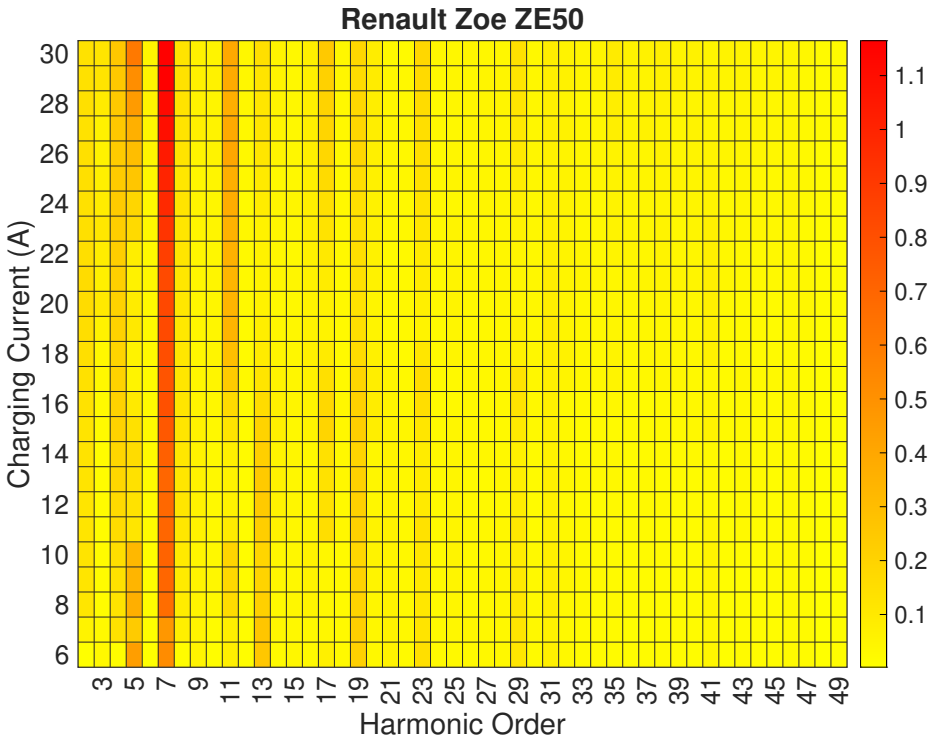


(d) Renault Zoe ZE50

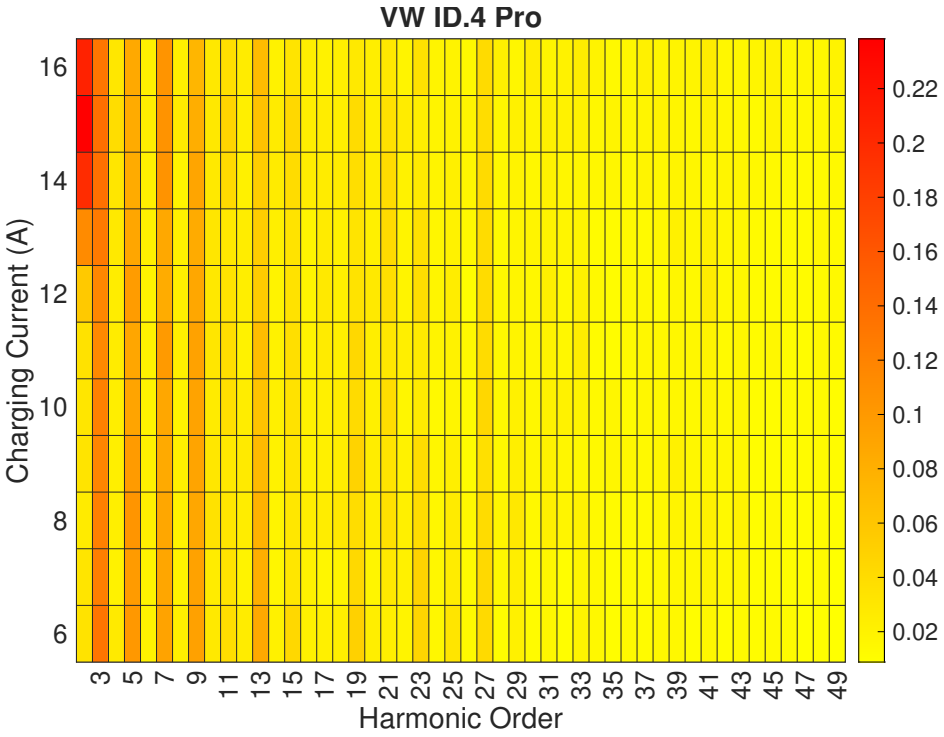


(e) VW ID.4 Pro

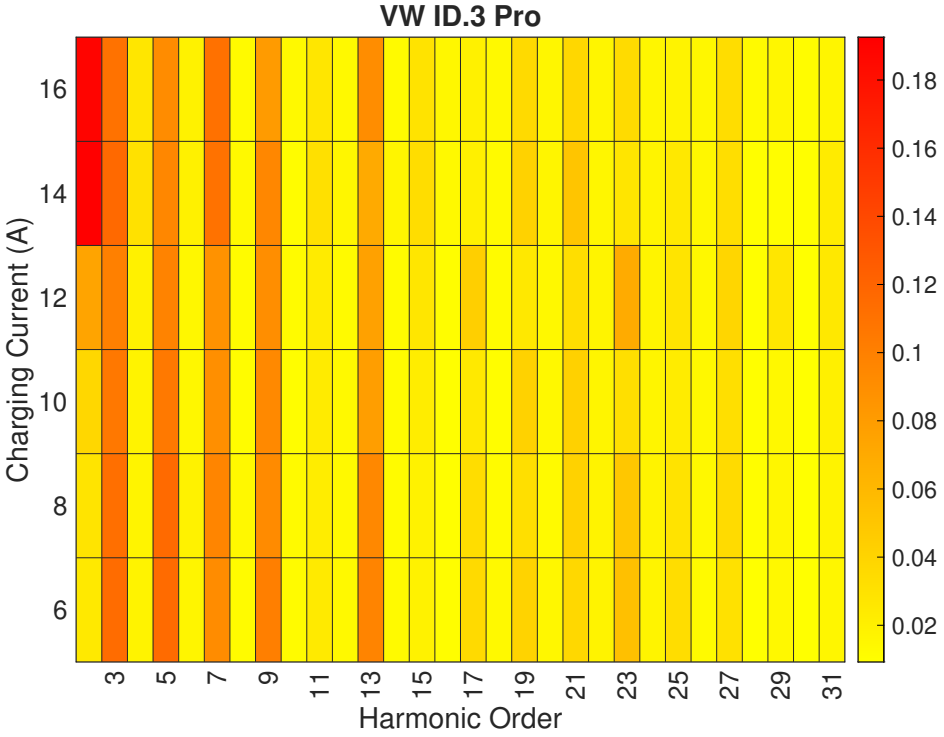


(f) VW ID.3 Pro

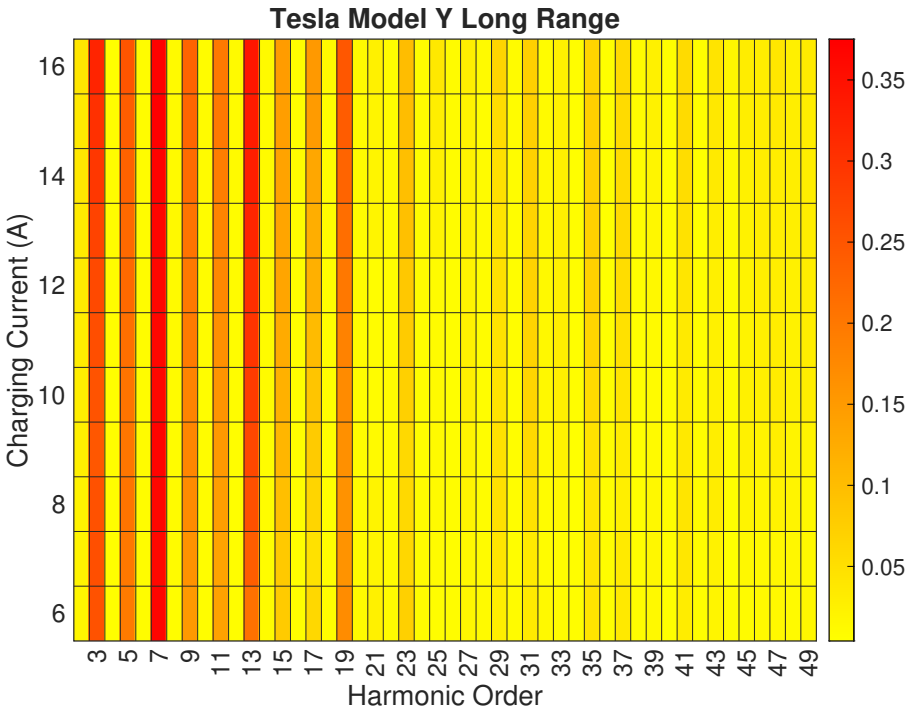


(g) Tesla Model Y Long Range

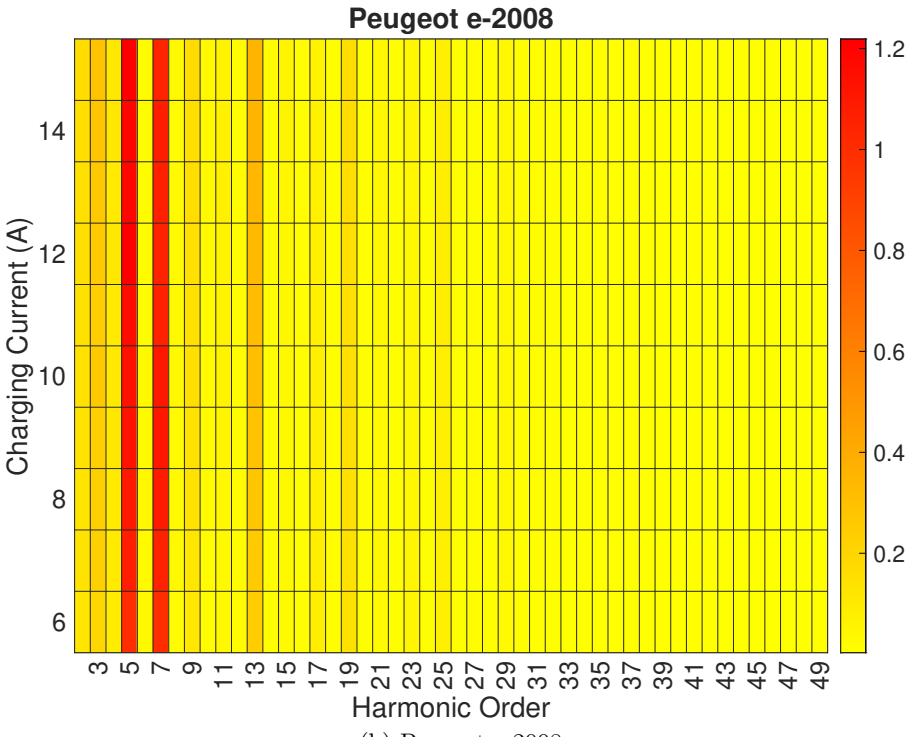


(h) Peugeot e-2008

Figure 4.5: Individual current harmonic amplitudes (A) across different charging rates for all tested EVs.

tial impact on power quality. Figure 4.5 confirms that these harmonics consistently have the highest magnitudes across all tested EVs. Beyond amplitude considerations, phase angles of dominant harmonics play a crucial role, especially when multiple EVs charge simultaneously. The alignment of phase angles among high-magnitude harmonics determines whether they reinforce or cancel each other out at the PCC. This interplay of harmonic phase relationships can significantly influence the aggregated harmonic distortion introduced into the power system.

## 4.3 Phase Angle Analysis

The phase angles of harmonic components determine their relative alignment and influence on overall harmonic summation. This section examines the statistical distribution of phase angles for various harmonic orders, evaluating their role in constructive and destructive interference. The analysis investigates phase angle variations across multiple EV charging scenarios, emphasising instances of harmonic cancellation and amplification.

Harmonic orders, similar to fundamental currents and voltages, are represented in a complex form that includes both amplitude and phase angle. Therefore, incorporating phase angle analysis is essential for a comprehensive harmonic assessment. Among the individual harmonics observed across all EVs, the 5th, 7th, and 9th harmonics exhibit the highest amplitudes, highlighting the need to examine these specific harmonics further. While their amplitudes are considerable in relation to power quality standards, phase angles must also be considered, as they determine whether harmonics reinforce or mitigate each other when summed. Due to phase angle variations across different EVs for the same harmonic order, the cumulative harmonic impact during simultaneous EV charging is lower than the direct arithmetic sum of individual harmonic amplitudes. However, if multiple EVs of the same model charge at identical rates, their harmonic contributions will sum arithmetically without cancellation effects.

Figure 4.6 presents the polar plot of the 3rd, 5th, and 7th harmonics, illustrating their phase angle distribution across different EVs and charging rates. The objective is

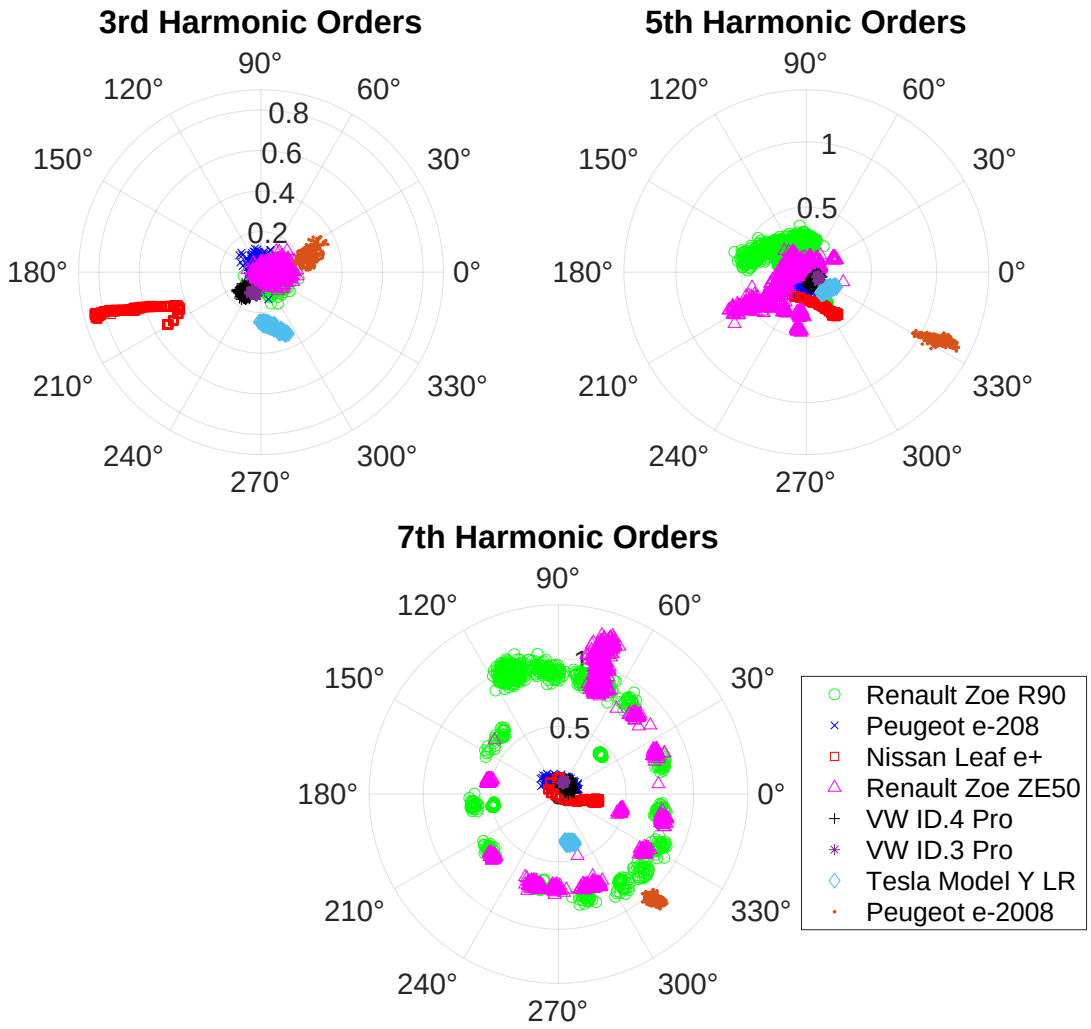


Figure 4.6: Phase angles of (in degrees) 3rd, 5th and 7th harmonic orders for all EVs.

to determine whether harmonics of the same order exhibit a concentrated or dispersed distribution among various EV models. For instance, the harmonic components of the Peugeot e-2008 appear clustered within specific angular regions, whereas those of the Renault Zoe R90 and Nissan Leaf e+ are more widely spread. Notably, the 3rd harmonic of the Peugeot e-2008 falls within the 0 to 30-degree range, while the same harmonic for the Nissan Leaf e+ is observed between 180 and 210 degrees. Given this 180-degree phase shift, partial harmonic cancellation is expected when these two vehicles charge simultaneously.

Circular data analysis is applied further to examine the behaviour of phase angles

beyond graphical representation. Unlike conventional statistical methods, such as mean and variance calculations, circular data requires specialized techniques since angular values wrap around at 360 degrees. For example, if two harmonic phase angles are 1° and 359°, a standard mean calculation would yield 180°, whereas the correct circular mean is 0°. To address this, MATLAB functions from [198] compute the mean and variance of phase angles.

Table 4.2: Circular descriptive statistics for phase angles (in degrees).

| Charging Current (A) | Harmonic Order | | | | | |
|---|---|---|---|---|---|---|
| | 3 | | 5 | | 7 | |
| | Mean | Variance | Mean | Variance | Mean | Variance |
| 6 | -117.3 | 13.4 | -73.9 | 13.6 | 92.9 | 37.8 |
| 7 | -66.5 | 36.7 | -92.9 | 37.8 | 17.2 | 26.4 |
| 8 | -91.9 | 38.3 | -77.7 | 17.6 | 70.0 | 44.6 |
| 9 | -89.9 | 42.3 | -77.7 | 12.7 | -110.4 | 48.8 |
| 10 | -105.6 | 36.3 | -57.1 | 11.3 | -15.1 | 50.0 |
| 11 | -123.7 | 47.8 | -63.3 | 25.4 | -62.7 | 31.7 |
| 12 | -123.9 | 35.8 | -39.4 | 30.8 | -15.4 | 38.7 |
| 13 | -120.7 | 43.7 | -51.8 | 38.3 | -45.4 | 29.4 |
| 14 | -115.3 | 29.8 | -32.7 | 31.1 | -4.2 | 33.1 |
| 15 | -42.1 | 48.5 | -54.2 | 32.4 | -27.3 | 31.5 |
| 16 | -113.8 | 17.2 | -17.0 | 34.7 | 5.8 | 18.7 |

The extent of harmonic cancellation across multiple EVs charging simultaneously was evaluated by collectively analyzing the phase angles of the 3rd, 5th, and 7th harmonic orders for charging currents between 6 A and 16 A. The results show that the variance for these harmonic orders ranges between 10 and 50 degrees, suggesting that when multiple EVs charge at the same rate, the overall harmonic contribution will be slightly lower than the direct arithmetic sum of individual harmonics. However, complete cancellation remains unlikely due to phase angle dispersion. A detailed summary of the circular mean and variance for selected harmonic orders is provided in Table 4.2.

## 4.4 Chapter Summary

This chapter presented a detailed statistical analysis of harmonic distortions observed during EV charging, with a focus on THD, individual harmonic amplitudes, and phase angles. The findings revealed that $THD_I$ decreased as the charging current increased, demonstrating a strong negative correlation for most EVs. Polynomial regression models, all with $R^2$ values greater than 0.85, effectively estimated $THD_I$ based on normalized charging current. In contrast, $THD_V$ remained relatively stable across all EVs and stayed well within the limits set by IEC and IEEE standards. Importantly, voltage distortion was primarily attributed to background harmonics from the supply side rather than the EVs themselves.

The amplitude analysis identified the 3rd, 5th, and 7th harmonics as the dominant contributors to distortion, with the 7th harmonic consistently exhibiting the highest magnitude across all vehicles. However, the relationship between harmonic amplitude and charging current varied depending on the specific harmonic order and vehicle, indicating that amplitude behaviour was influenced by complex, vehicle-specific characteristics.

Phase angle analysis highlighted that differences in harmonic phase among EVs enabled partial cancellation when multiple vehicles charged simultaneously. Circular statistical analysis revealed that phase angles were dispersed, with variances ranging from 10° to 50°, which limited full cancellation but still reduced the cumulative harmonic impact at the PCC.

Overall, the chapter provided a robust statistical foundation for modelling and optimizing EV charging strategies to minimize harmonic emissions. These insights can support the development of advanced simulation models and contribute to ensuring compliance with power quality standards in future electric mobility scenarios.

# Chapter 5

# Power Quality Assessment of EV Smart charging

This chapter examines the power quality implications of EV charging, focusing on both single and multiple EV charging scenarios. The analysis considers key power quality parameters, such as $THD_I$ and individual harmonics. The chapter is structured into two main sections: the first investigates power quality issues associated with individual EV charging, while the second explores the cumulative effects of multiple EVs charging simultaneously. Furthermore, a detailed case study based on laboratory measurements provides empirical insights into real-world charging conditions. Additionally, a Monte Carlo simulation approach is employed to model the probabilistic nature of EV charging behaviours and their potential impacts on power distribution networks. Through this assessment, the findings presented in this chapter contribute to the development of strategies for mitigating power quality disturbances caused by EV charging.

## 5.1 Power Quality Assessment-Single EV Charging

The evaluation of power quality for both single and multiple EV charging scenarios involves analyzing harmonic content by industry standards (outlined in Section 2.6). The assessment is relatively straightforward in the case of single EV charging, requiring a direct comparison of individual harmonic levels against the permissible limits. How-

ever, the analysis becomes more complex when multiple EVs charge simultaneously. This complexity arises from two key factors: First, the vector summation of harmonic components must account for their magnitudes and phase angles. Second, as the number of concurrently charging EVs increases, the range of possible EV combinations and charging states expands significantly, necessitating a probabilistic methodology to evaluate their collective impact.

The IEC 61000-3-2 standard is a widely recognized guideline for assessing power quality in single EV charging, setting maximum allowable current levels for individual harmonic orders (as detailed in Table 2.7). Figure 5.1 illustrates a heatmap depicting harmonic violations across all tested vehicles and harmonic orders. The results indicate that four out of the eight vehicles, namely the Renault Zoe R90, Renault Zoe ZE50, Tesla Model Y Long Range, and Peugeot e-2008, exceed the standard's permissible limits for multiple harmonic components. Notably, the 19th harmonic (950 Hz), which is likely associated with the switching frequency of on-board power electronics [199], consistently surpasses the threshold in all cases. However, the 7th harmonic does not exhibit comparable exceedance levels despite its previously highlighted high amplitude. This finding underscores the necessity of evaluating lower-amplitude harmonics in power quality assessment, as their impact may still be significant in meeting compliance requirements.

Another notable observation is the similarity in $THD_I$ trends between the Tesla Model Y and the Nissan Leaf e+, where $THD_I$ fluctuates between 4% and 10%. However, while none of the individual harmonics in the Nissan Leaf e+ surpass the IEC 61000-3-2 limits, six different harmonic orders in the Tesla Model Y exceed these thresholds. Interestingly, despite exhibiting higher $THD_I$ at lower charging currents, most of the Tesla Model Y's harmonic violations, specifically the 17th, 23rd, 31st, and 35th harmonics, occur at higher charging currents rather than at lower levels.

The results presented in this section highlight dissimilarities between $THD_I$ levels and individual harmonic violations. Notably, the lowest $THD_I$ values occur when charging power approaches its maximum capacity (e.g., 16 A). However, at higher charging rates, there is a significant increase in the number of individual harmonic violations

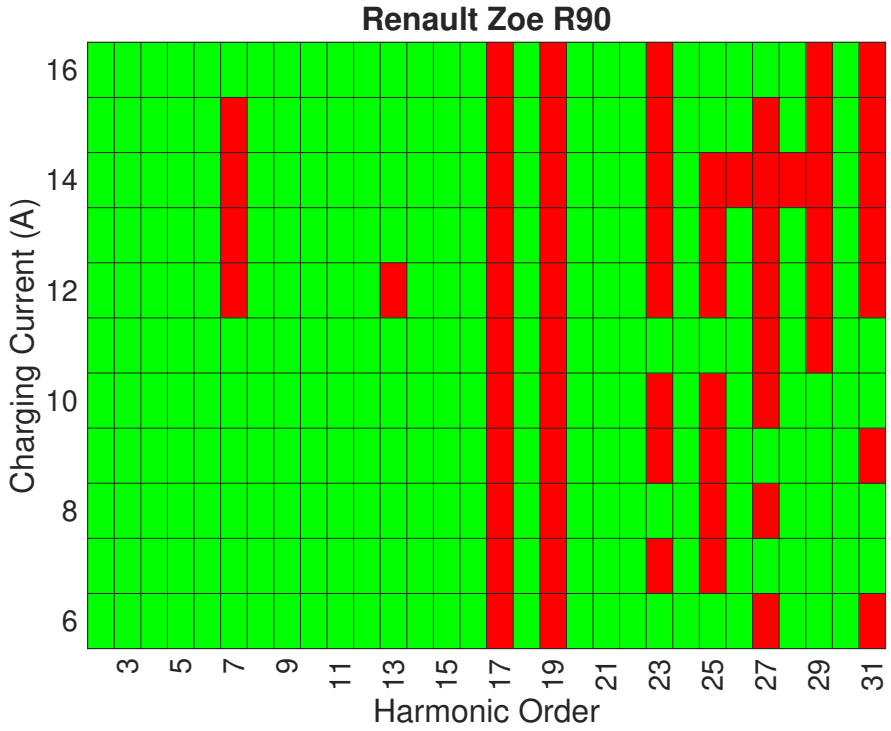


(a) Renault Zoe R90

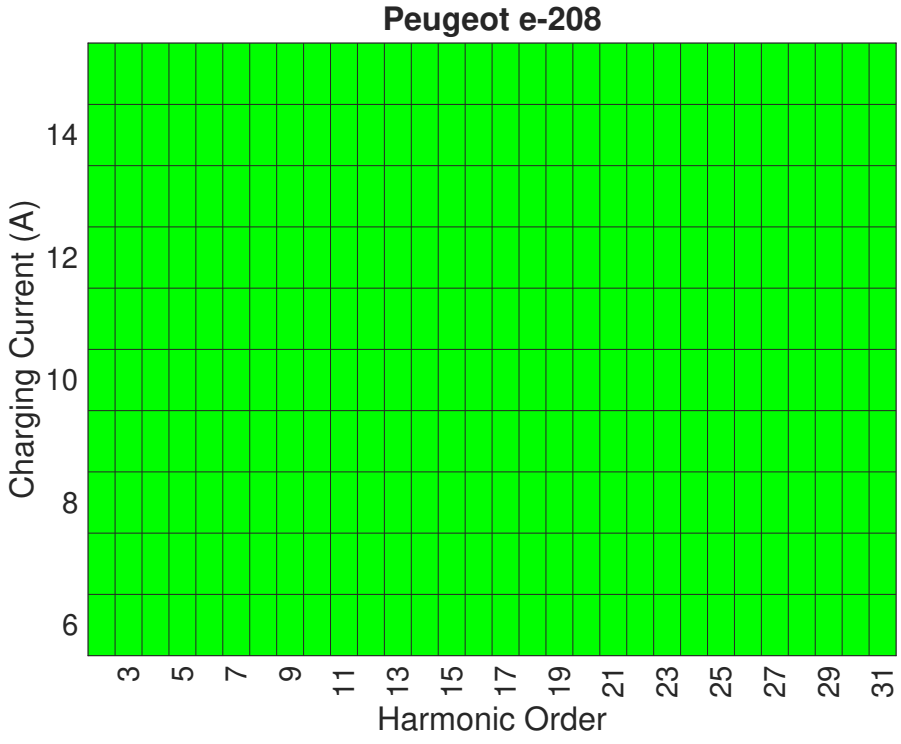


(b) Peugeot e-208

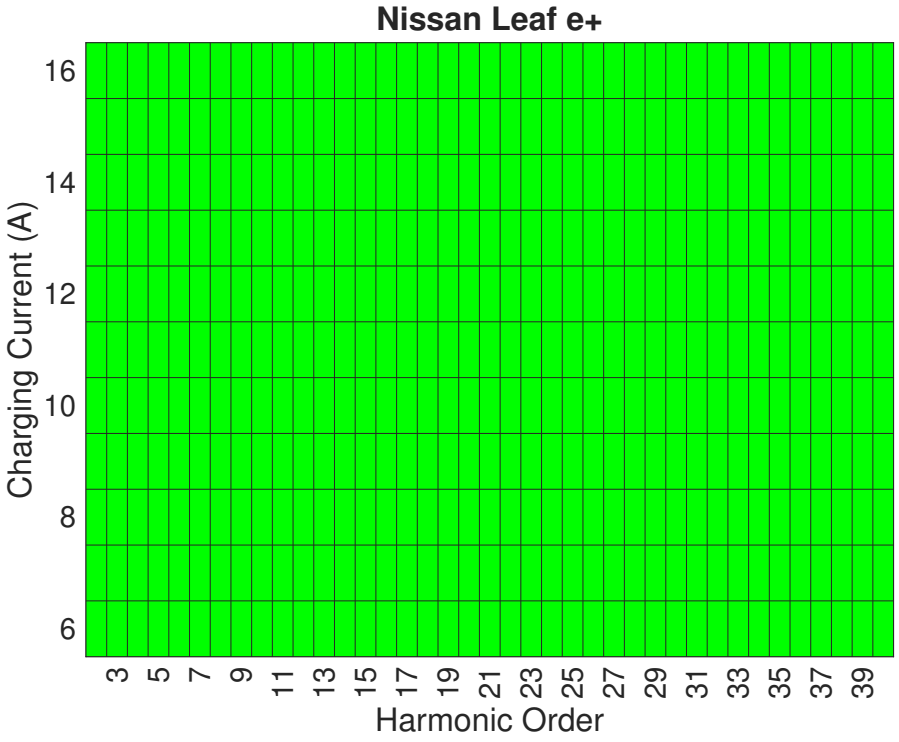


(c) Nissan Leaf e+

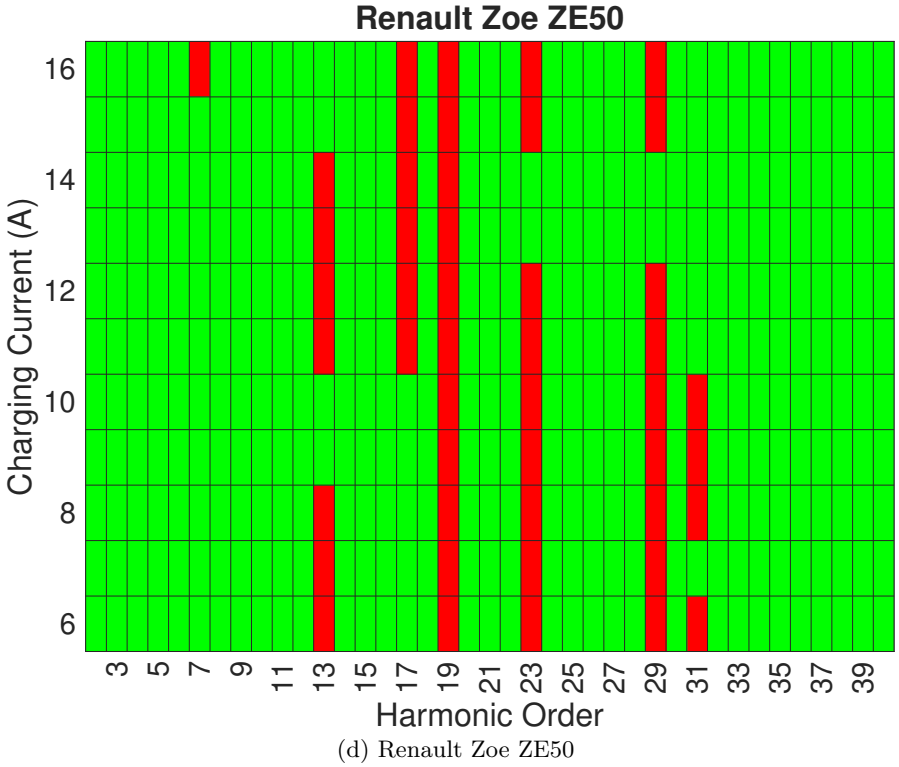


(d) Renault Zoe ZE50

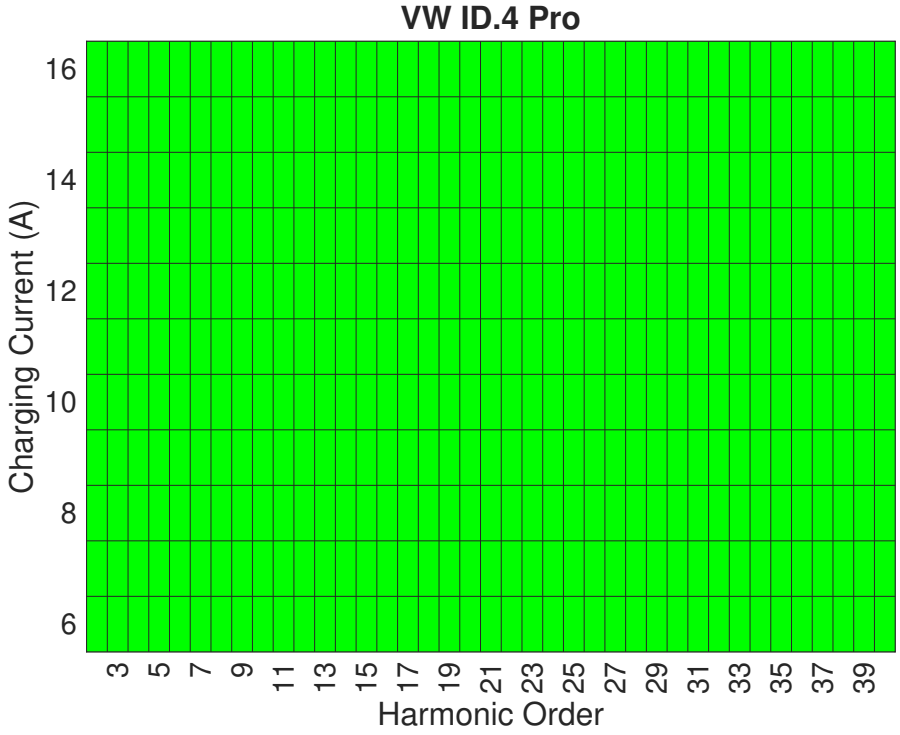


(e) VW ID.4 Pro

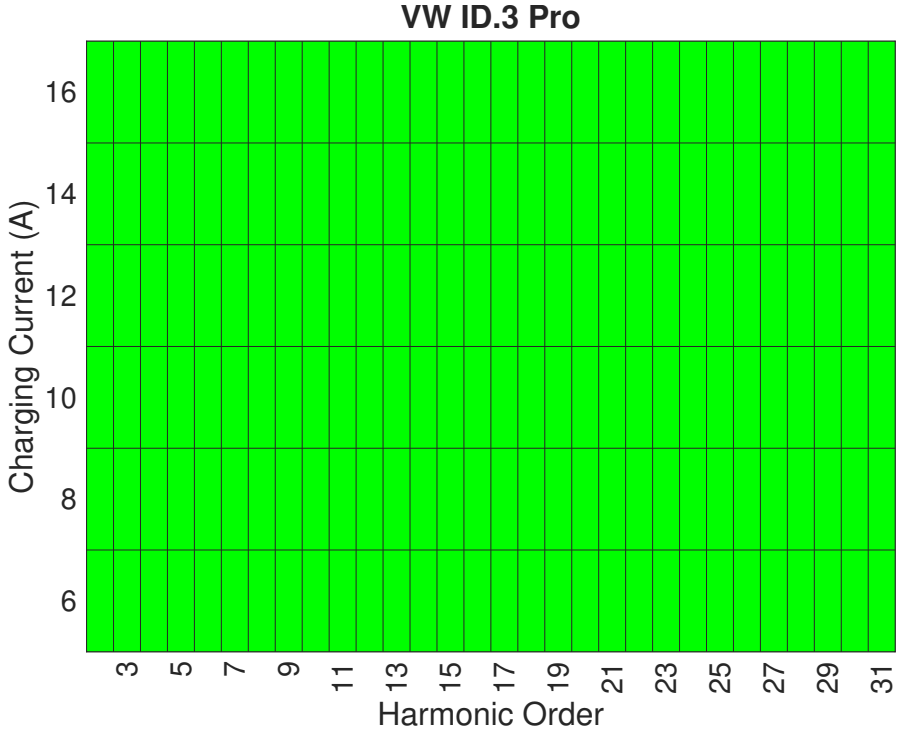


(f) VW ID.3 Pro

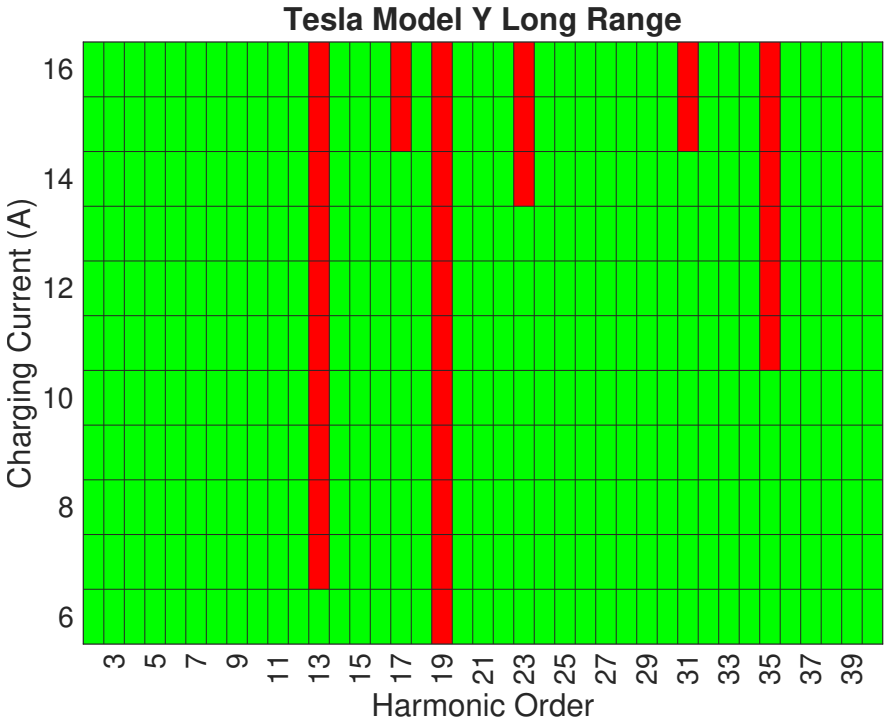


(g) Tesla Model Y Long Range

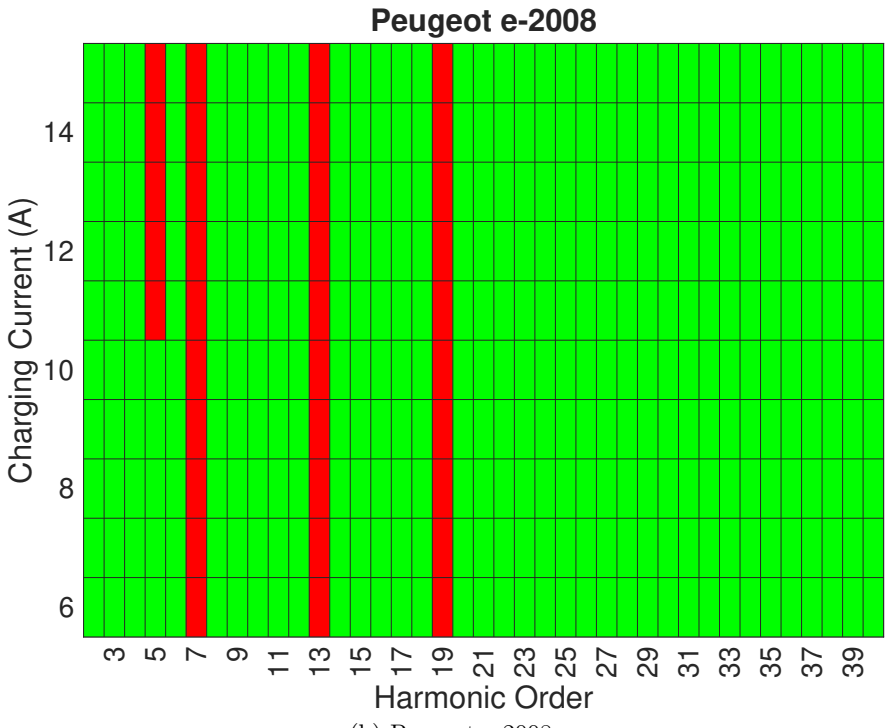


(h) Peugeot e-2008

Figure 5.1: Violation of individual current harmonics against the IEC 61000-3-2 standard for all tested EVs.

compared to lower charging rates. Furthermore, EVs with similar $THD_I$ levels can exhibit vastly different harmonic profiles and compliance outcomes. For instance, while both the Tesla Model Y and Nissan Leaf e+ have a $THD_I$ of 10% at a 6 A charging rate, only the Tesla Model Y exceeds harmonic limits. In contrast, the Nissan Leaf e+ remains within permissible thresholds.

## 5.2 Power Quality Assessment-Multiple EV Charging

An essential consideration in harmonic analysis is the accurate representation of harmonic current summation. When multiple loads are connected to the same bus, the total harmonic current injected into the system is the vector sum of the individual harmonic currents [200]. Since harmonic currents are vector quantities, both their magnitudes and phase angles must be taken into account for proper summation. The presence of various devices with distinct circuit topologies can lead to differences in harmonic phase angles, potentially resulting in a lower overall magnitude than the arithmetic sum of the individual harmonic currents [157]. To assess the combined effects of harmonic cancellation and amplification, it is necessary to consider the "absolute" harmonic phase angle, which defines the angle between current harmonics and the fundamental voltage, as outlined in IEC 61000-3-12 [172]. This differs from harmonic power flow studies, which focus on the "relative" harmonic phase angle, representing the angle between harmonic voltage and harmonic current.

Two distinct approaches are utilized to evaluate the overall harmonic emissions from multiple EVs. The first approach involves laboratory measurements of three EVs charging at different rates, while the second employs a Monte Carlo simulation to explore a wide range of EV charging scenarios under varying charging conditions.

### 5.2.1 Lab Measurements Case Study

This section presents an experimental analysis of harmonic emissions from the simultaneous charging of three EVs. Three power quality analyzers were assigned to monitor each vehicle individually to capture detailed measurements, while an additional power

Figure 5.2: 3 EVs (Tesla Y Long Range, Renault Zoe R90 and Peugeot e-2008) charging simultaneously.

Table 5.1: Charging currents for Tesla Model Y Long Range, Renault Zoe R90, and Peugeot e-2008 charging simultaneously.

| Tesla Model Y Long Range (A) | Renault Zoe R90 (A) | Peugeot e-2008 (A) |
|---|---|---|
| 6 | 6 | 6 |
| 9 | 9 | 9 |
| 12 | 12 | 12 |
| 15 | 15 | 15 |

analyzer was used to record the data at the PCC. The experiment was conducted using the Tesla Model Y Long Range, Renault Zoe R90, and Peugeot e-2008, which were selected based on vehicle availability. As illustrated in Figure 5.2, these vehicles were charged concurrently under four different charging current settings designed to replicate potential smart charging scenarios. The specific charging configurations are detailed in Table 5.1.

The variation of $THD_I$ and $THD_V$ in response to changing smart charging currents is illustrated in Figure 5.3. The expected trend of decreasing $THD_I$ with increasing charging current is clearly observed. However, the results indicate that smart charging has no significant impact on voltage harmonics, as $THD_V$ for both individual vehicles and the PCC remains consistently within the range of 1.65% to 1.85%. This is well below the 5% limit established by IEC 61000-2-4. As previously discussed in Figure 4.4, EV charging does not contribute to increased voltage harmonic distortion.

Furthermore, the concurrent charging of the three EVs significantly attenuates in-

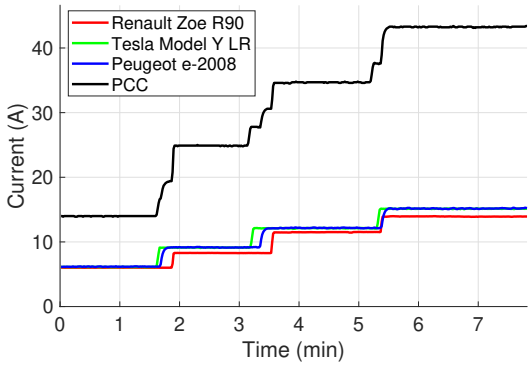


(a) Charging current vs. time

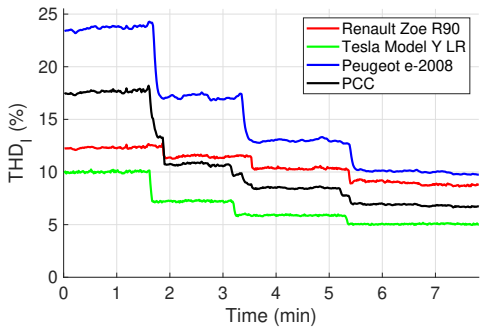


(b) Current harmonic distortion ($THD_I$) vs. time

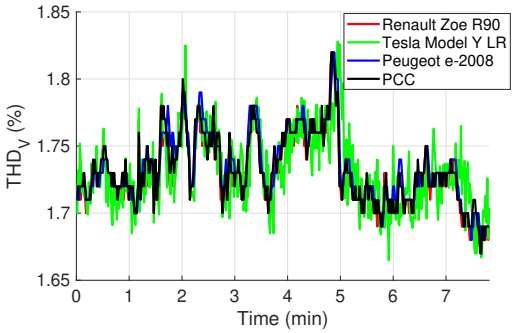


(c) Voltage harmonic distortion ($THD_V$) vs. time

Figure 5.3: Measurement results of three EVs charging simultaneously.

dividual harmonic components, effectively reducing $THD_I$ at the PCC. This reduction occurs due to the phase angle diversity of the harmonic currents generated by each vehicle, leading to partial cancellation when summed at the PCC. The extent of this cancellation effect depends on the relative phase angles and magnitudes of the individual harmonics. A detailed explanation of this phenomenon, including the mathematical representation of harmonic summation and cancellation, is provided in Section 2.4.1.

In this experiment, four distinct charging scenarios resulted in four different stages of analysis. In the first scenario, where all three EVs charged simultaneously at 6 A (6 A-6 A-6 A), the $THD_I$ measured at the PCC was lower than that of the Peugeot e-2008 alone. In the other three scenarios, the $THD_I$ at the PCC was lower than the corresponding $THD_I$ values of two out of the three individual vehicles. These findings reinforce the reliability of the results and highlight that the extent of harmonic

cancellation varies depending on the specific charging conditions. Given the practical limitations of laboratory testing with a large number of EV combinations, the subsequent section introduces a Monte Carlo simulation approach to evaluate the harmonic effects of a greater number of EVs charging at varying rates.

### 5.2.2 Background of Monte Carlo Simulation

Monte Carlo simulation is a probabilistic technique that uses repeated random sampling to estimate the behaviour of systems with inherent uncertainties [201]. Unlike deterministic models, which assume fixed inputs, Monte Carlo methods incorporate input variability through probability distributions, yielding a distribution of possible outcomes and enabling more robust decision-making [202].

The general process involves: (1) defining a deterministic model, (2) assigning probability distributions to uncertain parameters, (3) generating random samples, (4) computing model outputs for each sample, and (5) statistically analyzing the results to evaluate trends and risks.

In electrical engineering, Monte Carlo simulations are widely used to assess power system reliability, model load flow under uncertainty, and evaluate the impacts of variable renewable generation [203–205]. They are especially valuable for analyzing EV charging impacts on distribution networks, allowing utilities to account for stochastic user behaviour, charging rates, and EV penetration levels [206, 207]. These insights inform infrastructure planning, the modelling of uncertainties in EV charging behaviour, and comprehensive power quality evaluations.

### 5.2.3 Implementation of Monte Carlo Simulation for Multiple EV Charging

The Monte Carlo simulation is constructed using experimentally measured EV harmonic data as its fundamental input. Each EV is represented as a stochastic harmonic source whose behaviour depends on two discrete variables: the vehicle model and its charging current.

The ***simulation inputs*** are defined as follows:

- **EV model ($m$)**: One of the eight experimentally tested EVs listed in Table 3.2. The EV model is sampled from a discrete uniform distribution, such that each EV has an equal probability of 1/8 in each Monte Carlo iteration.
- **Charging current ($I$)**: The charging current is sampled from a discrete uniform distribution whose range depends on the case study:
  - Case Study 1: $I \in \{6, 7, 8, 9, 10\}$ A
  - Case Study 2: $I \in \{11, 12, \ldots, I_{\max,m}\}$ A

  where $I_{\max,m}$ is the experimentally measured maximum charging current of EV model $m$.
- **Harmonic database**: For each EV model $m$ and charging current $I$, the single-EV laboratory measurements provide the magnitude and phase angle of all measured harmonic orders. Each harmonic is represented as a complex phasor

$$\underline{I}_h(m, I) = I_h(m, I)\angle\phi_h(m, I), \tag{5.1}$$

  where $I_h$ and $\phi_h$ are directly obtained from the experimental dataset.

The ***simulation outputs*** are:

- Aggregated harmonic phasors at the PCC
- Computation of $\text{THD}_\text{I}$ for each iteration
- Probability distributions of $\text{THD}_\text{I}$
- Probability of exceeding IEEE 519 and IEC 61000-3-12 limits

To accurately model smart charging operations, a Monte Carlo simulation is developed to incorporate stochastic elements, accounting for variations in vehicle types and charging current rates. The simulation generates a dataset that enables the estimation of probabilistic distributions for key parameters. As the number of iterations increases, the reliability of the results improves. The Monte Carlo simulation follows four primary steps for a predefined number of EVs charging simultaneously, varying from 1 to 10:

- **Step 1:** Randomly select an EV type and assign a charging current within the defined range.
- **Step 2:** Compute $\mathrm{THD_I}$ using vector algebra by performing the vector summation of individual harmonic components.
- **Step 3:** Repeat Steps 1 and 2 one million times, recording the resulting $\mathrm{THD_I}$ for each iteration.
- **Step 4:** Determine the probability of exceeding harmonic limits by evaluating the recorded $\mathrm{THD_I}$ values against industry standards. The probability of exceeding the threshold, denoted as $\mathbb{P}_{\mathbb{F}}$, is given by:

$$\mathbb{P}_{\mathbb{F}} = \frac{N_F}{N_T}, \tag{5.2}$$

  where $N_F$ represents the number of simulation instances exceeding industry standards, and $N_T$ denotes the total number of iterations, set to one million. Evaluating (5.2) requires comparing each simulation result with established harmonic limits.

Two distinct case studies are conducted within the Monte Carlo framework:

- **Case Study 1:** Simulates EV charging during peak demand periods, where the charging current is constrained between 6 A and 10 A.
- **Case Study 2:** Examines off-peak charging scenarios, considering charging currents exceeding 11 A.

Algorithm 1 summarizes the Monte Carlo workflow used to estimate probabilistic harmonic distortion levels under multiple-EV charging. An essential aspect of Monte Carlo simulations is determining the necessary number of iterations to capture the inherent randomness of the system accurately. To establish this, the probability of failure for five EVs charging simultaneously is selected as a key harmonic assessment index. The number of iterations is varied from 1 to 10 million, and the probability of failure

**Algorithm 1** Monte Carlo Simulation for Probabilistic Harmonic Aggregation

**Require:**
$N_T = 1,000,000$ (Total iterations)
$N \in \{1, \ldots, 10\}$ (Simultaneous fleet size)
$\mathcal{L}$ (Empirical database: magnitudes $A_{h,m,I}$ and phase angles $\theta_{h,m,I}$)
$CaseStudy$ (Charging current range: Case 1 [6–10 A] or Case 2 [11 A+])
$Thresholds$ (IEEE 519 / IEC 61000 limits)
**Ensure:**
$\mathbb{P}_F$ (Probability of exceeding limits), Empirical distribution of $\mathrm{THD}_{\mathrm{I},\Sigma}$
$N_F \leftarrow 0$ ▷ Initialize violation counter
**for** $k = 1$ **to** $N_T$ **do**
  **Step 1: Stochastic Sampling**
  **for** $n = 1$ **to** $N$ **do**
    Sample EV model $m_n \sim \mathrm{DiscreteUniform}(1, 8)$
    Sample current $I_n \sim \mathrm{DiscreteUniform}(CaseStudy)$
    Retrieve phasors $(A_{h,n}, \theta_{h,n})$ for harmonic orders $h = 2, \ldots, 49$
  **end for**
  **Step 2: Vector Aggregation at PCC**
  **for** $h = 2$ **to** 49 **do**
    $\underline{I}_{h,\Sigma}(k) \leftarrow \sum_{n=1}^{N} A_{h,n} \cdot e^{j\theta_{h,n}}$ ▷ Complex vector summation
  **end for**
  **Step 3: Evaluation**
  Compute total aggregated distortion:
  $\mathrm{THD}_{\mathrm{I},\Sigma}(k) \leftarrow \frac{\sqrt{\sum_{h=2}^{49} |\underline{I}_{h,\Sigma}(k)|^2}}{|\underline{I}_{1,\Sigma}(k)|} \times 100\%$
  **Step 4: Violation Recording**
  **if** $\mathrm{THD}_{\mathrm{I},\Sigma}(k) > Limit$ **or** any individual order $|\underline{I}_{h,\Sigma}(k)| > Threshold$ **then**
    $N_F \leftarrow N_F + 1$
  **end if**
**end for**
**Step 5: Statistical Output**
$\mathbb{P}_F \leftarrow N_F / N_T$ ▷ Calculate Probability of Failure
**return** $\mathbb{P}_F$, Distribution of $\mathrm{THD}_{\mathrm{I},\Sigma}$

is computed, as shown in Figure 5.4. The results indicate that the probability stabilizes beyond $10^5$ iterations. However, to ensure statistical robustness, each simulation scenario is executed for one million iterations across all EV charging scenarios, ranging from 1 to 10 EVs, to encompass a sufficiently diverse set of possible charging conditions.

The Monte Carlo simulation relies on two key stochastic inputs. The first input concerns the selection of vehicle types, as detailed in Table 3.2, while the second input corresponds to the random charging current in Amps, along with the associated har-

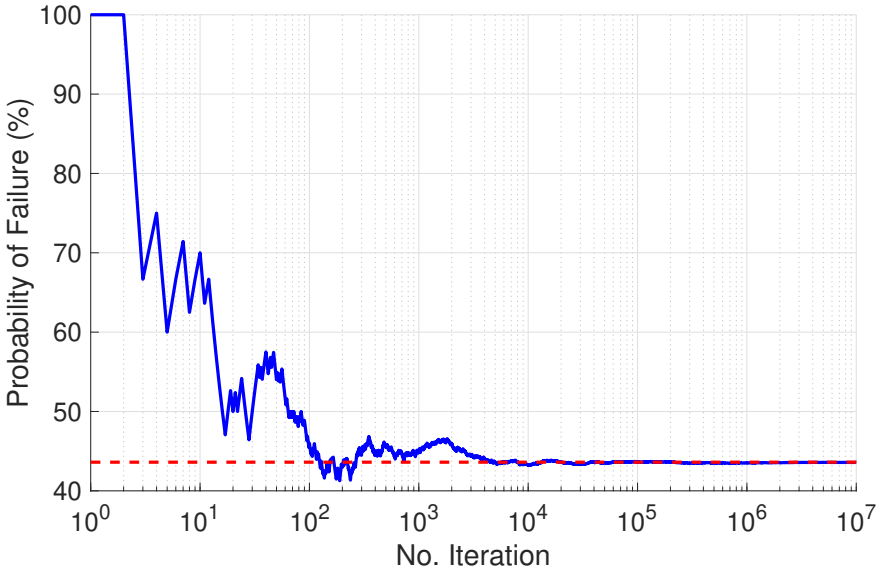


Figure 5.4: Monte Carlo number of iterations decision considering Case Study 1 and 5 EVs charging simultaneously in accordance to 5% $THD_I$ limits.

monic amplitude and phase angle derived from single EV charging experiments. The vehicle type is assumed to follow a discrete uniform distribution, where each of the eight vehicle models has an equal selection probability of 1/8 in each iteration of the simulation.

For Case Study 1, the charging current is randomly drawn from a discrete uniform distribution ranging from 6 A to 10 A, ensuring that only integer values within this range are considered. Similarly, in Case Study 2, the charging current is randomly assigned from a discrete uniform distribution spanning from 11 A to the maximum charging current for each EV, as specified in Table 3.2.

In each iteration of the simulation, $THD_I$ is determined by performing a vector summation of the individual harmonics that contribute to the overall harmonic content. The results for multiple EVs charging simultaneously are illustrated in Figure 5.5, which shows the distribution of $THD_I$ values and the probability of exceeding specified thresholds of 5% and 8%. The box plots in the figure represent the interquartile range, with the boxes spanning the 25th to 75th percentiles and the central red marker denoting the median value. The whiskers extend to the most extreme values within a

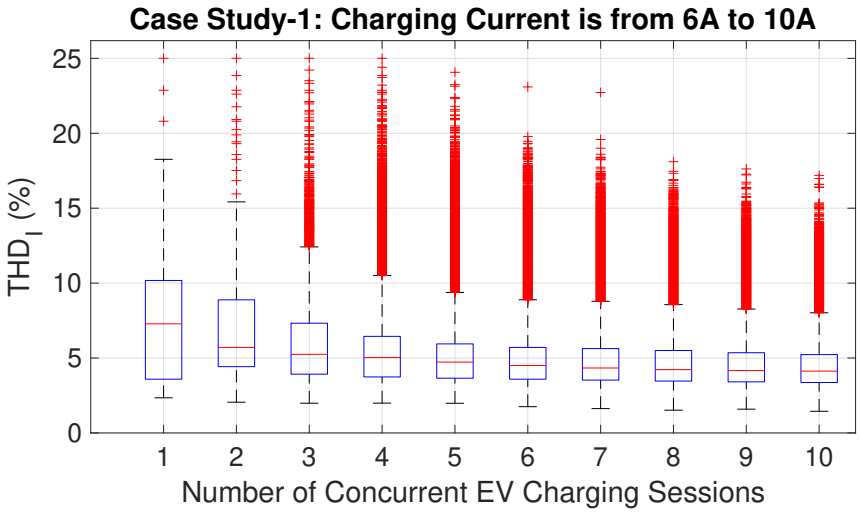


(a) $THD_I$ results for multiple EVs (Case Study-1)

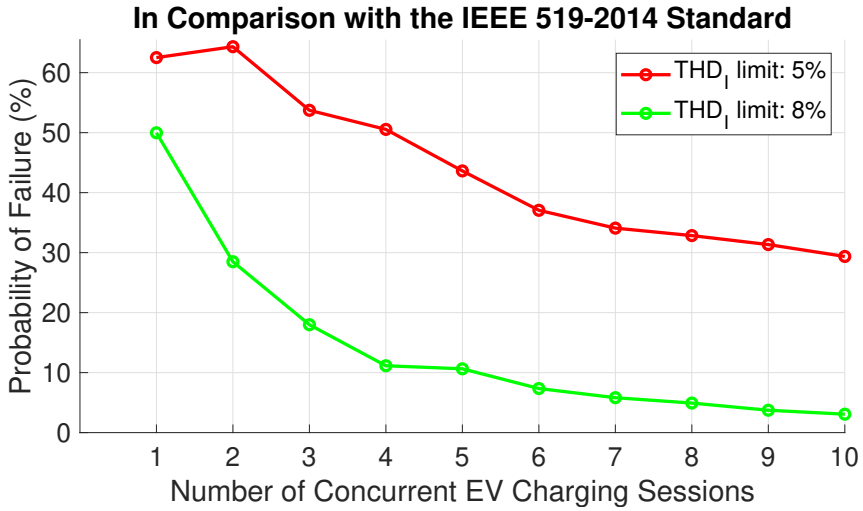


(b) Compliance comparison with IEEE 519-2014 limits

Figure 5.5: Simulation results of multiple simultaneous EV charging for Case Study-1.

non-outlier range, while outliers are displayed individually using a '+' marker symbol.

As observed in Figure 5.5, $THD_I$ exhibits a decreasing trend as the number of simultaneously charging EVs increases. This reduction is attributed to the cancellation effects of different harmonic orders, leading to a lower overall harmonic distortion. Consequently, the probability of surpassing specific $THD_I$ thresholds also follows a declining pattern.

In addition, the second case study, designed to simulate off-peak charging scenarios,

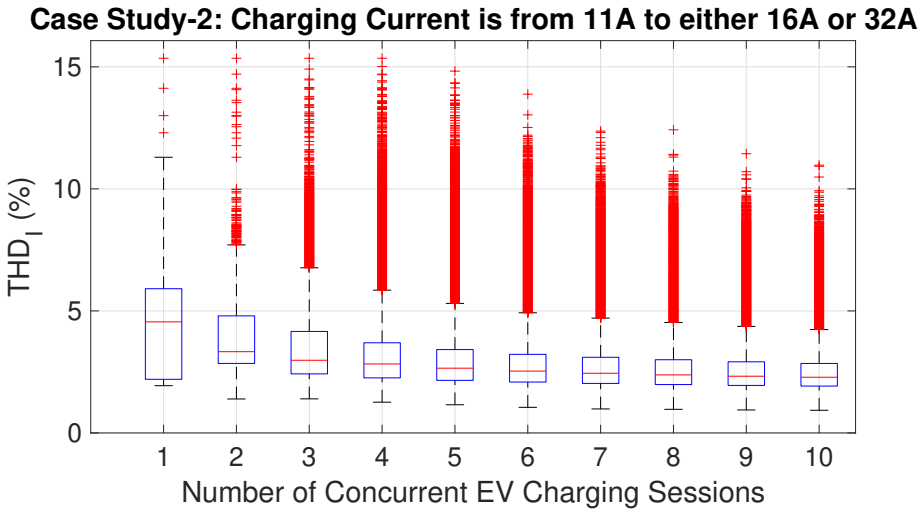


(a) $THD_I$ results for multiple EVs (Case Study-2)

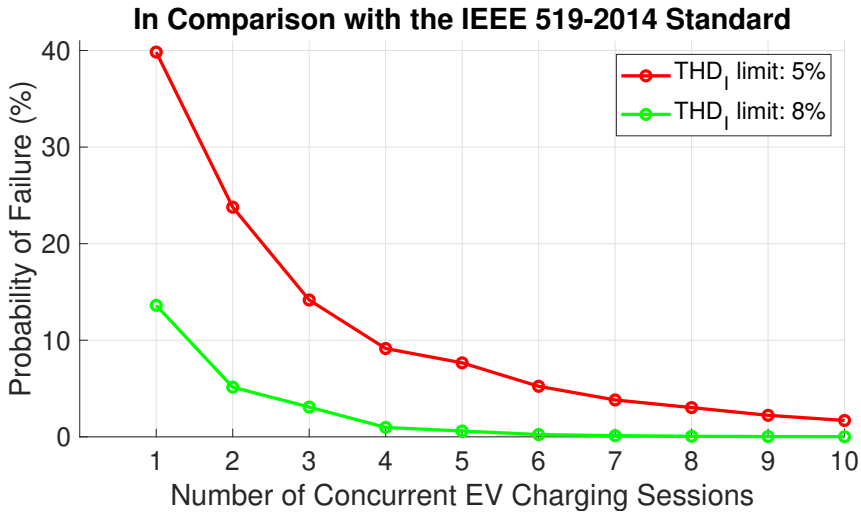


(b) Compliance comparison with IEEE 519-2014 limits

Figure 5.6: Simulation results of multiple simultaneous EV charging for Case Study-2.

was conducted by adjusting the smart charging currents accordingly. The findings from Case Study 2 are illustrated in Figure 5.6. Compared to Case Study 1, the results indicate that increasing the charging currents leads to a nearly 50% reduction in $THD_I$. As a result, the probability of exceeding $THD_I$ limits also declines significantly.

For instance, in the first case study, the probability of surpassing the 5% $THD_I$ threshold while charging ten EVs was approximately 30%. However, in Case Study 2, this probability was reduced by a factor of ten. These findings highlight a critical

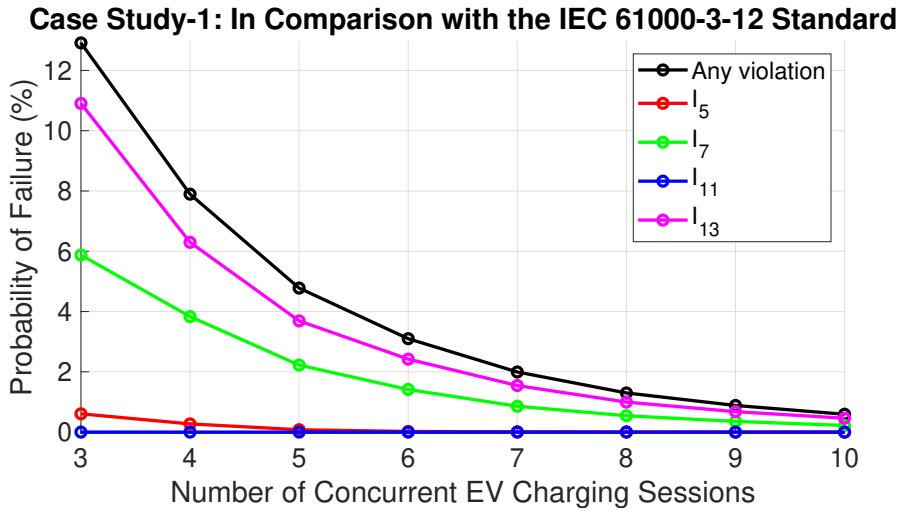


(a) Case Study-1: Individual harmonic violations (IEC 61000-3-12)

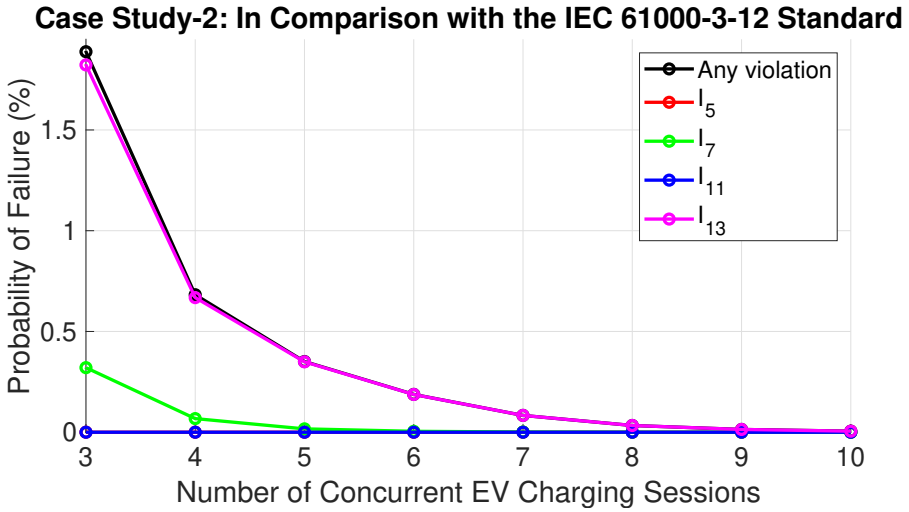


(b) Case Study-2: Individual harmonic violations (IEC 61000-3-12)

Figure 5.7: Exceeding individual harmonic current limits for two case studies based on the IEC 61000-3-12 power quality standard.

trade-off: while lower charging currents help mitigate peak demand on the grid, they can also lead to increased harmonic emissions, potentially affecting power quality within distribution networks.

In addition to evaluating overall $THD_I$, it is equally important to assess individual harmonics against the predefined thresholds set by power quality standards. To this end, Case Study 1 and Case Study 2 are compared by analyzing the 5th, 7th, 11th,

and 13th harmonic orders, whose permissible limits are specified in the IEC 61000-3-12 standard. Figure 5.7 illustrates the probability of exceeding these harmonic limits under different charging scenarios.

Since the IEC 61000-3-12 standard applies to scenarios where the total charging current exceeds 16 A, the analysis begins with three EVs charging simultaneously (as three EVs charging at 6 A each result in a total PCC current of 18 A). Each case is simulated one million times, and the probability of exceeding harmonic limits is determined by calculating the ratio of violation occurrences to the total number of iterations.

Beyond assessing the violations of the 5th, 7th, 11th, and 13th harmonics individually, the overall probability of exceeding harmonic limits is also analyzed. As expected, the occurrence of harmonic violations is significantly higher in Case Study 1 compared to Case Study 2. Among all examined harmonics, the 13th harmonic exhibits the highest probability of exceeding the permissible thresholds.

Figure 5.7 reveals that most harmonic violations tend to occur simultaneously, as there is minimal variation between the probability of any single harmonic exceeding its limit and that of the 13th harmonic. This indicates that when a violation occurs, multiple harmonics are likely to exceed their limits concurrently. Consistent with the $THD_I$ analysis, the probability of exceeding harmonic limits in Case Study 2 remains considerably lower, highlighting the effectiveness of higher smart charging currents in mitigating harmonic emissions.

It is important to note that this simulation study analyzes various combinations of EVs and charging rates rather than full charging sessions involving multiple vehicles. In a real-world scenario, a typical charging session lasts several hours, during which individual vehicles may experience fluctuating charging rates. These variations are further influenced by the battery SoC, as charging currents decrease significantly once the SoC exceeds 80-90%. Despite these considerations, the findings provide valuable insights, particularly in defining vehicle-specific charging ranges suitable for smart charging applications.

For example, the most unfavourable scenario for multiple EV charging would occur

if several Peugeot e-2008 vehicles were charging simultaneously at low current levels. If $N$ of these vehicles were to charge concurrently at 6 Amps, the resulting $THD_I$ (%) would be approximately 25%. In contrast, vehicles such as the VW ID.4 Pro would not require any specific charging restrictions, as their $THD_I$ levels consistently remain below 5%.

## 5.3 Chapter Summary

Chapter 5 focused on evaluating the impact of EV charging on power quality, with an emphasis on both single and multiple EV scenarios. The analysis was conducted through laboratory experiments and supported by Monte Carlo simulations to reflect real-world uncertainties in charging behaviour.

In the case of single EV charging, the study compared harmonic emissions against the IEC 61000-3-2 standard. Results indicated that four out of the eight tested EVs, Renault Zoe R90, Renault Zoe ZE50, Tesla Model Y Long Range, and Peugeot e-2008, exceeded permissible limits for individual harmonic components, despite some of them having relatively moderate $THD_I$ values. This highlighted that relying solely on $THD_I$ could overlook specific harmonic violations, as vehicles with similar $THD_I$ levels exhibited different harmonic profiles and compliance outcomes.

The multiple EV charging assessment was based on a laboratory experiment involving the simultaneous charging of three EVs. Results showed that the $THD_I$ at the PCC was reduced compared to individual vehicle measurements. This reduction was attributed to harmonic phase angle diversity, which led to partial cancellation of current harmonics. On the other hand, $THD_V$ remained unaffected by EV charging and consistently fell below regulatory thresholds, indicating that EV charging had minimal impact on voltage distortion.

To extend the analysis beyond the limitations of lab testing, a Monte Carlo simulation framework was introduced. This simulation modelled smart charging behaviour by incorporating stochastic variations in EV types and charging currents. Two case studies were considered: Case Study 1 simulated charging at low currents (6 –10 A) typical

of peak demand periods, while Case Study 2 represented off-peak charging at higher currents (above 11 A). The simulation demonstrated that $THD_I$ and the probability of exceeding harmonic limits both decreased as the number of simultaneously charging EVs increased. Furthermore, Case Study 2 resulted in significantly lower harmonic distortion, with nearly a tenfold reduction in violation probability compared to Case Study 1.

The analysis also showed that certain harmonic orders, particularly the 13th, were more prone to violations. Additionally, some EV models, such as the Peugeot e-2008, presented higher harmonic emissions under low-current conditions, making them more critical in the context of grid power quality.

In conclusion, Chapter 5 established that smart charging strategies and probabilistic modelling were essential for managing the harmonic impacts of EV integration. While low-current charging helped alleviate grid loading during peak times, it also increased harmonic distortion. Thus, a careful balance had to be maintained between load management and power quality, especially in scenarios involving high EV penetration.

# Chapter 6

# Transformer Aging Under Harmonic Emissions from EV Smart Charging

The previous chapters presented a detailed statistical analysis of harmonic emissions from EVs under smart charging conditions, revealing the relationship between charging current, harmonic amplitude, and phase angle dispersion, and further evaluated the compliance of harmonic emissions against established power quality standards. Building on these insights, this chapter focuses on quantifying the effects of harmonic-rich loading on distribution transformers. A thermal-electrical model is employed to assess transformer aging under various EV charging scenarios. Transformer losses, top-oil and hot-spot temperatures, aging acceleration factor, and transformer lifetime are estimated according to IEEE C57.91-2011 [161], and harmonic impacts are incorporated in line with IEEE C57.110-2018 [208] standards. To address the observed challenges, a rule-based EV charging management strategy is proposed to mitigate transformer aging in heavily loaded network conditions, offering practical guidance for balancing asset longevity with rising EV demand.

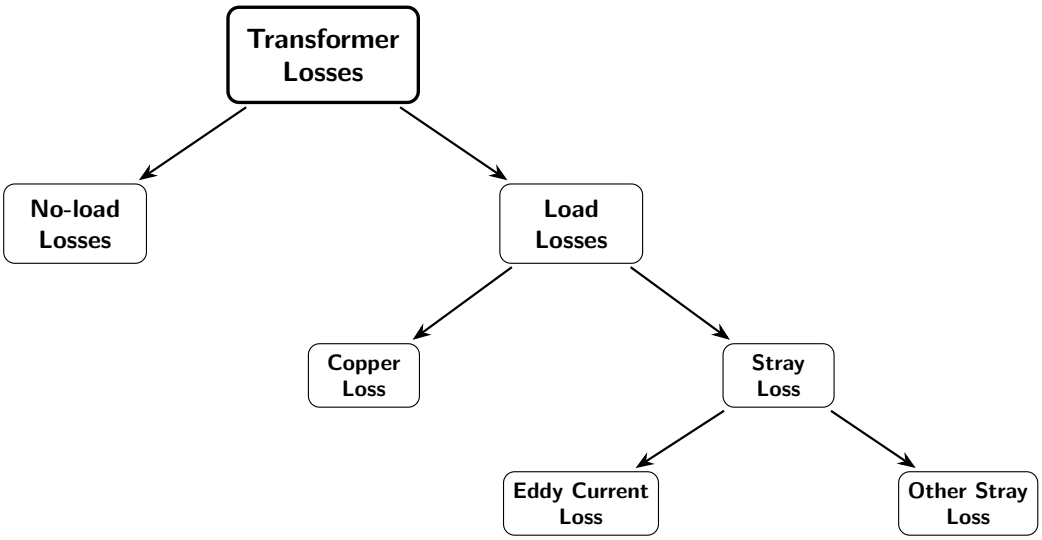


Figure 6.1: Transformer losses diagram.

## 6.1 Modelling Distribution Transformer Losses for Harmonic Analysis

While electrical loading is a key factor in evaluating transformer performance, it provides only a partial understanding of the operational stresses. In addition to electrical loading, thermal loads resulting from increased current flow must also be considered when assessing a transformer's lifespan. The total power loss in a transformer, denoted as $P_{TL}$, can be broadly classified into no-load losses ($P_{NL}$) and load losses ($P_{LL}$), as illustrated in Figure 6.1. No-load loss occurs whenever the transformer is energized, regardless of whether it supplies power to a load. Conversely, load loss is dependent on actual loading conditions and primarily results from winding resistance. Load loss can be further divided into copper loss ($P_{CL}$) and stray loss ($P_{SL}$). This relationship can be mathematically represented as follows [161]:

$$P_{TL} = P_{NL} + P_{LL} = P_{NL} + (P_{CL} + P_{SL}). \tag{6.1}$$

These losses collectively contribute to heat build-up within the transformer, leading to an increase in top-oil and hot-spot temperatures. Prolonged exposure to excessive

thermal stress can accelerate the degradation of insulation materials, shorten the transformer's operational lifespan, and ultimately affect the reliability of the power distribution network. Therefore, a comprehensive evaluation of both electrical and thermal loading is essential for accurately assessing transformer performance, particularly in EV-integrated power grids.

Copper losses, denoted as $P_{CL}$, refer to the energy dissipation caused by electrical resistance within the transformer windings. These losses are determined using the $I^2R$ formula, where $I$ represents the current flowing through the windings, and $R$ denotes the electrical resistance of the conductors.

Stray losses, represented as $P_{SL}$, originate from currents induced by stray magnetic fields within the transformer core and other structural components. Unlike copper losses, these losses are not directly linked to the primary or secondary winding currents but arise due to interactions between the magnetic fields and the transformer's structural elements. Stray losses can be further divided into winding eddy-current losses ($P_{ECL}$) and other stray losses ($P_{OSL}$).

Winding eddy-current losses, $P_{ECL}$, occur due to circulating currents induced in conductive materials by alternating magnetic fields. These currents generate heat, adding to the transformer's thermal stress and accelerating the aging of insulation materials. In contrast, $P_{OSL}$ represents losses in non-winding components such as the core, structural supports, and cooling systems. The total load losses, $P_{LL}$, encompass both copper and stray losses and can be expressed mathematically as follows:

$$P_{LL} = P_{CL} + P_{SL} = P_{CL} + (P_{ECL} + P_{OSL}). \tag{6.2}$$

One of the primary effects of harmonic distortion is the increase in the root mean square (RMS) value of the load current. The RMS value is a key parameter for assessing both the thermal and electrical stresses imposed on transformer windings, and it is notably affected by the presence of harmonic components. In particular, the RMS load current, $I_L^h$, depends on the contribution of multiple harmonic orders, extending from the fundamental frequency up to the highest considered harmonic order, $h_{\max}$. This

relationship can be mathematically represented as:

$$I_L^h = \sqrt{\sum_{h=1}^{h_{\max}} I_h^2}, \tag{6.3}$$

In this equation, $I_h$ denotes the RMS load current corresponding to the $h$-th harmonic order. This expression underscores the combined influence of multiple harmonic frequencies on the overall load current, demonstrating that even lower-order harmonics can significantly impact the total RMS value.

The various components of load loss, $P_{LL}$, increase proportionally to the square of the load current, though their dependence on frequency is more nuanced. Copper losses, $P_{CL}$, are affected by the skin effect, which raises conductor resistance at higher frequencies; however, this impact remains minimal for smaller conductors. In contrast, eddy-current losses within transformer windings, $P_{ECL}$, scale approximately with the square of frequency, as elevated frequencies generate stronger circulating currents, leading to increased energy dissipation. Eddy-current losses occurring in non-winding structural components, $P_{OSL}$, exhibit a sub-quadratic frequency dependence, with an exponent of 0.8, indicating a less pronounced increase compared to $P_{ECL}$. These losses, caused by stray magnetic fields interacting with the transformer's structural elements, significantly contribute to thermal stress. Considering these frequency-dependent factors, the total load losses in a transformer subjected to distorted currents can be mathematically represented as:

$$P_{LL}^h = P_{CL}^h + P_{ECL}^h + P_{OSL}^h, \tag{6.4}$$

which can equivalently be written as:

$$P_{LL}^h = (P_{CL}^r + F_{HL}^{ec} P_{ECL}^r + F_{HL}^{os} P_{OSL}^r) \times I_{L,pu}^2. \tag{6.5}$$

In these expressions, $P_{CL}^r$ denotes the reference copper losses at the nominal frequency, while $P_{ECL}^r$ and $P_{OSL}^r$ correspond to the reference values for eddy-current losses and other stray losses, respectively. The factors $F_{HL}^{ec}$ and $F_{HL}^{os}$ serve as harmonic loss coefficients, quantifying the influence of harmonic distortion on $P_{ECL}$ and $P_{OSL}$. Ad-

ditionally, $I_{L,pu}$ represents the per-unit load current, which normalizes the actual load current with respect to the transformer's rated current.

In harmonic distortion analysis, the superscript $h$ signifies the contribution of harmonic components, while the superscript $r$ represents rated operating conditions in terms of load and frequency. To evaluate the influence of harmonics on transformer performance, the per-unit harmonic load current, $I_{L,pu}$, is defined as the proportion of the harmonic load current relative to the rated load current. This relationship is mathematically formulated as:

$$I_{L,pu} = \frac{I_L^h}{I_L^r}, \tag{6.6}$$

In this expression, $I_L^h$ represents the RMS load current at a given harmonic order, while $I_L^r$ corresponds to the RMS load current under rated operating conditions. The per-unit system provides a standardized approach to normalizing the harmonic load current, enabling a more effective comparison and analysis of harmonic impacts concerning the transformer's rated performance.

Additionally, the harmonic loss factors, represented as $F_{HL}^{ec}$ for winding eddy currents and $F_{HL}^{os}$ for other stray losses, serve to quantify the impact of harmonic distortion on various load loss components within the transformer. These factors are determined using the following mathematical expressions [208]:

$$F_{HL}^{ec} = \frac{\sum_{h=1}^{h_{\max}} I_h^2 \times h^2}{\sum_{h=1}^{h_{\max}} I_h^2}, \tag{6.7}$$

$$F_{HL}^{os} = \frac{\sum_{h=1}^{h_{\max}} I_h^2 \times h^{0.8}}{\sum_{h=1}^{h_{\max}} I_h^2}, \tag{6.8}$$

In this context, $I_h$ represents the RMS load current corresponding to the $h$-th harmonic order, while $h_{\max}$ denotes the highest harmonic order included in the analysis. The harmonic loss factor associated with winding eddy currents, $F_{HL}^{ec}$, follows a quadratic relationship with the harmonic order, meaning that higher-order harmonics disproportionately increase eddy-current losses within transformer windings. On

the other hand, the harmonic loss factor for other stray losses, $F_{HL}^{os}$, follows a sub-quadratic dependency, characterized by an exponent of 0.8. This implies that although higher-order harmonics contribute to stray losses, their effect is relatively less significant compared to their influence on eddy-current losses.

### 6.1.1 Transformer Temperature Rise Modeling

The transformer's top-oil temperature ($\theta_{TO}$) can be calculated by initially determining the load losses under harmonic conditions and subsequently using the following equation to estimate the temperature rise.

$$\theta_{TO} = \theta_A + \Delta\theta_{TO}, \tag{6.9}$$

In this equation, $\Delta\theta_{TO}$ denotes the increase in top-oil temperature relative to the ambient temperature ($\theta_A$). The value of $\Delta\theta_{TO}$ is determined using the following expression:

$$\Delta\theta_{TO} = \Delta\theta_{TO}^{r} \times \left(\frac{P_{LL}^{h} + P_{NL}}{P_{LL}^{r} + P_{NL}}\right)^{0.8}, \tag{6.10}$$

In this formulation, $\Delta\theta_{TO}^{r}$ represents the temperature difference between the top-oil layer and the ambient temperature under rated operating conditions, as provided by the transformer manufacturer. The term $P_{LL}^{h}$ corresponds to the load losses arising from harmonic currents, while $P_{LL}^{r}$ denotes the load loss under rated conditions, and $P_{NL}$ accounts for the no-load loss. As harmonic currents increase, the associated rise in $P_{LL}^{h}$ leads to higher overall load losses, subsequently elevating $\Delta\theta_{TO}$ and, in turn, $\theta_{TO}$. Elevated top-oil temperatures can accelerate insulation aging, weaken the dielectric strength of insulating materials, and ultimately reduce the transformer's service life.

Once the top-oil temperature ($\theta_{TO}$) is assigned, the corresponding hot-spot temperature ($\theta_{HS}$) within the transformer windings can be calculated using the following equation:

$$\theta_{HS} = \theta_{TO} + \Delta\theta_{HS}, \tag{6.11}$$

where $\Delta\theta_{HS}$ denotes the increase in temperature at the hot spot relative to the top-oil

temperature. The hot-spot temperature rise, $\Delta\theta_{HS}$, is determined using the following equation:

$$\Delta\theta_{HS} = \Delta\theta_{HS}^{r} \times \left(\frac{P_{LL}^{h}}{P_{LL}^{r}}\right)^{0.8}, \tag{6.12}$$

where $\Delta\theta_{HS}^{r}$ represents the temperature difference between the hot spot and the top-oil layer under rated operating conditions. Elevated hot-spot temperatures pose a significant risk as they accelerate the aging process of the transformer's insulation materials. An increase in $\theta_{HS}$ speeds up thermal degradation, weakening the dielectric properties and ultimately shortening the transformer's service life [32, 161]. Moreover, excessive $\theta_{HS}$ can result in uneven thermal distribution within the windings, leading to localized overheating that further deteriorates the structural and electrical integrity of the transformer [209].

### 6.1.2 Transformer Lifetime Modelling

For a transformer with a nominal winding temperature rise of 55 °C, the aging acceleration factor, $F_{AA}$, is standardized at 1.0 when the hot-spot temperature (HST) reaches 110 °C. This factor serves as an indicator of insulation aging relative to standard operating conditions. As the HST exceeds 110 °C, $F_{AA}$ increases, signifying an accelerated deterioration of the insulation. The mathematical expression defining this relationship is taken directly from IEEE C57.91 Standard [161] and given as:

$$F_{AA} = \exp\left(\frac{15000}{383} - \frac{15000}{\theta_{HS} + 273}\right), \tag{6.13}$$

where $\theta_{HS}$ is the hot-spot temperature.

When operating under rated conditions with a HST of 110 °C, the aging acceleration factor $F_{AA}$ is defined as 1.0, indicating that the transformer insulation degrades at its expected rate. The standard insulation lifespan, $\text{Life}_{\text{norm}}$, for a transformer functioning under these conditions is specified as 20.55 years (or 180,000 hours) [161]. This reference value provides a benchmark for evaluating the actual lifespan of transformers experiencing thermal stress due to harmonic distortions.

The actual lifespan of a distribution transformer, $\text{Life}_{\text{real}}$, can be estimated by mod-

ifying the standard insulation life to reflect the transformer's real operating conditions. This adjustment is made using the aging acceleration factor, as expressed in the following equation:

$$\text{Life}_{\text{real}} = \frac{\text{Life}_{\text{norm}}}{F_{AA}}. \tag{6.14}$$

In this equation, $\text{Life}_{\text{real}}$ denotes the projected service life of the transformer, incorporating the effects of elevated thermal stress caused by harmonic-induced load losses. When $F_{AA}$ exceeds 1.0, $\text{Life}_{\text{real}}$ decreases accordingly, indicating a faster rate of insulation degradation and a reduced transformer lifespan. To provide a holistic overview of the analytical methodology, Figure 6.2 outlines the systematic progression of the assessment, tracking the data flow from initial harmonic and thermal parameters through to the final determination of the transformer's operational lifespan.

## 6.2 Monte Carlo Simulation for Transformer Aging

A Monte Carlo simulation is designed to account for the uncertainties associated with different numbers and types of EVs charging on a distribution transformer, considering the unique harmonic emission characteristics of each EV model. By employing this statistical approach, the simulation outputs facilitate the estimation of transformer aging parameters, with the accuracy and reliability of the results improving as the number of iterations increases. The simulation process follows five key steps specifically tailored to the distribution transformer examined in this study:

- **Step 1**: Generate harmonic emission profiles for each EV during charging, utilizing from empirical measurement data.
- **Step 2**: Establish the maximum number of EVs that can charge simultaneously, considering the constraints imposed by the charging current.
- **Step 3**: Randomly select EVs and compute the vector summation of their individual harmonic components based on their respective harmonic emission characteristics.

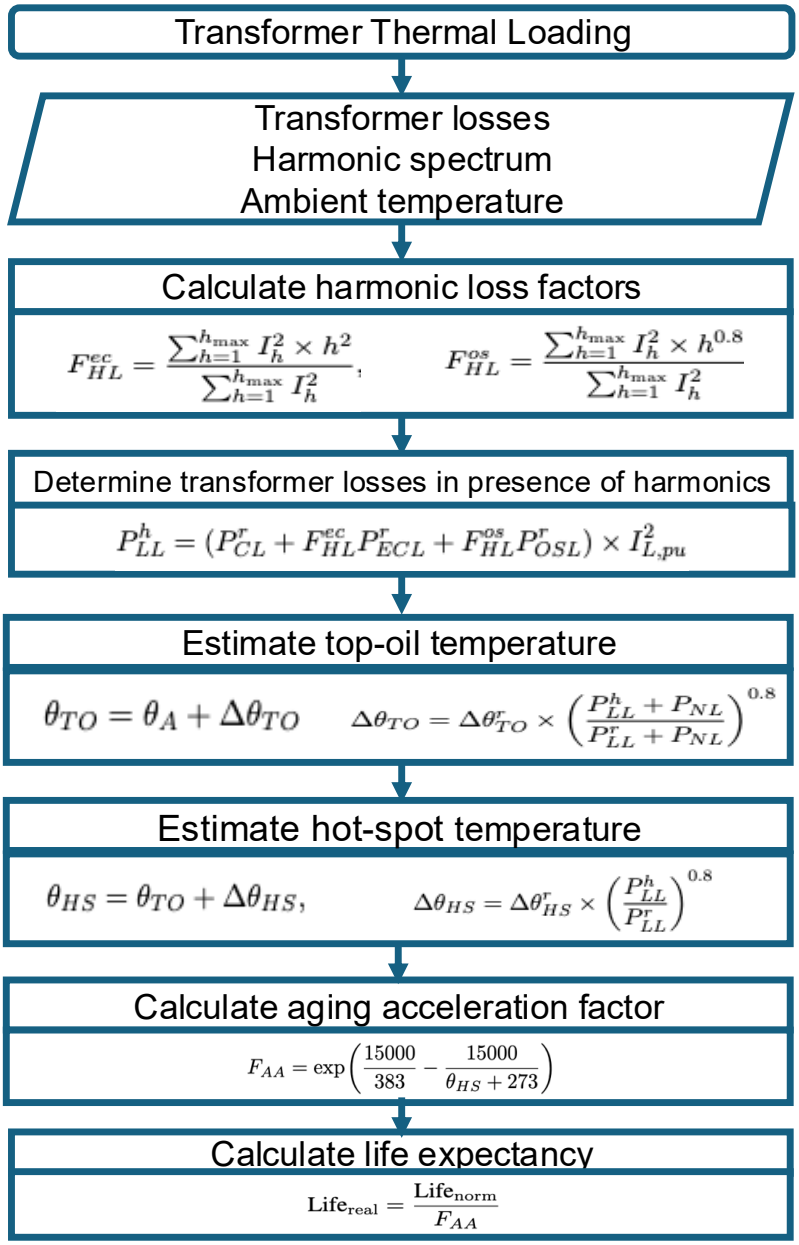


Figure 6.2: Flowchart illustrating the transformer aging assessment framework.

- **Step 4**: Evaluate transformer losses by integrating the aggregated harmonic contributions, followed by calculating the top-oil temperature, hot-spot temperature, aging acceleration factor, and estimated transformer lifespan.

- **Step 5**: Repeat Steps 3 and 4 for one million iterations to construct a comprehensive dataset for analyzing transformer losses and associated performance

metrics.

## 6.3 Case Study - I: Full Load Conditions

The electrical load imposed on a distribution transformer is a key factor in evaluating its capacity to accommodate EV charging. The maximum allowable number of EVs that can charge simultaneously without exceeding the transformer's rated capacity is directly influenced by the selected charging current. In this study, the number of EVs that can be charged concurrently is determined using (6.15), assuming that all vehicles charge at a consistent current level within a smart charging framework.

$$N = \frac{S \times \mathrm{PF}}{I \times V \times \phi}, \tag{6.15}$$

where $S$ represents the apparent power rating of the transformer, $PF$ denotes the power factor, $I$ corresponds to the charging current, $V$ is the single-phase voltage, and $\phi$ indicates the number of phases.

Considering a three-phase charging configuration with a single-phase voltage of 230 V, the maximum number of EVs capable of concurrent charging at a specific current level can be determined from the rated capacity of the transformer. For this analysis, a distribution transformer with representative parameters from the literature [210, 211], specifically rated at 160 kVA with a power factor of 0.95, is employed (see Table 6.1). Using these transformer specifications, the maximum simultaneous EV charging capacity ($N_{\mathrm{EV}}$) is computed as follows:

$$N = \frac{160{,}000 \times 0.95}{6 \times 230 \times 3} = 36.71 \approx 36,$$

This calculation shows that up to 36 EVs can be charged simultaneously without surpassing the transformer's rated capacity. However, if the charging current is increased to 15 A, the maximum number of EVs that can charge concurrently is reduced to:

Table 6.1: Overview of Technical Specifications of Distribution Transformer

| Parameter | Value | Parameter | Value |
|---|---|---|---|
| Rated power | 160 kVA | No-load loss | 330 W |
| Primary voltage | 11 kV | Full-load loss | 2650 W |
| Secondary voltage | 400 V | Ambient Temperature | 30 °C |
| Power factor | 0.95 | Rated top-oil temperature, $\Delta\theta^r_{TO}$ | 55 °C |
| Normal Insulation Life | 180,000 h | Rated hot-spot temperature, $\Delta\theta^r_{HS}$ | 25 °C |

$$N = \frac{160{,}000 \times 0.95}{15 \times 230 \times 3} = 14.69 \approx 14,$$

In this scenario, only 14 EVs can be charged concurrently without exceeding the transformer's rated capacity. This demonstrates the trade-off between charging current and the number of EVs that can be supported simultaneously. While higher charging currents reduce the total number of EVs that can be charged at once, lower charging currents enable more vehicles to connect. However, lower currents may also introduce additional operational challenges, such as prolonged charging durations or increased harmonic emissions, which could affect overall power quality.

### 6.3.1 Transformer Lifetime Analysis

This section examines the impact of harmonic currents generated by EV charging on a distribution transformer. Figure 6.3 presents a graphical summary of key outcomes, illustrating variations in hot-spot temperature (HST), aging acceleration factor ($F_{AA}$), and transformer lifetime. These visual representations provide crucial insights into the extent of harmonic-induced stress on transformer performance. The findings highlight the significant influence of charging current levels on the aging dynamics of a fully loaded 160 kVA transformer. At lower charging currents (e.g., 6 A), a greater number of EVs are required to fully load the transformer, whereas higher charging currents (e.g., 13–15 A) result in fewer EVs reaching the transformer's rated capacity. This underscores how different smart charging strategies can impact transformer degradation and overall longevity.

The HST graph in Figure 6.3a reveals that the highest HST occurs at lower charging

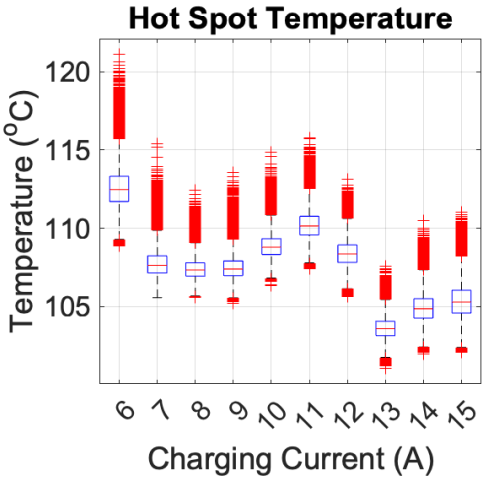


(a) Hotspot temperature (HST)

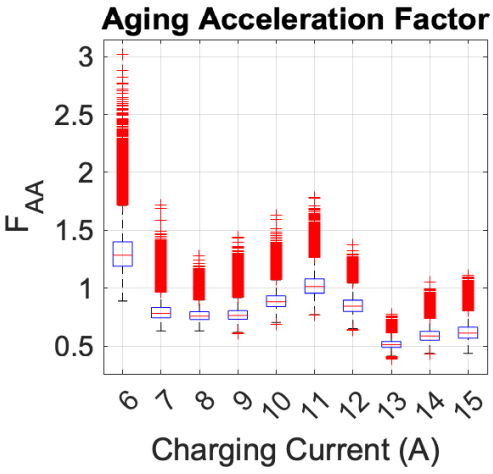


(b) Aging acceleration factor ($F_{AA}$)

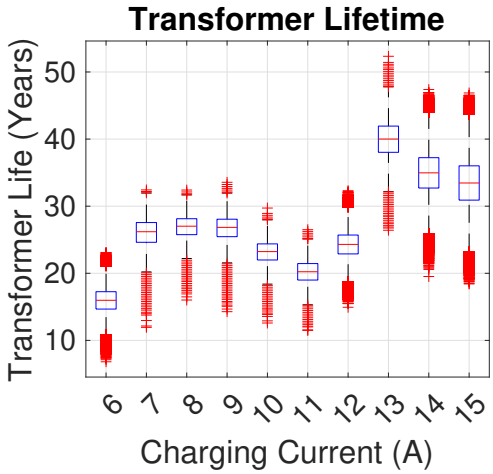


(c) Transformer lifetime

Figure 6.3: Overview of the transformer aging metrics under full load conditions.

currents, particularly at 6 A, where it approaches 120 °C. This increase is attributed to elevated harmonic distortions, which exacerbate thermal stress on the transformer. In contrast, at higher charging currents (e.g., 13–15 A), HST decreases and stabilizes around 105 °C. This trend indicates that transformers experience lower thermal stress at higher charging rates due to the reduction in harmonic-induced losses, thereby mitigating excessive heating effects.

The $F_{AA}$ graph in 6.3b follows a similar pattern to the HST, showing a sharp increase at lower charging currents. This indicates accelerated insulation aging, which

considerably shortens the transformer's operational lifespan. This effect is further reflected in the transformer lifetime graph in Figure 6.3c, where at 6 A, corresponding to the highest HST and $F_{AA}$ values, the projected transformer lifespan drops below 10 years in certain cases. In contrast, at higher charging currents (13–15 A), the combined reduction in thermal and harmonic stresses significantly extends the transformer lifespan, exceeding 40 years. These findings highlight the strong correlation between charging current, harmonic-induced thermal effects, and transformer aging.

These findings underscore the necessity of implementing harmonics-averse smart charging strategies to balance reducing electrical loading and minimizing harmonic-induced thermal stress on transformers. The adverse effects of harmonic distortions can be mitigated by strategically optimising charging currents, thereby prolonging the lifespan and enhancing the overall resilience of power distribution networks. This approach is crucial in ensuring grid infrastructure's long-term reliability and sustainability as EV adoption continues to grow.

Figure 6.4 illustrates the impact of harmonic distortion on transformer aging compared to a non-harmonic scenario across different charging currents. The findings reveal that harmonic distortion from smart charging significantly accelerates transformer aging. Nevertheless, at specific charging currents, particularly in the 13–15 A range, the aging rates under harmonic conditions closely match, or even slightly improve upon, those observed in the non-harmonic case. This indicates that the impact of harmonics on transformer thermal stress and aging is not purely linear, but varies depending on the loading level and the specific harmonic characteristics of the EV chargers involved. These insights highlight the necessity of harmonics-averse smart charging strategies to optimize transformer performance, ensuring both grid stability and the reliable integration of EVs into distribution networks.

### 6.3.2 Rule-based EV Charging Management

Based on the findings depicted in Figure 6.3 and Figure 6.4, the following *rule-based EV charging management* guidelines are suggested:

- **Optimal Charging Rate:** A charging current of 13 A provides the best balance

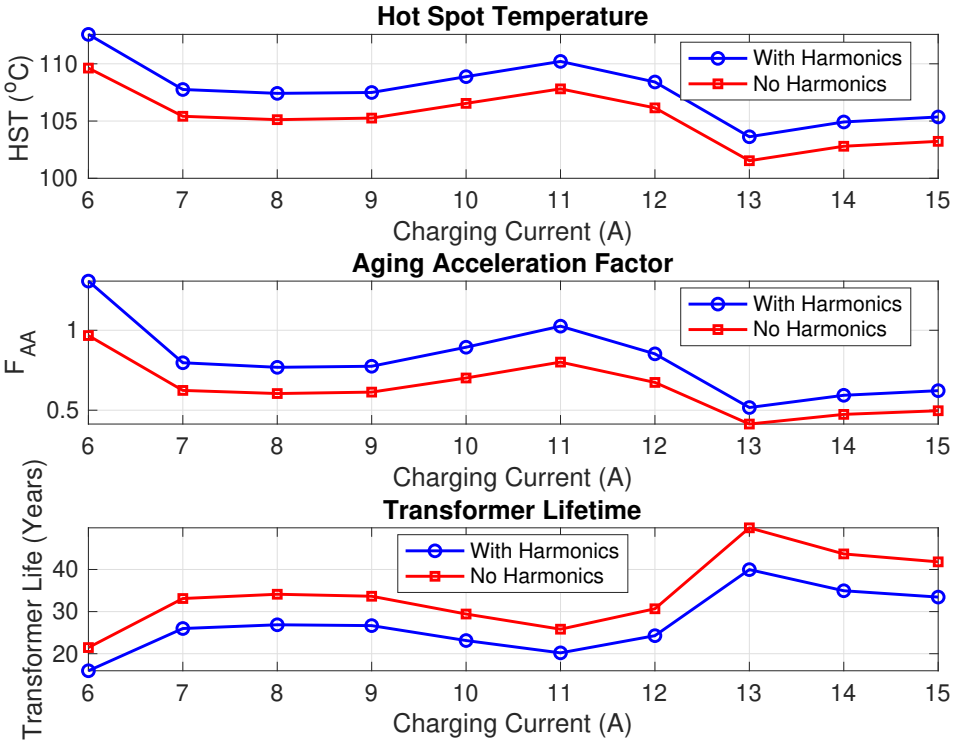


Figure 6.4: Comparison of transformer aging under harmonic distorted and non-harmonic distorted conditions.

by significantly reducing transformer aging while supporting a practical number of simultaneous EV connections (approximately 16 vehicles).

- **Acceptable Lower Rates:** When lower charging currents are required, such as during residential overnight charging, 9 A, 8 A, or 7 A are preferable, albeit extending the total charging duration.

- **Rates to Avoid:** Charging at 6 A, despite accommodating the highest number of simultaneous connections (up to 36 EVs), notably accelerates transformer aging. Thus, if lower current levels are unavoidable, opting for at least 7 A is recommended.

The rule-based, harmonics-averse EV charging management strategy for peak hours is illustrated in Figure 6.5. As shown, charging currents are dynamically modified

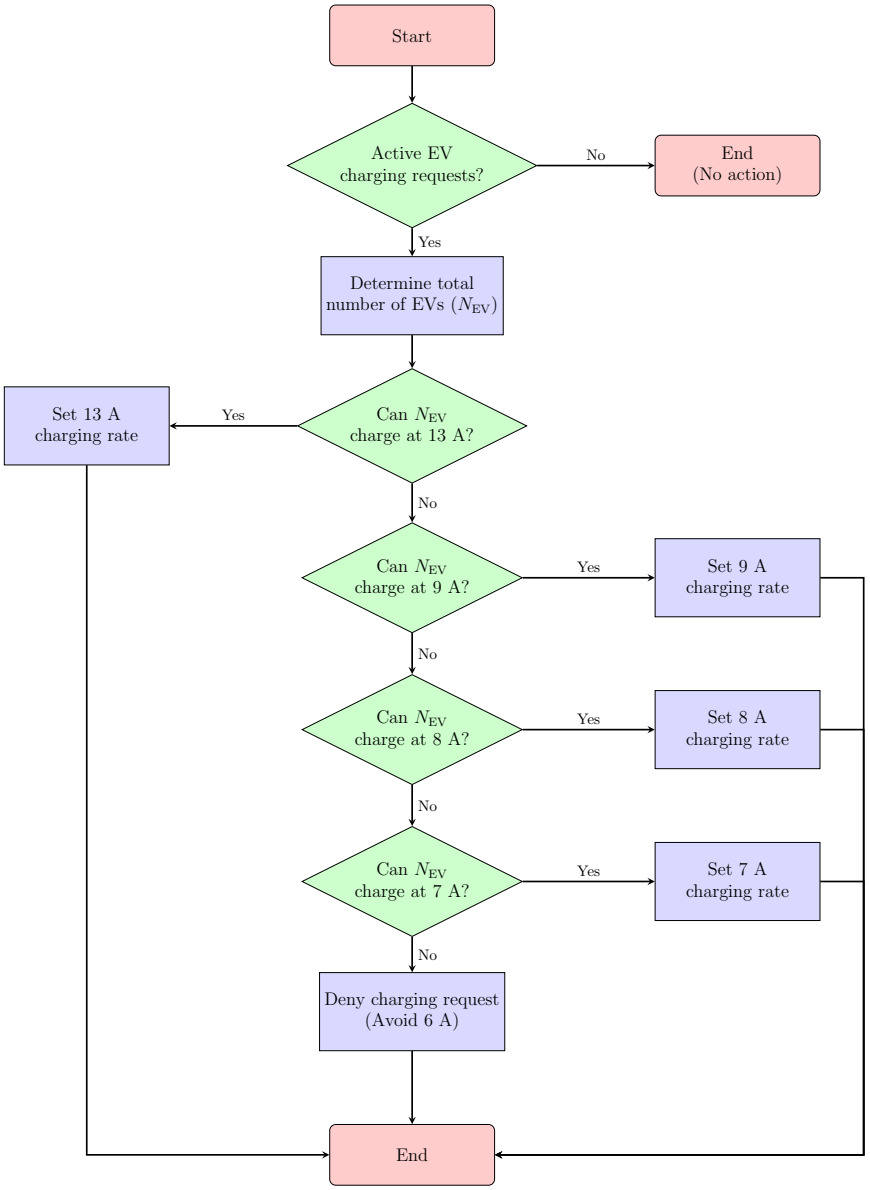


Figure 6.5: Rule-based EV charging management for new connection requests during peak hours.

according to the number of EVs connected, aiming to maintain transformer load within its rated capacity while mitigating harmonic distortions. Whenever an additional EV initiates a charging request, the available transformer capacity is recalculated using equation (6.15).

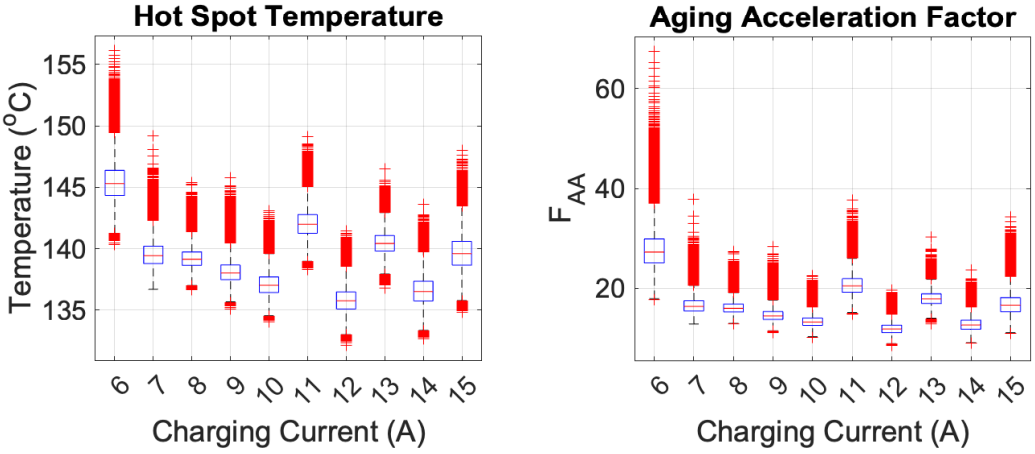


(a) Hotspot temperature (HST)

(b) Aging acceleration factor ($F_{AA}$)

(c) Transformer lifetime

Figure 6.6: Overview of transformer aging metrics under 25% transformer overloading allowance.

## 6.4 Case Study - II: Overloading Conditions

It should be highlighted that the suggested rule-based EV charging management method can easily be adapted to accommodate conditions permitting transformer overload. For example, Figure 6.6 presents simulation results for a scenario where the transformer operates with an overload margin of 25%, thus allowing additional EVs to connect. Nonetheless, adopting such an operating approach significantly compromises transformer longevity. Elevated HST surpassing 110 °C substantially accelerate $F_{AA}$, drastically reducing the transformer's lifespan. In this overloaded scenario, even a single

hour of operation corresponds to the $F_{AA}$ of approximately 15 to 20 times greater than full load conditions.

The proposed rule-based framework offers inherent flexibility and can be easily adjusted to handle transformer overloading scenarios with minimal alterations. For instance, instead of maintaining a fixed charging current of 13 A, a marginally reduced value such as 12 A could be implemented to alleviate excessive thermal stress. Additionally, the decision-making logic could be refined by introducing supplementary charging levels, like 10 A, thereby enhancing operational versatility. It is essential to highlight that charging at the lowest rate of 6 A is still not recommended due to its inefficiency and the potential for excessively prolonging charging durations.

It is crucial to highlight that the presented analysis specifically addresses scenarios involving heavily loaded networks. For partially loaded networks, the HST typically remains below the critical threshold of 110°C, making transformer aging a less critical problem. Nevertheless, compliance to harmonic distortion limits, as defined by industry standards such as IEEE 519 and IEC 61000, emerges as the primary operational constraint under these conditions. This distinction underscores the necessity of implementing harmonics-aware smart charging strategies, dynamically adjusting EV charging rates based on real-time transformer loading and harmonic conditions.

## 6.5 Chapter Summary

This chapter presented a comprehensive methodology to assess and mitigate the aging of distribution transformers under the influence of harmonic distortion caused by EV charging. It began by modelling transformer losses, dividing them into no-load and load losses. The latter included copper losses, winding eddy-current losses, and other stray losses. Due to harmonic components, these losses were shown to increase not only with current magnitude but also with frequency.

Harmonics were modelled through RMS current calculations that incorporated contributions from individual harmonic orders. The chapter introduced harmonic loss factors to quantify the effects of frequency on eddy-current and stray losses, emphasizing

that higher-order harmonics disproportionately accelerated transformer heating. This thermal impact was analyzed using models that estimated the top-oil and hot-spot temperatures, which were key indicators of transformer health. As the hot-spot temperature increased, the insulation deteriorated more rapidly, reducing transformer life. The chapter applied IEEE C57.91-2011 and IEEE C57.110-2018 standards to calculate an aging acceleration factor, which was then used to estimate the transformer's remaining lifespan under real-world harmonic-stressed conditions.

A Monte Carlo simulation was implemented to incorporate uncertainty in EV charging behaviour. This simulation accounted for variations in EV models, charging rates, and harmonic profiles. A case study focusing on a 160 kVA transformer under full-load conditions demonstrated how different charging currents influenced transformer aging. Results showed that lower charging currents (e.g., 6 A) allowed more EVs to connect but resulted in elevated harmonic emissions and thermal stress, significantly reducing transformer lifespan to under 10 years. In contrast, higher charging currents (e.g., 13–15 A) resulted in fewer EV connections but reduced harmonic distortion, yielding hot-spot temperatures below critical thresholds and extending the transformer lifespan beyond 40 years.

The findings led to a proposed rule-based EV charging management strategy. Charging at 13 A was recommended as the optimal rate, balancing the number of EVs supported and transformer longevity. Lower currents (7–9 A) were considered acceptable for overnight or low-demand periods, while 6 A was generally discouraged due to its severe impact on transformer aging.

A comparative analysis between harmonic and non-harmonic conditions revealed that harmonics significantly influenced transformer performance at lower charging currents, whereas at higher currents, the difference was negligible or even favourable. The chapter also examined transformer overloading scenarios, demonstrating that temporary overloading could accommodate more EVs, but at the cost of accelerated aging and drastically reduced transformer lifespan.

Overall, the chapter underscored the importance of harmonics-averse charging strategies tailored to transformer loading conditions. It highlighted that managing EV charg-

ing for both electrical load and harmonic emissions was essential to prolong transformer life, ensure power quality, and maintain the resilience of distribution networks as the adoption of EVs increases.

# Chapter 7

# Harmonics-Aware Smart Charging

The previous chapter investigated how harmonic emissions from EV smart charging influence transformer aging under heavily loaded conditions. However, the presence of harmonic distortion introduces distinct operational challenges in partially-loaded distribution networks. Although transformers in these scenarios may not be subject to significant thermal stress, the cumulative harmonic emissions from EV charging can negatively affect power quality. This leads to potential violations of harmonic distortion limits defined by international standards. Consequently, EV charging station operators and DNOs must ensure compliance with industry standards, including IEEE 519 and IEC 61000, which typically prescribe a THD limit of around 5%, with variations based on specific circuit and network configurations.

Given the increasing penetration of EVs and the widespread adoption of smart charging technologies that allow advanced scheduling of charging sessions, developing effective strategies for managing harmonic emissions is crucial. In this context, harmonics-aware smart charging emerges as a promising approach to actively minimize harmonic emissions while simultaneously achieving load balancing and peak shaving objectives.

Accordingly, this chapter has two primary objectives. First, it develops a harmonics-

aware smart charging framework tailored for partially-loaded networks, where transformer thermal limits are generally non-binding, but compliance with power-quality constraints, particularly THD limits, becomes the dominant operational requirement. Second, it provides a quantitative comparison between a conventional smart charging formulation that does not consider harmonic constraints and an extended formulation that explicitly enforces THD limits. This comparison is conducted using a large-scale EV parking lot case study, enabling an assessment of the trade-offs between power-quality compliance and the level of energy delivery requested by EV fleets.

The precise modelling and aggregation of harmonic emissions from multiple EV chargers are at the core of developing a *harmonics-aware smart charging* framework. This modelling is essential for effectively predicting the total harmonic current injected into the network and assessing compliance with established harmonic limits. Consequently, the following subsection outlines the methodology employed for individual EV harmonic modelling, the vector summation of harmonics, and the subsequent aggregation of harmonic emissions at the PCC. This comprehensive modelling approach serves as the foundation for evaluating and implementing harmonics-aware smart charging strategies.

## 7.1 Smart Charging Harmonic Emissions

The input data for this analysis were collected from controlled smart charging experiments, with comprehensive methodologies documented in Chapter 3. It should be reiterated that this investigation focuses exclusively on current harmonic emissions, as voltage harmonics exhibit negligible variation across different charging currents, as previously demonstrated in Chapter 4.

All vehicles in this study were charged in 1 A increments, starting from the minimum allowable charging current of 6 A. While previous chapters have used charging current (A) as the primary variable, this chapter adopts per-phase charging power (kW) for consistency and ease of comparison across different EVs. Charging power is calculated by multiplying the charging current by the single-phase voltage (230 V); thus, 6 A

Table 7.1: Quadratic polynomial fitting parameters for THD as a function of charging power.

| EV Model | $p_1$ | $p_2$ | $p_3$ | $R^2$ |
|---|---|---|---|---|
| Renault Zoe R90 | 0.26 | -3.41 | 16.14 | 0.9675 |
| Peugeot e-208 | 0.82 | -5.39 | 11.42 | 0.8634 |
| Nissan Leaf e+ | 0.41 | -4.16 | 13.98 | 0.9235 |
| VW ID.3 Pro | 0.73 | -4.63 | 9.36 | 0.9734 |
| Renault Zoe ZE50 | 0.48 | -5.26 | 18.92 | 0.9681 |
| VW ID.4 Pro | 0.86 | -5.26 | 10.28 | 0.9167 |
| Tesla Model Y Long Range | 1.00 | -7.17 | 18.07 | 0.9920 |
| Peugeot e-2008 | 1.94 | -15.76 | 42.74 | 0.9928 |

corresponds to a power of 1.38 kW.

As previously emphasized in this thesis, an inverse relationship exists between charging rate and harmonic emissions. This trend is further investigated here using the power-based representation. For reference, the maximum single-phase charging power is $16\,\mathrm{A} \times 230\,\mathrm{V} = 3.68\,\mathrm{kW}$, while three-phase systems can support up to 11 kW. This standardized power-based approach enables a clearer comparative analysis of harmonic behaviour across all tested EVs.

To characterize the relationship between harmonic behaviour and charging power, a quadratic polynomial fit was applied to each EV dataset as follows:

$$THD(x) = p_1 x^2 + p_2 x + p_3,$$

where $x$ represents the per-phase charging power in kilowatts, and $p_1$, $p_2$, and $p_3$ are the fitted polynomial coefficients. This analytical formulation allows the harmonic behaviour to be embedded within optimization-based smart charging strategies, effectively capturing the nonlinear nature of the THD–power relationship.

As presented in Table 7.1, the polynomial models demonstrate strong predictive performance, with coefficients of determination ($R^2$) consistently above 0.86, in several instances exceeding 0.99. These convex quadratic models form the basis for the optimization framework discussed in Section 7.3. Notably, this modelling approach addresses a key limitation of the experimental data, where charging rates are restricted to

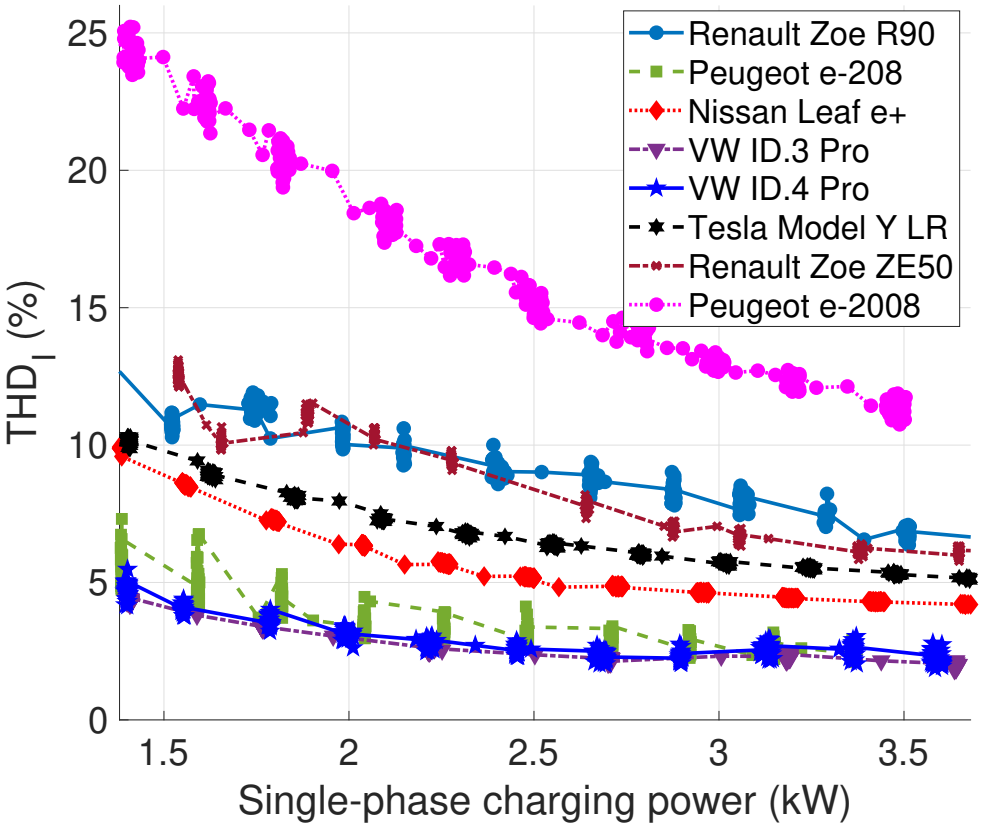


Figure 7.1: Relationship between EV charging power and THD (per phase).

discrete values due to measurement constraints. By employing continuous polynomial functions, the analysis can accommodate a broader and more flexible range of charging rates, offering improved applicability for real-world optimization and control strategies.

Figure 7.1 illustrates the overall correlation between per-phase charging power and THD, highlighting a general decline in THD with increasing charging power. This trend underpins the harmonics-aware smart charging strategy developed in this study, allowing for designing EV charging schedules that simultaneously consider grid capacity constraints and harmonic distortion compliance.

## 7.2 Harmonics Modelling

While modelling the harmonic emissions of a single EV can be achieved using the polynomial fitting parameters outlined in Table 7.1, estimating the aggregate harmonic emissions from multiple EVs, regardless of whether they are the same model charging at different rates or various models operating at distinct power levels, poses significant challenges. This complexity arises from the absence of a closed-form expression that simultaneously addresses both the amplitude and phase angle of individual harmonic components.

The combined harmonic emissions from multiple EVs must be computed using vector algebra, where each harmonic order is represented as a phasor incorporating both magnitude and phase angle. Specifically, an individual harmonic can be expressed in exponential form as $A \cdot e^{j\theta}$, or in rectangular form as $A \cdot (\cos(\theta) + j\sin(\theta))$, with $A$ denoting the amplitude and $\theta$ the corresponding phase angle. When multiple EVs contribute to the same harmonic order, their phasor components are summed vectorially. The resulting aggregated vector is then used to calculate the THD that the formulation provided earlier in Chapter 4.

Incorporating vector summation of harmonics into optimization frameworks is inherently challenging, as the individual harmonic magnitudes, $I_h$, and their corresponding phase angles may cancel out unpredictably. Moreover, the existing literature lacks analytical models that adequately represent harmonic cancellation effects arising from multiple EVs acting as harmonic sources. Without closed-form expressions, integrating this behavior into optimization would require a brute-force search through all possible charging configurations. This approach becomes computationally impractical for real-time or large-scale implementations.

To overcome this challenge, we introduce a computationally efficient approximation that provides a conservative upper bound for THD. As demonstrated both empirically and through a Monte Carlo simulation in Chapter 5, simultaneous charging of multiple EVs leads to a natural harmonic cancellation effect, whereby the combined THD is typically lower than the simple sum of individual contributions. The reduction in

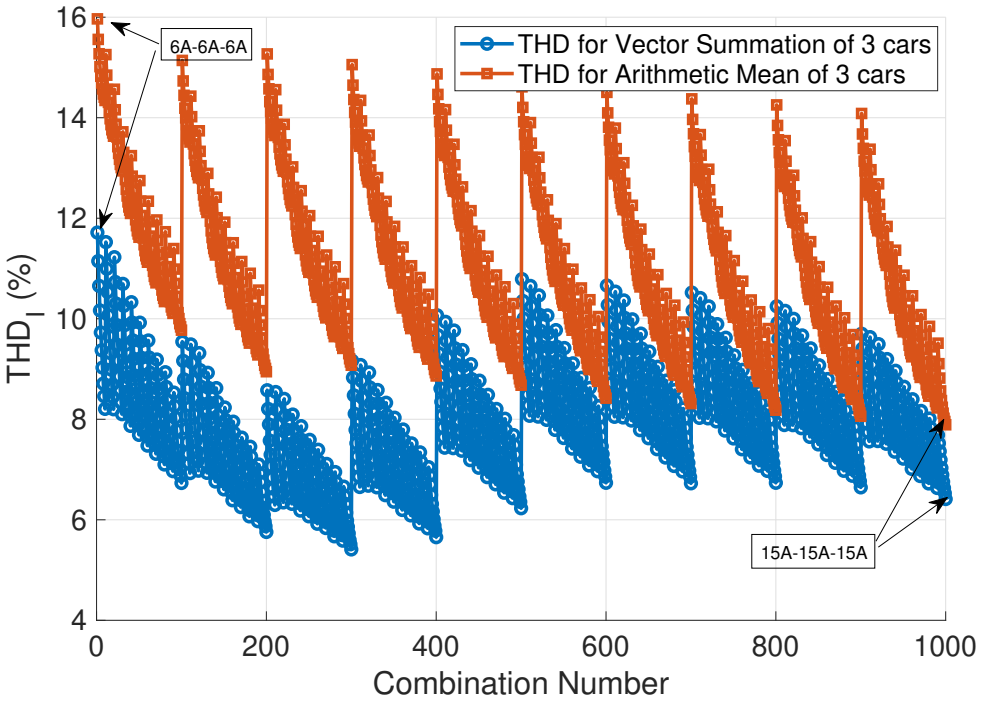


Figure 7.2: Vector summation versus arithmetic mean comparison of THD with 3 EVs charging

THD occurs due to variations in phase angles, which lead to partial cancellation of the harmonic components. From a mathematical standpoint, this phenomenon is attributed to phasor addition, where each harmonic order is projected using $\cos(\theta)$ and $\sin(\theta)$, thereby reducing the magnitude of the resulting vector.

Consequently, the arithmetic average of individual THD values is a practical and conservative estimate for the overall THD. This approach enables the optimization process to bypass computationally intensive vector summations while ensuring compliance with THD constraints. Letting $THD_i$ represent the harmonic contribution from the $i^{\text{th}}$ EV, the aggregated approximation can be expressed as:

$$THD_{\text{total}} \lessapprox \frac{1}{N} \sum_{i=1}^{N} THD_i, \tag{7.1}$$

where $N$ is the total number of simultaneously charging EVs.

Figure 7.2 compares the arithmetic mean and vector summation of current har-

monic emissions for three EV models, Tesla Model Y Long Range, Peugeot e-2008, and Renault Zoe R90, charged simultaneously at the same current levels. The x-axis denotes various charging combinations, ranging from the lowest setting (6 A, 6 A, 6 A) to the highest (15 A, 15 A, 15 A). The results clearly demonstrate that the arithmetic mean consistently overestimates the total THD compared to vector-based summation. This finding supports the use of the arithmetic mean as a conservative upper-bound approximation.

This approximation significantly simplifies the implementation of harmonics-aware smart charging optimization. Instead of performing complex vector-based harmonic summations across all possible EV charging rate combinations, the optimization process can impose THD constraints using the arithmetic mean derived from the fitted polynomial models. This approach facilitates the practical application of harmonics-aware smart charging in real-world scenarios, such as large-scale parking areas and public charging stations, without introducing excessive computational burden. Consequently, this section lays the groundwork for a mathematically efficient method to estimate the cumulative harmonic emissions from multiple EVs, which serves as the foundation for the optimization strategy introduced in the following section.

## 7.3 Harmonics-Aware Smart Charging

This section outlines the mathematical formulation of two optimization problems related to smart charging. The first represents a conventional smart charging strategy based on practical charging rates, while the second builds upon it by explicitly integrating THD constraints into the optimization framework.

Let $i = \{1, 2, \ldots, N\}$ represent the index set of EVs arriving at a charging station that operates over discrete time intervals $t = \{1, 2, \ldots, T\}$. Each vehicle arrives at time slot $a_i \in T$ and departs at $d_i \in T$, where the charging window $d_i - a_i$ must be strictly greater than a minimum threshold $M$ for all $i$, ensuring sufficient time for participation in the charging process. Accordingly, the first constraint enforces a

minimum connection duration and is formulated as:

$$d_i - a_i \geq M, \quad \forall i. \tag{7.2}$$

Let $k = \{1, 2, \ldots, K\}$ represent the index set of EV types (for example, $k = 1$ corresponds to the Tesla Model Y). Each EV $i$ has a charging requirement $D_i$ in kilowatt-hours (kWh). The charging decision for EV $i$ is captured by the vector $\boldsymbol{x_i} \in \mathbb{R}^{1\times T}$, defined over the planning horizon $T$. Furthermore, let $\boldsymbol{x^t}$ denote the vector comprising the charging rates of all EVs at a specific time slot $t$.

Due to technical limitations, charging currents can only take specific values (charging constraints): they can either be zero (indicating that no charging is occurring) or fall within the range of 6 A to 16 A. These currents correspond to per-phase charging powers ranging from $c_{\min} = 1.38\,\text{kW}$ to $c_{\max} = 3.68\,\text{kW}$. Values below 6 A are technically infeasible, resulting in a discontinuous set of allowable charging rates. Although all chargers are assumed to operate in three-phase mode, this analysis is conducted on a per-phase basis. The constraint on charging power is therefore defined as follows [212]:

$$\boldsymbol{x_i}(t) \in \{0\} \cup [c_{\min}, c_{\max}], \quad \forall i, \forall t. \tag{7.3}$$

In addition, the total charging power drawn by all EVs at any given time $t$ must not exceed the system-wide capacity limit $C$, which reflects physical infrastructure constraints such as transformer and feeder capabilities. This system-level (capacity) constraint is formulated as:

$$\sum_{i=1}^{N} \boldsymbol{x_i}(t) \leq C, \quad \forall t, \tag{7.4}$$

Here, $C$ is typically defined as a fraction of the maximum peak load capacity, for example, $C = 0.75 \times N \times 3.68\,\text{kW}$, which reflects a 25% reduction in required infrastructure capacity enabled by coordinated smart charging. This formulation underscores the importance of smart charging in avoiding costly over-dimensioning of grid infrastructure to accommodate simultaneous peak EV demand.

To maintain service quality, a minimum energy delivery constraint $D_{\min}$ is enforced

to ensure that each EV receives at least a certain proportion of its total energy demand $D_i$. This requirement is formulated as

$$\sum_{t=a_i}^{d_i} \boldsymbol{x_i}(t) \geq D_{\min} \times D_i, \quad \forall i. \tag{7.5}$$

A specific value for $D_{\min}$ is 0.9, which corresponds to delivering 90% of the requested energy, ensuring a balance between customer satisfaction and operational flexibility.

### 7.3.1 Optimization Problem I: Smart Charging without THD Constraints

The aim of the first optimization problem is to ensure fair charging by minimizing the discrepancy between each EV's actual allocated energy $\boldsymbol{x_i}$ and its requested energy demand $D_i$. Assuming uniform priority across all EVs, the objective function is expressed as:

$$\sum_{i=1}^{N} \left( \frac{\sum_{t=a_i}^{d_i} \boldsymbol{x_i}(t)}{D_i} - 1 \right)^2. \tag{7.6}$$

Accordingly, **Optimization Problem I** is formulated as:

$$\begin{aligned} \text{Minimize:} \quad & (7.6) \\ \text{Subject to:} \quad & (7.2),\ (7.3),\ (7.4),\ (7.5). \end{aligned}$$

Since the optimization is performed over 1-hour time intervals, the charging power vector $x(t)$ expressed in kW is numerically equal to the energy delivered in kWh within each time slot. This enables a direct comparison with the energy demand $D$ used in the constraint formulation.

### 7.3.2 Optimization Problem II: Smart Charging with THD constraints

The second optimization formulation builds upon the first optimization by introducing a constraint on THD. Specifically, at each time slot $t$, the cumulative THD, computed based on the set of active EV charging rates $\boldsymbol{x^t}$ and their corresponding EV types $\boldsymbol{k^t}$,

must remain below a defined threshold $h_{\text{lim}}$, typically set to 5%. This requirement is expressed by the following constraint:

$$\text{THD}(\boldsymbol{x^t}, \boldsymbol{k^t}) \leq h_{\text{lim}}, \quad \forall t. \tag{7.7}$$

Beyond minimizing deviations from requested energy demands, the objective function includes a penalty term for any THD violations. This penalized objective is expressed as:

$$\sum_{i=1}^{N} \left( \frac{\sum_{t=a_i}^{d_i} \boldsymbol{x_i}(t)}{D_i} - 1 \right)^2 + \omega \sum_{t \in \bar{T}} \left( \text{THD}(\boldsymbol{x^t}, \boldsymbol{k^t}) - h_{\text{lim}} \right)^2, \tag{7.8}$$

where $\bar{T}$ denotes the set of time slots in which the THD limit is exceeded, and $\omega \gg 0$ is a large penalty coefficient that enforces the harmonic constraint.

Thus, **Optimization Problem II** is defined as:

$$\begin{aligned} \text{Minimize:} \quad & (7.8) \\ \text{Subject to:} \quad & (7.2),\ (7.3),\ (7.4),\ (7.5),\ (7.7). \end{aligned}$$

To summarize, Optimization Problem I prioritizes fair and efficient charging across EVs, whereas Optimization Problem II enhances this framework by directly integrating harmonic distortion limits. This integration enables smart charging strategies that comply with power quality standards.

## 7.4 Particle Swarm Optimization

Particle Swarm Optimization (PSO) [213] is selected as the solution methodology for both optimization problems presented in this chapter. Prior to this choice, several alternative techniques, including Genetic Algorithms and gradient-based nonlinear solvers, were evaluated. However, these approaches either failed to converge or produced infeasible solutions due to the nonconvex and discontinuous structure of the feasible region arising from discrete EV charging rates specified in equation (7.3) and THD constraints.

In contrast, PSO demonstrated reliable convergence and consistently generated feasible solutions while maintaining computational efficiency. Its ability to handle discontinuities, mixed-integer decision variables, and non-differentiable objective functions makes it particularly well suited for the harmonics-aware smart charging problem considered in this study [214, 215].

PSO is a population-based, stochastic optimization algorithm inspired by the collective behaviour of social organisms, such as birds flocking or fish schooling [214]. It operates by initializing a population of candidate solutions, known as "particles", that explore the multidimensional solution space in search of an optimal configuration. Let $P$ denote the total number of particles. At each iteration, every particle $p \in \{1, 2, \ldots, P\}$ maintains two key attributes: its current position $X_p$, which represents a candidate solution (e.g., charging schedule), and a velocity vector $V_p$, which determines its direction and speed of movement through the solution space.

Each particle evaluates the objective function at its current position and keeps track of the best solution it has encountered thus far, denoted as the personal best position $P_p$. Simultaneously, the global best solution $G$ found by the entire swarm is also recorded. The position and velocity of each particle are updated at each iteration based on both individual experience and social learning mechanisms. A weighted combination of the following components governs the velocity update rule:

- The *inertia term ($w$)*, which retains a portion of the previous velocity to maintain momentum.
- The *cognitive component ($c_1$)*, which encourages the particle to return to its personal best position.
- The *social component ($c_2$)*, which pulls the particle toward the global best solution found by the swarm.

Mathematically, the velocity and position of particle $p$ at iteration $t$ are updated as follows [216]:

$$V_p^{(t+1)} = wV_p^{(t)} + c_1 r_1 (P_p - X_p^{(t)}) + c_2 r_2 (G - X_p^{(t)}), \tag{7.9}$$

$$X_p^{(t+1)} = X_p^{(t)} + V_p^{(t+1)}, \tag{7.10}$$

where $w$ is the inertia weight, $c_1$ and $c_2$ are the cognitive and social acceleration coefficients, respectively, and $r_1$ and $r_2$ are uniformly distributed random numbers in [0, 1]. These parameters govern the balance between exploration (global search) and exploitation (local refinement), and must be carefully selected to ensure convergence and solution quality.

A more detailed PSO implementation tailored for EV charging can be found in [217], where similar methodologies are adapted for real-time scheduling scenarios. In the context of this thesis, PSO serves as a powerful and flexible meta-heuristic for solving complex optimization problems arising from large-scale EV integration, particularly in the presence of nonlinear harmonic behaviours and infrastructure constraints. If a proposed solution violates any constraints, such as system capacity or THD limits, a penalty is added to the objective value to discourage infeasible configurations.

## 7.5 Water Filling Algorithm

The optimization framework employed in this study is detailed in Algorithm 2, which is based on a PSO-driven optimization strategy. A key component of this framework is the subroutine RepairSolution, which ensures that all operational constraints are satisfied. These include the constraints defined in (7.2), (7.3), (7.4), (7.5), and (7.7). Furthermore, RepairSolution monitors the set of actively charging EVs dynamically, updating the corresponding THD contributions in real-time. This includes removing EVs that have either completed their charging session or are temporarily deactivated within the current scheduling interval.

To guarantee compliance with both the charging rate constraint (7.3) and the minimum energy delivery requirement (7.5), the RepairSolution subroutine incorporates a "Water Filling" strategy. This mechanism proceeds through the following steps:

**Algorithm 2** PSO-based Harmonics-Aware Smart Charging Optimization

**Input:** EV data ($N$, $\{a_i, d_i, D_i\}$, types), charging constraints ((7.3), (7.4), (7.5), (7.7)), PSO parameters (swarm size, max iterations, inertia $w$, coefficients $c_1$, $c_2$)
Generate arrival, departure, and demand profiles for EVs
**for** each scenario (Optimization Problem I: $\omega = 0$, Optimization Problem II: $\omega > 0$) **do**
    Initialize PSO swarm: random charging schedules $x_p$ and velocities $v_p$
    Apply RepairSolution to each $x_p$ to ensure feasibility
    Evaluate objective ((7.6) or (7.8)), update $p_{\text{best}}$
    Identify global best $g_{\text{best}}$
    **for** $iter = 1$ to max iterations **do**
        **for** each particle $p$ **do**
            Apply RepairSolution to $x_p$
            Evaluate objective, update $p_{\text{best}}$ and $g_{\text{best}}$ if improved
            Update velocity:

$$v_p \leftarrow w v_p + c_1(p_{\text{best}} - x_p) + c_2(g_{\text{best}} - x_p)$$

            Update position:

$$x_p \leftarrow x_p + v_p$$

            Enforce constraints (7.3), (7.4), (7.5), (7.7)
        **end for**
    **end for**
    **Output:** Optimal charging schedule $x_{\text{opt}} = \text{RepairSolution}(g_{\text{best}})$
**end for**

1. Initially, any charging rate below the minimum threshold $c_{\min}$ is set to zero:

$$x_i(t) = 0, \quad \text{if } x_i(t) < c_{\min}, \quad \forall i, t. \tag{7.11}$$

2. Next, if the total energy delivered does not satisfy the minimum required amount $D_{\min} \times D_i$, the algorithm assigns the minimum allowable charging rate $c_{\min}$ to idle time slots, continuing this process until the requirement is met or no inactive slots remain.

3. Should the demand constraint still remain unmet, the algorithm uniformly increases the charging rates of all active time slots, initially set to $c_{\min}$, in a stepwise manner up to $c_{\max}$, ensuring that the aggregate charging load at each time slot does not violate the system-wide capacity constraint given by (7.4).

4. Lastly, for each time slot $t$, THD is evaluated against the threshold defined in (7.7). If the THD exceeds the allowed limit $h_{\text{lim}}$, the algorithm alters the charging

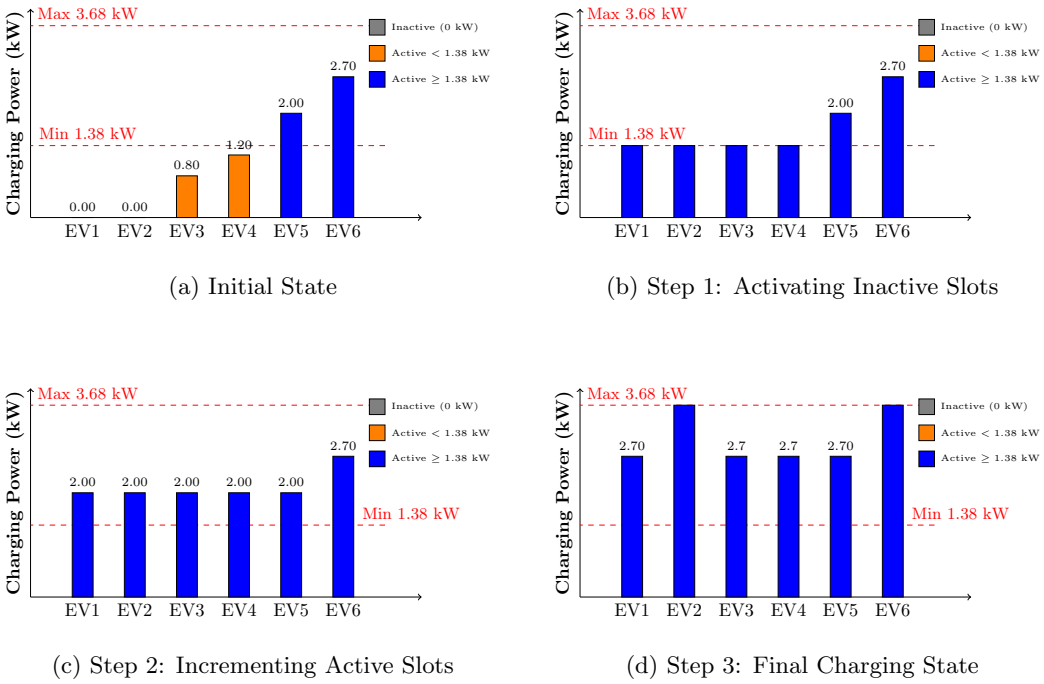


(a) Initial State

(b) Step 1: Activating Inactive Slots

(c) Step 2: Incrementing Active Slots

(d) Step 3: Final Charging State

Figure 7.3: Step-by-step illustration of the Water Filling Algorithm for dynamic slot allocation.

rates of EVs that contribute most significantly to the distortion, repeating this process until the constraint is satisfied.

This structured and iterative Water Filling approach ensures that the charging schedules adhere to all key constraints while focusing on meeting user energy requirements and staying within harmonic distortion limits.

Figure 7.3 depicts a sample scenario illustrating the Water Filling Algorithm. In the initial configuration (Figure 7.3a), EV1 and EV2 are not charging (0 kW), while the remaining vehicles are charging at different power levels. According to the limits defined in (7.3), the allowable charging range is between $c_{\min} = 1.38\,\text{kW}$ and $c_{\max} = 3.68\,\text{kW}$. Charging slots with power below $c_{\min}$ (e.g., EV3 at 0.8 kW, EV4 at 1.2 kW) are shown in orange, whereas those meeting or exceeding the minimum threshold (e.g., EV5 at 2.0 kW, EV6 at 2.7 kW) are displayed in blue.

In Step 1 (Figure 7.3b), all EVs that were either inactive or operating below the

minimum threshold are brought up to $c_{\min}$. As a result, EV1 and EV2 are activated at 1.38 kW, while EV3 and EV4 are raised to the same level. EV5 and EV6 remain unchanged, as their initial charging levels already exceed the minimum requirement.

In Step 2 (Figure 7.3c), if the minimum energy demand is still unmet, the algorithm uniformly increases all active charging slots until the demand is satisfied or the upper bound $c_{\max}$ is reached. For example, EV1 to EV5 are raised to 2.0 kW, while EV6 remains at 2.7 kW.

In Step 3 (Figure 7.3d), the final charging allocation is shown: each EV receives at least $c_{\min}$, and some reach the maximum limit. In this case, EV2 and EV6 are restricted at 3.68 kW, while the remaining vehicles charge at approximately 2.7 kW, thus maximizing available capacity while meeting demand and complying with harmonic constraints.

## 7.6 Case-Study: Large-scale EV Parking Lots

A large-scale EV parking lot scenario is considered for evaluation as a case-study. A total of 200 EVs are assumed to request charging services at a workplace facility operating between 6:00 am and 11:00 pm. Each vehicle remains connected for a minimum of 8 hours, reflecting typical workday parking behaviour. To simulate realistic variability in user behaviour, both arrival and departure times are generated using a uniform distribution. Similarly, per-phase charging demands are uniformly distributed between 20 kWh and 30 kWh, corresponding to a total demand of 60 kWh to 90 kWh for three-phase charging systems.

The EV fleet consists of $k = 8$ distinct vehicle types, introduced in Section 3, with each vehicle selected with equal probability (0.125). The charging infrastructure comprises standardized 11 kW three-phase AC chargers, equivalent to 3.68 kW per phase. According to IEEE 519-2014 standards, the THD limit is set to 5%. The system operator guarantees that at least 90% of each vehicle's requested energy is delivered. Charging power is bounded between $c_{\min} = 1.38$ kW (corresponding to 6 A) and $c_{\max} = 3.68$ kW (16 A), with 0 kW representing idle states. The per-phase capacity

constraint is set to approximately 480 kW, computed as $200 \times 0.65 \times 3.68$. Each EV's harmonic behaviour is represented using second-order polynomial models, as detailed in Table 7.1.

The PSO algorithm is configured as follows, based on values commonly adopted in the literature [218], and further tuned through experimental trials:

- Swarm size: 100
- Maximum number of iterations: 500
- Inertia weight: 0.7
- Cognitive coefficient: 1.4
- Social coefficient: 1.4

These parameters aim to balance computational time and solution accuracy in the large-scale optimization problem.

Figure 7.4 illustrates the arrival and departure distributions of EVs, along with the number of actively connected vehicles over the day. The outcomes of the simulation are shown in Figures 7.5 and 7.6, which compare the performance of two distinct optimization frameworks: Optimization Problem I, which does not include THD constraints, and Optimization Problem II, which incorporates THD limits into the scheduling process.

Figure 7.5 shows the hourly power consumption profile of the charging station, which closely aligns with the EV arrival and departure trends illustrated in Figure 7.4. The peak load is observed around 3:00 pm, when up to 198 EVs are connected, collectively requesting approximately 450 kW per phase. Figure 7.6 provides a comparison of THD levels under both optimization approaches. As anticipated, the conventional smart charging framework without THD enforcement exceeds the 5% threshold during much of the peak period. In contrast, Optimization Problem II, which incorporates THD constraints, successfully maintains harmonic distortion within acceptable limits. To ensure strict adherence to the THD requirement, the penalty coefficient $\omega$ is set to one million, as lower values were found to permit constraint violations.

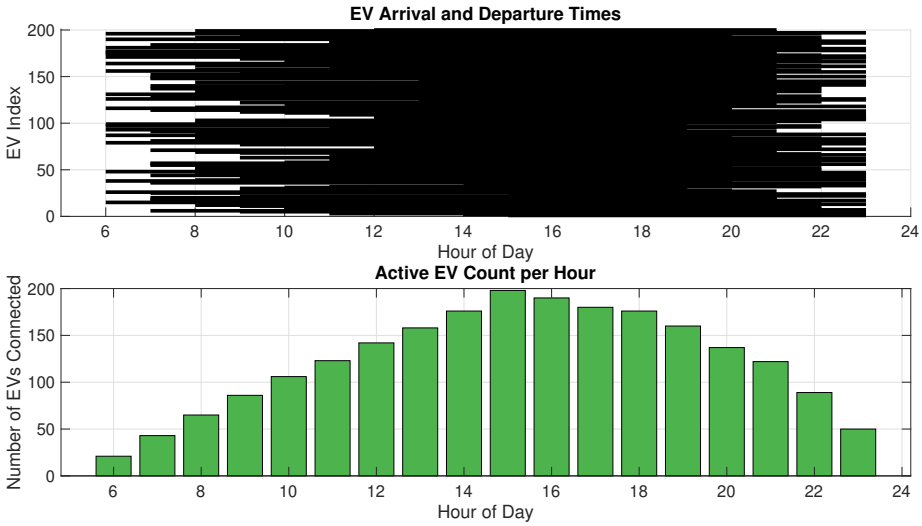


Figure 7.4: Arrival/departure times and the number of active EVs at the charging station.

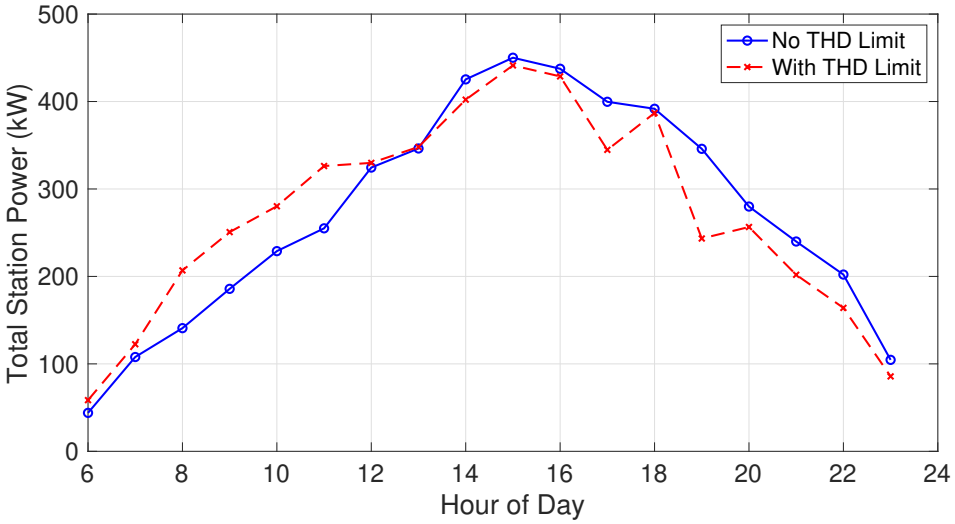


Figure 7.5: Hourly electrical power usage for Optimization Problems I (no THD limit) and II (with THD limit).

The effectiveness of the THD-aware smart charging framework in maintaining harmonic levels within acceptable limits stems from two key operational strategies. First, as shown in Figure 7.1, charging at higher power levels tends to reduce individual harmonic emissions. Consequently, the algorithm prioritizes operating EVs at their maximum allowable charging rates whenever possible. Second, during intervals when

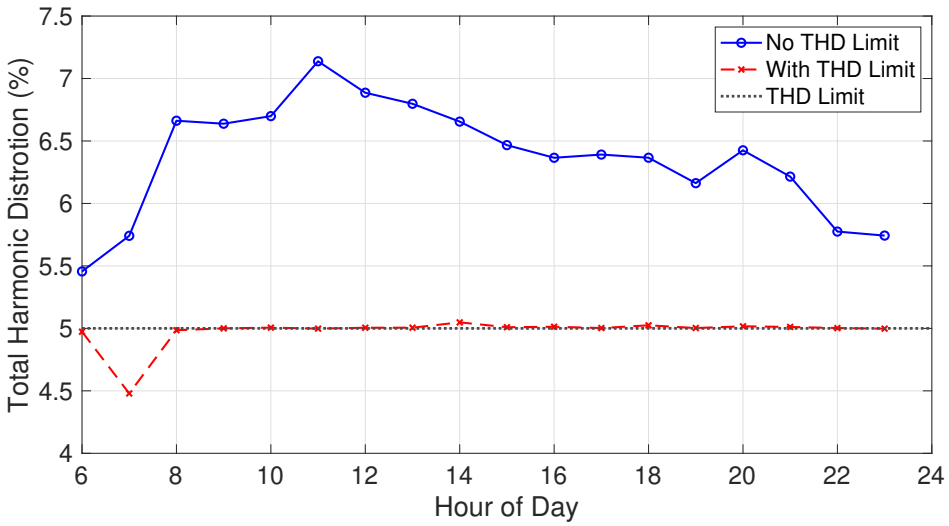


Figure 7.6: THD comparison for both optimization cases.

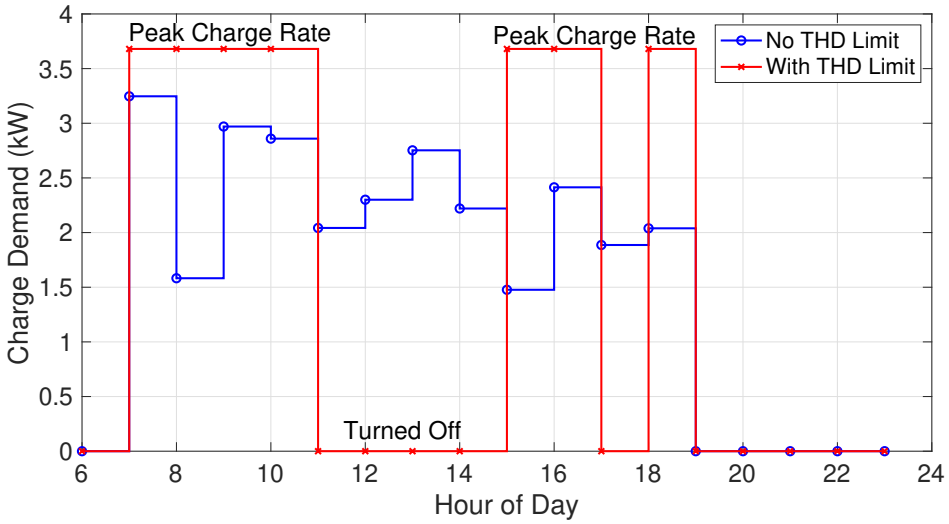


Figure 7.7: Example of THD-aware smart charging for Peugeot e-2008.

the THD approaches the regulatory threshold, selected EVs are temporarily deactivated, thereby eliminating their harmonic contributions. These two principles form the foundation of the harmonics-aware smart charging mechanism embedded in Optimization Problem II. A representative example is shown in Figure 7.7, where the charging profile of a Peugeot e-2008 reveals two intervals, between 11:00 am and 3:00 pm, and again from 5:00 pm to 6:00 pm, during which the vehicle is completely turned off to

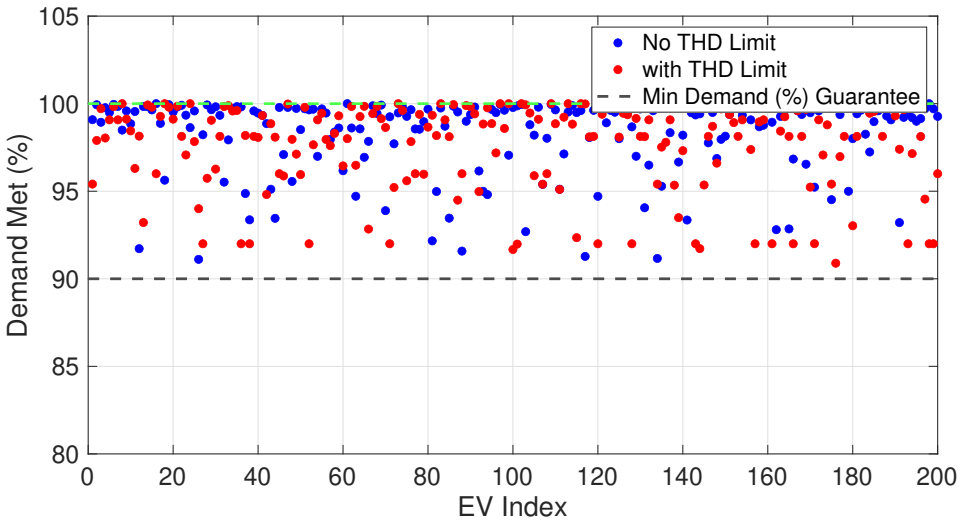


Figure 7.8: Demand completion rates for 200 EVs under both optimization frameworks.

comply with THD limits. Outside of these periods, it charges at its full rated capacity.

It is essential to assess the impact of these strategies on overall energy delivery. Figure 7.8 illustrates the demand completion rates for both optimization approaches. In both scenarios, the 90% minimum energy delivery requirement is met for all EVs. Under the THD-constrained optimization framework, 97.6% of the total requested energy is delivered, compared to 98.9% in the unconstrained case. This minor reduction represents an acceptable compromise for ensuring compliance with power quality standards. Additionally, fewer than 1.5% of EVs fail to receive their full requested energy in both scenarios. This deficit typically occurs when the requested energy exceeds what can be physically delivered within the parking period. For instance, if an EV requests 30 kWh but is limited to a maximum delivery of $3.68 \times 8 = 29.44$ kWh per phase over 8 hours, it would not receive the full amount. Despite these constraints, the harmonics-aware smart charging approach effectively maintains THD within limits without relying on additional hardware solutions such as active filtering devices.

Finally, it is important to highlight that, as demonstrated in Section 4, certain EV models, such as the Peugeot e-2008, generate significantly higher levels of harmonic distortion than others. The existence of such vehicles can reduce the effectiveness of station-level THD mitigation. Therefore, DNOs may consider implementing measures

such as limiting the connection of high-THD EVs during peak periods or mandating the use of vehicles with harmonics-compliant on-board chargers.

## 7.7 Chapter Summary

This chapter addressed the challenges of harmonic distortion in partially-loaded distribution networks, where thermal stress on transformers was minimal. However, cumulative harmonic emissions from EV charging could lead to violations of power quality standards such as IEEE 519. It highlighted the need for harmonics-aware smart charging strategies that actively managed THD while achieving typical objectives like load balancing and demand fulfilment.

The chapter began by modelling the harmonic emissions of individual EVs using second-order polynomial functions that related THD to per-phase charging power. These models enabled the integration of harmonic constraints into optimization frameworks and provided a continuous representation of harmonic behaviour for scheduling purposes.

Due to the complexity of vector summation in aggregating harmonic emissions from multiple EVs (involving both amplitude and phase angles), a conservative and computationally efficient approach was proposed: using the arithmetic mean of individual THD values as an upper-bound approximation of the aggregated THD. This method enabled tractable optimization without the need for costly phasor-level calculations, as validated by experimental comparisons.

Two smart charging optimization problems were then formulated. The first (Optimization Problem I) aimed to fairly allocate charging energy without considering harmonic limits. The second (Optimization Problem II) extended the first by incorporating a THD constraint, ensuring the THD remained below regulatory thresholds. Both optimization problems were solved using a customized PSO algorithm selected for its effectiveness in handling discontinuity in charging rates. A Water Filling Algorithm was introduced as a repair strategy to enforce the feasibility of charging rates, energy delivery, and THD limits.

A case study simulated a large-scale EV parking lot scenario involving 200 vehicles with diverse charging needs, harmonic profiles, and connection times. Unlike conventional smart charging, the results demonstrated that harmonics-aware smart charging (Optimization Problem II) effectively maintained THD below the 5% threshold. This was achieved through two strategies: prioritizing high charging rates (which reduced THD) and selectively deactivating high-emission EVs during peak harmonic periods.

Despite the added constraints, the harmonics-aware strategy met the 90% minimum energy delivery requirement and achieved 97.6% of the total requested energy, only slightly lower than the 98.9% in the unconstrained case. The study also emphasized the excessive impact of specific high-THD EV models, such as the Peugeot e-2008, on overall power quality. The chapter concluded by suggesting that system operators could enforce harmonics compliance policies or restrict high-emission EVs during peak times to preserve network performance.

Overall, this chapter established a practical and computationally efficient approach to harmonics mitigation in partially-loaded networks using harmonics-aware smart charging, ensuring regulatory compliance without requiring additional hardware infrastructure.

# Chapter 8

# Conclusions and Future Work

This final chapter synthesizes the main contributions, findings, and implications of the research presented throughout the thesis. It highlights how this work enhances the understanding of harmonic impacts caused by EV smart charging on power quality and transformer aging in distribution networks. The chapter also critically reflects on the study's limitations and outlines potential directions for future research, building upon the measurement-analysis-quantification-solution framework developed in this work. It is organized into three sections: overall conclusions, study limitations, and future research directions.

## 8.1 Conclusions

This thesis investigated the harmonic impacts of EV smart charging on power quality and transformer aging in low-voltage power distribution systems. The work followed a structured, multi-stage methodology that progressed from empirical measurement to statistical analysis, probabilistic modelling, and finally to the development of harmonics-aware charging solutions. These efforts addressed key gaps in understanding how EV charging behaviour interacts with power quality standards, infrastructure stress, and control strategies—contributing valuable knowledge to the development of sustainable EV-grid integration. The research was guided by six core questions, which are addressed below through a synthesis of experimental results, simulation findings,

and optimization analyses.

The first phase of this research focused on understanding the nature and variability of harmonic emissions from different EVs under smart charging conditions. To address the question, "*How do different EV models behave in terms of harmonic emissions across varying smart charging current levels, and what is the relationship between charging rate and harmonic distortion?*", a detailed experimental dataset was collected. Eight commercially available EV models were tested across a range of charging currents, with current and voltage harmonics captured at 1 A intervals. The results revealed a clear inverse relationship between charging current and current total harmonic distortion ($THD_I$): lower current levels produced significantly higher harmonic distortion. Moreover, the extent and pattern of harmonic emissions varied considerably across EV models. For instance, the Peugeot e-2008 consistently showed the highest $THD_I$ values, peaking at 25%, while other EV models like the Tesla Model Y and Renault Zoe displayed non-compliant harmonic profiles despite moderate $THD_I$. These findings confirmed that harmonic emissions are both current-dependent and vehicle-specific, necessitating model-level characterization.

Building on this, the second part of the analysis examined the cumulative effect of simultaneous EV charging on grid-connected points. To answer the question, "*What is the cumulative harmonic impact of multiple EVs charging simultaneously, and how do phase angle variations influence harmonic cancellation effects at the point of common coupling (PCC)?*", both laboratory measurements and Monte Carlo simulations were employed. The analysis demonstrated that harmonic cancellation occurred due to diversity in phase angles across EVs, which reduced overall $THD_I$ at the PCC in multi-EV simultaneous charging scenarios. However, this effect was probabilistic and not guaranteed—certain combinations of EVs and charging rates still resulted in severe distortion. In extreme cases, $THD_I$ exceeded 25%, despite partial cancellation. This showed that while aggregation can mitigate harmonic distortion, reliance on cancellation effects alone is insufficient to ensure regulatory compliance, especially under uncontrolled charging behaviour.

To assess whether current regulatory frameworks are adequate for this evolving

landscape, the thesis investigated the question, "*To what extent do current harmonic emission standards (e.g., IEC 61000-3-2, IEC 61000-3-12) adequately capture the dynamic and variable conditions introduced by smart charging?*", the empirical results were benchmarked against IEC harmonic current limits. Four out of eight EVs violated individual harmonic order limits—even when $THD_I$ remained below established compliance thresholds. These discrepancies revealed that standards focused solely on rated conditions and aggregate metrics such as THD fail to capture real-world smart charging effects. Vehicles exhibited highly variable harmonic behaviour across different current levels, which was not reflected in existing compliance tests. This underscores the need for revised standards that incorporate dynamic test profiles across multiple charging points, rather than assessing EVs only under fixed maximum-rated conditions.

Transformer performance under harmonic-rich loading formed the focus of the next research phase. The fourth research question, "*How do harmonic-rich load conditions affect transformer performance, particularly in terms of thermal stress, aging acceleration, and estimated lifetime, under different loading scenarios?*", was answered using a thermal-electrical model based on IEEE C57.91 and IEEE C57.110 standards. The model incorporated harmonic loss coefficients and calculated top-oil and hot-spot temperatures to estimate the aging acceleration factor and lifetime. Monte Carlo simulations were used to model uncertainty in EVs and charging behaviour. The findings showed that transformer degradation was significantly accelerated when many EVs charged concurrently at low current levels—where harmonic content is the highest. For example, scenarios with 6 A charging currents reduced transformer lifetime to less than 10 years due to hot-spot temperatures exceeding 120 °C. In contrast, charging at 13–15 A resulted in much lower thermal stress and extended transformer lifespan beyond 40 years. This demonstrated that transformer aging is not merely a function of load magnitude but is strongly influenced by harmonic distortion characteristics.

In response to these technical challenges, the thesis developed practical strategies for harmonics-aware EV charging. The fifth research question, "*How can harmonics-aware smart charging strategies be developed and optimized to comply with power quality standards, minimize transformer aging, and ensure adequate energy delivery?*", was ad-

dressed through two solutions. First, a rule-based control strategy was proposed for heavily loaded transformers. It recommended an optimal charging range—13 A as the preferred current during peak periods, and 7–9 A for off-peak scenarios—to strike a balance between minimizing aging and maintaining charging capacity. Second, an optimization framework was formulated for partially loaded networks. This framework integrated second-order polynomial models of THD as a function of charging power and used a Particle Swarm Optimization (PSO) algorithm with a Water Filling repair mechanism. A case study involving 200 EVs confirmed that this strategy successfully constrained THD below 5% (IEEE 519 limit) while still delivering over 97% of the requested energy. These results illustrated that harmonics-aware charging is not only feasible but also effective at reducing power quality risks without sacrificing user satisfaction.

Finally, the thesis investigated the broader system-level trade-offs. To answer the sixth question, "*What trade-offs emerge between minimizing harmonic emissions and meeting user energy demand, and how can these be addressed through smart charging control mechanisms?*", the optimization framework was stress-tested under diverse conditions. The results indicated that minimizing THD often required deprioritizing certain high-emission EVs or shifting charging sessions to off-peak periods. While this introduced minor deviations from optimal energy delivery (a 1.3% reduction compared to unconstrained scheduling), it enabled full compliance with harmonic limits and avoided the need for costly mitigation hardware such as active filters. Moreover, by prioritizing EVs with lower emission profiles or allocating higher charging currents, the algorithm achieved power quality compliance with minimal operational sacrifice. These outcomes demonstrate that harmonics-aware control can align grid needs with consumer demand through intelligent, real-time scheduling.

In conclusion, this thesis provided a structured and holistic framework for evaluating and mitigating the harmonic impacts of EV smart charging. It answered all six research questions through a rigorous sequence of measurement, statistical profiling, power quality assessment, and control optimization. The contributions include a unique empirical dataset, insights into standard compliance shortcomings, and action-

able charging strategies for different grid loading conditions. The findings demonstrate that harmonic distortion is a critical dimension of EV-grid interaction, one that must be addressed alongside energy management. Future EV charging infrastructure must incorporate harmonics-aware strategies into both policy and system design to ensure scalable, efficient, and reliable operation of low-carbon power networks.

## 8.2 Limitations of Research

While this thesis provides a comprehensive analysis of harmonic emissions and mitigation strategies associated with EV smart charging, several limitations must be acknowledged. These limitations are presented to reflect the progress of the research:

1. **Experimental Dataset Scope:** The empirical dataset was limited to eight commercially available EV models due to laboratory access and vehicle availability. Although these models represent a diverse range of on-board charging technologies, the findings may not fully capture the harmonic behaviour of newer or older vehicle models, variations due to firmware updates, or long-term battery aging effects. Expanding the dataset to include a broader spectrum of EV types would enhance the generalizability of the harmonic characterization.

2. **Grid-Level Factors and External Interactions:** This study primarily focused on EV-generated harmonics without explicitly modelling background harmonic distortion, voltage imbalances, or the effects of long feeder lengths—all of which are prevalent in real-world distribution networks. These external conditions may influence the interaction between EV loads and the existing grid, potentially amplifying or mitigating harmonic emissions observed in controlled laboratory settings.

3. **Transformer Modelling Scope and Assumptions:** The transformer thermal aging analysis was based on a single 160 kVA distribution transformer under a fixed ambient temperature of 30 °C. While this represents typical residential network conditions, it does not capture the diversity of transformer ratings (e.g.,

25–100 kVA) found in rural or semi-urban settings, nor the daily and seasonal fluctuations in ambient temperature that significantly influence thermal performance and insulation degradation. As a result, the conclusions regarding transformer lifespan and optimal charging currents may not be directly transferable to all deployment scenarios. Future models incorporating variable ambient profiles and a range of transformer capacities would provide more representative aging assessments across diverse network conditions.

4. **Harmonic Aggregation Modelling:** The harmonic aggregation in the multi-EV smart charging scenarios was modelled using second-order polynomial regression and arithmetic averaging to estimate total THD. While this approach enabled tractable optimization, it did not account for precise vector summation of harmonics, which depends on both amplitude and phase angle. Although conservative and validated against empirical data, this simplification may lead to overconstrained optimization results and slight underutilization of available charging capacity.

This structured overview of limitations highlights areas where further research can extend the findings of this thesis and enhance the robustness of future harmonics-aware EV charging frameworks.

## 8.3 Future Work

Building on the contributions and addressing the limitations identified in this thesis, several promising research directions are proposed for future work:

1. The EV harmonic dataset developed in this study can be expanded to include a broader range of vehicles, including newer models, EVs with aged battery and charger components, and tests under different battery SoC and ambient temperatures. These additions would improve the representativeness and accuracy of harmonic models under real-world operational conditions.

2. Future studies should also consider the coexistence of EVs with other harmonic-generating sources such as PV systems, wind turbines, and other power-electronic-interfaced loads. Incorporating these additional sources will enable a more detailed and comprehensive analysis of harmonic interactions in modern distribution networks, particularly under scenarios of high renewable energy penetration.

3. Transformer aging models will be enhanced by incorporating dynamic ambient temperatures, diurnal and seasonal fluctuations, and thermal memory effects. These improvements would enable more realistic estimates of insulation aging and transformer lifetime across diverse climatic and loading environments.

4. The Monte Carlo simulation framework introduced in this thesis will be extended to cover a wider spectrum of transformer sizes and substation configurations, including low-rated rural transformers. Such generalization will help assess the scalability of proposed harmonics mitigation and transformer protection strategies for both urban and rural distribution networks.

5. In addition to transformer health, future simulation studies will investigate harmonic imbalance phenomena under unbalanced phase loading. Dedicated metrics and indices for harmonic imbalance, analogous to traditional voltage imbalance metrics, will be developed to support comprehensive power quality assessments in networks with mixed single-phase and three-phase EV charging.

6. Advanced meta-models, such as neural networks and response surface methodologies, will be explored to improve the accuracy of harmonic summation approximations in optimization tasks. These models can address the limitations of arithmetic averaging and reduce conservativeness without sacrificing computational efficiency in large-scale smart charging problems.

7. Integration of advanced distribution network simulators such as OpenDSS or DigSILENT PowerFactory will be implemented to evaluate the combined effects of voltage drops, harmonic propagation, and grid-side interactions in three-phase unbalanced networks. This will enable an integrated evaluation of THD, trans-

former aging, voltage imbalance, flicker, and resonant conditions under high EV penetration.

8. Finally, further investigation will be dedicated to the regulatory and standardization landscape. Specifically, future research will aim to propose dynamic harmonic compliance protocols for smart controllable loads, including EVs. This includes updates to IEC 61000-3-2 and IEC 61000-3-12, as well as the feasibility of implementing real-time harmonic monitoring and mitigation controls at the charger or aggregator level.

This thesis advances the understanding of harmonic emissions associated with EV smart charging and their implications for power quality and transformer aging in low-voltage distribution networks. By combining high-resolution empirical measurements, probabilistic simulations, compliance analyses, and harmonics-aware optimization strategies, it addresses a critical gap in the integration of flexible EV charging within power systems.

The methodologies and findings presented in this thesis contribute a comprehensive framework that enables system operators, regulators, and researchers to quantify, predict, and manage the harmonic impacts of smart charging across varying network conditions and EV types. In doing so, the work establishes the technical and analytical basis needed to support the wider deployment of smart charging solutions while protecting grid stability and infrastructure longevity.

By integrating measurement, modelling, simulation, and charging management, this thesis advances the practical adoption of harmonics-aware smart charging and offers valuable guidance for shaping future standards and policies. Ultimately, this work contributes to the reliable and sustainable deployment of large-scale EV infrastructure within modern and future power systems.

# Appendix A

# Harmonic Data: Amplitudes and Phase Angles of Individual Harmonic Orders Across EV-Specific Charging Levels

This appendix presents detailed harmonic data for eight EVs individually charged under smart charging conditions. For each EV, the amplitude (A) and phase angle ($\theta$) in degrees of each harmonic order have been measured across the full range of charging currents specific to that vehicle, from its minimum to maximum allowable levels. The vehicles analyzed include the Renault Zoe R90, Peugeot e-208, Nissan Leaf e+, VW ID.3 Pro, Renault Zoe ZE50, VW ID.4 Pro, Tesla Model Y Long Range, and Peugeot e-2008. These harmonic profiles vary with charging current and are critical for evaluating the impact of smart charging on power quality under realistic operating conditions.

Table A.1: Renault Zoe R90 — Harmonic Orders $h_2$ to $h_9$

| **Harmonic Order** | **h2** | | **h3** | | **h4** | | **h5** | | **h6** | | **h7** | | **h8** | | **h9** | |
|---|---|---|---|---|---|---|---|---|---|---|---|---|---|---|---|---|
| **Charging Rate (A)** | **A** | $\theta$ | **A** | $\theta$ | **A** | $\theta$ | **A** | $\theta$ | **A** | $\theta$ | **A** | $\theta$ | **A** | $\theta$ | **A** | $\theta$ |
| **6** | 0.00 | -171.63 | 0.03 | -98.22 | 0.01 | 21.75 | 0.28 | -58.85 | 0.01 | -170.93 | 0.49 | -169.92 | 0.01 | 84.32 | 0.05 | -129.82 |
| **7** | 0.04 | -45.77 | 0.01 | -27.97 | 0.10 | -164.92 | 0.21 | 164.24 | 0.01 | 30.06 | 0.42 | 45.02 | 0.06 | 106.19 | 0.04 | 129.47 |
| **8** | 0.11 | 6.49 | 0.01 | -31.32 | 0.09 | -103.17 | 0.05 | -147.07 | 0.02 | 88.76 | 0.60 | 139.24 | 0.09 | -153.61 | 0.05 | -111.93 |
| **9** | 0.12 | 17.11 | 0.02 | -76.56 | 0.11 | -78.11 | 0.02 | -67.92 | 0.03 | 90.71 | 0.63 | -172.28 | 0.10 | -101.81 | 0.07 | -44.81 |
| **10** | 0.13 | 22.41 | 0.02 | -96.67 | 0.12 | -59.80 | 0.03 | -38.02 | 0.04 | 108.73 | 0.65 | -141.49 | 0.10 | -62.52 | 0.05 | -4.32 |
| **11** | 0.13 | 35.04 | 0.01 | 102.09 | 0.13 | -38.10 | 0.06 | 25.31 | 0.02 | 172.17 | 0.69 | -102.12 | 0.12 | -25.02 | 0.06 | 38.70 |
| **12** | 0.13 | 39.29 | 0.01 | -76.13 | 0.14 | -24.39 | 0.14 | 93.18 | 0.02 | -153.01 | 0.79 | -74.71 | 0.15 | -3.03 | 0.07 | 72.05 |
| **13** | 0.15 | 47.37 | 0.03 | -103.36 | 0.15 | -15.28 | 0.17 | 95.92 | 0.01 | -99.91 | 0.82 | -54.75 | 0.15 | 21.57 | 0.07 | 100.70 |
| **14** | 0.13 | 53.52 | 0.03 | -116.79 | 0.17 | -8.70 | 0.16 | 97.41 | 0.02 | -152.91 | 0.84 | -42.43 | 0.15 | 35.98 | 0.10 | 106.64 |
| **15** | 0.14 | 50.77 | 0.05 | -87.99 | 0.18 | 1.55 | 0.19 | 111.74 | 0.03 | -154.91 | 0.84 | -27.54 | 0.14 | 46.54 | 0.05 | 107.75 |
| **16** | 0.14 | 58.53 | 0.02 | -77.46 | 0.18 | 6.29 | 0.18 | 101.75 | 0.03 | -171.05 | 0.76 | -8.61 | 0.12 | 55.88 | 0.05 | 151.47 |
| **17** | 0.13 | 75.60 | 0.03 | -86.10 | 0.18 | 15.23 | 0.20 | 92.59 | 0.02 | -83.80 | 0.80 | 16.56 | 0.14 | 73.02 | 0.05 | -177.90 |
| **18** | 0.15 | 101.11 | 0.03 | -33.19 | 0.21 | 24.63 | 0.22 | 83.42 | 0.01 | -81.81 | 0.85 | 52.02 | 0.12 | 85.99 | 0.04 | -125.66 |
| **19** | 0.16 | 104.86 | 0.03 | -7.91 | 0.22 | 28.45 | 0.23 | 90.88 | 0.01 | -75.29 | 0.87 | 66.02 | 0.13 | 93.74 | 0.03 | -118.31 |
| **20** | 0.16 | 109.95 | 0.05 | -2.59 | 0.24 | 32.37 | 0.25 | 103.05 | 0.02 | -33.96 | 0.88 | 78.33 | 0.13 | 98.51 | 0.03 | -115.14 |
| **21** | 0.18 | 120.34 | 0.04 | -14.18 | 0.23 | 34.17 | 0.25 | 98.14 | 0.02 | -14.71 | 0.90 | 92.90 | 0.13 | 113.23 | 0.02 | -98.38 |
| **22** | 0.17 | 122.16 | 0.06 | -32.27 | 0.25 | 38.93 | 0.24 | 95.54 | 0.01 | -70.52 | 0.96 | 99.31 | 0.12 | 104.25 | 0.02 | -90.93 |
| **23** | 0.19 | 128.42 | 0.06 | -36.40 | 0.24 | 40.07 | 0.25 | 98.52 | 0.02 | -21.61 | 0.98 | 108.01 | 0.14 | 116.86 | 0.02 | -81.18 |
| **24** | 0.17 | 127.56 | 0.06 | -9.31 | 0.26 | 43.05 | 0.25 | 120.42 | 0.01 | -10.02 | 0.96 | 109.90 | 0.13 | 118.04 | 0.02 | -83.91 |
| **25** | 0.19 | 128.37 | 0.08 | -24.74 | 0.26 | 42.35 | 0.27 | 126.20 | 0.01 | 0.25 | 0.98 | 110.52 | 0.13 | 124.93 | 0.02 | -103.65 |
| **26** | 0.19 | 124.82 | 0.07 | -21.66 | 0.25 | 45.76 | 0.30 | 138.63 | 0.00 | 19.29 | 0.96 | 110.24 | 0.14 | 127.71 | 0.03 | -74.52 |
| **27** | 0.19 | 127.62 | 0.10 | -20.12 | 0.27 | 44.39 | 0.33 | 146.38 | 0.02 | -15.87 | 0.96 | 111.49 | 0.14 | 129.93 | 0.01 | -98.00 |
| **28** | 0.18 | 124.03 | 0.07 | -12.96 | 0.26 | 46.42 | 0.33 | 147.19 | 0.02 | -48.79 | 0.96 | 112.48 | 0.14 | 127.13 | 0.02 | -87.06 |
| **29** | 0.18 | 120.95 | 0.08 | -12.92 | 0.27 | 45.07 | 0.38 | 153.13 | 0.02 | -138.53 | 0.96 | 113.36 | 0.16 | 131.40 | 0.02 | -69.95 |
| **30** | 0.20 | 125.12 | 0.08 | -11.63 | 0.27 | 44.99 | 0.40 | 161.02 | 0.00 | -55.96 | 0.97 | 113.57 | 0.15 | 135.69 | 0.02 | -64.63 |
| **31** | 0.21 | 122.96 | 0.09 | -19.24 | 0.27 | 49.72 | 0.44 | 163.25 | 0.01 | -76.24 | 0.97 | 114.21 | 0.15 | 141.78 | 0.03 | -78.68 |
| **32** | 0.20 | 121.73 | 0.08 | -35.03 | 0.29 | 46.22 | 0.46 | 169.31 | 0.01 | -106.97 | 0.96 | 114.26 | 0.16 | 142.19 | 0.03 | -78.19 |

Table A.2: Renault Zoe R90 — Harmonic Orders $h_{10}$ to $h_{16}$

| **Harmonic Order** | **h10** | | **h11** | | **h12** | | **h13** | | **h14** | | **h15** | | **h16** | |
|---|---|---|---|---|---|---|---|---|---|---|---|---|---|---|
| **Charging Rate (A)** | **A** | $\theta$ | **A** | $\theta$ | **A** | $\theta$ | **A** | $\theta$ | **A** | $\theta$ | **A** | $\theta$ | **A** | $\theta$ |
| **6** | 0.01 | 174.77 | 0.03 | 174.25 | 0.01 | 120.13 | 0.17 | -178.62 | 0.01 | -140.53 | 0.01 | -160.21 | 0.02 | -146.45 |
| **7** | 0.06 | 3.10 | 0.10 | 158.19 | 0.01 | 143.72 | 0.12 | -170.60 | 0.04 | -108.20 | 0.00 | -57.45 | 0.02 | -118.47 |
| **8** | 0.04 | 123.23 | 0.12 | -54.79 | 0.01 | -74.00 | 0.17 | 3.80 | 0.02 | 107.49 | 0.02 | -35.86 | 0.04 | 122.52 |
| **9** | 0.04 | -145.30 | 0.14 | 23.32 | 0.02 | -7.01 | 0.20 | 91.41 | 0.02 | -140.01 | 0.02 | 47.25 | 0.05 | -105.60 |
| **10** | 0.02 | -95.58 | 0.14 | 70.23 | 0.01 | 9.99 | 0.18 | 156.12 | 0.02 | -29.77 | 0.01 | 144.55 | 0.03 | -27.96 |
| **11** | 0.00 | 110.24 | 0.14 | 121.22 | 0.01 | 42.14 | 0.18 | -138.48 | 0.03 | 75.62 | 0.01 | -121.11 | 0.03 | 75.57 |
| **12** | 0.02 | 103.47 | 0.18 | 130.10 | 0.01 | -47.77 | 0.23 | -119.76 | 0.04 | 119.73 | 0.01 | -165.93 | 0.02 | 83.11 |
| **13** | 0.03 | 107.37 | 0.19 | 158.28 | 0.03 | 96.15 | 0.21 | -85.45 | 0.06 | 162.88 | 0.01 | 21.60 | 0.03 | 152.76 |
| **14** | 0.03 | 143.04 | 0.18 | 176.37 | 0.01 | 92.74 | 0.17 | -69.08 | 0.05 | 177.35 | 0.00 | 58.29 | 0.03 | 166.24 |
| **15** | 0.03 | 159.05 | 0.18 | -172.99 | 0.02 | 121.58 | 0.17 | -37.06 | 0.05 | -136.05 | 0.02 | -117.31 | 0.03 | -131.15 |
| **16** | 0.02 | -176.46 | 0.18 | -125.42 | 0.00 | 170.41 | 0.14 | 6.15 | 0.06 | -121.07 | 0.01 | 129.52 | 0.03 | -69.98 |
| **17** | 0.05 | -149.27 | 0.26 | -98.32 | 0.02 | -62.06 | 0.10 | 36.46 | 0.05 | -86.39 | 0.01 | -94.14 | 0.03 | -50.12 |
| **18** | 0.04 | -104.18 | 0.33 | -61.85 | 0.01 | -77.97 | 0.07 | 65.57 | 0.06 | -46.55 | 0.01 | -53.47 | 0.03 | 30.90 |
| **19** | 0.05 | -68.37 | 0.37 | -47.52 | 0.01 | 159.88 | 0.05 | 80.97 | 0.06 | -33.95 | 0.01 | 92.52 | 0.04 | 38.58 |
| **20** | 0.05 | -58.67 | 0.39 | -33.58 | 0.01 | 153.39 | 0.05 | 71.31 | 0.06 | -13.97 | 0.02 | -71.23 | 0.04 | 55.47 |
| **21** | 0.06 | -42.52 | 0.42 | -16.34 | 0.02 | 4.33 | 0.05 | 44.34 | 0.04 | -4.70 | 0.01 | 162.33 | 0.03 | 84.76 |
| **22** | 0.04 | -22.29 | 0.42 | -7.49 | 0.01 | 166.70 | 0.05 | 44.65 | 0.07 | 8.10 | 0.01 | 21.92 | 0.05 | 117.18 |
| **23** | 0.05 | -31.51 | 0.44 | 1.62 | 0.01 | 172.06 | 0.05 | 48.48 | 0.04 | 24.80 | 0.02 | 111.36 | 0.04 | 107.25 |
| **24** | 0.04 | -18.61 | 0.46 | 9.98 | 0.00 | -17.16 | 0.04 | 61.15 | 0.05 | 31.98 | 0.01 | 29.35 | 0.04 | 119.38 |
| **25** | 0.05 | -30.02 | 0.44 | 11.68 | 0.01 | 98.87 | 0.04 | 81.22 | 0.05 | 28.61 | 0.02 | 71.80 | 0.04 | 121.87 |
| **26** | 0.04 | -12.56 | 0.43 | 16.97 | 0.01 | 119.88 | 0.06 | 78.29 | 0.07 | 34.34 | 0.01 | 116.34 | 0.03 | 148.19 |
| **27** | 0.05 | -24.21 | 0.44 | 20.91 | 0.01 | -6.23 | 0.06 | 103.49 | 0.06 | 38.86 | 0.01 | 23.83 | 0.04 | 135.02 |
| **28** | 0.04 | -17.67 | 0.46 | 22.84 | 0.01 | 104.23 | 0.07 | 112.66 | 0.06 | 51.55 | 0.01 | -101.19 | 0.03 | 145.13 |
| **29** | 0.05 | -26.83 | 0.45 | 26.56 | 0.01 | 123.74 | 0.06 | 112.62 | 0.05 | 65.27 | 0.01 | 103.34 | 0.04 | 152.13 |
| **30** | 0.06 | -9.11 | 0.44 | 28.33 | 0.02 | 128.30 | 0.07 | 131.47 | 0.04 | 57.62 | 0.01 | 77.73 | 0.06 | 154.11 |
| **31** | 0.04 | 7.34 | 0.47 | 30.62 | 0.01 | 7.94 | 0.09 | 130.15 | 0.06 | 61.83 | 0.02 | 167.30 | 0.04 | 163.49 |
| **32** | 0.05 | -15.22 | 0.44 | 33.46 | 0.01 | 176.72 | 0.07 | 130.53 | 0.05 | 70.25 | 0.01 | 117.86 | 0.05 | 162.20 |

Table A.3: Renault Zoe R90 — Harmonic Orders $h_{17}$ to $h_{24}$

| **Harmonic Order** | **h17** | | **h18** | | **h19** | | **h20** | | **h21** | | **h22** | | **h23** | | **h24** | |
|---|---|---|---|---|---|---|---|---|---|---|---|---|---|---|---|---|
| **Charging Rate (A)** | **A** | $\theta$ | **A** | $\theta$ | **A** | $\theta$ | **A** | $\theta$ | **A** | $\theta$ | **A** | $\theta$ | **A** | $\theta$ | **A** | $\theta$ |
| **6** | 0.16 | -13.15 | 0.01 | -130.59 | 0.40 | 10.61 | 0.01 | -131.30 | 0.03 | -6.08 | 0.02 | -113.03 | 0.09 | -162.04 | 0.01 | -116.62 |
| **7** | 0.24 | 132.45 | 0.02 | -0.11 | 0.31 | -128.66 | 0.04 | 119.19 | 0.04 | -130.50 | 0.04 | -167.80 | 0.11 | 166.05 | 0.01 | -59.23 |
| **8** | 0.31 | -26.19 | 0.01 | -31.77 | 0.28 | 104.51 | 0.01 | -11.57 | 0.03 | -165.85 | 0.05 | 83.80 | 0.08 | 60.85 | 0.00 | 84.61 |
| **9** | 0.35 | 97.59 | 0.01 | -89.56 | 0.27 | -128.64 | 0.02 | 20.73 | 0.02 | 4.72 | 0.06 | -99.88 | 0.11 | -154.43 | 0.01 | -71.81 |
| **10** | 0.37 | 169.80 | 0.01 | 88.91 | 0.27 | -54.34 | 0.03 | 90.09 | 0.02 | 84.54 | 0.05 | -15.24 | 0.10 | -76.58 | 0.00 | 136.72 |
| **11** | 0.38 | -101.93 | 0.01 | -153.48 | 0.27 | 52.54 | 0.01 | -162.01 | 0.04 | -146.32 | 0.06 | 97.08 | 0.08 | 36.31 | 0.01 | -121.58 |
| **12** | 0.25 | -62.45 | 0.02 | 170.37 | 0.13 | 145.52 | 0.02 | -118.92 | 0.03 | -30.76 | 0.05 | -163.14 | 0.10 | 148.78 | 0.01 | 33.73 |
| **13** | 0.25 | -17.10 | 0.01 | -143.72 | 0.13 | -163.65 | 0.03 | -47.44 | 0.03 | 56.22 | 0.03 | -94.50 | 0.11 | -146.03 | 0.01 | 163.50 |
| **14** | 0.26 | 11.75 | 0.01 | -89.65 | 0.13 | -122.99 | 0.04 | -15.42 | 0.04 | 59.10 | 0.05 | -56.51 | 0.13 | -105.95 | 0.02 | 124.18 |
| **15** | 0.26 | 48.88 | 0.00 | 89.96 | 0.13 | -85.32 | 0.03 | 21.85 | 0.03 | 92.94 | 0.06 | -9.13 | 0.12 | -55.60 | 0.01 | 155.24 |
| **16** | 0.37 | 104.72 | 0.01 | 74.85 | 0.22 | -41.91 | 0.04 | 55.06 | 0.05 | 130.64 | 0.05 | -4.26 | 0.09 | -36.07 | 0.01 | 173.65 |
| **17** | 0.35 | 144.02 | 0.01 | 86.23 | 0.28 | 35.40 | 0.04 | 79.74 | 0.05 | -171.72 | 0.04 | 11.62 | 0.03 | -122.70 | 0.01 | -139.59 |
| **18** | 0.19 | -158.39 | 0.02 | -66.70 | 0.30 | 130.79 | 0.08 | 91.52 | 0.04 | -55.23 | 0.02 | 34.00 | 0.18 | -64.91 | 0.01 | -43.03 |
| **19** | 0.14 | -140.05 | 0.00 | 16.71 | 0.26 | 165.85 | 0.07 | 129.68 | 0.04 | 15.47 | 0.04 | 55.98 | 0.22 | -20.27 | 0.00 | -157.46 |
| **20** | 0.13 | -121.83 | 0.01 | -23.94 | 0.29 | -161.61 | 0.07 | 146.17 | 0.05 | 35.07 | 0.02 | 99.28 | 0.24 | 16.04 | 0.01 | 90.58 |
| **21** | 0.10 | -106.80 | 0.02 | 51.80 | 0.27 | -118.23 | 0.08 | 176.70 | 0.05 | 93.97 | 0.06 | 101.11 | 0.24 | 55.98 | 0.01 | -128.73 |
| **22** | 0.06 | -116.26 | 0.02 | 38.82 | 0.27 | -104.20 | 0.08 | -164.04 | 0.04 | 133.82 | 0.06 | 120.84 | 0.24 | 73.68 | 0.01 | -112.14 |
| **23** | 0.07 | -126.16 | 0.02 | 87.90 | 0.25 | -72.23 | 0.09 | -147.98 | 0.05 | 176.32 | 0.04 | 145.14 | 0.23 | 95.60 | 0.02 | -79.73 |
| **24** | 0.07 | -91.15 | 0.01 | 75.30 | 0.27 | -68.80 | 0.08 | -138.64 | 0.05 | -177.44 | 0.05 | 164.73 | 0.25 | 112.80 | 0.01 | 70.94 |
| **25** | 0.10 | -68.09 | 0.01 | 101.71 | 0.26 | -66.92 | 0.09 | -132.53 | 0.03 | 173.94 | 0.05 | 170.78 | 0.23 | 122.46 | 0.01 | -55.23 |
| **26** | 0.11 | -44.56 | 0.02 | 79.34 | 0.26 | -62.83 | 0.10 | -123.99 | 0.05 | -169.10 | 0.06 | 174.03 | 0.22 | 126.94 | 0.02 | -22.15 |
| **27** | 0.16 | -36.54 | 0.02 | 113.23 | 0.26 | -62.24 | 0.08 | -106.34 | 0.04 | -151.69 | 0.06 | -178.88 | 0.23 | 141.76 | 0.01 | -5.30 |
| **28** | 0.18 | -30.26 | 0.01 | 100.04 | 0.27 | -56.03 | 0.09 | -105.06 | 0.04 | -165.25 | 0.04 | -148.51 | 0.24 | 147.70 | 0.01 | -111.35 |
| **29** | 0.20 | -25.42 | 0.01 | 127.34 | 0.28 | -51.33 | 0.09 | -84.48 | 0.03 | 173.96 | 0.03 | -137.56 | 0.22 | 156.34 | 0.00 | -43.24 |
| **30** | 0.23 | -15.67 | 0.01 | 84.24 | 0.29 | -55.41 | 0.09 | -93.30 | 0.04 | 171.45 | 0.05 | -152.10 | 0.20 | 165.25 | 0.01 | -33.80 |
| **31** | 0.25 | -17.64 | 0.01 | 127.63 | 0.31 | -52.18 | 0.09 | -85.33 | 0.05 | 161.55 | 0.05 | -122.51 | 0.20 | 171.02 | 0.02 | 18.55 |
| **32** | 0.28 | -5.85 | 0.01 | 32.25 | 0.29 | -50.86 | 0.09 | -79.58 | 0.04 | -177.14 | 0.03 | -121.38 | 0.21 | 177.51 | 0.01 | -13.92 |

Table A.4: Renault Zoe R90 — Harmonic Orders $h_{25}$ to $h_{31}$

| **Harmonic Order** | **h25** | | **h26** | | **h27** | | **h28** | | **h29** | | **h30** | | **h31** | |
|---|---|---|---|---|---|---|---|---|---|---|---|---|---|---|
| **Charging Rate (A)** | **A** | $\theta$ | **A** | $\theta$ | **A** | $\theta$ | **A** | $\theta$ | **A** | $\theta$ | **A** | $\theta$ | **A** | $\theta$ |
| **6** | 0.07 | 172.05 | 0.02 | -92.02 | 0.08 | 149.50 | 0.01 | 17.76 | 0.02 | 167.35 | 0.00 | -67.84 | 0.08 | 96.73 |
| **7** | 0.12 | -153.25 | 0.00 | -20.05 | 0.08 | -139.99 | 0.01 | 8.09 | 0.04 | -178.47 | 0.00 | -169.24 | 0.06 | -84.04 |
| **8** | 0.14 | -179.58 | 0.03 | 9.45 | 0.07 | -168.34 | 0.02 | 91.53 | 0.01 | 146.56 | 0.01 | 51.61 | 0.05 | -93.83 |
| **9** | 0.13 | 0.44 | 0.02 | -178.41 | 0.08 | 42.65 | 0.01 | -4.99 | 0.03 | -138.65 | 0.02 | -96.11 | 0.07 | 133.93 |
| **10** | 0.10 | 109.63 | 0.02 | -78.56 | 0.08 | 165.20 | 0.02 | 79.54 | 0.05 | -49.50 | 0.01 | 51.67 | 0.06 | -75.72 |
| **11** | 0.07 | -103.97 | 0.01 | 47.57 | 0.08 | -48.66 | 0.02 | -131.43 | 0.08 | 94.29 | 0.01 | 178.92 | 0.04 | 117.69 |
| **12** | 0.11 | -1.31 | 0.01 | 151.22 | 0.10 | 51.23 | 0.01 | -95.49 | 0.12 | 179.57 | 0.02 | -69.57 | 0.06 | -95.96 |
| **13** | 0.09 | 73.05 | 0.01 | -119.48 | 0.09 | 120.01 | 0.01 | 39.39 | 0.15 | -97.74 | 0.01 | 42.62 | 0.09 | -7.66 |
| **14** | 0.10 | 118.59 | 0.03 | -91.44 | 0.09 | -174.08 | 0.02 | 109.56 | 0.14 | -34.89 | 0.01 | -70.00 | 0.08 | 56.05 |
| **15** | 0.08 | 178.86 | 0.01 | -53.29 | 0.09 | -130.30 | 0.04 | -174.57 | 0.14 | 26.59 | 0.00 | -30.18 | 0.09 | 129.44 |
| **16** | 0.07 | -116.46 | 0.01 | 4.56 | 0.06 | -50.68 | 0.02 | -133.84 | 0.09 | 78.48 | 0.01 | -83.24 | 0.08 | -143.63 |
| **17** | 0.06 | -10.30 | 0.02 | 117.84 | 0.06 | 60.55 | 0.02 | -60.75 | 0.09 | 124.24 | 0.00 | 13.50 | 0.09 | -22.80 |
| **18** | 0.07 | 128.63 | 0.01 | -170.83 | 0.07 | -146.34 | 0.02 | -73.39 | 0.13 | -179.58 | 0.01 | -33.48 | 0.05 | 132.05 |
| **19** | 0.07 | -172.71 | 0.01 | -60.44 | 0.08 | -77.50 | 0.01 | -55.24 | 0.13 | -149.55 | 0.01 | -43.58 | 0.04 | -133.52 |
| **20** | 0.05 | -143.04 | 0.01 | -24.17 | 0.07 | -35.87 | 0.01 | -26.21 | 0.14 | -111.88 | 0.01 | 76.38 | 0.04 | -47.55 |
| **21** | 0.04 | -97.25 | 0.02 | 67.35 | 0.07 | 11.31 | 0.02 | 32.30 | 0.15 | -75.41 | 0.01 | 109.53 | 0.07 | 27.05 |
| **22** | 0.03 | -52.62 | 0.03 | 69.50 | 0.07 | 43.37 | 0.01 | 134.69 | 0.13 | -55.64 | 0.00 | 175.39 | 0.07 | 52.93 |
| **23** | 0.05 | -30.05 | 0.03 | 124.39 | 0.07 | 90.57 | 0.02 | 125.43 | 0.15 | -28.20 | 0.01 | -71.96 | 0.09 | 100.52 |
| **24** | 0.05 | -6.29 | 0.03 | 117.79 | 0.06 | 87.96 | 0.03 | 149.89 | 0.13 | 2.79 | 0.02 | -82.70 | 0.07 | 120.77 |
| **25** | 0.04 | -9.57 | 0.02 | 125.49 | 0.06 | 96.91 | 0.02 | 145.15 | 0.14 | 14.21 | 0.01 | -104.98 | 0.08 | 130.97 |
| **26** | 0.03 | 17.48 | 0.03 | 120.43 | 0.07 | 105.92 | 0.03 | 150.16 | 0.15 | 23.02 | 0.01 | -28.97 | 0.07 | 123.62 |
| **27** | 0.04 | 1.01 | 0.02 | 157.29 | 0.07 | 104.59 | 0.02 | 169.95 | 0.15 | 48.20 | 0.00 | 37.36 | 0.05 | 133.33 |
| **28** | 0.04 | 28.22 | 0.03 | 168.48 | 0.06 | 110.77 | 0.01 | 179.21 | 0.15 | 53.71 | 0.01 | -35.35 | 0.05 | 159.93 |
| **29** | 0.04 | 42.42 | 0.03 | 172.46 | 0.06 | 110.04 | 0.03 | -143.98 | 0.15 | 70.04 | 0.02 | -79.03 | 0.01 | 138.09 |
| **30** | 0.04 | 15.75 | 0.03 | 170.49 | 0.08 | 114.94 | 0.01 | -108.89 | 0.14 | 76.96 | 0.02 | 127.66 | 0.02 | 109.11 |
| **31** | 0.03 | 18.70 | 0.02 | 173.73 | 0.06 | 122.50 | 0.02 | -167.64 | 0.17 | 81.69 | 0.04 | -4.39 | 0.03 | 60.36 |
| **32** | 0.03 | 13.01 | 0.03 | -153.55 | 0.07 | 124.82 | 0.00 | 46.87 | 0.15 | 88.91 | 0.00 | -68.06 | 0.03 | 108.49 |

Table A.5: Peugeot e-208 — Harmonic Orders $h_2$ to $h_9$

| **Harmonic Order** | **h2** | | **h3** | | **h4** | | **h5** | | **h6** | | **h7** | | **h8** | | **h9** | |
|---|---|---|---|---|---|---|---|---|---|---|---|---|---|---|---|---|
| **Charging Rate (A)** | **A** | $\theta$ | **A** | $\theta$ | **A** | $\theta$ | **A** | $\theta$ | **A** | $\theta$ | **A** | $\theta$ | **A** | $\theta$ | **A** | $\theta$ |
| **6** | 0.11 | -90.00 | 0.04 | 107.65 | 0.09 | -124.12 | 0.13 | -86.67 | 0.02 | -105.68 | 0.13 | 19.66 | 0.01 | 7.83 | 0.02 | -87.77 |
| **7** | 0.13 | -90.02 | 0.03 | 82.84 | 0.10 | -124.42 | 0.13 | -97.28 | 0.01 | -71.71 | 0.12 | 39.68 | 0.01 | 46.53 | 0.02 | -55.36 |
| **8** | 0.12 | -83.85 | 0.03 | 103.68 | 0.10 | -120.82 | 0.15 | -104.11 | 0.02 | -74.17 | 0.11 | 57.44 | 0.01 | 31.45 | 0.02 | -73.66 |
| **9** | 0.10 | -85.17 | 0.04 | 103.82 | 0.10 | -113.57 | 0.13 | -108.99 | 0.01 | -76.19 | 0.10 | 71.24 | 0.02 | 39.90 | 0.02 | -64.02 |
| **10** | 0.10 | -80.25 | 0.04 | 122.41 | 0.11 | -114.68 | 0.16 | -111.02 | 0.02 | -65.44 | 0.11 | 81.61 | 0.01 | 38.63 | 0.03 | -76.56 |
| **11** | 0.05 | -82.54 | 0.03 | 114.95 | 0.11 | -102.31 | 0.16 | -112.45 | 0.02 | -128.78 | 0.10 | 95.15 | 0.02 | 46.17 | 0.02 | -65.14 |
| **12** | 0.03 | -70.82 | 0.03 | 99.22 | 0.11 | -107.86 | 0.16 | -112.36 | 0.02 | -93.43 | 0.10 | 106.58 | 0.02 | 51.74 | 0.02 | -89.00 |
| **13** | 0.03 | -94.22 | 0.02 | 102.87 | 0.11 | -101.35 | 0.17 | -111.30 | 0.01 | -84.80 | 0.12 | 116.51 | 0.01 | 59.24 | 0.02 | -51.40 |
| **14** | 0.03 | 66.42 | 0.01 | 113.26 | 0.13 | -101.80 | 0.16 | -113.49 | 0.02 | -80.60 | 0.11 | 120.93 | 0.01 | 58.63 | 0.02 | -54.55 |
| **15** | 0.06 | 76.21 | 0.03 | 86.52 | 0.12 | -95.91 | 0.18 | -113.78 | 0.02 | -93.97 | 0.11 | 129.51 | 0.00 | 15.84 | 0.02 | -62.80 |

Table A.6: Peugeot e-208 — Harmonic Orders $h_{10}$ to $h_{16}$



| **Harmonic Order** | **h10** | | **h11** | | **h12** | | **h13** | | **h14** | | **h15** | | **h16** | |
|---|---|---|---|---|---|---|---|---|---|---|---|---|---|---|
| **Charging Rate (A)** | **A** | $\theta$ | **A** | $\theta$ | **A** | $\theta$ | **A** | $\theta$ | **A** | $\theta$ | **A** | $\theta$ | **A** | $\theta$ |
| **6** | 0.02 | 33.62 | 0.08 | -76.01 | 0.01 | -0.31 | 0.06 | -109.00 | 0.01 | -165.91 | 0.02 | 71.99 | 0.02 | 158.42 |
| **7** | 0.01 | 47.71 | 0.07 | -83.82 | 0.01 | 20.06 | 0.06 | -97.33 | 0.01 | -139.85 | 0.02 | 75.00 | 0.03 | 160.25 |
| **8** | 0.03 | 39.85 | 0.05 | -50.88 | 0.01 | 73.79 | 0.06 | -92.86 | 0.01 | -147.54 | 0.01 | 81.53 | 0.03 | 171.54 |
| **9** | 0.02 | 47.02 | 0.04 | -68.49 | 0.01 | 39.24 | 0.05 | -80.88 | 0.01 | -111.46 | 0.01 | 92.30 | 0.02 | -162.38 |
| **10** | 0.05 | 48.18 | 0.02 | -29.55 | 0.00 | 131.33 | 0.04 | -86.62 | 0.01 | -107.88 | 0.01 | 99.83 | 0.02 | -157.85 |
| **11** | 0.04 | 50.22 | 0.00 | 146.43 | 0.01 | 58.04 | 0.03 | -89.26 | 0.01 | -50.59 | 0.01 | 104.05 | 0.03 | -166.68 |
| **12** | 0.05 | 49.44 | 0.01 | 126.45 | 0.01 | -143.33 | 0.03 | -92.28 | 0.01 | -13.35 | 0.02 | 109.57 | 0.02 | -147.72 |
| **13** | 0.04 | 64.42 | 0.04 | 156.63 | 0.01 | -6.38 | 0.02 | -130.02 | 0.01 | 63.17 | 0.02 | 107.22 | 0.02 | -154.94 |
| **14** | 0.05 | 55.54 | 0.05 | 155.77 | 0.01 | 98.34 | 0.02 | -177.55 | 0.01 | 36.97 | 0.02 | 120.60 | 0.01 | -124.67 |
| **15** | 0.06 | 57.00 | 0.06 | 146.70 | 0.00 | 21.30 | 0.03 | -170.66 | 0.01 | 42.16 | 0.01 | 123.27 | 0.01 | -132.26 |

Table A.7: Peugeot e-208 — Harmonic Orders $h_{17}$ to $h_{24}$

| **Harmonic Order** | **h17** | | **h18** | | **h19** | | **h20** | | **h21** | | **h22** | | **h23** | | **h24** | |
|---|---|---|---|---|---|---|---|---|---|---|---|---|---|---|---|---|
| **Charging Rate (A)** | **A** | $\theta$ | **A** | $\theta$ | **A** | $\theta$ | **A** | $\theta$ | **A** | $\theta$ | **A** | $\theta$ | **A** | $\theta$ | **A** | $\theta$ |
| **6** | 0.03 | -70.99 | 0.01 | -131.09 | 0.03 | 166.95 | 0.00 | 55.29 | 0.00 | -27.11 | 0.02 | -36.73 | 0.04 | 11.27 | 0.00 | 149.51 |
| **7** | 0.04 | -73.09 | 0.01 | -84.32 | 0.04 | -166.53 | 0.00 | 128.94 | 0.01 | -17.04 | 0.01 | -8.36 | 0.04 | 30.94 | 0.01 | 172.19 |
| **8** | 0.06 | -72.26 | 0.00 | 172.44 | 0.05 | -139.97 | 0.01 | 155.15 | 0.01 | -3.35 | 0.01 | -6.27 | 0.04 | 49.80 | 0.00 | 148.21 |
| **9** | 0.07 | -63.86 | 0.01 | -44.96 | 0.06 | -124.92 | 0.02 | 174.24 | 0.01 | -3.44 | 0.01 | 72.80 | 0.02 | 72.96 | 0.00 | -103.35 |
| **10** | 0.07 | -61.61 | 0.00 | 18.13 | 0.07 | -108.75 | 0.01 | 178.32 | 0.00 | -35.73 | 0.01 | 105.91 | 0.02 | 73.26 | 0.00 | 147.26 |
| **11** | 0.07 | -52.66 | 0.01 | 18.88 | 0.08 | -102.07 | 0.02 | -162.88 | 0.01 | -9.31 | 0.01 | 131.58 | 0.00 | 156.05 | 0.00 | 2.40 |
| **12** | 0.07 | -48.53 | 0.00 | 41.82 | 0.08 | -94.76 | 0.01 | -157.23 | 0.01 | -12.96 | 0.01 | 145.26 | 0.01 | -140.86 | 0.00 | 33.32 |
| **13** | 0.07 | -45.18 | 0.01 | -44.52 | 0.08 | -89.90 | 0.01 | -145.41 | 0.01 | 9.03 | 0.01 | 131.11 | 0.01 | -141.51 | 0.00 | 142.14 |
| **14** | 0.06 | -38.20 | 0.00 | 6.03 | 0.08 | -88.48 | 0.01 | -135.02 | 0.01 | -5.99 | 0.01 | 129.68 | 0.01 | -79.37 | 0.00 | 0.64 |
| **15** | 0.05 | -31.94 | 0.00 | 59.68 | 0.07 | -87.89 | 0.01 | -119.02 | 0.01 | -9.90 | 0.01 | 125.97 | 0.02 | -83.16 | 0.00 | 95.35 |

Table A.8: Peugeot e-208 — Harmonic Orders $h_{25}$ to $h_{31}$



| **Harmonic Order** | **h25** | | **h26** | | **h27** | | **h28** | | **h29** | | **h30** | | **h31** | |
|---|---|---|---|---|---|---|---|---|---|---|---|---|---|---|
| **Charging Rate (A)** | **A** | $\theta$ | **A** | $\theta$ | **A** | $\theta$ | **A** | $\theta$ | **A** | $\theta$ | **A** | $\theta$ | **A** | $\theta$ |
| **6** | 0.01 | 120.32 | 0.01 | -81.33 | 0.02 | -4.77 | 0.00 | 134.00 | 0.01 | -172.87 | 0.01 | 67.37 | 0.01 | -90.22 |
| **7** | 0.01 | 67.99 | 0.01 | -75.40 | 0.02 | 7.27 | 0.01 | -117.27 | 0.01 | -136.31 | 0.00 | -2.30 | 0.01 | -79.66 |
| **8** | 0.01 | 101.76 | 0.01 | -17.71 | 0.01 | 30.64 | 0.01 | -94.30 | 0.01 | -42.06 | 0.00 | 61.75 | 0.01 | -48.62 |
| **9** | 0.01 | 147.43 | 0.01 | -17.26 | 0.02 | 26.05 | 0.00 | -22.53 | 0.01 | 19.80 | 0.00 | -100.38 | 0.02 | -8.17 |
| **10** | 0.02 | -165.98 | 0.01 | -7.41 | 0.02 | 50.69 | 0.01 | -67.94 | 0.00 | -24.64 | 0.00 | 87.83 | 0.02 | 11.79 |
| **11** | 0.02 | -140.75 | 0.01 | 52.96 | 0.02 | 52.84 | 0.00 | -147.40 | 0.01 | -13.23 | 0.00 | 88.78 | 0.02 | 16.69 |
| **12** | 0.03 | -131.81 | 0.00 | 120.98 | 0.02 | 63.16 | 0.00 | 138.96 | 0.01 | -78.79 | 0.00 | -27.02 | 0.02 | 30.73 |
| **13** | 0.04 | -123.02 | 0.00 | -168.42 | 0.02 | 56.99 | 0.01 | 131.88 | 0.01 | -104.36 | 0.00 | -153.46 | 0.01 | -4.43 |
| **14** | 0.05 | -106.23 | 0.00 | -3.54 | 0.02 | 72.23 | 0.01 | 165.01 | 0.02 | -98.19 | 0.00 | -77.73 | 0.01 | 3.13 |
| **15** | 0.05 | -98.08 | 0.00 | -51.49 | 0.01 | 78.60 | 0.01 | -157.64 | 0.03 | -95.15 | 0.00 | 116.40 | 0.01 | -31.62 |

Table A.9: Nissan Leaf e+ — Harmonic Orders $h_2$ to $h_9$

| **Harmonic Order** | **h2** | | **h3** | | **h4** | | **h5** | | **h6** | | **h7** | | **h8** | | **h9** | |
|---|---|---|---|---|---|---|---|---|---|---|---|---|---|---|---|---|
| **Charging Rate (A)** | **A** | $\theta$ | **A** | $\theta$ | **A** | $\theta$ | **A** | $\theta$ | **A** | $\theta$ | **A** | $\theta$ | **A** | $\theta$ | **A** | $\theta$ |
| **6** | 0.00 | -175.77 | 0.53 | -150.71 | 0.00 | 168.98 | 0.20 | -151.52 | 0.00 | 122.27 | 0.12 | 86.14 | 0.00 | 22.81 | 0.04 | 59.86 |
| **7** | 0.00 | -178.21 | 0.49 | -151.13 | 0.00 | 178.72 | 0.23 | -141.13 | 0.00 | 141.97 | 0.10 | 126.38 | 0.00 | 25.98 | 0.09 | 143.64 |
| **8** | 0.00 | -172.07 | 0.46 | -153.47 | 0.00 | -166.71 | 0.22 | -127.90 | 0.00 | 171.31 | 0.08 | 154.02 | 0.00 | 27.54 | 0.15 | 166.61 |
| **9** | 0.00 | 174.40 | 0.44 | -155.33 | 0.00 | 169.10 | 0.21 | -115.31 | 0.00 | 149.77 | 0.05 | 169.78 | 0.00 | 44.81 | 0.16 | 179.16 |
| **10** | 0.00 | 179.24 | 0.44 | -156.35 | 0.00 | -176.27 | 0.20 | -103.25 | 0.00 | 149.74 | 0.02 | -152.47 | 0.00 | 45.33 | 0.16 | -168.95 |
| **11** | 0.00 | -175.88 | 0.44 | -157.96 | 0.00 | -158.77 | 0.21 | -93.76 | 0.00 | 166.27 | 0.03 | -59.50 | 0.00 | 39.43 | 0.15 | -158.00 |
| **12** | 0.00 | -174.28 | 0.46 | -158.89 | 0.00 | -179.77 | 0.22 | -85.63 | 0.00 | 173.67 | 0.06 | -40.92 | 0.00 | 39.93 | 0.15 | -148.53 |
| **13** | 0.00 | 171.02 | 0.48 | -159.49 | 0.00 | -161.78 | 0.23 | -80.09 | 0.00 | 169.06 | 0.09 | -32.73 | 0.00 | 22.87 | 0.14 | -140.57 |
| **14** | 0.00 | 168.63 | 0.50 | -160.33 | 0.00 | -179.61 | 0.24 | -75.91 | 0.00 | 174.51 | 0.10 | -27.99 | 0.00 | 40.17 | 0.14 | -134.08 |
| **15** | 0.00 | 173.31 | 0.52 | -161.05 | 0.00 | 175.62 | 0.25 | -72.79 | 0.00 | 160.95 | 0.12 | -24.75 | 0.00 | 38.09 | 0.14 | -129.24 |
| **16** | 0.01 | 166.85 | 0.55 | -162.24 | 0.00 | -162.58 | 0.26 | -68.60 | 0.00 | 169.49 | 0.14 | -21.20 | 0.00 | 47.24 | 0.14 | -125.82 |
| **17** | 0.01 | 166.76 | 0.57 | -162.79 | 0.00 | 176.90 | 0.27 | -68.15 | 0.00 | 160.62 | 0.15 | -18.72 | 0.00 | 44.11 | 0.14 | -123.06 |
| **18** | 0.01 | 165.28 | 0.60 | -163.31 | 0.00 | -175.99 | 0.27 | -67.83 | 0.00 | 160.47 | 0.16 | -16.49 | 0.00 | 37.89 | 0.14 | -120.69 |
| **19** | 0.01 | 163.31 | 0.62 | -163.61 | 0.00 | -157.47 | 0.28 | -66.16 | 0.00 | 171.50 | 0.17 | -15.27 | 0.00 | 37.12 | 0.14 | -119.27 |
| **20** | 0.01 | 165.80 | 0.65 | -163.58 | 0.00 | -164.65 | 0.29 | -64.03 | 0.00 | 167.38 | 0.19 | -13.81 | 0.00 | 39.19 | 0.14 | -117.30 |
| **21** | 0.01 | 167.57 | 0.68 | -164.03 | 0.00 | -162.59 | 0.30 | -62.06 | 0.00 | 158.07 | 0.20 | -12.74 | 0.00 | 23.09 | 0.14 | -116.13 |
| **22** | 0.01 | 167.20 | 0.70 | -164.46 | 0.00 | -163.12 | 0.31 | -62.50 | 0.00 | 167.23 | 0.21 | -11.22 | 0.00 | 28.20 | 0.15 | -114.93 |
| **23** | 0.01 | 171.77 | 0.73 | -164.97 | 0.00 | -162.60 | 0.32 | -61.68 | 0.00 | 161.51 | 0.22 | -10.78 | 0.00 | 38.15 | 0.15 | -113.79 |
| **24** | 0.01 | -178.22 | 0.75 | -165.20 | 0.00 | -151.92 | 0.34 | -59.88 | 0.00 | 171.28 | 0.23 | -10.36 | 0.00 | 33.65 | 0.15 | -112.85 |
| **25** | 0.01 | 170.75 | 0.77 | -165.82 | 0.00 | -137.88 | 0.36 | -58.23 | 0.00 | 162.22 | 0.25 | -11.61 | 0.00 | 34.86 | 0.16 | -111.52 |
| **26** | 0.01 | 178.98 | 0.80 | -165.77 | 0.00 | -130.26 | 0.37 | -56.78 | 0.00 | 156.74 | 0.27 | -10.68 | 0.00 | 28.63 | 0.16 | -110.37 |
| **27** | 0.01 | 170.20 | 0.82 | -165.64 | 0.00 | -144.01 | 0.38 | -56.71 | 0.00 | 143.93 | 0.28 | -9.71 | 0.00 | 35.45 | 0.17 | -109.55 |
| **28** | 0.01 | 171.62 | 0.84 | -165.51 | 0.00 | -149.78 | 0.39 | -55.24 | 0.00 | 158.82 | 0.30 | -9.54 | 0.00 | 34.31 | 0.17 | -107.53 |

Table A.10: Nissan Leaf e+ — Harmonic Orders $h_{10}$ to $h_{17}$

| **Harmonic Order** | **h10** | | **h11** | | **h12** | | **h13** | | **h14** | | **h15** | | **h16** | | **h17** | |
|---|---|---|---|---|---|---|---|---|---|---|---|---|---|---|---|---|
| **Charging Rate (A)** | **A** | $\theta$ | **A** | $\theta$ | **A** | $\theta$ | **A** | $\theta$ | **A** | $\theta$ | **A** | $\theta$ | **A** | $\theta$ | **A** | $\theta$ |
| **6** | 0.00 | -126.48 | 0.08 | 14.91 | 0.00 | 66.73 | 0.01 | -100.30 | 0.00 | -103.24 | 0.02 | 61.68 | 0.00 | 117.57 | 0.02 | 122.72 |
| **7** | 0.00 | -130.60 | 0.08 | 65.33 | 0.00 | 32.80 | 0.04 | 47.53 | 0.00 | -97.10 | 0.07 | 1.24 | 0.00 | 119.07 | 0.03 | -59.65 |
| **8** | 0.00 | -148.79 | 0.11 | 115.10 | 0.00 | 31.75 | 0.09 | 101.31 | 0.00 | -97.72 | 0.09 | 37.12 | 0.00 | 135.90 | 0.06 | -14.23 |
| **9** | 0.00 | -162.39 | 0.12 | 138.49 | 0.00 | 56.91 | 0.12 | 127.61 | 0.00 | -77.57 | 0.09 | 72.69 | 0.00 | 134.33 | 0.05 | 33.49 |
| **10** | 0.00 | -166.27 | 0.12 | 153.97 | 0.00 | 53.33 | 0.13 | 143.00 | 0.00 | -77.42 | 0.09 | 95.01 | 0.00 | 124.72 | 0.05 | 72.77 |
| **11** | 0.00 | -153.40 | 0.10 | 168.38 | 0.00 | 54.42 | 0.12 | 156.53 | 0.00 | -87.67 | 0.08 | 111.15 | 0.00 | 154.89 | 0.04 | 100.21 |
| **12** | 0.00 | -154.52 | 0.09 | -177.58 | 0.00 | 60.30 | 0.12 | 167.80 | 0.00 | -72.40 | 0.07 | 124.97 | 0.00 | 118.53 | 0.04 | 122.78 |
| **13** | 0.00 | -150.72 | 0.09 | -166.15 | 0.00 | 70.51 | 0.12 | 176.35 | 0.00 | -79.61 | 0.07 | 137.97 | 0.00 | 145.69 | 0.03 | 146.14 |
| **14** | 0.00 | -148.38 | 0.09 | -154.66 | 0.00 | 68.31 | 0.11 | -176.90 | 0.00 | -57.31 | 0.06 | 149.65 | 0.00 | 122.24 | 0.03 | 163.52 |
| **15** | 0.00 | -154.39 | 0.08 | -145.94 | 0.00 | 62.37 | 0.11 | -170.27 | 0.00 | -60.88 | 0.06 | 158.65 | 0.00 | 131.77 | 0.03 | 177.68 |
| **16** | 0.00 | -154.99 | 0.08 | -138.25 | 0.00 | 87.59 | 0.11 | -165.48 | 0.00 | -80.40 | 0.05 | 167.37 | 0.00 | 147.55 | 0.04 | -170.17 |
| **17** | 0.00 | -150.67 | 0.08 | -132.17 | 0.00 | 71.97 | 0.11 | -162.05 | 0.00 | -69.10 | 0.05 | 174.69 | 0.00 | 129.85 | 0.04 | -158.51 |
| **18** | 0.00 | -154.37 | 0.08 | -127.83 | 0.00 | 69.26 | 0.11 | -159.35 | 0.00 | -51.79 | 0.05 | -176.83 | 0.00 | 126.15 | 0.04 | -151.50 |
| **19** | 0.00 | -151.51 | 0.08 | -123.61 | 0.00 | 72.13 | 0.11 | -156.59 | 0.00 | -53.52 | 0.05 | -171.19 | 0.00 | 143.40 | 0.04 | -146.08 |
| **20** | 0.00 | -150.62 | 0.08 | -118.66 | 0.00 | 78.50 | 0.11 | -154.98 | 0.00 | -40.22 | 0.05 | -165.20 | 0.00 | 126.48 | 0.04 | -142.45 |
| **21** | 0.00 | -151.43 | 0.08 | -114.59 | 0.00 | 75.86 | 0.11 | -153.21 | 0.00 | -63.63 | 0.05 | -162.52 | 0.00 | 163.01 | 0.05 | -141.39 |
| **22** | 0.00 | -149.84 | 0.08 | -112.14 | 0.00 | 87.08 | 0.11 | -150.56 | 0.00 | -58.19 | 0.05 | -161.02 | 0.00 | 165.91 | 0.05 | -140.04 |
| **23** | 0.00 | -152.23 | 0.09 | -110.88 | 0.00 | 85.60 | 0.12 | -148.80 | 0.00 | -39.84 | 0.06 | -157.35 | 0.00 | 120.74 | 0.05 | -140.27 |
| **24** | 0.00 | -152.62 | 0.09 | -109.42 | 0.00 | 87.29 | 0.12 | -147.84 | 0.00 | -57.02 | 0.06 | -154.09 | 0.00 | 149.89 | 0.06 | -141.18 |
| **25** | 0.00 | -153.03 | 0.10 | -107.02 | 0.00 | 79.04 | 0.13 | -145.84 | 0.00 | -50.14 | 0.07 | -151.70 | 0.00 | 157.92 | 0.06 | -141.39 |
| **26** | 0.00 | -157.74 | 0.10 | -105.30 | 0.00 | 74.58 | 0.13 | -145.26 | 0.00 | -38.13 | 0.07 | -149.81 | 0.00 | 105.06 | 0.07 | -140.64 |
| **27** | 0.00 | -150.25 | 0.10 | -103.40 | 0.00 | 70.53 | 0.14 | -143.60 | 0.00 | -43.79 | 0.08 | -147.98 | 0.00 | 137.20 | 0.07 | -144.72 |
| **28** | 0.00 | -155.81 | 0.12 | -98.84 | 0.00 | 79.70 | 0.15 | -141.77 | 0.00 | -48.14 | 0.09 | -146.24 | 0.00 | 129.76 | 0.08 | -143.57 |

Table A.11: Nissan Leaf e+ — Harmonic Orders $h_{18}$ to $h_{25}$

| **Harmonic Order** | **h18** | | **h19** | | **h20** | | **h21** | | **h22** | | **h23** | | **h24** | | **h25** | |
|---|---|---|---|---|---|---|---|---|---|---|---|---|---|---|---|---|
| **Charging Rate (A)** | **A** | $\theta$ | **A** | $\theta$ | **A** | $\theta$ | **A** | $\theta$ | **A** | $\theta$ | **A** | $\theta$ | **A** | $\theta$ | **A** | $\theta$ |
| **6** | 0.00 | -8.91 | 0.06 | 102.85 | 0.00 | 6.41 | 0.03 | 3.25 | 0.00 | -104.71 | 0.04 | -13.54 | 0.00 | 123.51 | 0.00 | -117.08 |
| **7** | 0.00 | -165.32 | 0.04 | 135.24 | 0.00 | 114.98 | 0.01 | 53.15 | 0.00 | -83.36 | 0.04 | 18.11 | 0.00 | 104.80 | 0.01 | 54.90 |
| **8** | 0.00 | -173.92 | 0.01 | 42.00 | 0.00 | 98.43 | 0.03 | -62.03 | 0.00 | -63.66 | 0.03 | -22.32 | 0.00 | 107.34 | 0.02 | 157.59 |
| **9** | 0.00 | -106.81 | 0.04 | 74.96 | 0.00 | -113.12 | 0.04 | -24.67 | 0.00 | -92.86 | 0.05 | -19.17 | 0.00 | 134.83 | 0.02 | -113.48 |
| **10** | 0.00 | -102.32 | 0.06 | 101.46 | 0.00 | -111.66 | 0.04 | 10.07 | 0.00 | -78.14 | 0.05 | 7.33 | 0.00 | 168.64 | 0.02 | -70.59 |
| **11** | 0.00 | -119.62 | 0.07 | 119.31 | 0.00 | -120.58 | 0.04 | 38.19 | 0.00 | -51.46 | 0.06 | 27.21 | 0.00 | 120.87 | 0.01 | -5.11 |
| **12** | 0.00 | -96.83 | 0.08 | 133.12 | 0.00 | -124.64 | 0.03 | 62.69 | 0.00 | -44.80 | 0.06 | 44.69 | 0.00 | 120.41 | 0.01 | 43.60 |
| **13** | 0.00 | -107.73 | 0.08 | 144.58 | 0.00 | -136.61 | 0.03 | 80.85 | 0.00 | -45.91 | 0.06 | 56.72 | 0.00 | 85.38 | 0.02 | 63.78 |
| **14** | 0.00 | -117.77 | 0.09 | 153.86 | 0.00 | -99.15 | 0.03 | 97.92 | 0.00 | -49.15 | 0.06 | 69.67 | 0.00 | 85.86 | 0.02 | 92.69 |
| **15** | 0.00 | -65.34 | 0.09 | 161.44 | 0.00 | -85.01 | 0.03 | 112.58 | 0.00 | -39.32 | 0.06 | 80.59 | 0.00 | 62.45 | 0.02 | 106.50 |
| **16** | 0.00 | -125.02 | 0.09 | 168.52 | 0.00 | -86.49 | 0.03 | 127.86 | 0.00 | -55.26 | 0.06 | 91.00 | 0.00 | 174.79 | 0.03 | 119.99 |
| **17** | 0.00 | -58.35 | 0.09 | 173.17 | 0.00 | -136.83 | 0.03 | 138.20 | 0.00 | -49.54 | 0.06 | 97.06 | 0.00 | -164.67 | 0.03 | 127.81 |
| **18** | 0.00 | -72.74 | 0.10 | 176.95 | 0.00 | -88.23 | 0.03 | 148.35 | 0.00 | -43.55 | 0.06 | 107.15 | 0.00 | -70.74 | 0.03 | 133.13 |
| **19** | 0.00 | -69.15 | 0.10 | 179.48 | 0.00 | -91.87 | 0.03 | 153.98 | 0.00 | -24.78 | 0.06 | 114.03 | 0.00 | 86.16 | 0.04 | 137.10 |
| **20** | 0.00 | -66.16 | 0.11 | -177.42 | 0.00 | -60.66 | 0.04 | 155.93 | 0.00 | -32.21 | 0.07 | 117.38 | 0.00 | -154.66 | 0.04 | 136.72 |
| **21** | 0.00 | -117.95 | 0.11 | -174.69 | 0.00 | -148.94 | 0.04 | 157.45 | 0.00 | -44.99 | 0.08 | 121.71 | 0.00 | -147.67 | 0.05 | 138.89 |
| **22** | 0.00 | -63.58 | 0.12 | -173.06 | 0.00 | -84.97 | 0.05 | 158.81 | 0.00 | -47.72 | 0.08 | 124.45 | 0.00 | -169.64 | 0.06 | 142.76 |
| **23** | 0.00 | -50.70 | 0.13 | -172.19 | 0.00 | -54.72 | 0.05 | 159.65 | 0.00 | -36.79 | 0.09 | 126.83 | 0.00 | -112.60 | 0.07 | 140.99 |
| **24** | 0.00 | -64.86 | 0.14 | -171.10 | 0.00 | -88.56 | 0.06 | 159.68 | 0.00 | -34.49 | 0.10 | 127.79 | 0.00 | -126.89 | 0.08 | 139.29 |
| **25** | 0.00 | -51.91 | 0.14 | -170.77 | 0.00 | -31.84 | 0.07 | 159.55 | 0.00 | -29.31 | 0.11 | 129.74 | 0.00 | -132.55 | 0.08 | 137.50 |
| **26** | 0.00 | -51.28 | 0.15 | -170.86 | 0.00 | -75.72 | 0.08 | 159.50 | 0.00 | -26.11 | 0.12 | 130.68 | 0.00 | -96.84 | 0.09 | 136.57 |
| **27** | 0.00 | -56.18 | 0.16 | -170.94 | 0.00 | 120.69 | 0.09 | 158.79 | 0.00 | -17.98 | 0.13 | 131.28 | 0.00 | -128.68 | 0.10 | 135.31 |
| **28** | 0.00 | -52.14 | 0.17 | -170.62 | 0.00 | -98.59 | 0.10 | 157.37 | 0.00 | -23.21 | 0.14 | 130.85 | 0.00 | -120.96 | 0.11 | 133.02 |

Table A.12: Nissan Leaf e+ — Harmonic Orders $h_{26}$ to $h_{33}$

| **Harmonic Order** | **h26** | | **h27** | | **h28** | | **h29** | | **h30** | | **h31** | | **h32** | | **h33** | |
|---|---|---|---|---|---|---|---|---|---|---|---|---|---|---|---|---|
| **Charging Rate (A)** | **A** | $\theta$ | **A** | $\theta$ | **A** | $\theta$ | **A** | $\theta$ | **A** | $\theta$ | **A** | $\theta$ | **A** | $\theta$ | **A** | $\theta$ |
| **6** | 0.00 | -12.13 | 0.03 | -51.52 | 0.00 | -120.12 | 0.01 | 34.08 | 0.00 | -22.26 | 0.01 | -111.20 | 0.00 | 125.01 | 0.02 | -102.46 |
| **7** | 0.00 | -23.91 | 0.02 | -44.26 | 0.00 | -140.56 | 0.01 | 99.91 | 0.00 | -55.10 | 0.01 | -152.88 | 0.00 | 146.34 | 0.02 | -67.40 |
| **8** | 0.00 | -13.42 | 0.01 | -62.23 | 0.00 | -94.32 | 0.02 | 100.13 | 0.00 | -68.72 | 0.00 | -178.70 | 0.00 | 152.16 | 0.02 | -46.53 |
| **9** | 0.00 | -9.61 | 0.03 | -87.52 | 0.00 | -12.13 | 0.02 | 178.88 | 0.00 | 4.57 | 0.02 | -161.47 | 0.00 | 135.14 | 0.00 | -63.58 |
| **10** | 0.00 | 8.75 | 0.04 | -60.97 | 0.00 | -75.57 | 0.02 | -136.64 | 0.00 | 17.72 | 0.03 | -130.23 | 0.00 | 157.53 | 0.01 | -106.62 |
| **11** | 0.00 | 31.51 | 0.04 | -39.95 | 0.00 | -29.87 | 0.02 | -101.13 | 0.00 | 39.97 | 0.03 | -102.50 | 0.00 | -168.17 | 0.02 | -88.35 |
| **12** | 0.00 | 27.09 | 0.04 | -16.79 | 0.00 | 9.56 | 0.01 | -68.02 | 0.00 | -1.12 | 0.03 | -80.86 | 0.00 | -160.15 | 0.02 | -61.54 |
| **13** | 0.00 | 36.18 | 0.03 | 3.17 | 0.00 | -86.69 | 0.01 | -27.71 | 0.00 | -29.55 | 0.02 | -60.13 | 0.00 | -125.41 | 0.02 | -36.23 |
| **14** | 0.00 | 36.41 | 0.03 | 19.29 | 0.00 | 42.90 | 0.01 | 12.25 | 0.00 | 24.69 | 0.02 | -41.97 | 0.00 | -131.20 | 0.03 | -16.65 |
| **15** | 0.00 | 24.15 | 0.03 | 31.17 | 0.00 | -88.92 | 0.01 | 50.21 | 0.00 | 43.27 | 0.02 | -26.96 | 0.00 | -115.47 | 0.03 | -0.07 |
| **16** | 0.00 | 28.63 | 0.03 | 43.96 | 0.00 | -17.38 | 0.01 | 73.76 | 0.00 | 41.81 | 0.02 | -8.06 | 0.00 | -109.43 | 0.03 | 14.86 |
| **17** | 0.00 | 38.09 | 0.03 | 56.86 | 0.00 | -18.45 | 0.02 | 88.80 | 0.00 | 79.89 | 0.02 | 9.32 | 0.00 | -113.73 | 0.03 | 24.27 |
| **18** | 0.00 | 46.74 | 0.03 | 63.56 | 0.00 | 1.80 | 0.02 | 92.92 | 0.00 | 49.38 | 0.02 | 22.22 | 0.00 | -113.06 | 0.03 | 36.37 |
| **19** | 0.00 | 48.96 | 0.04 | 70.27 | 0.00 | -91.45 | 0.02 | 97.01 | 0.00 | 30.07 | 0.02 | 32.30 | 0.00 | -117.13 | 0.04 | 43.27 |
| **20** | 0.00 | 54.06 | 0.04 | 74.73 | 0.00 | -4.50 | 0.03 | 98.82 | 0.00 | 77.24 | 0.02 | 44.98 | 0.00 | -115.79 | 0.05 | 46.89 |
| **21** | 0.00 | 62.06 | 0.05 | 80.84 | 0.00 | 49.21 | 0.03 | 98.10 | 0.00 | 68.50 | 0.03 | 51.04 | 0.00 | -86.75 | 0.05 | 49.53 |
| **22** | 0.00 | 68.17 | 0.06 | 85.97 | 0.00 | 21.63 | 0.04 | 93.06 | 0.00 | 75.16 | 0.04 | 53.02 | 0.00 | -88.80 | 0.06 | 49.90 |
| **23** | 0.00 | 57.46 | 0.07 | 89.10 | 0.00 | 19.92 | 0.05 | 91.14 | 0.00 | 113.98 | 0.05 | 56.00 | 0.00 | -114.85 | 0.07 | 51.33 |
| **24** | 0.00 | 63.73 | 0.08 | 91.85 | 0.00 | 4.10 | 0.06 | 92.40 | 0.00 | 76.85 | 0.06 | 59.17 | 0.00 | -83.02 | 0.08 | 51.96 |
| **25** | 0.00 | 66.15 | 0.09 | 93.90 | 0.00 | -9.81 | 0.07 | 92.53 | 0.00 | 70.06 | 0.07 | 59.34 | 0.00 | -113.59 | 0.09 | 51.57 |
| **26** | 0.00 | 57.25 | 0.09 | 94.75 | 0.00 | -68.29 | 0.08 | 90.61 | 0.00 | 136.32 | 0.08 | 60.79 | 0.00 | -112.62 | 0.10 | 52.40 |
| **27** | 0.00 | 71.92 | 0.11 | 95.00 | 0.00 | 26.05 | 0.09 | 90.09 | 0.00 | 94.22 | 0.09 | 60.60 | 0.00 | -166.38 | 0.11 | 51.11 |
| **28** | 0.00 | 71.94 | 0.12 | 94.75 | 0.00 | -19.50 | 0.10 | 88.23 | 0.00 | 119.80 | 0.10 | 60.86 | 0.00 | -110.65 | 0.12 | 50.57 |

Table A.13: Nissan Leaf e+ — Harmonic Orders $h_{34}$ to $h_{41}$

| **Harmonic Order** | **h34** | | **h35** | | **h36** | | **h37** | | **h38** | | **h49** | | **h40** | | **h41** | |
|---|---|---|---|---|---|---|---|---|---|---|---|---|---|---|---|---|
| **Charging Rate (A)** | **A** | $\theta$ | **A** | $\theta$ | **A** | $\theta$ | **A** | $\theta$ | **A** | $\theta$ | **A** | $\theta$ | **A** | $\theta$ | **A** | $\theta$ |
| **6** | 0.00 | 17.25 | 0.02 | 9.09 | 0.00 | -135.20 | 0.01 | 166.79 | 0.00 | 121.76 | 0.00 | -62.33 | 0.00 | -71.58 | 0.01 | -16.24 |
| **7** | 0.00 | 13.42 | 0.03 | -19.15 | 0.00 | -113.35 | 0.02 | -130.95 | 0.00 | 118.75 | 0.01 | -178.89 | 0.00 | -68.48 | 0.02 | 78.89 |
| **8** | 0.00 | 79.76 | 0.03 | 4.77 | 0.00 | -165.45 | 0.01 | -130.08 | 0.00 | 127.10 | 0.00 | 130.01 | 0.00 | -43.58 | 0.02 | 61.95 |
| **9** | 0.00 | 46.43 | 0.03 | 44.62 | 0.00 | -130.87 | 0.00 | 113.59 | 0.00 | 118.94 | 0.01 | 87.44 | 0.00 | -125.59 | 0.02 | 70.24 |
| **10** | 0.00 | 72.56 | 0.02 | 80.73 | 0.00 | -110.29 | 0.02 | 164.10 | 0.00 | 126.48 | 0.02 | 125.26 | 0.00 | -12.55 | 0.03 | 97.31 |
| **11** | 0.00 | 83.38 | 0.01 | 88.89 | 0.00 | -70.18 | 0.02 | -161.26 | 0.00 | 145.36 | 0.02 | 160.79 | 0.00 | 24.38 | 0.03 | 125.09 |
| **12** | 0.00 | 101.02 | 0.01 | 83.90 | 0.00 | -84.03 | 0.02 | -137.56 | 0.00 | 143.95 | 0.02 | -175.34 | 0.00 | 4.61 | 0.03 | 146.59 |
| **13** | 0.00 | 106.93 | 0.01 | 75.90 | 0.00 | -47.40 | 0.02 | -117.70 | 0.00 | 163.62 | 0.02 | -157.53 | 0.00 | 68.24 | 0.03 | 163.56 |
| **14** | 0.00 | 125.16 | 0.01 | 66.34 | 0.00 | -49.77 | 0.02 | -97.52 | 0.00 | 179.74 | 0.02 | -141.44 | 0.00 | -108.49 | 0.03 | 178.91 |
| **15** | 0.00 | 130.81 | 0.02 | 70.88 | 0.00 | -35.12 | 0.02 | -77.54 | 0.00 | -176.67 | 0.02 | -122.30 | 0.00 | -5.04 | 0.03 | -169.24 |
| **16** | 0.00 | 155.37 | 0.02 | 76.03 | 0.00 | -56.48 | 0.02 | -54.72 | 0.00 | -140.24 | 0.02 | -99.06 | 0.00 | 76.00 | 0.03 | -158.64 |
| **17** | 0.00 | 163.55 | 0.02 | 76.26 | 0.00 | -45.59 | 0.02 | -39.89 | 0.00 | -148.95 | 0.02 | -81.74 | 0.00 | 73.27 | 0.02 | -145.65 |
| **18** | 0.00 | 154.64 | 0.03 | 74.24 | 0.00 | -15.55 | 0.03 | -23.67 | 0.00 | -171.95 | 0.02 | -57.48 | 0.00 | 46.29 | 0.02 | -124.66 |
| **19** | 0.00 | 159.69 | 0.03 | 74.26 | 0.00 | -21.49 | 0.03 | -10.74 | 0.00 | -175.65 | 0.02 | -40.91 | 0.00 | 39.47 | 0.02 | -106.91 |
| **20** | 0.00 | 160.49 | 0.04 | 72.91 | 0.00 | 4.70 | 0.04 | -4.98 | 0.00 | -158.02 | 0.03 | -32.30 | 0.00 | 109.20 | 0.03 | -92.25 |
| **21** | 0.00 | 117.29 | 0.04 | 68.78 | 0.00 | -1.27 | 0.04 | 0.25 | 0.00 | -76.10 | 0.04 | -25.93 | 0.00 | -130.66 | 0.03 | -77.16 |
| **22** | 0.00 | 155.33 | 0.05 | 63.72 | 0.00 | -26.96 | 0.05 | 4.29 | 0.00 | -111.29 | 0.05 | -20.90 | 0.00 | 123.27 | 0.04 | -66.58 |
| **23** | 0.00 | 156.79 | 0.06 | 60.07 | 0.00 | 13.01 | 0.06 | 6.80 | 0.00 | -139.56 | 0.05 | -18.70 | 0.00 | 100.62 | 0.05 | -59.57 |
| **24** | 0.00 | 153.30 | 0.06 | 56.31 | 0.00 | -19.07 | 0.07 | 7.85 | 0.00 | -107.91 | 0.06 | -18.18 | 0.00 | 142.41 | 0.06 | -56.54 |
| **25** | 0.00 | -176.01 | 0.07 | 54.37 | 0.00 | -6.62 | 0.08 | 8.25 | 0.00 | -140.59 | 0.07 | -17.78 | 0.00 | 111.51 | 0.06 | -53.15 |
| **26** | 0.00 | -177.80 | 0.07 | 51.54 | 0.00 | 78.11 | 0.09 | 8.82 | 0.00 | -156.98 | 0.08 | -16.69 | 0.00 | 98.52 | 0.07 | -51.66 |
| **27** | 0.00 | 148.76 | 0.08 | 47.89 | 0.00 | 35.73 | 0.10 | 7.96 | 0.00 | -163.13 | 0.09 | -17.16 | 0.00 | 99.30 | 0.08 | -51.99 |
| **28** | 0.00 | 173.29 | 0.09 | 42.89 | 0.00 | 41.99 | 0.10 | 5.97 | 0.00 | -111.11 | 0.09 | -18.39 | 0.00 | 119.48 | 0.09 | -53.31 |

Table A.14: Nissan Leaf e+ — Harmonic Orders $h_{42}$ to $h_{49}$

| **Harmonic Order** | **h42** | | **h43** | | **h44** | | **h45** | | **h46** | | **h47** | | **h48** | | **h49** | |
|---|---|---|---|---|---|---|---|---|---|---|---|---|---|---|---|---|
| **Charging Rate (A)** | **A** | $\theta$ | **A** | $\theta$ | **A** | $\theta$ | **A** | $\theta$ | **A** | $\theta$ | **A** | $\theta$ | **A** | $\theta$ | **A** | $\theta$ |
| **6** | 0.00 | 150.09 | 0.01 | 175.59 | 0.00 | 46.46 | 0.01 | 143.55 | 0.00 | 44.34 | 0.01 | 86.55 | 0.00 | -88.17 | 0.02 | -4.13 |
| **7** | 0.00 | -122.84 | 0.02 | 85.58 | 0.00 | 37.12 | 0.01 | 28.29 | 0.00 | 100.32 | 0.01 | -36.72 | 0.00 | -133.55 | 0.01 | -49.99 |
| **8** | 0.00 | -70.73 | 0.01 | 92.42 | 0.00 | -111.00 | 0.00 | -34.61 | 0.00 | -159.95 | 0.01 | -164.35 | 0.00 | 149.19 | 0.00 | 45.01 |
| **9** | 0.00 | 175.02 | 0.01 | 81.68 | 0.00 | 11.87 | 0.00 | 18.13 | 0.00 | 144.04 | 0.00 | -141.34 | 0.00 | -52.85 | 0.01 | 58.52 |
| **10** | 0.00 | -58.36 | 0.02 | 95.39 | 0.00 | -39.91 | 0.01 | 56.50 | 0.00 | -164.02 | 0.00 | -14.05 | 0.00 | -69.33 | 0.01 | 43.43 |
| **11** | 0.00 | 88.34 | 0.02 | 126.48 | 0.00 | -37.04 | 0.02 | 95.03 | 0.00 | -167.30 | 0.01 | 81.98 | 0.00 | -131.34 | 0.01 | 71.61 |
| **12** | 0.00 | -129.35 | 0.03 | 150.50 | 0.00 | -24.86 | 0.02 | 123.67 | 0.00 | -159.38 | 0.01 | 121.30 | 0.00 | -7.09 | 0.02 | 99.87 |
| **13** | 0.00 | -36.00 | 0.03 | 170.52 | 0.00 | 85.33 | 0.02 | 146.45 | 0.00 | -170.17 | 0.01 | 149.73 | 0.00 | 124.35 | 0.02 | 121.07 |
| **14** | 0.00 | -31.28 | 0.03 | -173.40 | 0.00 | 17.23 | 0.02 | 167.28 | 0.00 | -103.24 | 0.01 | 173.52 | 0.00 | 15.83 | 0.02 | 141.15 |
| **15** | 0.00 | -20.37 | 0.02 | -158.44 | 0.00 | 28.47 | 0.02 | -177.22 | 0.00 | -86.82 | 0.01 | -164.38 | 0.00 | 23.34 | 0.02 | 160.99 |
| **16** | 0.00 | -101.09 | 0.02 | -141.22 | 0.00 | -173.56 | 0.01 | -152.97 | 0.00 | -126.37 | 0.01 | -143.48 | 0.00 | -34.63 | 0.02 | -179.20 |
| **17** | 0.00 | 54.36 | 0.02 | -124.99 | 0.00 | 105.39 | 0.02 | -128.50 | 0.00 | -119.32 | 0.02 | -121.84 | 0.00 | 56.66 | 0.02 | -162.01 |
| **18** | 0.00 | -47.03 | 0.02 | -110.11 | 0.00 | 85.78 | 0.02 | -110.06 | 0.00 | -52.52 | 0.02 | -105.25 | 0.00 | 38.36 | 0.02 | -144.19 |
| **19** | 0.00 | -19.95 | 0.03 | -97.59 | 0.00 | 94.88 | 0.02 | -100.04 | 0.00 | 101.26 | 0.02 | -94.44 | 0.00 | 102.68 | 0.02 | -133.32 |
| **20** | 0.00 | -5.80 | 0.03 | -86.10 | 0.00 | 100.65 | 0.02 | -87.82 | 0.00 | 74.28 | 0.03 | -90.63 | 0.00 | 69.79 | 0.03 | -126.99 |
| **21** | 0.00 | -81.10 | 0.04 | -76.93 | 0.00 | -14.96 | 0.03 | -83.89 | 0.00 | -77.18 | 0.03 | -88.98 | 0.00 | 10.27 | 0.03 | -123.15 |
| **22** | 0.00 | -38.17 | 0.04 | -70.80 | 0.00 | -39.65 | 0.03 | -84.06 | 0.00 | -86.00 | 0.04 | -90.78 | 0.00 | 49.84 | 0.04 | -121.95 |
| **23** | 0.00 | 44.43 | 0.05 | -68.30 | 0.00 | 76.21 | 0.04 | -82.91 | 0.00 | 3.03 | 0.04 | -91.58 | 0.00 | 56.95 | 0.04 | -122.36 |
| **24** | 0.00 | 93.33 | 0.06 | -66.43 | 0.00 | -128.95 | 0.05 | -83.13 | 0.00 | -94.49 | 0.05 | -93.30 | 0.00 | 57.72 | 0.05 | -123.58 |
| **25** | 0.00 | 82.13 | 0.07 | -65.66 | 0.00 | 61.89 | 0.05 | -84.09 | 0.00 | -21.14 | 0.05 | -95.22 | 0.00 | 65.88 | 0.05 | -126.06 |
| **26** | 0.00 | 55.62 | 0.07 | -64.82 | 0.00 | 69.57 | 0.06 | -84.75 | 0.00 | -1.64 | 0.05 | -96.92 | 0.00 | 92.84 | 0.06 | -127.49 |
| **27** | 0.00 | 7.38 | 0.08 | -66.51 | 0.00 | 41.86 | 0.06 | -87.33 | 0.00 | -15.64 | 0.06 | -101.55 | 0.00 | 85.40 | 0.06 | -131.24 |
| **28** | 0.00 | 77.68 | 0.09 | -67.41 | 0.00 | 58.73 | 0.07 | -88.74 | 0.00 | -31.98 | 0.06 | -106.02 | 0.00 | 56.81 | 0.07 | -135.61 |

Table A.15: VW ID.3 Pro — Harmonic Orders $h_2$ to $h_9$

| **Harmonic Order** | **h2** | | **h3** | | **h4** | | **h5** | | **h6** | | **h7** | | **h8** | | **h9** | |
|---|---|---|---|---|---|---|---|---|---|---|---|---|---|---|---|---|
| **Charging Rate (A)** | **A** | $\theta$ | **A** | $\theta$ | **A** | $\theta$ | **A** | $\theta$ | **A** | $\theta$ | **A** | $\theta$ | **A** | $\theta$ | **A** | $\theta$ |
| **6** | 0.02 | -83.09 | 0.12 | -102.55 | 0.02 | -6.65 | 0.12 | -32.90 | 0.01 | 4.88 | 0.09 | 67.55 | 0.01 | 34.31 | 0.10 | -74.09 |
| **8** | 0.03 | -82.68 | 0.11 | -103.70 | 0.01 | -6.23 | 0.12 | -35.30 | 0.01 | -9.12 | 0.10 | 65.56 | 0.01 | 22.37 | 0.09 | -73.98 |
| **10** | 0.04 | -78.51 | 0.11 | -110.01 | 0.01 | -16.57 | 0.11 | -25.62 | 0.01 | 1.04 | 0.09 | 65.96 | 0.01 | 13.01 | 0.09 | -68.14 |
| **12** | 0.07 | -79.92 | 0.10 | -115.47 | 0.02 | -56.01 | 0.10 | -18.65 | 0.01 | -9.35 | 0.09 | 68.90 | 0.01 | 19.31 | 0.09 | -65.34 |
| **14** | 0.19 | -81.91 | 0.12 | -116.22 | 0.03 | -104.00 | 0.10 | -18.94 | 0.01 | -57.35 | 0.11 | 67.66 | 0.01 | 55.64 | 0.10 | -71.43 |
| **16** | 0.19 | -77.55 | 0.11 | -117.69 | 0.03 | -101.04 | 0.09 | -22.61 | 0.01 | -62.95 | 0.11 | 66.88 | 0.01 | 25.36 | 0.08 | -60.73 |



Table A.16: VW ID.3 Pro — Harmonic Orders $h_{10}$ to $h_{16}$

| **Harmonic Order** | **h10** | | **h11** | | **h12** | | **h13** | | **h14** | | **h15** | | **h16** | |
|---|---|---|---|---|---|---|---|---|---|---|---|---|---|---|
| **Charging Rate (A)** | **A** | $\theta$ | **A** | $\theta$ | **A** | $\theta$ | **A** | $\theta$ | **A** | $\theta$ | **A** | $\theta$ | **A** | $\theta$ |
| **6** | 0.01 | -1.46 | 0.02 | -112.89 | 0.01 | 13.86 | 0.10 | -129.79 | 0.01 | 25.84 | 0.02 | 112.74 | 0.01 | 16.23 |
| **8** | 0.01 | 0.00 | 0.02 | -94.57 | 0.01 | 4.78 | 0.09 | -126.69 | 0.01 | 5.33 | 0.02 | 95.11 | 0.01 | 8.78 |
| **10** | 0.01 | 14.39 | 0.02 | -98.57 | 0.01 | 12.89 | 0.08 | -128.44 | 0.01 | 26.04 | 0.02 | 97.36 | 0.01 | 24.19 |
| **12** | 0.01 | 26.80 | 0.02 | -66.60 | 0.01 | 30.39 | 0.08 | -119.03 | 0.01 | 38.29 | 0.03 | 109.85 | 0.01 | 58.29 |
| **14** | 0.01 | 15.46 | 0.03 | -96.11 | 0.01 | 82.58 | 0.07 | -129.71 | 0.02 | 91.14 | 0.03 | 90.29 | 0.01 | 47.57 |
| **16** | 0.01 | 90.03 | 0.03 | -88.46 | 0.01 | 61.43 | 0.09 | -127.50 | 0.01 | 66.17 | 0.03 | 97.54 | 0.01 | 77.10 |

Table A.17: VW ID.3 Pro — Harmonic Orders $h_{17}$ to $h_{24}$

| **Harmonic Order** | **h17** | | **h18** | | **h19** | | **h20** | | **h21** | | **h22** | | **h23** | | **h24** | |
|---|---|---|---|---|---|---|---|---|---|---|---|---|---|---|---|---|
| **Charging Rate (A)** | **A** | $\theta$ | **A** | $\theta$ | **A** | $\theta$ | **A** | $\theta$ | **A** | $\theta$ | **A** | $\theta$ | **A** | $\theta$ | **A** | $\theta$ |
| **6** | 0.04 | 152.43 | 0.01 | -19.96 | 0.04 | -115.28 | 0.01 | -5.49 | 0.04 | 37.44 | 0.01 | 11.75 | 0.05 | -144.69 | 0.01 | -9.32 |
| **8** | 0.03 | 143.13 | 0.01 | -11.98 | 0.03 | -101.68 | 0.01 | 17.62 | 0.04 | 32.45 | 0.01 | 1.06 | 0.05 | -145.74 | 0.01 | -17.07 |
| **10** | 0.01 | 93.46 | 0.01 | -15.47 | 0.04 | -122.30 | 0.01 | 12.07 | 0.04 | 52.80 | 0.01 | 25.60 | 0.03 | -107.43 | 0.01 | -2.87 |
| **12** | 0.04 | 143.18 | 0.01 | 2.49 | 0.00 | 168.13 | 0.01 | 25.91 | 0.03 | 56.99 | 0.01 | 15.09 | 0.07 | -133.60 | 0.01 | 3.12 |
| **14** | 0.01 | -5.87 | 0.01 | 19.47 | 0.04 | -114.33 | 0.01 | 75.11 | 0.05 | 51.69 | 0.01 | 41.52 | 0.02 | -110.43 | 0.02 | 6.07 |
| **16** | 0.02 | 107.29 | 0.01 | 43.16 | 0.04 | -117.79 | 0.01 | 64.81 | 0.04 | 49.73 | 0.01 | 41.92 | 0.03 | -134.79 | 0.01 | 17.71 |



Table A.18: VW ID.3 Pro — Harmonic Orders $h_{25}$ to $h_{31}$

| **Harmonic Order** | **h25** | | **h26** | | **h27** | | **h28** | | **h29** | | **h30** | | **h31** | |
|---|---|---|---|---|---|---|---|---|---|---|---|---|---|---|
| **Charging Rate (A)** | **A** | $\theta$ | **A** | $\theta$ | **A** | $\theta$ | **A** | $\theta$ | **A** | $\theta$ | **A** | $\theta$ | **A** | $\theta$ |
| **6** | 0.03 | -120.26 | 0.01 | -5.13 | 0.03 | 74.58 | 0.01 | 20.17 | 0.01 | 123.82 | 0.01 | 38.74 | 0.02 | -6.89 |
| **8** | 0.02 | -122.22 | 0.01 | -9.32 | 0.04 | 72.31 | 0.01 | 32.38 | 0.02 | 116.77 | 0.01 | 28.19 | 0.02 | 0.92 |
| **10** | 0.01 | -24.07 | 0.01 | 13.39 | 0.03 | 98.88 | 0.01 | 24.82 | 0.01 | -94.75 | 0.01 | 23.30 | 0.02 | -10.26 |
| **12** | 0.02 | -134.64 | 0.01 | 19.02 | 0.04 | 88.81 | 0.01 | 42.81 | 0.03 | 18.68 | 0.01 | 23.52 | 0.03 | -9.06 |
| **14** | 0.02 | -127.12 | 0.01 | 28.44 | 0.03 | 116.56 | 0.01 | 24.96 | 0.01 | -76.45 | 0.01 | 21.52 | 0.02 | -1.00 |
| **16** | 0.01 | 87.64 | 0.01 | 36.70 | 0.03 | 90.48 | 0.01 | 50.07 | 0.02 | -128.51 | 0.01 | 2.76 | 0.02 | -46.83 |

Table A.19: Renault Zoe ZE50 — Harmonic Orders $h_2$ to $h_9$

| **Harmonic Order** | **h2** | | **h3** | | **h4** | | **h5** | | **h6** | | **h7** | | **h8** | | **h9** | |
|---|---|---|---|---|---|---|---|---|---|---|---|---|---|---|---|---|
| **Charging Rate (A)** | **A** | $\theta$ | **A** | $\theta$ | **A** | $\theta$ | **A** | $\theta$ | **A** | $\theta$ | **A** | $\theta$ | **A** | $\theta$ | **A** | $\theta$ |
| **6** | 0.00 | -153.24 | 0.03 | -125.97 | 0.01 | 30.22 | 0.44 | -97.79 | 0.00 | 134.59 | 0.52 | 169.80 | 0.02 | 134.36 | 0.05 | -150.06 |
| **7** | 0.06 | -67.77 | 0.03 | -78.28 | 0.14 | -177.65 | 0.24 | 23.84 | 0.01 | 7.80 | 0.47 | -17.03 | 0.07 | 58.71 | 0.05 | 64.11 |
| **8** | 0.12 | 38.52 | 0.01 | 24.04 | 0.13 | -96.18 | 0.36 | -144.89 | 0.00 | 47.97 | 0.65 | -138.26 | 0.09 | -145.71 | 0.05 | 18.29 |
| **9** | 0.12 | 51.61 | 0.02 | 2.42 | 0.14 | -75.80 | 0.34 | -118.49 | 0.00 | 15.69 | 0.70 | -102.67 | 0.10 | -102.58 | 0.05 | 62.63 |
| **10** | 0.13 | 58.16 | 0.02 | 25.71 | 0.15 | -59.91 | 0.33 | -97.77 | 0.00 | 168.98 | 0.71 | -73.85 | 0.10 | -63.20 | 0.05 | 92.72 |
| **11** | 0.12 | 36.08 | 0.00 | 71.34 | 0.16 | -45.06 | 0.12 | -168.97 | 0.01 | 124.67 | 0.70 | -107.20 | 0.11 | -32.87 | 0.06 | 38.73 |
| **12** | 0.12 | 32.25 | 0.02 | 132.55 | 0.17 | -35.64 | 0.13 | 148.78 | 0.01 | 63.28 | 0.69 | -104.27 | 0.12 | -13.33 | 0.06 | 36.18 |
| **13** | 0.13 | 37.91 | 0.01 | 129.59 | 0.18 | -28.47 | 0.14 | 148.13 | 0.01 | 80.38 | 0.70 | -91.99 | 0.12 | 4.24 | 0.06 | 59.23 |
| **14** | 0.13 | 43.66 | 0.00 | -169.44 | 0.19 | -16.94 | 0.16 | 132.40 | 0.02 | 113.08 | 0.73 | -67.24 | 0.11 | 26.88 | 0.06 | 76.25 |
| **15** | 0.13 | 58.91 | 0.01 | -159.66 | 0.21 | -7.40 | 0.14 | 136.65 | 0.02 | 131.70 | 0.76 | -33.81 | 0.12 | 45.68 | 0.06 | 115.41 |
| **16** | 0.14 | 69.81 | 0.01 | -116.60 | 0.21 | -4.75 | 0.10 | 137.18 | 0.01 | 128.11 | 0.80 | -13.75 | 0.12 | 50.74 | 0.05 | 128.83 |
| **17** | 0.14 | 85.44 | 0.03 | 2.57 | 0.20 | 4.92 | 0.04 | 127.76 | 0.01 | 138.62 | 0.78 | 22.09 | 0.11 | 72.86 | 0.04 | 168.88 |
| **18** | 0.15 | 95.30 | 0.03 | 24.43 | 0.20 | 9.73 | 0.05 | 32.52 | 0.02 | 178.55 | 0.81 | 45.03 | 0.11 | 75.80 | 0.03 | -172.07 |
| **19** | 0.15 | 104.37 | 0.05 | 32.05 | 0.21 | 14.98 | 0.10 | 26.85 | 0.01 | -143.81 | 0.82 | 66.78 | 0.11 | 88.59 | 0.03 | 176.14 |
| **20** | 0.16 | 105.28 | 0.10 | 27.28 | 0.21 | 19.44 | 0.08 | 63.14 | 0.02 | -159.21 | 0.83 | 70.67 | 0.11 | 95.47 | 0.04 | 171.45 |
| **21** | 0.16 | 105.66 | 0.07 | 21.92 | 0.22 | 17.15 | 0.06 | 130.81 | 0.02 | -175.28 | 0.83 | 70.47 | 0.11 | 101.62 | 0.04 | -159.12 |
| **22** | 0.15 | 105.07 | 0.08 | 16.41 | 0.23 | 21.54 | 0.07 | -179.49 | 0.02 | 178.32 | 0.88 | 69.98 | 0.12 | 103.66 | 0.04 | 175.93 |
| **23** | 0.14 | 104.62 | 0.11 | 7.95 | 0.23 | 24.65 | 0.17 | -170.02 | 0.02 | -172.67 | 0.93 | 70.26 | 0.12 | 108.02 | 0.04 | 173.62 |
| **24** | 0.14 | 107.59 | 0.09 | -3.11 | 0.24 | 27.11 | 0.19 | -158.68 | 0.03 | -176.74 | 0.98 | 71.56 | 0.12 | 110.55 | 0.04 | -149.02 |
| **25** | 0.14 | 103.53 | 0.07 | -9.58 | 0.24 | 29.26 | 0.26 | -150.73 | 0.03 | 175.58 | 1.00 | 71.05 | 0.11 | 120.21 | 0.04 | -169.53 |
| **26** | 0.14 | 103.95 | 0.05 | -25.87 | 0.24 | 30.54 | 0.30 | -138.79 | 0.04 | -175.65 | 1.04 | 75.09 | 0.13 | 119.20 | 0.05 | -145.89 |
| **27** | 0.13 | 103.37 | 0.06 | -26.85 | 0.25 | 31.70 | 0.36 | -141.55 | 0.04 | -174.49 | 1.10 | 74.26 | 0.12 | 127.04 | 0.06 | -142.01 |
| **28** | 0.14 | 101.05 | 0.09 | -11.51 | 0.25 | 31.03 | 0.46 | -148.29 | 0.05 | -174.22 | 1.12 | 71.67 | 0.13 | 124.43 | 0.05 | -148.35 |
| **29** | 0.14 | 101.61 | 0.13 | -8.67 | 0.25 | 31.89 | 0.52 | -150.50 | 0.03 | -174.41 | 1.16 | 72.23 | 0.13 | 127.25 | 0.06 | -144.45 |
| **30** | 0.14 | 101.22 | 0.12 | -9.03 | 0.25 | 36.18 | 0.61 | -151.43 | 0.03 | -172.52 | 1.16 | 71.60 | 0.12 | 130.46 | 0.06 | -133.20 |

Table A.20: Renault Zoe ZE50 — Harmonic Orders $h_{10}$ to $h_{17}$

| **Harmonic Order** | **h10** | | **h11** | | **h12** | | **h13** | | **h14** | | **h15** | | **h16** | | **h17** | |
|---|---|---|---|---|---|---|---|---|---|---|---|---|---|---|---|---|
| **Charging Rate (A)** | **A** | $\theta$ | **A** | $\theta$ | **A** | $\theta$ | **A** | $\theta$ | **A** | $\theta$ | **A** | $\theta$ | **A** | $\theta$ | **A** | $\theta$ |
| **6** | 0.01 | -164.32 | 0.08 | 61.66 | 0.00 | 174.58 | 0.26 | 133.85 | 0.02 | -95.76 | 0.04 | 129.78 | 0.02 | 158.39 | 0.07 | -120.83 |
| **7** | 0.02 | 13.80 | 0.07 | -12.32 | 0.01 | -179.11 | 0.25 | 102.02 | 0.04 | -80.21 | 0.03 | 119.25 | 0.03 | 100.86 | 0.04 | -58.10 |
| **8** | 0.03 | 16.31 | 0.16 | -3.42 | 0.01 | -140.43 | 0.20 | -163.99 | 0.02 | -44.20 | 0.03 | -74.94 | 0.05 | -48.38 | 0.01 | -108.61 |
| **9** | 0.04 | 69.00 | 0.18 | 49.35 | 0.01 | -83.41 | 0.20 | -106.05 | 0.04 | 24.38 | 0.03 | -1.13 | 0.05 | 42.05 | 0.02 | -163.61 |
| **10** | 0.03 | 108.42 | 0.19 | 102.63 | 0.01 | -38.35 | 0.19 | -52.19 | 0.03 | 94.95 | 0.03 | 86.61 | 0.06 | 112.68 | 0.04 | -110.17 |
| **11** | 0.03 | 95.00 | 0.09 | 70.25 | 0.01 | -32.15 | 0.22 | -139.23 | 0.06 | 85.81 | 0.03 | 6.35 | 0.03 | 148.22 | 0.15 | -118.19 |
| **12** | 0.02 | 99.36 | 0.06 | 53.60 | 0.01 | -5.32 | 0.24 | -135.22 | 0.06 | 126.52 | 0.03 | 11.80 | 0.03 | -160.10 | 0.14 | -99.20 |
| **13** | 0.03 | 124.83 | 0.06 | 82.11 | 0.01 | -36.94 | 0.25 | -111.68 | 0.06 | 144.70 | 0.03 | 42.28 | 0.02 | -137.79 | 0.13 | -56.26 |
| **14** | 0.02 | 137.88 | 0.07 | 97.47 | 0.01 | 34.96 | 0.22 | -66.21 | 0.05 | -162.67 | 0.03 | 109.00 | 0.02 | -88.08 | 0.14 | 1.69 |
| **15** | 0.03 | -162.09 | 0.13 | -177.22 | 0.01 | 77.06 | 0.20 | -5.83 | 0.07 | -110.25 | 0.03 | -170.41 | 0.04 | -56.50 | 0.19 | 66.23 |
| **16** | 0.04 | -145.57 | 0.17 | -140.58 | 0.01 | 89.88 | 0.16 | 34.46 | 0.07 | -88.88 | 0.04 | -120.25 | 0.05 | -34.36 | 0.18 | 103.74 |
| **17** | 0.04 | -106.54 | 0.24 | -88.81 | 0.01 | 79.41 | 0.12 | 100.13 | 0.05 | -47.56 | 0.03 | -35.43 | 0.06 | 16.27 | 0.14 | 162.47 |
| **18** | 0.04 | -82.88 | 0.29 | -60.33 | 0.01 | -179.03 | 0.09 | 157.52 | 0.04 | -14.72 | 0.02 | 15.05 | 0.07 | 61.45 | 0.09 | -166.57 |
| **19** | 0.04 | -50.63 | 0.34 | -33.42 | 0.01 | -142.42 | 0.08 | -130.10 | 0.03 | 24.53 | 0.02 | 108.74 | 0.06 | 82.82 | 0.05 | -161.86 |
| **20** | 0.04 | -38.61 | 0.34 | -23.81 | 0.02 | -168.89 | 0.06 | -131.18 | 0.03 | 31.26 | 0.02 | 79.67 | 0.06 | 103.02 | 0.05 | -124.49 |
| **21** | 0.04 | -28.20 | 0.34 | -19.99 | 0.01 | -127.27 | 0.05 | -139.59 | 0.04 | 21.04 | 0.02 | 102.51 | 0.06 | 117.22 | 0.08 | -102.95 |
| **22** | 0.03 | -43.86 | 0.35 | -18.94 | 0.02 | -131.87 | 0.06 | -164.87 | 0.03 | 9.24 | 0.02 | 118.33 | 0.06 | 119.74 | 0.10 | -96.54 |
| **23** | 0.04 | -46.74 | 0.35 | -12.87 | 0.01 | -135.68 | 0.06 | 173.19 | 0.04 | 29.36 | 0.02 | 147.28 | 0.07 | 124.55 | 0.13 | -78.93 |
| **24** | 0.04 | -40.95 | 0.37 | -9.30 | 0.01 | -120.38 | 0.08 | -177.27 | 0.04 | 57.23 | 0.03 | 111.65 | 0.07 | 132.42 | 0.14 | -74.94 |
| **25** | 0.05 | -40.62 | 0.37 | -8.39 | 0.02 | -178.25 | 0.09 | -177.68 | 0.03 | 45.28 | 0.02 | 124.02 | 0.06 | 130.11 | 0.17 | -67.15 |
| **26** | 0.05 | -29.65 | 0.41 | -4.55 | 0.01 | -175.02 | 0.11 | -177.29 | 0.04 | 55.27 | 0.03 | 117.90 | 0.07 | 141.18 | 0.18 | -63.60 |
| **27** | 0.05 | -37.91 | 0.39 | -3.24 | 0.01 | -160.60 | 0.12 | 176.39 | 0.04 | 59.49 | 0.02 | 101.34 | 0.07 | 142.31 | 0.19 | -56.58 |
| **28** | 0.04 | -25.52 | 0.37 | 0.75 | 0.02 | -139.69 | 0.12 | 164.81 | 0.04 | 56.98 | 0.02 | 139.70 | 0.07 | 151.27 | 0.20 | -48.08 |
| **29** | 0.04 | -37.92 | 0.39 | 4.72 | 0.02 | -133.12 | 0.12 | 159.73 | 0.05 | 69.52 | 0.01 | -174.77 | 0.07 | 158.81 | 0.21 | -41.71 |
| **30** | 0.03 | -26.41 | 0.39 | 4.91 | 0.02 | -123.42 | 0.14 | 156.94 | 0.05 | 81.72 | 0.02 | 98.06 | 0.07 | 167.12 | 0.25 | -36.06 |

Table A.21: Renault Zoe ZE50 — Harmonic Orders $h_{18}$ to $h_{25}$

| **Harmonic Order** | **h18** | | **h19** | | **h20** | | **h21** | | **h22** | | **h23** | | **h24** | | **h25** | |
|---|---|---|---|---|---|---|---|---|---|---|---|---|---|---|---|---|
| **Charging Rate (A)** | **A** | $\theta$ | **A** | $\theta$ | **A** | $\theta$ | **A** | $\theta$ | **A** | $\theta$ | **A** | $\theta$ | **A** | $\theta$ | **A** | $\theta$ |
| **6** | 0.01 | 47.31 | 0.22 | -22.39 | 0.03 | -70.12 | 0.06 | -88.12 | 0.01 | 23.44 | 0.15 | -79.33 | 0.01 | -57.99 | 0.01 | -96.89 |
| **7** | 0.01 | 167.12 | 0.21 | 82.67 | 0.02 | -11.77 | 0.06 | 71.97 | 0.02 | -130.28 | 0.11 | 127.02 | 0.00 | 149.63 | 0.02 | 71.14 |
| **8** | 0.01 | 101.44 | 0.19 | 24.44 | 0.03 | -83.97 | 0.05 | 79.18 | 0.02 | -42.79 | 0.11 | -149.81 | 0.01 | -138.65 | 0.03 | 33.64 |
| **9** | 0.01 | -171.51 | 0.20 | 112.71 | 0.05 | 23.37 | 0.05 | 175.11 | 0.01 | 56.68 | 0.10 | -54.88 | 0.01 | 18.56 | 0.04 | 169.11 |
| **10** | 0.00 | -88.25 | 0.18 | -168.13 | 0.06 | 115.17 | 0.05 | -86.73 | 0.01 | 143.84 | 0.12 | 42.81 | 0.00 | 80.95 | 0.04 | -86.40 |
| **11** | 0.01 | 40.87 | 0.21 | 93.57 | 0.05 | 150.76 | 0.06 | 153.02 | 0.02 | 29.31 | 0.13 | -62.81 | 0.01 | -55.90 | 0.03 | 68.96 |
| **12** | 0.01 | 157.83 | 0.21 | 101.32 | 0.03 | -135.48 | 0.05 | 160.15 | 0.01 | 56.24 | 0.09 | -62.36 | 0.00 | -12.43 | 0.03 | 127.73 |
| **13** | 0.02 | 152.20 | 0.21 | 142.54 | 0.03 | -87.53 | 0.05 | -153.73 | 0.02 | 76.95 | 0.09 | -20.29 | 0.00 | -161.38 | 0.04 | 166.13 |
| **14** | 0.02 | 179.49 | 0.20 | -147.41 | 0.03 | -40.39 | 0.05 | -92.06 | 0.02 | 155.90 | 0.08 | 65.62 | 0.01 | -172.80 | 0.03 | -113.90 |
| **15** | 0.02 | -97.97 | 0.22 | -45.49 | 0.07 | 8.89 | 0.05 | 18.98 | 0.02 | -134.93 | 0.11 | -159.55 | 0.01 | -61.99 | 0.03 | -34.07 |
| **16** | 0.01 | -5.08 | 0.21 | 11.23 | 0.08 | 56.01 | 0.04 | 91.11 | 0.02 | -49.00 | 0.15 | -85.51 | 0.00 | 12.31 | 0.01 | 6.90 |
| **17** | 0.01 | 57.06 | 0.19 | 105.26 | 0.08 | 117.03 | 0.04 | -163.47 | 0.02 | 60.95 | 0.16 | 20.30 | 0.01 | 147.17 | 0.02 | -5.86 |
| **18** | 0.01 | -156.68 | 0.16 | 174.96 | 0.06 | 155.13 | 0.03 | -98.50 | 0.01 | -179.51 | 0.11 | 89.79 | 0.00 | 148.88 | 0.04 | 31.22 |
| **19** | 0.01 | -103.07 | 0.15 | -98.85 | 0.04 | -169.02 | 0.01 | 24.87 | 0.02 | -79.39 | 0.05 | 171.22 | 0.01 | 117.43 | 0.04 | 107.86 |
| **20** | 0.01 | -79.49 | 0.14 | -88.79 | 0.05 | -147.22 | 0.01 | 1.71 | 0.01 | -69.83 | 0.07 | 175.17 | 0.00 | -95.90 | 0.04 | 143.86 |
| **21** | 0.01 | -89.65 | 0.14 | -95.36 | 0.06 | -137.14 | 0.02 | -21.31 | 0.01 | -32.60 | 0.09 | -179.50 | 0.01 | -89.79 | 0.04 | 117.34 |
| **22** | 0.00 | -117.16 | 0.15 | -101.41 | 0.06 | -129.52 | 0.02 | -23.92 | 0.01 | -33.76 | 0.09 | 175.67 | 0.01 | -122.59 | 0.03 | 144.90 |
| **23** | 0.00 | 89.86 | 0.14 | -99.62 | 0.06 | -119.31 | 0.02 | -46.69 | 0.01 | -69.12 | 0.11 | -167.58 | 0.02 | -78.85 | 0.04 | 154.51 |
| **24** | 0.02 | -74.96 | 0.14 | -107.92 | 0.06 | -109.01 | 0.02 | -7.47 | 0.01 | -62.58 | 0.13 | -164.93 | 0.02 | -106.69 | 0.03 | 176.19 |
| **25** | 0.01 | -53.01 | 0.15 | -100.99 | 0.06 | -100.09 | 0.02 | -10.08 | 0.01 | -106.64 | 0.13 | -165.06 | 0.01 | -47.08 | 0.03 | 177.10 |
| **26** | 0.01 | -74.47 | 0.18 | -95.18 | 0.07 | -90.79 | 0.03 | -7.18 | 0.01 | -65.42 | 0.15 | -167.71 | 0.02 | -44.21 | 0.02 | -164.49 |
| **27** | 0.01 | 12.33 | 0.18 | -96.07 | 0.08 | -90.30 | 0.03 | -13.38 | 0.00 | 87.25 | 0.15 | -156.28 | 0.02 | -116.07 | 0.02 | -155.03 |
| **28** | 0.01 | -14.32 | 0.18 | -97.75 | 0.08 | -70.55 | 0.03 | -2.82 | 0.02 | -105.67 | 0.16 | -144.77 | 0.01 | -47.64 | 0.02 | -174.47 |
| **29** | 0.01 | -139.38 | 0.16 | -90.72 | 0.09 | -63.83 | 0.02 | -18.98 | 0.01 | -88.10 | 0.17 | -136.70 | 0.00 | -55.53 | 0.03 | -136.93 |
| **30** | 0.01 | 131.20 | 0.18 | -95.01 | 0.08 | -61.27 | 0.03 | -14.10 | 0.01 | -121.68 | 0.18 | -135.02 | 0.02 | -58.74 | 0.02 | -130.72 |

Table A.22: Renault Zoe ZE50 — Harmonic Orders $h_{26}$ to $h_{33}$

| **Harmonic Order** | **h26** | | **h27** | | **h28** | | **h29** | | **h30** | | **h31** | | **h32** | | **h33** | |
|---|---|---|---|---|---|---|---|---|---|---|---|---|---|---|---|---|
| **Charging Rate (A)** | **A** | $\theta$ | **A** | $\theta$ | **A** | $\theta$ | **A** | $\theta$ | **A** | $\theta$ | **A** | $\theta$ | **A** | $\theta$ | **A** | $\theta$ |
| **6** | 0.00 | 15.30 | 0.02 | 134.59 | 0.01 | -135.87 | 0.12 | -10.21 | 0.01 | -173.35 | 0.07 | 110.53 | 0.01 | -115.06 | 0.02 | 30.18 |
| **7** | 0.01 | -144.40 | 0.01 | 96.04 | 0.01 | -71.87 | 0.12 | -13.36 | 0.01 | 147.40 | 0.06 | 153.29 | 0.01 | 140.50 | 0.02 | 126.73 |
| **8** | 0.01 | -74.27 | 0.01 | -66.60 | 0.02 | -35.55 | 0.11 | -71.28 | 0.01 | -43.85 | 0.08 | 147.61 | 0.02 | -23.90 | 0.02 | -169.90 |
| **9** | 0.02 | 51.81 | 0.02 | 31.31 | 0.03 | 135.16 | 0.10 | 68.17 | 0.01 | -40.90 | 0.08 | -64.67 | 0.03 | 119.09 | 0.01 | 1.44 |
| **10** | 0.01 | -173.98 | 0.01 | 154.04 | 0.02 | -117.01 | 0.08 | -176.33 | 0.00 | 13.53 | 0.07 | 76.92 | 0.03 | -85.61 | 0.01 | 167.47 |
| **11** | 0.02 | 0.36 | 0.01 | -7.32 | 0.02 | 65.62 | 0.11 | 36.62 | 0.00 | 37.62 | 0.07 | -93.73 | 0.02 | 81.01 | 0.01 | -30.48 |
| **12** | 0.02 | 49.05 | 0.01 | -9.36 | 0.02 | 126.41 | 0.08 | 22.80 | 0.00 | -161.62 | 0.06 | -75.60 | 0.02 | 158.72 | 0.02 | -48.85 |
| **13** | 0.01 | 127.47 | 0.01 | 99.97 | 0.02 | -158.75 | 0.07 | 88.43 | 0.00 | -31.21 | 0.07 | -14.69 | 0.03 | -135.39 | 0.01 | 53.53 |
| **14** | 0.02 | -174.06 | 0.02 | -173.85 | 0.02 | -72.37 | 0.06 | -162.18 | 0.01 | 174.35 | 0.06 | 93.44 | 0.03 | -23.89 | 0.02 | 137.96 |
| **15** | 0.02 | -107.20 | 0.02 | -14.11 | 0.01 | 14.62 | 0.10 | 10.20 | 0.01 | -71.99 | 0.06 | -90.99 | 0.02 | 50.87 | 0.01 | -72.64 |
| **16** | 0.03 | -114.32 | 0.01 | 61.91 | 0.02 | -42.38 | 0.13 | 91.86 | 0.01 | -8.26 | 0.06 | 3.40 | 0.02 | 76.34 | 0.02 | 89.04 |
| **17** | 0.03 | -58.59 | 0.02 | -117.99 | 0.03 | 43.86 | 0.12 | -135.08 | 0.01 | 123.60 | 0.07 | 177.31 | 0.03 | 132.64 | 0.02 | -86.34 |
| **18** | 0.02 | 5.81 | 0.03 | -38.49 | 0.03 | 87.38 | 0.05 | -28.75 | 0.01 | 62.60 | 0.07 | -60.91 | 0.05 | 176.42 | 0.01 | 51.62 |
| **19** | 0.01 | 27.95 | 0.02 | 40.22 | 0.02 | 117.11 | 0.06 | 154.51 | 0.00 | -106.51 | 0.09 | 59.43 | 0.03 | -100.96 | 0.02 | -175.22 |
| **20** | 0.02 | 61.75 | 0.02 | 86.25 | 0.03 | 161.14 | 0.03 | 168.00 | 0.01 | -86.65 | 0.08 | 85.64 | 0.03 | -79.00 | 0.01 | -153.14 |
| **21** | 0.03 | 78.68 | 0.03 | 113.97 | 0.02 | 168.12 | 0.02 | 129.77 | 0.00 | 91.74 | 0.08 | 89.39 | 0.04 | -69.10 | 0.02 | -142.39 |
| **22** | 0.02 | 98.74 | 0.03 | 97.75 | 0.02 | -152.17 | 0.03 | 103.50 | 0.01 | 40.02 | 0.07 | 95.90 | 0.04 | -47.82 | 0.02 | -154.01 |
| **23** | 0.03 | 124.10 | 0.03 | 106.79 | 0.03 | -145.14 | 0.05 | 81.51 | 0.01 | 61.87 | 0.07 | 100.95 | 0.03 | -22.15 | 0.01 | -103.21 |
| **24** | 0.03 | 101.47 | 0.04 | 100.52 | 0.03 | -144.55 | 0.06 | 95.80 | 0.00 | -32.76 | 0.06 | 95.39 | 0.04 | 0.79 | 0.01 | -83.98 |
| **25** | 0.03 | 144.84 | 0.03 | 135.79 | 0.03 | -124.88 | 0.08 | 87.26 | 0.00 | -165.55 | 0.05 | 101.24 | 0.04 | 6.12 | 0.01 | -71.09 |
| **26** | 0.03 | 147.96 | 0.03 | 111.84 | 0.03 | -120.99 | 0.10 | 105.31 | 0.01 | 81.71 | 0.05 | 64.76 | 0.03 | 49.25 | 0.02 | 141.26 |
| **27** | 0.02 | -176.23 | 0.03 | 129.48 | 0.03 | -93.87 | 0.10 | 104.76 | 0.02 | 117.65 | 0.07 | 75.57 | 0.05 | 9.86 | 0.02 | 155.63 |
| **28** | 0.02 | -174.91 | 0.03 | 113.99 | 0.04 | -94.15 | 0.12 | 121.03 | 0.01 | 99.10 | 0.06 | 85.41 | 0.04 | 38.84 | 0.01 | 134.23 |
| **29** | 0.03 | -165.62 | 0.04 | 132.13 | 0.03 | -74.35 | 0.12 | 126.62 | 0.00 | 177.91 | 0.07 | 84.91 | 0.05 | 63.81 | 0.00 | -134.06 |
| **30** | 0.03 | -164.65 | 0.03 | 135.56 | 0.02 | -67.00 | 0.14 | 128.26 | 0.01 | -36.23 | 0.07 | 88.31 | 0.04 | 67.13 | 0.02 | -137.37 |

Table A.23: Renault Zoe ZE50 — Harmonic Orders $h_{34}$ to $h_{41}$

| **Harmonic Order** | **h34** | | **h35** | | **h36** | | **h37** | | **h38** | | **h49** | | **h40** | | **h41** | |
|---|---|---|---|---|---|---|---|---|---|---|---|---|---|---|---|---|
| **Charging Rate (A)** | **A** | $\theta$ | **A** | $\theta$ | **A** | $\theta$ | **A** | $\theta$ | **A** | $\theta$ | **A** | $\theta$ | **A** | $\theta$ | **A** | $\theta$ |
| **6** | 0.00 | 164.02 | 0.01 | -53.88 | 0.00 | 52.90 | 0.02 | -68.66 | 0.00 | 108.57 | 0.02 | 66.27 | 0.01 | -174.45 | 0.04 | -152.79 |
| **7** | 0.01 | 21.90 | 0.02 | 118.27 | 0.00 | -161.95 | 0.01 | 161.61 | 0.01 | 94.22 | 0.02 | -61.42 | 0.01 | 140.67 | 0.04 | 135.10 |
| **8** | 0.01 | 107.20 | 0.01 | -51.52 | 0.01 | -164.45 | 0.01 | -30.24 | 0.01 | -45.67 | 0.02 | -155.22 | 0.00 | -2.54 | 0.04 | 103.71 |
| **9** | 0.02 | -63.46 | 0.01 | 63.08 | 0.01 | 74.77 | 0.00 | 122.33 | 0.01 | -157.45 | 0.02 | 14.01 | 0.00 | -22.49 | 0.05 | -59.18 |
| **10** | 0.00 | 124.57 | 0.00 | -121.39 | 0.00 | -54.25 | 0.01 | -130.94 | 0.01 | 26.48 | 0.02 | -169.12 | 0.01 | 87.26 | 0.05 | 123.30 |
| **11** | 0.01 | -120.09 | 0.01 | 10.16 | 0.01 | -28.25 | 0.01 | 27.61 | 0.00 | -143.29 | 0.02 | -6.81 | 0.00 | -101.39 | 0.04 | -67.83 |
| **12** | 0.01 | 25.12 | 0.02 | 13.15 | 0.01 | 93.10 | 0.02 | 74.82 | 0.01 | -56.53 | 0.02 | 21.81 | 0.01 | 73.10 | 0.02 | -68.60 |
| **13** | 0.01 | 155.64 | 0.03 | 103.08 | 0.00 | 10.58 | 0.02 | 153.89 | 0.01 | 65.57 | 0.02 | 84.72 | 0.01 | 139.99 | 0.02 | 14.19 |
| **14** | 0.01 | -165.27 | 0.03 | -137.67 | 0.00 | -7.12 | 0.02 | -103.02 | 0.01 | -177.90 | 0.02 | -122.47 | 0.01 | -95.25 | 0.03 | -178.18 |
| **15** | 0.01 | -26.80 | 0.01 | -41.10 | 0.02 | 60.26 | 0.00 | 25.96 | 0.01 | -160.07 | 0.02 | 82.67 | 0.00 | -54.32 | 0.05 | 34.73 |
| **16** | 0.01 | -6.98 | 0.03 | -83.34 | 0.00 | 149.84 | 0.01 | -20.85 | 0.01 | -129.02 | 0.02 | -153.31 | 0.00 | 18.55 | 0.04 | 145.26 |
| **17** | 0.01 | -38.06 | 0.04 | 31.22 | 0.02 | 110.16 | 0.01 | 85.75 | 0.01 | -44.53 | 0.03 | 56.36 | 0.00 | 22.73 | 0.02 | 46.30 |
| **18** | 0.01 | 27.27 | 0.04 | 87.01 | 0.00 | -171.04 | 0.01 | -154.60 | 0.01 | -7.26 | 0.01 | -143.55 | 0.01 | 74.25 | 0.06 | -174.91 |
| **19** | 0.01 | 119.73 | 0.03 | 93.26 | 0.01 | -61.23 | 0.01 | -120.14 | 0.02 | 83.57 | 0.02 | -3.30 | 0.01 | 155.15 | 0.06 | -47.42 |
| **20** | 0.00 | 82.41 | 0.03 | 160.56 | 0.01 | -48.19 | 0.01 | 24.13 | 0.01 | 111.07 | 0.02 | 17.90 | 0.01 | 128.78 | 0.06 | -16.19 |
| **21** | 0.01 | -71.64 | 0.02 | 178.66 | 0.01 | 57.73 | 0.01 | -114.73 | 0.01 | 151.79 | 0.03 | 21.16 | 0.01 | -36.28 | 0.07 | 5.90 |
| **22** | 0.01 | -154.35 | 0.04 | -146.63 | 0.01 | -15.87 | 0.01 | -12.99 | 0.03 | 170.53 | 0.02 | 28.20 | 0.01 | -46.90 | 0.07 | 6.29 |
| **23** | 0.01 | -154.17 | 0.04 | -114.59 | 0.02 | -8.33 | 0.02 | 33.07 | 0.02 | -161.70 | 0.02 | 28.87 | 0.01 | -154.64 | 0.07 | 40.03 |
| **24** | 0.01 | -153.82 | 0.04 | -99.51 | 0.01 | 13.71 | 0.01 | 32.44 | 0.02 | -159.60 | 0.03 | 35.37 | 0.03 | -130.65 | 0.04 | 52.36 |
| **25** | 0.01 | -120.12 | 0.04 | -72.87 | 0.02 | -12.56 | 0.02 | 43.66 | 0.01 | -117.59 | 0.02 | 71.60 | 0.01 | -159.67 | 0.05 | 55.69 |
| **26** | 0.01 | -36.70 | 0.05 | -63.52 | 0.00 | -38.01 | 0.02 | 37.12 | 0.04 | -108.56 | 0.01 | 102.41 | 0.01 | 54.76 | 0.04 | 66.61 |
| **27** | 0.01 | -25.80 | 0.07 | -45.39 | 0.02 | 89.82 | 0.03 | 113.33 | 0.02 | -89.90 | 0.02 | 22.93 | 0.00 | 131.97 | 0.02 | 66.57 |
| **28** | 0.01 | -21.17 | 0.07 | -20.73 | 0.02 | 110.84 | 0.02 | 136.29 | 0.02 | -58.01 | 0.02 | 49.45 | 0.01 | -166.44 | 0.01 | 65.37 |
| **29** | 0.01 | -105.00 | 0.08 | 3.68 | 0.01 | 113.23 | 0.02 | 67.67 | 0.03 | -63.06 | 0.01 | 115.19 | 0.01 | -62.83 | 0.00 | 115.53 |
| **30** | 0.01 | -157.79 | 0.08 | 11.65 | 0.01 | -48.81 | 0.02 | 118.81 | 0.03 | -72.04 | 0.02 | -23.69 | 0.02 | 10.17 | 0.01 | 112.89 |

Table A.24: Renault Zoe ZE50 — Harmonic Orders $h_{42}$ to $h_{49}$

| **Harmonic Order** | **h42** | | **h43** | | **h44** | | **h45** | | **h46** | | **h47** | | **h48** | | **h49** | |
|---|---|---|---|---|---|---|---|---|---|---|---|---|---|---|---|---|
| **Charging Rate (A)** | **A** | $\theta$ | **A** | $\theta$ | **A** | $\theta$ | **A** | $\theta$ | **A** | $\theta$ | **A** | $\theta$ | **A** | $\theta$ | **A** | $\theta$ |
| **6** | 0.00 | 72.94 | 0.03 | -24.80 | 0.00 | 139.54 | 0.02 | -67.27 | 0.01 | 126.10 | 0.02 | -126.99 | 0.00 | 83.93 | 0.01 | 59.88 |
| **7** | 0.00 | -56.80 | 0.02 | -63.54 | 0.00 | 27.55 | 0.02 | -43.39 | 0.00 | -89.61 | 0.02 | -57.50 | 0.00 | 61.74 | 0.02 | 161.83 |
| **8** | 0.01 | -60.18 | 0.02 | 17.68 | 0.01 | -51.97 | 0.02 | 102.30 | 0.00 | 80.83 | 0.02 | 130.85 | 0.00 | -150.85 | 0.01 | 105.28 |
| **9** | 0.00 | 142.15 | 0.02 | -147.92 | 0.01 | -156.80 | 0.02 | -51.00 | 0.00 | -76.71 | 0.02 | -12.12 | 0.00 | 60.76 | 0.01 | -25.23 |
| **10** | 0.00 | -91.43 | 0.02 | 16.50 | 0.01 | 60.97 | 0.02 | 125.98 | 0.00 | -77.03 | 0.02 | -155.61 | 0.00 | -36.07 | 0.01 | -169.05 |
| **11** | 0.00 | -140.10 | 0.03 | 158.97 | 0.01 | -43.83 | 0.02 | -96.72 | 0.00 | 31.10 | 0.02 | -30.58 | 0.00 | 50.36 | 0.02 | -113.54 |
| **12** | 0.00 | -93.57 | 0.03 | -161.51 | 0.01 | 73.24 | 0.01 | -73.79 | 0.00 | 172.34 | 0.02 | -27.97 | 0.00 | 97.50 | 0.01 | -44.83 |
| **13** | 0.00 | -150.83 | 0.03 | -84.24 | 0.01 | 155.24 | 0.01 | 12.63 | 0.00 | -113.89 | 0.02 | 63.26 | 0.00 | 171.80 | 0.01 | 33.73 |
| **14** | 0.00 | 51.77 | 0.03 | 70.10 | 0.01 | -71.17 | 0.02 | 162.90 | 0.00 | 15.92 | 0.02 | -123.90 | 0.00 | -117.52 | 0.01 | -146.81 |
| **15** | 0.01 | -52.29 | 0.03 | -72.97 | 0.01 | 93.72 | 0.02 | 49.00 | 0.01 | -61.27 | 0.02 | 143.98 | 0.00 | -22.20 | 0.00 | 31.67 |
| **16** | 0.00 | -54.36 | 0.03 | 96.25 | 0.01 | 52.31 | 0.02 | -164.27 | 0.01 | 126.38 | 0.03 | -65.51 | 0.00 | 29.59 | 0.00 | -70.99 |
| **17** | 0.00 | -175.96 | 0.04 | -58.28 | 0.01 | -142.92 | 0.02 | 87.95 | 0.01 | 48.03 | 0.02 | 170.57 | 0.00 | 150.12 | 0.01 | 132.53 |
| **18** | 0.01 | 104.19 | 0.02 | 88.67 | 0.00 | 144.51 | 0.02 | -126.02 | 0.01 | 162.55 | 0.02 | 5.43 | 0.00 | 171.81 | 0.01 | 28.55 |
| **19** | 0.01 | -115.63 | 0.02 | -46.94 | 0.01 | -115.15 | 0.01 | 57.63 | 0.01 | -17.19 | 0.03 | 158.44 | 0.01 | -81.40 | 0.01 | -130.86 |
| **20** | 0.01 | 174.54 | 0.02 | -14.30 | 0.01 | -62.25 | 0.02 | 86.67 | 0.01 | -74.84 | 0.03 | -158.62 | 0.01 | 178.55 | 0.01 | -101.31 |
| **21** | 0.01 | 148.80 | 0.02 | -41.73 | 0.01 | -46.18 | 0.02 | 93.46 | 0.01 | 2.96 | 0.03 | -152.95 | 0.00 | -162.10 | 0.01 | -100.27 |
| **22** | 0.00 | -98.25 | 0.02 | -53.48 | 0.01 | 5.21 | 0.02 | 76.42 | 0.01 | 81.50 | 0.03 | -132.91 | 0.01 | 20.86 | 0.00 | 1.06 |
| **23** | 0.00 | 120.17 | 0.02 | -75.12 | 0.01 | -104.66 | 0.03 | 97.70 | 0.01 | -8.08 | 0.02 | -107.27 | 0.00 | 112.13 | 0.00 | -4.67 |
| **24** | 0.01 | -19.34 | 0.03 | -56.01 | 0.01 | 40.39 | 0.03 | 104.53 | 0.01 | -37.81 | 0.02 | -115.06 | 0.01 | 51.41 | 0.00 | -88.59 |
| **25** | 0.01 | -108.22 | 0.03 | -58.36 | 0.01 | 139.54 | 0.02 | 104.48 | 0.01 | -0.95 | 0.02 | -120.14 | 0.00 | -94.60 | 0.00 | 74.37 |
| **26** | 0.00 | 118.68 | 0.04 | -69.04 | 0.01 | 126.01 | 0.03 | 97.27 | 0.01 | -94.91 | 0.02 | -88.05 | 0.01 | 82.78 | 0.01 | 154.66 |
| **27** | 0.01 | -175.44 | 0.03 | -42.36 | 0.01 | -176.55 | 0.02 | 125.93 | 0.01 | -85.21 | 0.01 | -103.12 | 0.00 | 173.55 | 0.01 | 165.37 |
| **28** | 0.01 | -63.20 | 0.03 | -43.55 | 0.01 | -169.12 | 0.02 | 100.67 | 0.01 | 8.73 | 0.02 | -137.33 | 0.00 | 5.24 | 0.01 | -138.59 |
| **29** | 0.02 | 51.51 | 0.04 | -12.45 | 0.01 | 142.76 | 0.03 | 156.34 | 0.01 | -171.89 | 0.01 | -110.14 | 0.01 | -92.85 | 0.01 | -163.89 |
| **30** | 0.01 | 84.08 | 0.05 | -24.15 | 0.01 | -113.86 | 0.03 | 150.41 | 0.02 | 141.69 | 0.02 | -133.33 | 0.00 | -67.51 | 0.01 | -149.03 |

Table A.25: VW ID.4 Pro — Harmonic Orders $h_2$ to $h_9$

| **Harmonic Order** | **h2** | | **h3** | | **h4** | | **h5** | | **h6** | | **h7** | | **h8** | | **h9** | |
|---|---|---|---|---|---|---|---|---|---|---|---|---|---|---|---|---|
| **Charging Rate (A)** | **A** | $\theta$ | **A** | $\theta$ | **A** | $\theta$ | **A** | $\theta$ | **A** | $\theta$ | **A** | $\theta$ | **A** | $\theta$ | **A** | $\theta$ |
| **6** | 0.02 | -104.98 | 0.13 | -131.26 | 0.00 | -37.40 | 0.10 | -68.63 | 0.00 | -127.26 | 0.09 | 23.43 | 0.00 | 99.54 | 0.09 | -143.25 |
| **7** | 0.02 | -106.84 | 0.12 | -129.90 | 0.00 | -52.35 | 0.10 | -63.06 | 0.01 | -143.19 | 0.09 | 29.33 | 0.01 | 118.73 | 0.09 | -128.96 |
| **8** | 0.02 | -120.01 | 0.12 | -128.42 | 0.00 | 97.80 | 0.10 | -60.24 | 0.00 | -177.37 | 0.09 | 36.89 | 0.00 | -40.63 | 0.08 | -123.27 |
| **9** | 0.03 | -100.52 | 0.12 | -127.37 | 0.01 | 59.22 | 0.10 | -52.53 | 0.01 | 33.14 | 0.08 | 42.06 | 0.01 | -7.56 | 0.09 | -115.60 |
| **10** | 0.02 | -100.12 | 0.12 | -125.84 | 0.00 | -75.29 | 0.09 | -46.70 | 0.00 | -172.71 | 0.09 | 48.98 | 0.00 | 76.19 | 0.09 | -107.11 |
| **11** | 0.03 | -95.63 | 0.11 | -127.85 | 0.00 | 65.59 | 0.09 | -42.62 | 0.00 | -93.91 | 0.10 | 46.61 | 0.01 | 95.06 | 0.09 | -91.29 |
| **12** | 0.05 | -88.36 | 0.12 | -128.14 | 0.00 | -141.84 | 0.10 | -32.94 | 0.00 | -90.47 | 0.08 | 48.78 | 0.01 | 164.32 | 0.09 | -92.06 |
| **13** | 0.11 | -88.74 | 0.13 | -123.28 | 0.02 | -119.21 | 0.09 | -27.27 | 0.01 | -173.04 | 0.09 | 56.85 | 0.01 | 159.53 | 0.08 | -94.63 |
| **14** | 0.20 | -88.87 | 0.14 | -126.81 | 0.02 | -109.51 | 0.08 | -29.83 | 0.01 | -169.66 | 0.10 | 54.09 | 0.01 | 138.41 | 0.09 | -89.13 |
| **15** | 0.24 | -85.57 | 0.14 | -129.04 | 0.03 | -102.92 | 0.08 | -32.79 | 0.01 | -158.30 | 0.10 | 56.52 | 0.01 | 112.83 | 0.08 | -77.77 |
| **16** | 0.21 | -84.22 | 0.13 | -126.20 | 0.02 | -117.88 | 0.08 | -32.19 | 0.01 | 177.82 | 0.10 | 56.75 | 0.01 | 81.60 | 0.07 | -72.27 |



Table A.26: VW ID.4 Pro — Harmonic Orders $h_{10}$ to $h_{17}$

| **Harmonic Order** | **h10** | | **h11** | | **h12** | | **h13** | | **h14** | | **h15** | | **h16** | | **h17** | |
|---|---|---|---|---|---|---|---|---|---|---|---|---|---|---|---|---|
| **Charging Rate (A)** | **A** | $\theta$ | **A** | $\theta$ | **A** | $\theta$ | **A** | $\theta$ | **A** | $\theta$ | **A** | $\theta$ | **A** | $\theta$ | **A** | $\theta$ |
| **6** | 0.00 | -34.18 | 0.03 | 151.20 | 0.00 | -81.07 | 0.08 | 121.85 | 0.00 | -94.85 | 0.04 | 19.60 | 0.00 | -134.53 | 0.02 | 54.60 |
| **7** | 0.01 | 26.51 | 0.03 | 163.55 | 0.00 | -45.10 | 0.08 | 138.74 | 0.01 | -25.61 | 0.03 | 28.92 | 0.00 | -79.37 | 0.01 | 140.57 |
| **8** | 0.00 | 131.27 | 0.02 | 179.62 | 0.01 | 30.11 | 0.08 | 153.89 | 0.00 | 48.89 | 0.03 | 31.86 | 0.01 | 128.76 | 0.00 | -55.65 |
| **9** | 0.01 | -83.76 | 0.02 | 147.56 | 0.01 | 177.66 | 0.07 | 165.53 | 0.01 | 52.38 | 0.03 | 36.13 | 0.00 | 124.03 | 0.00 | 179.11 |
| **10** | 0.01 | -33.29 | 0.03 | -144.74 | 0.01 | -119.01 | 0.06 | 166.91 | 0.01 | 45.67 | 0.03 | 56.05 | 0.00 | 38.97 | 0.01 | 175.70 |
| **11** | 0.00 | 96.19 | 0.04 | -136.87 | 0.00 | -166.42 | 0.07 | -173.17 | 0.00 | -14.14 | 0.03 | 62.36 | 0.00 | -23.38 | 0.01 | 146.20 |
| **12** | 0.00 | -105.53 | 0.03 | -136.59 | 0.00 | 60.30 | 0.05 | -170.21 | 0.01 | 35.91 | 0.03 | 80.39 | 0.01 | 43.93 | 0.02 | 160.22 |
| **13** | 0.01 | 101.58 | 0.02 | -127.28 | 0.00 | 85.70 | 0.05 | -164.67 | 0.01 | 57.00 | 0.03 | 76.23 | 0.01 | 18.74 | 0.02 | 161.86 |
| **14** | 0.00 | 43.00 | 0.04 | -130.41 | 0.00 | 104.71 | 0.05 | -169.91 | 0.01 | 66.73 | 0.04 | 80.57 | 0.01 | 28.46 | 0.02 | -175.58 |
| **15** | 0.01 | 14.80 | 0.04 | -126.49 | 0.01 | -39.61 | 0.06 | -161.46 | 0.01 | 55.80 | 0.04 | 77.83 | 0.01 | 51.34 | 0.01 | 123.18 |
| **16** | 0.01 | 93.01 | 0.03 | -125.67 | 0.01 | 77.47 | 0.07 | -152.03 | 0.01 | 30.89 | 0.03 | 92.29 | 0.01 | 66.03 | 0.00 | 60.37 |

Table A.27: VW ID.4 Pro — Harmonic Orders $h_{18}$ to $h_{25}$

| **Harmonic Order** | **h18** | | **h19** | | **h20** | | **h21** | | **h22** | | **h23** | | **h24** | | **h25** | |
|---|---|---|---|---|---|---|---|---|---|---|---|---|---|---|---|---|
| **Charging Rate (A)** | **A** | $\theta$ | **A** | $\theta$ | **A** | $\theta$ | **A** | $\theta$ | **A** | $\theta$ | **A** | $\theta$ | **A** | $\theta$ | **A** | $\theta$ |
| **6** | 0.00 | -14.89 | 0.05 | 80.90 | 0.00 | -166.84 | 0.02 | -76.66 | 0.00 | -27.00 | 0.05 | 47.22 | 0.00 | -73.04 | 0.03 | 17.22 |
| **7** | 0.00 | 82.16 | 0.04 | 104.02 | 0.01 | 124.39 | 0.03 | -87.95 | 0.01 | 14.04 | 0.05 | 62.63 | 0.00 | -64.35 | 0.02 | 30.30 |
| **8** | 0.01 | -150.78 | 0.03 | 119.85 | 0.01 | -100.34 | 0.03 | -84.45 | 0.01 | 19.89 | 0.04 | 104.82 | 0.00 | 61.98 | 0.02 | 61.59 |
| **9** | 0.00 | 172.93 | 0.04 | 129.40 | 0.00 | -15.28 | 0.03 | -58.75 | 0.01 | 103.39 | 0.03 | 125.09 | 0.00 | -5.85 | 0.02 | 76.34 |
| **10** | 0.00 | 79.58 | 0.03 | 149.27 | 0.00 | -75.36 | 0.03 | -33.38 | 0.01 | 65.12 | 0.02 | 139.68 | 0.00 | 44.74 | 0.01 | 59.04 |
| **11** | 0.00 | 85.87 | 0.04 | 157.78 | 0.01 | 112.49 | 0.02 | -24.11 | 0.01 | 172.55 | 0.02 | 152.30 | 0.00 | -177.31 | 0.01 | 71.20 |
| **12** | 0.01 | 90.17 | 0.02 | 166.60 | 0.01 | 155.07 | 0.03 | -9.46 | 0.00 | -44.46 | 0.04 | 166.23 | 0.00 | -35.21 | 0.02 | 96.78 |
| **13** | 0.00 | -23.53 | 0.02 | 173.25 | 0.00 | 58.76 | 0.03 | -5.92 | 0.00 | -72.32 | 0.03 | -169.06 | 0.01 | -71.42 | 0.02 | 129.19 |
| **14** | 0.01 | 8.30 | 0.03 | 168.69 | 0.01 | 69.50 | 0.04 | 13.13 | 0.00 | 51.36 | 0.02 | -163.83 | 0.01 | -74.59 | 0.02 | 128.41 |
| **15** | 0.00 | 21.30 | 0.03 | -171.68 | 0.01 | -33.97 | 0.03 | 5.12 | 0.01 | 51.26 | 0.02 | -160.84 | 0.00 | 73.63 | 0.01 | 81.70 |
| **16** | 0.01 | 45.66 | 0.02 | 164.91 | 0.01 | 2.46 | 0.02 | 25.90 | 0.01 | -12.94 | 0.03 | -168.29 | 0.01 | -25.54 | 0.01 | 102.17 |



Table A.28: VW ID.4 Pro — Harmonic Orders $h_{26}$ to $h_{33}$

| **Harmonic Order** | **h26** | | **h27** | | **h28** | | **h29** | | **h30** | | **h31** | | **h32** | | **h33** | |
|---|---|---|---|---|---|---|---|---|---|---|---|---|---|---|---|---|
| **Charging Rate (A)** | **A** | $\theta$ | **A** | $\theta$ | **A** | $\theta$ | **A** | $\theta$ | **A** | $\theta$ | **A** | $\theta$ | **A** | $\theta$ | **A** | $\theta$ |
| **6** | 0.00 | 110.52 | 0.04 | -99.15 | 0.00 | -65.06 | 0.02 | -86.55 | 0.00 | -153.84 | 0.01 | 69.01 | 0.00 | 55.16 | 0.02 | -54.46 |
| **7** | 0.00 | 14.46 | 0.04 | -89.62 | 0.00 | -0.69 | 0.02 | -77.37 | 0.00 | -100.94 | 0.01 | 121.70 | 0.00 | 118.53 | 0.01 | -24.35 |
| **8** | 0.00 | 178.89 | 0.04 | -53.16 | 0.00 | -10.19 | 0.03 | -56.28 | 0.00 | 63.47 | 0.01 | 161.63 | 0.01 | -118.27 | 0.01 | 12.26 |
| **9** | 0.00 | 174.39 | 0.04 | -25.78 | 0.00 | -76.31 | 0.02 | -26.07 | 0.00 | -82.07 | 0.01 | -173.12 | 0.00 | 80.76 | 0.01 | 50.57 |
| **10** | 0.00 | -153.26 | 0.04 | -11.59 | 0.00 | 14.35 | 0.02 | 4.98 | 0.00 | -7.56 | 0.01 | 179.21 | 0.00 | 132.84 | 0.01 | 79.87 |
| **11** | 0.00 | -58.84 | 0.04 | 7.97 | 0.00 | 151.92 | 0.02 | 5.59 | 0.00 | -2.33 | 0.01 | -141.01 | 0.00 | 166.46 | 0.02 | 80.91 |
| **12** | 0.00 | 42.46 | 0.04 | 17.25 | 0.00 | 24.98 | 0.01 | -16.86 | 0.01 | -113.21 | 0.02 | -104.40 | 0.01 | -159.64 | 0.02 | 91.23 |
| **13** | 0.00 | -43.95 | 0.04 | 34.88 | 0.00 | 26.08 | 0.01 | 11.99 | 0.01 | -56.98 | 0.01 | -72.30 | 0.00 | -166.09 | 0.01 | 88.34 |
| **14** | 0.01 | -21.55 | 0.04 | 58.77 | 0.00 | -128.57 | 0.01 | 64.66 | 0.01 | -99.63 | 0.01 | -103.67 | 0.01 | -75.67 | 0.01 | 177.17 |
| **15** | 0.01 | -19.82 | 0.04 | 59.76 | 0.01 | -46.04 | 0.01 | 115.60 | 0.00 | 65.33 | 0.01 | -117.31 | 0.01 | -132.45 | 0.01 | 124.01 |
| **16** | 0.00 | -7.89 | 0.04 | 47.28 | 0.01 | 25.09 | 0.01 | 50.22 | 0.01 | -5.21 | 0.01 | -105.44 | 0.00 | -58.37 | 0.02 | 133.29 |

Table A.29: VW ID.4 Pro — Harmonic Orders $h_{34}$ to $h_{41}$

| **Harmonic Order** | **h34** | | **h35** | | **h36** | | **h37** | | **h38** | | **h49** | | **h40** | | **h41** | |
|---|---|---|---|---|---|---|---|---|---|---|---|---|---|---|---|---|
| **Charging Rate (A)** | **A** | $\theta$ | **A** | $\theta$ | **A** | $\theta$ | **A** | $\theta$ | **A** | $\theta$ | **A** | $\theta$ | **A** | $\theta$ | **A** | $\theta$ |
| **6** | 0.00 | -89.40 | 0.00 | -8.74 | 0.00 | -129.72 | 0.01 | 10.09 | 0.00 | -66.38 | 0.01 | -149.53 | 0.00 | -37.07 | 0.01 | 33.38 |
| **7** | 0.00 | 131.51 | 0.00 | 61.46 | 0.00 | -133.76 | 0.01 | 42.56 | 0.00 | -69.67 | 0.01 | -111.09 | 0.01 | -21.07 | 0.02 | 70.97 |
| **8** | 0.00 | -133.51 | 0.00 | 105.80 | 0.00 | 38.78 | 0.01 | 78.10 | 0.00 | 75.98 | 0.01 | -83.46 | 0.01 | 64.70 | 0.02 | 129.75 |
| **9** | 0.00 | 137.33 | 0.01 | 160.35 | 0.00 | 175.63 | 0.01 | 148.88 | 0.01 | 149.90 | 0.02 | -60.71 | 0.00 | -93.67 | 0.01 | 158.78 |
| **10** | 0.00 | -119.23 | 0.01 | -113.79 | 0.00 | 22.66 | 0.00 | -149.19 | 0.00 | 92.40 | 0.01 | 6.77 | 0.00 | 157.40 | 0.01 | 172.33 |
| **11** | 0.00 | 55.33 | 0.00 | -83.84 | 0.00 | 3.28 | 0.01 | -115.97 | 0.00 | 1.28 | 0.01 | -12.35 | 0.00 | -16.75 | 0.01 | -125.10 |
| **12** | 0.00 | 83.56 | 0.01 | 74.67 | 0.00 | -130.04 | 0.01 | 156.84 | 0.00 | -50.93 | 0.00 | 6.85 | 0.00 | 20.54 | 0.02 | -126.53 |
| **13** | 0.00 | 87.09 | 0.01 | 46.63 | 0.00 | -104.12 | 0.00 | 179.00 | 0.01 | -72.46 | 0.01 | 49.67 | 0.00 | -11.85 | 0.02 | -111.66 |
| **14** | 0.00 | -11.90 | 0.01 | -42.23 | 0.00 | 143.85 | 0.01 | -79.29 | 0.00 | -99.50 | 0.01 | 72.34 | 0.00 | -77.46 | 0.01 | -97.73 |
| **15** | 0.00 | -115.52 | 0.01 | -26.53 | 0.00 | -43.46 | 0.01 | -87.76 | 0.00 | -89.92 | 0.00 | 103.85 | 0.00 | -68.39 | 0.01 | -82.11 |
| **16** | 0.00 | -84.74 | 0.01 | -1.67 | 0.00 | -19.03 | 0.01 | -50.69 | 0.00 | 105.31 | 0.01 | -17.32 | 0.01 | -118.35 | 0.02 | -71.63 |



Table A.30: VW ID.4 Pro — Harmonic Orders $h_{42}$ to $h_{49}$

| **Harmonic Order** | **h42** | | **h43** | | **h44** | | **h45** | | **h46** | | **h47** | | **h48** | | **h49** | |
|---|---|---|---|---|---|---|---|---|---|---|---|---|---|---|---|---|
| **Charging Rate (A)** | **A** | $\theta$ | **A** | $\theta$ | **A** | $\theta$ | **A** | $\theta$ | **A** | $\theta$ | **A** | $\theta$ | **A** | $\theta$ | **A** | $\theta$ |
| **6** | 0.00 | 70.33 | 0.01 | -19.16 | 0.00 | -99.28 | 0.01 | -144.89 | 0.00 | -177.72 | 0.01 | -149.41 | 0.00 | 19.47 | 0.00 | -136.01 |
| **7** | 0.01 | 47.27 | 0.01 | 33.92 | 0.00 | 30.31 | 0.01 | -108.21 | 0.00 | 164.87 | 0.00 | -85.79 | 0.00 | -158.00 | 0.01 | -65.63 |
| **8** | 0.00 | -26.83 | 0.02 | 87.28 | 0.00 | 26.26 | 0.01 | -57.14 | 0.00 | -160.17 | 0.01 | -55.79 | 0.00 | 117.93 | 0.00 | 0.12 |
| **9** | 0.01 | 6.84 | 0.01 | 122.77 | 0.00 | -103.23 | 0.01 | 10.96 | 0.00 | 43.43 | 0.01 | -7.13 | 0.00 | 47.55 | 0.01 | -12.08 |
| **10** | 0.00 | -104.21 | 0.01 | 125.41 | 0.00 | 34.54 | 0.01 | 2.52 | 0.00 | 28.62 | 0.01 | -59.78 | 0.00 | 108.32 | 0.00 | 160.39 |
| **11** | 0.00 | 168.47 | 0.01 | -178.20 | 0.00 | 152.58 | 0.01 | 20.17 | 0.00 | 97.63 | 0.01 | 28.53 | 0.00 | -163.15 | 0.01 | 118.05 |
| **12** | 0.00 | -89.77 | 0.01 | -122.39 | 0.00 | -149.33 | 0.01 | -7.63 | 0.00 | -107.41 | 0.01 | 13.80 | 0.00 | -168.93 | 0.01 | 111.58 |
| **13** | 0.00 | 64.24 | 0.01 | -169.93 | 0.00 | 153.98 | 0.00 | -10.39 | 0.00 | -169.03 | 0.01 | -60.78 | 0.00 | -143.87 | 0.01 | -133.79 |
| **14** | 0.00 | -130.25 | 0.01 | -146.38 | 0.00 | -176.50 | 0.00 | 96.14 | 0.00 | -102.87 | 0.00 | 57.90 | 0.00 | -154.08 | 0.01 | -162.26 |
| **15** | 0.00 | -154.47 | 0.01 | -126.32 | 0.00 | -33.85 | 0.01 | 76.93 | 0.01 | 44.06 | 0.01 | 59.72 | 0.00 | -106.17 | 0.01 | -165.83 |
| **16** | 0.00 | -168.15 | 0.01 | -66.32 | 0.00 | -171.68 | 0.01 | 73.25 | 0.00 | -25.88 | 0.01 | 97.44 | 0.00 | -59.46 | 0.01 | -169.80 |

Table A.31: Tesla Model Y LR — Harmonic Orders $h_2$ to $h_9$

| **Harmonic Order** | **h2** | | **h3** | | **h4** | | **h5** | | **h6** | | **h7** | | **h8** | | **h9** | |
|---|---|---|---|---|---|---|---|---|---|---|---|---|---|---|---|---|
| **Charging Rate (A)** | **A** | $\theta$ | **A** | $\theta$ | **A** | $\theta$ | **A** | $\theta$ | **A** | $\theta$ | **A** | $\theta$ | **A** | $\theta$ | **A** | $\theta$ |
| **6** | 0.01 | -133.87 | 0.26 | -85.42 | 0.00 | -76.55 | 0.20 | -53.98 | 0.01 | -46.72 | 0.37 | -81.22 | 0.01 | -72.94 | 0.15 | 2.64 |
| **7** | 0.01 | -106.18 | 0.26 | -83.53 | 0.00 | 137.54 | 0.20 | -50.58 | 0.01 | -42.24 | 0.36 | -81.26 | 0.01 | -72.76 | 0.16 | 7.21 |
| **8** | 0.01 | -87.53 | 0.26 | -82.31 | 0.00 | -100.90 | 0.21 | -48.01 | 0.01 | -40.86 | 0.37 | -80.06 | 0.01 | -75.33 | 0.17 | 9.10 |
| **9** | 0.02 | -91.90 | 0.25 | -85.37 | 0.00 | 26.33 | 0.20 | -44.16 | 0.01 | -24.47 | 0.37 | -78.80 | 0.01 | -62.64 | 0.18 | 10.50 |
| **10** | 0.00 | -146.22 | 0.25 | -85.82 | 0.00 | 78.30 | 0.21 | -40.29 | 0.01 | -43.18 | 0.36 | -77.81 | 0.01 | -71.36 | 0.18 | 13.76 |
| **11** | 0.02 | -98.38 | 0.26 | -81.29 | 0.00 | 11.76 | 0.21 | -38.68 | 0.01 | -35.91 | 0.37 | -76.94 | 0.01 | -69.76 | 0.20 | 12.72 |
| **12** | 0.02 | -113.75 | 0.27 | -78.46 | 0.00 | -29.98 | 0.22 | -35.07 | 0.01 | -28.62 | 0.37 | -75.82 | 0.01 | -59.34 | 0.20 | 14.83 |
| **13** | 0.01 | -99.75 | 0.28 | -77.29 | 0.00 | 41.73 | 0.22 | -32.75 | 0.00 | -26.56 | 0.37 | -74.81 | 0.01 | -55.50 | 0.21 | 15.05 |
| **14** | 0.01 | -104.97 | 0.29 | -73.38 | 0.00 | 56.39 | 0.23 | -31.32 | 0.00 | -23.45 | 0.37 | -73.42 | 0.01 | -62.95 | 0.22 | 13.69 |
| **15** | 0.03 | -103.60 | 0.30 | -71.87 | 0.00 | -59.05 | 0.24 | -28.92 | 0.01 | -54.56 | 0.38 | -72.36 | 0.01 | -66.45 | 0.23 | 14.22 |
| **16** | 0.01 | -126.51 | 0.32 | -69.19 | 0.00 | 33.93 | 0.25 | -26.05 | 0.01 | -24.69 | 0.37 | -72.02 | 0.01 | -57.64 | 0.23 | 16.12 |



Table A.32: Tesla Model Y LR — Harmonic Orders $h_{10}$ to $h_{17}$

| **Harmonic Order** | **h10** | | **h11** | | **h12** | | **h13** | | **h14** | | **h15** | | **h16** | | **h17** | |
|---|---|---|---|---|---|---|---|---|---|---|---|---|---|---|---|---|
| **Charging Rate (A)** | **A** | $\theta$ | **A** | $\theta$ | **A** | $\theta$ | **A** | $\theta$ | **A** | $\theta$ | **A** | $\theta$ | **A** | $\theta$ | **A** | $\theta$ |
| **6** | 0.00 | -85.04 | 0.14 | -119.99 | 0.00 | -60.41 | 0.21 | -30.24 | 0.01 | -62.04 | 0.08 | -125.87 | 0.00 | -56.15 | 0.06 | -133.41 |
| **7** | 0.00 | -62.95 | 0.14 | -138.97 | 0.01 | -52.00 | 0.24 | -30.81 | 0.01 | -57.30 | 0.08 | -131.46 | 0.00 | -55.74 | 0.05 | -169.51 |
| **8** | 0.00 | -72.58 | 0.15 | -148.01 | 0.00 | -50.31 | 0.26 | -32.58 | 0.00 | -66.15 | 0.10 | -128.04 | 0.00 | -34.91 | 0.07 | -165.11 |
| **9** | 0.00 | -24.95 | 0.15 | -154.81 | 0.00 | -59.36 | 0.27 | -32.48 | 0.01 | -67.54 | 0.11 | -127.33 | 0.00 | -51.29 | 0.08 | -156.61 |
| **10** | 0.00 | -85.86 | 0.16 | -154.55 | 0.01 | -63.92 | 0.29 | -33.76 | 0.01 | -65.16 | 0.12 | -129.06 | 0.00 | -48.31 | 0.09 | -155.94 |
| **11** | 0.00 | -88.41 | 0.16 | -158.69 | 0.00 | -57.07 | 0.30 | -35.00 | 0.01 | -67.42 | 0.13 | -127.35 | 0.01 | -72.02 | 0.10 | -151.94 |
| **12** | 0.00 | -92.84 | 0.17 | -153.90 | 0.01 | -57.64 | 0.31 | -36.36 | 0.01 | -74.37 | 0.13 | -126.58 | 0.00 | -88.89 | 0.12 | -148.09 |
| **13** | 0.00 | -94.00 | 0.18 | -149.63 | 0.01 | -62.95 | 0.32 | -35.83 | 0.01 | -75.31 | 0.13 | -129.86 | 0.01 | -64.00 | 0.12 | -152.88 |
| **14** | 0.00 | -93.73 | 0.19 | -144.89 | 0.01 | -46.70 | 0.33 | -36.92 | 0.01 | -77.13 | 0.14 | -128.93 | 0.00 | -74.76 | 0.13 | -154.59 |
| **15** | 0.00 | -76.97 | 0.20 | -142.51 | 0.00 | -46.24 | 0.33 | -38.87 | 0.01 | -84.96 | 0.15 | -128.37 | 0.00 | -48.93 | 0.15 | -147.78 |
| **16** | 0.00 | -51.22 | 0.20 | -144.13 | 0.01 | -36.53 | 0.34 | -38.27 | 0.01 | -73.83 | 0.15 | -130.63 | 0.00 | -85.18 | 0.15 | -149.72 |

Table A.33: Tesla Model Y LR — Harmonic Orders $h_{18}$ to $h_{25}$

| **Harmonic Order** | **h18** | | **h19** | | **h20** | | **h21** | | **h22** | | **h23** | | **h24** | | **h25** | |
|---|---|---|---|---|---|---|---|---|---|---|---|---|---|---|---|---|
| **Charging Rate (A)** | **A** | $\theta$ | **A** | $\theta$ | **A** | $\theta$ | **A** | $\theta$ | **A** | $\theta$ | **A** | $\theta$ | **A** | $\theta$ | **A** | $\theta$ |
| **6** | 0.00 | -55.57 | 0.17 | -12.46 | 0.01 | -40.33 | 0.02 | 1.75 | 0.00 | -43.98 | 0.07 | -73.01 | 0.01 | -59.49 | 0.00 | 127.23 |
| **7** | 0.01 | -50.56 | 0.16 | -14.74 | 0.01 | -40.40 | 0.02 | 18.39 | 0.01 | -65.82 | 0.06 | -87.90 | 0.01 | -54.42 | 0.01 | 88.56 |
| **8** | 0.00 | -44.11 | 0.16 | -9.26 | 0.01 | -41.52 | 0.02 | 20.96 | 0.00 | -48.82 | 0.06 | -84.78 | 0.01 | -48.01 | 0.01 | 72.51 |
| **9** | 0.00 | -71.33 | 0.17 | -4.24 | 0.01 | -40.79 | 0.01 | 9.16 | 0.01 | -13.86 | 0.06 | -89.69 | 0.01 | -38.27 | 0.01 | 87.28 |
| **10** | 0.00 | -69.01 | 0.17 | -0.91 | 0.01 | -23.89 | 0.00 | -5.93 | 0.01 | -34.62 | 0.07 | -90.66 | 0.01 | -40.85 | 0.01 | 69.38 |
| **11** | 0.01 | -68.62 | 0.19 | -0.05 | 0.01 | -29.89 | 0.00 | -2.50 | 0.01 | -13.08 | 0.08 | -88.70 | 0.01 | -26.19 | 0.01 | 120.02 |
| **12** | 0.00 | -77.84 | 0.20 | -1.52 | 0.01 | -22.78 | 0.01 | 178.64 | 0.00 | -0.53 | 0.08 | -93.76 | 0.01 | -53.24 | 0.01 | 158.12 |
| **13** | 0.00 | -61.87 | 0.21 | -4.18 | 0.01 | -20.55 | 0.02 | -176.98 | 0.01 | -29.98 | 0.09 | -97.51 | 0.01 | -50.65 | 0.02 | 140.68 |
| **14** | 0.00 | -112.23 | 0.23 | -4.52 | 0.01 | -44.19 | 0.02 | 172.95 | 0.00 | -32.34 | 0.10 | -98.46 | 0.01 | -56.44 | 0.02 | 159.31 |
| **15** | 0.00 | -75.03 | 0.24 | -4.28 | 0.01 | -43.83 | 0.02 | 150.24 | 0.01 | -27.70 | 0.10 | -100.95 | 0.01 | -52.91 | 0.03 | -176.76 |
| **16** | 0.01 | -87.01 | 0.25 | -8.32 | 0.01 | -64.86 | 0.02 | 161.26 | 0.00 | -36.55 | 0.10 | -108.98 | 0.01 | -70.41 | 0.04 | 170.63 |



Table A.34: Tesla Model Y LR — Harmonic Orders $h_{26}$ to $h_{33}$

| **Harmonic Order** | **h26** | | **h27** | | **h28** | | **h29** | | **h30** | | **h31** | | **h32** | | **h33** | |
|---|---|---|---|---|---|---|---|---|---|---|---|---|---|---|---|---|
| **Charging Rate (A)** | **A** | $\theta$ | **A** | $\theta$ | **A** | $\theta$ | **A** | $\theta$ | **A** | $\theta$ | **A** | $\theta$ | **A** | $\theta$ | **A** | $\theta$ |
| **6** | 0.00 | -86.25 | 0.02 | 31.92 | 0.01 | 2.38 | 0.03 | -93.89 | 0.00 | -46.01 | 0.03 | 46.84 | 0.01 | 8.81 | 0.01 | 141.75 |
| **7** | 0.00 | -91.42 | 0.01 | 67.90 | 0.01 | 13.79 | 0.04 | -93.94 | 0.00 | -61.65 | 0.03 | 93.62 | 0.01 | 4.65 | 0.01 | -150.01 |
| **8** | 0.00 | -43.85 | 0.02 | 96.84 | 0.01 | 12.98 | 0.05 | -111.09 | 0.00 | -59.90 | 0.04 | 104.92 | 0.01 | -14.37 | 0.01 | -155.03 |
| **9** | 0.00 | -64.00 | 0.02 | 101.39 | 0.00 | -27.39 | 0.05 | -118.62 | 0.00 | -122.98 | 0.05 | 82.64 | 0.01 | -18.80 | 0.02 | -153.64 |
| **10** | 0.00 | -36.12 | 0.03 | 84.31 | 0.00 | -50.89 | 0.04 | -122.22 | 0.00 | -79.88 | 0.04 | 63.15 | 0.01 | -28.06 | 0.03 | -148.13 |
| **11** | 0.00 | -20.62 | 0.02 | 91.62 | 0.01 | -25.40 | 0.05 | -125.38 | 0.00 | -48.93 | 0.03 | 58.80 | 0.01 | -18.83 | 0.03 | -159.55 |
| **12** | 0.01 | -41.70 | 0.02 | 96.72 | 0.00 | 14.80 | 0.05 | -125.95 | 0.00 | -73.20 | 0.04 | 54.84 | 0.01 | -1.09 | 0.03 | -165.49 |
| **13** | 0.00 | -46.09 | 0.02 | 81.98 | 0.01 | 18.00 | 0.04 | -124.53 | 0.00 | -37.69 | 0.03 | 72.88 | 0.01 | 18.64 | 0.03 | -163.44 |
| **14** | 0.00 | -74.55 | 0.02 | 100.68 | 0.01 | 32.57 | 0.05 | -126.36 | 0.00 | -99.82 | 0.04 | 45.55 | 0.01 | 16.61 | 0.03 | -167.86 |
| **15** | 0.00 | -32.27 | 0.02 | 123.33 | 0.00 | 34.56 | 0.06 | -139.70 | 0.00 | -77.58 | 0.04 | 69.44 | 0.01 | 10.77 | 0.02 | -179.34 |
| **16** | 0.00 | -82.11 | 0.03 | 128.33 | 0.01 | -2.53 | 0.07 | -129.84 | 0.01 | -73.54 | 0.07 | 73.20 | 0.01 | 28.04 | 0.03 | -175.81 |

Table A.35: Tesla Model Y LR — Harmonic Orders $h_{34}$ to $h_{41}$

| **Harmonic Order** | **h34** | | **h35** | | **h36** | | **h37** | | **h38** | | **h49** | | **h40** | | **h41** | |
|---|---|---|---|---|---|---|---|---|---|---|---|---|---|---|---|---|
| **Charging Rate (A)** | **A** | $\theta$ | **A** | $\theta$ | **A** | $\theta$ | **A** | $\theta$ | **A** | $\theta$ | **A** | $\theta$ | **A** | $\theta$ | **A** | $\theta$ |
| **6** | 0.01 | -49.58 | 0.04 | -30.19 | 0.00 | 1.84 | 0.04 | -48.50 | 0.01 | -14.87 | 0.01 | 146.86 | 0.00 | -76.99 | 0.03 | -77.47 |
| **7** | 0.01 | -25.46 | 0.04 | -15.10 | 0.01 | 55.94 | 0.03 | -61.62 | 0.00 | 56.61 | 0.02 | 124.06 | 0.00 | -70.32 | 0.04 | -61.94 |
| **8** | 0.00 | 10.25 | 0.04 | -1.85 | 0.01 | 70.93 | 0.03 | -62.96 | 0.00 | 83.74 | 0.01 | 123.93 | 0.01 | -33.44 | 0.04 | -75.14 |
| **9** | 0.00 | 2.95 | 0.05 | 14.57 | 0.00 | 111.44 | 0.03 | -34.23 | 0.00 | 134.54 | 0.01 | 118.64 | 0.01 | -35.64 | 0.04 | -78.21 |
| **10** | 0.00 | 157.13 | 0.06 | 21.74 | 0.00 | 170.69 | 0.04 | -28.70 | 0.00 | -80.27 | 0.01 | 122.47 | 0.00 | -15.23 | 0.03 | -51.76 |
| **11** | 0.00 | -148.18 | 0.06 | 7.32 | 0.00 | 122.30 | 0.04 | -52.47 | 0.00 | -45.77 | 0.01 | 148.29 | 0.00 | 21.40 | 0.03 | -47.54 |
| **12** | 0.00 | -129.80 | 0.07 | -12.03 | 0.00 | 80.52 | 0.05 | -58.60 | 0.00 | -35.16 | 0.01 | 145.92 | 0.00 | 16.81 | 0.03 | -68.63 |
| **13** | 0.00 | -110.69 | 0.07 | -4.50 | 0.00 | 86.12 | 0.05 | -61.36 | 0.01 | -38.63 | 0.02 | 146.20 | 0.00 | -4.29 | 0.04 | -79.11 |
| **14** | 0.00 | -78.94 | 0.07 | -6.17 | 0.00 | 35.97 | 0.05 | -79.68 | 0.00 | -8.56 | 0.02 | 129.66 | 0.00 | -34.23 | 0.05 | -70.70 |
| **15** | 0.00 | -72.90 | 0.07 | -19.44 | 0.00 | -52.28 | 0.05 | -95.02 | 0.00 | 127.48 | 0.02 | 131.35 | 0.00 | -173.81 | 0.05 | -90.14 |
| **16** | 0.00 | -52.05 | 0.06 | -5.18 | 0.00 | -8.32 | 0.05 | -69.23 | 0.01 | -23.34 | 0.03 | 140.34 | 0.00 | 124.59 | 0.05 | -91.33 |



Table A.36: Tesla Model Y LR — Harmonic Orders $h_{42}$ to $h_{49}$

| **Harmonic Order** | **h42** | | **h43** | | **h44** | | **h45** | | **h46** | | **h47** | | **h48** | | **h49** | |
|---|---|---|---|---|---|---|---|---|---|---|---|---|---|---|---|---|
| **Charging Rate (A)** | **A** | $\theta$ | **A** | $\theta$ | **A** | $\theta$ | **A** | $\theta$ | **A** | $\theta$ | **A** | $\theta$ | **A** | $\theta$ | **A** | $\theta$ |
| **6** | 0.01 | -56.34 | 0.01 | -171.07 | 0.01 | -75.88 | 0.01 | 113.51 | 0.01 | -18.96 | 0.01 | 154.18 | 0.01 | -43.26 | 0.01 | 157.13 |
| **7** | 0.01 | -24.80 | 0.02 | -154.51 | 0.00 | -40.81 | 0.01 | 134.87 | 0.01 | -49.11 | 0.01 | 154.00 | 0.02 | -61.06 | 0.01 | 163.74 |
| **8** | 0.01 | 12.53 | 0.03 | -165.82 | 0.00 | -107.85 | 0.02 | 140.34 | 0.02 | -73.94 | 0.02 | 170.61 | 0.02 | -84.88 | 0.01 | 170.96 |
| **9** | 0.01 | 23.54 | 0.03 | -173.10 | 0.00 | -131.84 | 0.02 | 139.10 | 0.02 | -58.60 | 0.03 | -165.33 | 0.02 | -80.37 | 0.02 | -174.25 |
| **10** | 0.01 | 50.55 | 0.02 | -163.68 | 0.01 | 148.92 | 0.02 | 136.27 | 0.03 | -45.51 | 0.03 | -163.82 | 0.02 | -65.33 | 0.03 | -169.33 |
| **11** | 0.00 | 46.63 | 0.02 | -175.43 | 0.01 | 163.45 | 0.02 | 142.40 | 0.03 | -44.08 | 0.03 | -162.87 | 0.02 | -64.47 | 0.03 | -168.83 |
| **12** | 0.00 | 36.19 | 0.03 | -156.37 | 0.01 | -178.73 | 0.02 | 127.92 | 0.03 | -32.50 | 0.03 | -161.40 | 0.02 | -54.59 | 0.03 | -172.84 |
| **13** | 0.00 | 44.47 | 0.03 | -159.19 | 0.01 | -168.96 | 0.02 | 131.53 | 0.03 | -18.60 | 0.03 | -174.72 | 0.02 | -41.86 | 0.03 | -175.43 |
| **14** | 0.00 | -75.34 | 0.03 | -151.24 | 0.01 | -151.04 | 0.02 | 130.87 | 0.03 | -4.03 | 0.03 | -170.84 | 0.00 | 118.58 | 0.03 | -166.55 |
| **15** | 0.00 | -62.52 | 0.04 | -156.68 | 0.01 | -137.11 | 0.03 | 134.51 | 0.01 | -12.51 | 0.03 | -162.03 | 0.01 | -177.28 | 0.03 | -170.08 |
| **16** | 0.00 | -140.81 | 0.04 | -155.73 | 0.01 | -116.84 | 0.03 | 139.69 | 0.03 | -46.00 | 0.04 | -148.25 | 0.02 | -135.71 | 0.03 | -168.89 |

Table A.37: Peugeot e-2008 — Harmonic Orders $h_2$ to $h_9$

| **Harmonic Order** | **h2** | | **h3** | | **h4** | | **h5** | | **h6** | | **h7** | | **h8** | | **h9** | |
|---|---|---|---|---|---|---|---|---|---|---|---|---|---|---|---|---|
| **Charging Rate (A)** | **A** | $\theta$ | **A** | $\theta$ | **A** | $\theta$ | **A** | $\theta$ | **A** | $\theta$ | **A** | $\theta$ | **A** | $\theta$ | **A** | $\theta$ |
| **6** | 0.08 | 78.97 | 0.20 | 16.37 | 0.04 | -63.08 | 1.00 | -28.98 | 0.02 | -19.43 | 1.00 | -47.10 | 0.01 | -28.71 | 0.12 | -41.32 |
| **7** | 0.06 | 91.30 | 0.23 | 21.53 | 0.02 | -75.71 | 1.07 | -28.77 | 0.01 | 8.70 | 1.05 | -46.73 | 0.02 | -33.99 | 0.12 | -43.67 |
| **8** | 0.07 | 83.14 | 0.23 | 19.49 | 0.06 | -94.52 | 1.10 | -28.90 | 0.02 | -55.22 | 1.09 | -47.23 | 0.01 | -54.57 | 0.14 | -43.96 |
| **9** | 0.08 | 88.45 | 0.23 | 14.89 | 0.08 | -90.36 | 1.13 | -27.80 | 0.00 | 110.28 | 1.11 | -46.94 | 0.01 | -23.25 | 0.14 | -45.96 |
| **10** | 0.06 | 79.73 | 0.26 | 20.01 | 0.06 | -93.65 | 1.14 | -27.37 | 0.01 | -116.60 | 1.10 | -47.22 | 0.02 | -25.79 | 0.16 | -45.12 |
| **11** | 0.08 | 89.98 | 0.24 | 16.40 | 0.06 | -95.27 | 1.16 | -26.65 | 0.00 | 18.70 | 1.06 | -47.63 | 0.02 | -25.41 | 0.15 | -46.81 |
| **12** | 0.10 | 77.15 | 0.26 | 19.98 | 0.04 | -92.76 | 1.22 | -25.94 | 0.01 | -14.04 | 1.05 | -47.34 | 0.02 | -47.96 | 0.15 | -46.57 |
| **13** | 0.04 | 42.84 | 0.26 | 17.95 | 0.07 | -67.27 | 1.18 | -26.05 | 0.01 | -4.96 | 1.06 | -48.40 | 0.02 | -46.36 | 0.16 | -48.63 |
| **14** | 0.10 | 76.04 | 0.27 | 17.94 | 0.06 | -74.80 | 1.19 | -26.15 | 0.01 | -72.81 | 1.08 | -48.31 | 0.01 | -35.39 | 0.16 | -47.47 |
| **15** | 0.08 | 76.09 | 0.29 | 21.03 | 0.07 | -94.55 | 1.22 | -25.55 | 0.00 | -41.31 | 1.05 | -48.43 | 0.02 | -45.27 | 0.17 | -48.78 |



Table A.38: Peugeot e-2008 — Harmonic Orders $h_{10}$ to $h_{17}$

| **Harmonic Order** | **h10** | | **h11** | | **h12** | | **h13** | | **h14** | | **h15** | | **h16** | | **h17** | |
|---|---|---|---|---|---|---|---|---|---|---|---|---|---|---|---|---|
| **Charging Rate (A)** | **A** | $\theta$ | **A** | $\theta$ | **A** | $\theta$ | **A** | $\theta$ | **A** | $\theta$ | **A** | $\theta$ | **A** | $\theta$ | **A** | $\theta$ |
| **6** | 0.01 | -48.02 | 0.04 | 88.04 | 0.01 | -31.44 | 0.24 | -3.55 | 0.00 | -42.93 | 0.03 | 79.67 | 0.00 | 16.66 | 0.09 | -7.26 |
| **7** | 0.00 | -134.73 | 0.03 | 123.63 | 0.01 | -26.59 | 0.26 | -4.14 | 0.00 | -105.09 | 0.03 | 78.17 | 0.00 | 32.31 | 0.09 | -3.35 |
| **8** | 0.01 | -43.21 | 0.03 | 130.02 | 0.01 | -84.60 | 0.28 | -4.94 | 0.00 | 62.59 | 0.03 | 77.58 | 0.00 | 1.46 | 0.08 | -8.79 |
| **9** | 0.01 | -81.77 | 0.05 | 143.38 | 0.01 | -30.18 | 0.29 | -5.84 | 0.00 | 132.21 | 0.03 | 79.34 | 0.01 | 2.39 | 0.08 | -7.84 |
| **10** | 0.01 | -102.59 | 0.05 | 160.96 | 0.01 | -59.65 | 0.31 | -5.64 | 0.00 | -168.88 | 0.04 | 91.33 | 0.00 | -26.43 | 0.08 | -7.70 |
| **11** | 0.01 | -41.04 | 0.06 | 150.99 | 0.01 | -79.92 | 0.32 | -7.47 | 0.00 | 140.91 | 0.04 | 93.47 | 0.01 | 35.72 | 0.08 | -10.16 |
| **12** | 0.01 | -97.12 | 0.05 | 168.66 | 0.01 | -35.35 | 0.33 | -8.57 | 0.00 | -82.70 | 0.04 | 95.29 | 0.01 | 4.31 | 0.08 | -8.91 |
| **13** | 0.01 | -125.82 | 0.07 | -173.82 | 0.01 | -26.84 | 0.35 | -9.97 | 0.01 | -142.64 | 0.05 | 84.16 | 0.00 | -2.45 | 0.07 | -4.33 |
| **14** | 0.01 | -116.58 | 0.07 | -156.21 | 0.01 | -135.58 | 0.36 | -11.77 | 0.01 | 133.87 | 0.05 | 83.00 | 0.00 | -88.86 | 0.07 | -5.17 |
| **15** | 0.01 | -119.21 | 0.06 | -167.02 | 0.01 | -62.60 | 0.36 | -11.59 | 0.00 | -61.22 | 0.05 | 77.79 | 0.01 | -18.42 | 0.06 | -1.62 |

Table A.39: Peugeot e-2008 — Harmonic Orders $h_{18}$ to $h_{25}$

| **Harmonic Order** | **h18** | | **h19** | | **h20** | | **h21** | | **h22** | | **h23** | | **h24** | | **h25** | |
|---|---|---|---|---|---|---|---|---|---|---|---|---|---|---|---|---|
| **Charging Rate (A)** | **A** | $\theta$ | **A** | $\theta$ | **A** | $\theta$ | **A** | $\theta$ | **A** | $\theta$ | **A** | $\theta$ | **A** | $\theta$ | **A** | $\theta$ |
| **6** | 0.01 | 14.20 | 0.15 | -8.75 | 0.00 | -31.96 | 0.03 | 61.22 | 0.01 | 17.20 | 0.05 | 45.09 | 0.00 | 4.63 | 0.08 | 39.81 |
| **7** | 0.01 | -5.25 | 0.15 | -5.95 | 0.00 | 16.66 | 0.03 | 60.85 | 0.01 | 22.58 | 0.05 | 46.67 | 0.00 | 83.47 | 0.08 | 38.55 |
| **8** | 0.01 | -3.62 | 0.15 | -6.06 | 0.00 | -17.94 | 0.03 | 72.99 | 0.01 | 30.23 | 0.05 | 50.19 | 0.00 | 87.90 | 0.08 | 36.15 |
| **9** | 0.01 | -6.61 | 0.15 | -3.68 | 0.00 | 0.83 | 0.03 | 77.42 | 0.00 | 44.28 | 0.05 | 53.26 | 0.00 | 76.27 | 0.08 | 37.93 |
| **10** | 0.01 | -1.43 | 0.15 | -2.76 | 0.01 | 12.88 | 0.03 | 69.37 | 0.01 | 7.98 | 0.05 | 43.48 | 0.00 | 74.22 | 0.08 | 40.49 |
| **11** | 0.01 | -9.14 | 0.15 | -2.40 | 0.00 | 30.33 | 0.03 | 71.88 | 0.00 | 24.15 | 0.05 | 44.19 | 0.00 | 62.13 | 0.08 | 41.84 |
| **12** | 0.01 | -17.23 | 0.15 | -0.16 | 0.00 | 6.68 | 0.04 | 74.04 | 0.00 | 42.11 | 0.04 | 49.23 | 0.00 | 56.79 | 0.08 | 41.12 |
| **13** | 0.01 | -7.66 | 0.16 | 0.08 | 0.00 | 9.37 | 0.04 | 76.26 | 0.00 | 24.34 | 0.05 | 44.99 | 0.00 | 92.21 | 0.09 | 39.48 |
| **14** | 0.01 | -10.50 | 0.17 | -0.41 | 0.00 | 18.04 | 0.04 | 79.13 | 0.01 | 2.24 | 0.05 | 47.20 | 0.01 | 57.74 | 0.09 | 39.99 |
| **15** | 0.01 | -21.20 | 0.17 | -0.26 | 0.00 | 10.91 | 0.04 | 73.81 | 0.01 | 22.28 | 0.05 | 45.38 | 0.01 | 49.54 | 0.08 | 41.58 |

200

Table A.40: Peugeot e-2008 — Harmonic Orders $h_{26}$ to $h_{33}$

| **Harmonic Order** | **h26** | | **h27** | | **h28** | | **h29** | | **h30** | | **h31** | | **h32** | | **h33** | |
|---|---|---|---|---|---|---|---|---|---|---|---|---|---|---|---|---|
| **Charging Rate (A)** | **A** | $\theta$ | **A** | $\theta$ | **A** | $\theta$ | **A** | $\theta$ | **A** | $\theta$ | **A** | $\theta$ | **A** | $\theta$ | **A** | $\theta$ |
| **6** | 0.00 | 19.89 | 0.01 | 139.81 | 0.00 | 11.18 | 0.03 | 33.77 | 0.00 | -41.65 | 0.00 | 7.16 | 0.01 | 23.95 | 0.00 | -140.34 |
| **7** | 0.01 | 13.17 | 0.01 | 136.76 | 0.00 | -23.63 | 0.03 | 39.19 | 0.00 | 78.98 | 0.01 | 25.28 | 0.01 | 41.24 | 0.00 | -82.32 |
| **8** | 0.01 | 0.76 | 0.02 | 129.45 | 0.00 | 28.00 | 0.03 | 41.48 | 0.00 | -11.80 | 0.01 | 6.65 | 0.01 | 40.42 | 0.00 | -80.58 |
| **9** | 0.01 | 6.22 | 0.01 | 138.51 | 0.01 | 36.97 | 0.04 | 41.35 | 0.00 | 106.46 | 0.01 | 10.30 | 0.01 | 70.00 | 0.00 | -42.32 |
| **10** | 0.00 | 49.54 | 0.01 | 134.94 | 0.00 | 7.26 | 0.03 | 38.90 | 0.00 | 10.18 | 0.01 | 3.29 | 0.01 | 43.71 | 0.00 | -33.05 |
| **11** | 0.01 | -0.20 | 0.01 | 142.69 | 0.01 | 1.53 | 0.04 | 37.30 | 0.00 | 86.89 | 0.02 | 4.97 | 0.01 | 40.68 | 0.00 | -7.91 |
| **12** | 0.00 | 18.71 | 0.01 | 148.02 | 0.01 | 51.33 | 0.03 | 42.99 | 0.00 | -102.89 | 0.02 | 8.77 | 0.01 | 33.91 | 0.00 | 0.07 |
| **13** | 0.01 | 3.92 | 0.01 | 139.17 | 0.00 | -3.56 | 0.04 | 36.96 | 0.00 | 82.39 | 0.01 | -5.70 | 0.01 | 40.05 | 0.01 | -23.07 |
| **14** | 0.01 | 20.35 | 0.01 | 149.43 | 0.00 | 2.58 | 0.03 | 41.52 | 0.00 | 30.99 | 0.01 | -13.23 | 0.01 | 41.81 | 0.01 | -30.34 |
| **15** | 0.01 | 8.97 | 0.01 | 144.18 | 0.01 | 25.89 | 0.04 | 39.09 | 0.00 | 72.17 | 0.01 | 0.45 | 0.01 | 35.24 | 0.01 | -35.16 |

Table A.41: Peugeot e-2008 — Harmonic Orders $h_{34}$ to $h_{41}$

| **Harmonic Order** | **h34** | | **h35** | | **h36** | | **h37** | | **h38** | | **h49** | | **h40** | | **h41** | |
|---|---|---|---|---|---|---|---|---|---|---|---|---|---|---|---|---|
| **Charging Rate (A)** | **A** | $\theta$ | **A** | $\theta$ | **A** | $\theta$ | **A** | $\theta$ | **A** | $\theta$ | **A** | $\theta$ | **A** | $\theta$ | **A** | $\theta$ |
| **6** | 0.01 | 46.17 | 0.00 | 28.33 | 0.00 | 77.03 | 0.01 | -47.23 | 0.00 | 5.45 | 0.00 | 178.05 | 0.00 | 28.93 | 0.00 | 127.79 |
| **7** | 0.00 | 30.26 | 0.01 | 25.72 | 0.00 | 115.09 | 0.01 | -41.93 | 0.00 | 29.72 | 0.01 | 170.18 | 0.00 | -8.89 | 0.00 | 54.32 |
| **8** | 0.01 | 41.98 | 0.01 | 9.61 | 0.00 | 77.42 | 0.01 | -16.01 | 0.00 | 28.41 | 0.00 | -165.96 | 0.00 | 24.07 | 0.00 | 82.23 |
| **9** | 0.00 | 64.23 | 0.01 | 9.06 | 0.00 | 86.96 | 0.01 | -16.45 | 0.00 | 57.71 | 0.00 | 170.79 | 0.00 | 11.87 | 0.00 | 81.18 |
| **10** | 0.00 | 36.20 | 0.00 | 30.62 | 0.00 | 122.26 | 0.01 | -16.27 | 0.00 | 37.97 | 0.00 | 168.39 | 0.00 | 20.43 | 0.00 | 77.75 |
| **11** | 0.00 | 61.54 | 0.00 | 36.54 | 0.00 | 106.97 | 0.01 | -18.40 | 0.00 | 54.84 | 0.00 | 145.24 | 0.00 | 29.84 | 0.00 | 93.48 |
| **12** | 0.01 | 61.25 | 0.00 | 55.46 | 0.00 | 99.97 | 0.01 | -10.10 | 0.00 | 49.38 | 0.00 | 128.01 | 0.00 | -11.45 | 0.00 | 55.36 |
| **13** | 0.01 | 52.52 | 0.01 | 60.48 | 0.00 | 110.17 | 0.01 | -16.22 | 0.00 | 67.99 | 0.00 | 115.67 | 0.00 | -7.51 | 0.00 | 46.94 |
| **14** | 0.01 | 43.19 | 0.01 | 58.73 | 0.00 | 109.60 | 0.01 | -38.40 | 0.00 | 91.68 | 0.00 | 122.94 | 0.00 | 9.50 | 0.00 | 97.69 |
| **15** | 0.01 | 47.26 | 0.01 | 52.95 | 0.00 | -144.91 | 0.01 | -16.36 | 0.00 | 72.39 | 0.00 | 129.00 | 0.00 | -11.88 | 0.00 | 78.80 |



Table A.42: Peugeot e-2008 — Harmonic Orders $h_{42}$ to $h_{49}$

| **Harmonic Order** | **h42** | | **h43** | | **h44** | | **h45** | | **h46** | | **h47** | | **h48** | | **h49** | |
|---|---|---|---|---|---|---|---|---|---|---|---|---|---|---|---|---|
| **Charging Rate (A)** | **A** | $\theta$ | **A** | $\theta$ | **A** | $\theta$ | **A** | $\theta$ | **A** | $\theta$ | **A** | $\theta$ | **A** | $\theta$ | **A** | $\theta$ |
| **6** | 0.00 | -98.37 | 0.00 | 66.98 | 0.00 | -9.49 | 0.00 | 166.70 | 0.00 | 111.79 | 0.00 | -60.71 | 0.00 | -161.16 | 0.00 | -21.81 |
| **7** | 0.00 | -33.42 | 0.00 | 91.48 | 0.00 | -30.59 | 0.00 | 154.03 | 0.00 | 96.28 | 0.00 | -123.83 | 0.00 | -149.98 | 0.00 | -135.31 |
| **8** | 0.00 | -58.52 | 0.00 | 121.56 | 0.00 | -40.02 | 0.00 | 148.76 | 0.01 | 55.23 | 0.00 | -125.67 | 0.00 | -168.41 | 0.00 | 41.71 |
| **9** | 0.00 | -54.71 | 0.00 | 152.88 | 0.00 | -36.47 | 0.00 | 144.92 | 0.01 | 77.73 | 0.00 | -115.16 | 0.00 | -157.56 | 0.00 | 168.21 |
| **10** | 0.00 | -13.41 | 0.00 | 178.09 | 0.01 | -39.41 | 0.00 | 124.33 | 0.01 | 67.39 | 0.00 | -100.47 | 0.00 | -173.94 | 0.00 | 104.21 |
| **11** | 0.00 | -33.65 | 0.00 | 132.71 | 0.00 | -70.16 | 0.00 | 166.16 | 0.01 | 70.99 | 0.00 | -100.98 | 0.00 | -166.05 | 0.00 | 91.09 |
| **12** | 0.00 | -35.97 | 0.00 | 112.35 | 0.00 | -18.59 | 0.00 | 129.57 | 0.01 | 46.67 | 0.00 | -100.45 | 0.00 | -157.66 | 0.00 | 83.60 |
| **13** | 0.00 | -17.93 | 0.00 | 119.50 | 0.01 | -45.51 | 0.00 | 106.38 | 0.01 | 78.52 | 0.00 | -95.40 | 0.00 | -146.08 | 0.00 | 88.05 |
| **14** | 0.00 | 12.94 | 0.00 | 92.17 | 0.00 | -43.13 | 0.00 | 106.40 | 0.00 | 60.17 | 0.00 | -94.83 | 0.00 | -116.52 | 0.00 | 93.35 |
| **15** | 0.00 | 8.08 | 0.00 | -94.14 | 0.01 | -54.86 | 0.00 | 108.31 | 0.01 | 76.80 | 0.00 | -93.64 | 0.00 | -152.95 | 0.00 | 103.76 |

# Bibliography

[1] S. Fankhauser, S. M. Smith, M. Allen, K. Axelsson, T. Hale, C. Hepburn, J. M. Kendall, R. Khosla, J. Lezaun, E. Mitchell-Larson *et al.*, "The meaning of net zero and how to get it right," *Nature Climate Change*, vol. 12, no. 1, pp. 15–21, 2022.

[2] J. Rogelj, M. Den Elzen, N. Höhne, T. Fransen, H. Fekete, H. Winkler, R. Schaeffer, F. Sha, K. Riahi, and M. Meinshausen, "Paris Agreement climate proposals need a boost to keep warming well below 2 C," *Nature*, vol. 534, no. 7609, pp. 631–639, 2016.

[3] UNFCCC, "Paris agreement," in *report of the conference of the parties to the United Nations framework convention on climate change (21st session, 2015: Paris). Retrived December*, vol. 4, no. 2017. HeinOnline, 2015, p. 2.

[4] S. Jeudy-Hugo, L. L. Re, and C. Falduto, "Understanding countries' net-zero emissions targets," *OECD/IEA Climate Change Expert Group Papers*, 2021.

[5] O. C. Anika, S. G. Nnabuife, A. Bello, E. R. Okoroafor, B. Kuang, and R. Villa, "Prospects of low and zero-carbon renewable fuels in 1.5-degree net zero emission actualisation by 2050: A critical review," *Carbon Capture Science & Technology*, vol. 5, p. 100072, 2022.

[6] W. F. Lamb, T. Wiedmann, J. Pongratz, R. Andrew, M. Crippa, J. G. Olivier, D. Wiedenhofer, G. Mattioli, A. Al Khourdajie, J. House *et al.*, "A review of trends and drivers of greenhouse gas emissions by sector from 1990 to 2018," *Environmental Research Letters*, vol. 16, no. 7, p. 073005, 2021.

[7] European Environment Agency Road Transport. https://tinyurl.com/peju9dmd. Online; accessed June 25, 2025.

[8] 2024 uk greenhouse gas emissions, provisional figures.

[9] Phasing out the sale of new petrol and diesel cars from 2030 and support for zero emission vehicle (ZEV) transition. https://tinyurl.com/2c4n8va7. Online; accessed June 25, 2025.

[10] EV Data, Society of Motor Manufacturers and Traders. https://tinyurl.com/46pe42yj. Online; accessed June 25, 2025.

[11] International Energy Agency, "Global EV Outlook 2024," IEA, Tech. Rep., 2024.

[12] Can Power Grids Cope With Millions of EVs? https://tinyurl.com/4pfz626s. Online; accessed June 25, 2025.

[13] N. Brinkel, W. Schram, T. AlSkaif, I. Lampropoulos, and W. Van Sark, "Should we reinforce the grid? Cost and emission optimization of electric vehicle charging under different transformer limits," *Applied Energy*, vol. 276, p. 115285, 2020.

[14] M. Soleimani and M. Kezunovic, "Mitigating transformer loss of life and reducing the hazard of failure by the smart EV charging," *IEEE Transactions on Industry Applications*, vol. 56, no. 5, pp. 5974–5983, 2020.

[15] P. Richardson, D. Flynn, and A. Keane, "Impact assessment of varying penetrations of electric vehicles on low voltage distribution systems," in *IEEE PES general meeting*. IEEE, 2010, pp. 1–6.

[16] L. C. Hunter, G. Robinson, R. Sims, and S. Galloway, "From planning to deployment-insights into installing publicly-accessible journey EV charging infrastructure," in *EVI: Charging Ahead (EVI 2023)*, vol. 2023. IET, 2023, pp. 98–101.

[17] M. H. Tveit, K. Sevdari, M. Marinelli, and L. Calearo, "Behind-the-meter residential electric vehicle smart charging strategies: Danish cases," in *2022 Interna-*

*tional Conference on Renewable Energies and Smart Technologies (REST)*, vol. 1. IEEE, 2022, pp. 1–5.

[18] T. Zeng, H. Zhang, and S. Moura, "Solving overstay and stochasticity in PEV charging station planning with real data," *IEEE Transactions on Industrial Informatics*, vol. 16, no. 5, pp. 3504–3514, 2019.

[19] I. S. Bayram, A. Saad, R. Sims, A. Babu, C. Edmunds, and S. Galloway, "Statistical characterisation of public AC EV chargers in the UK," *IEEE Access*, 2023.

[20] L. Calearo, M. Marinelli, and C. Ziras, "A review of data sources for electric vehicle integration studies," *Renewable and Sustainable Energy Reviews*, vol. 151, p. 111518, 2021.

[21] S. Striani, K. Sevdari, P. B. Andersen, M. Marinelli, Y. Kobayashi, and K. Suzuki, "Autonomously distributed control of EV parking lot management for optimal grid integration," in *2022 International Conference on Renewable Energies and Smart Technologies (REST)*, vol. 1. IEEE, 2022, pp. 1–5.

[22] The Renewable Energy Consumer Code, "An introduction to electric vehicle home chargepoints," RECC, Tech. Rep., 2019.

[23] UK Government Electric vehicle smart charging. https://tinyurl.com/36p96eu9. Online; accessed June 25, 2025.

[24] Alternative Fuels Infrastructure Regulation. https://tinyurl.com/627fwkhy. Online; accessed June 25, 2025.

[25] C. McGarry, J. Dixon, J. Flower, W. Bukhsh, C. Brand, K. Bell, and S. Galloway, "Electrified heat and transport: Energy demand futures, their impacts on power networks and what it means for system flexibility," *Applied Energy*, vol. 360, p. 122836, 2024.

[26] Z. J. Lee, G. Lee, T. Lee, C. Jin, R. Lee, Z. Low, D. Chang, C. Ortega, and S. H. Low, "Adaptive charging networks: A framework for smart electric vehicle charging," *IEEE Transactions on Smart Grid*, vol. 12, no. 5, pp. 4339–4350, 2021.

[27] G. Barone, G. Brusco, D. Menniti, A. Pinnarelli, G. Polizzi, N. Sorrentino, P. Vizza, and A. Burgio, "How smart metering and smart charging may help a local energy community in collective self-consumption in presence of electric vehicles," *Energies*, vol. 13, no. 16, p. 4163, 2020.

[28] A. Khaligh and M. D'Antonio, "Global trends in high-power on-board chargers for electric vehicles," *IEEE Transactions on Vehicular Technology*, vol. 68, no. 4, pp. 3306–3324, 2019.

[29] S. Taghizadeh, M. Hossain, J. Lu, and W. Water, "A unified multi-functional on-board EV charger for power-quality control in household networks," *Applied Energy*, vol. 215, pp. 186–201, 2018.

[30] K. Sevdari, L. Calearo, B. H. Bakken, P. B. Andersen, and M. Marinelli, "Experimental validation of onboard electric vehicle chargers to improve the efficiency of smart charging operation," *Sustainable Energy Technologies and Assessments*, vol. 60, p. 103512, 2023.

[31] M. Senol, I. S. Bayram, Y. Naderi, and S. Galloway, "Electric vehicles under low temperatures: A review on battery performance, charging needs, and power grid impacts," *IEEE Access*, 2023.

[32] D. Alame, M. Azzouz, and N. Kar, "Assessing and mitigating impacts of electric vehicle harmonic currents on distribution systems," *Energies*, vol. 13, no. 12, p. 3257, 2020.

[33] A. Ulinuha and E. M. Sari, "The influence of harmonic distortion on losses and efficiency of three-phase distribution transformer," in *Journal of Physics: Conference Series*, vol. 1858, no. 1. IOP Publishing, 2021, p. 012084.

[34] M. Van den Berg, I. Lampropoulos, and T. AlSkaif, "Impact of electric vehicles charging demand on distribution transformers in an office area and determination of flexibility potential," *Sustainable Energy, Grids and Networks*, vol. 26, p. 100452, 2021.

[35] C. Francisco, *Harmonics, power systems, and smart grids.* CRC press, 2017.

[36] J. Yuan, L. Dorn-Gomba, A. D. Callegaro, J. Reimers, and A. Emadi, "A review of bidirectional on-board chargers for electric vehicles," *IEEE Access*, vol. 9, pp. 51 501–51 518, 2021.

[37] R. Pinyol, "Harmonics: Causes, effects and minimization," *Salicru White Papers*, 2015.

[38] T. Slangen, T. van Wijk, V. Ćuk, and J. Cobben, "The harmonic and supraharmonic emission of battery electric vehicles in the Netherlands," in *2020 International Conference on Smart Energy Systems and Technologies (SEST).* IEEE, 2020, pp. 1–6.

[39] S. Deilami and S. Muyeen, "An insight into practical solutions for electric vehicle charging in smart grid," *Energies*, vol. 13, no. 7, p. 1545, 2020.

[40] M. T. Hussain, N. B. Sulaiman, M. S. Hussain, and M. Jabir, "Optimal Management strategies to solve issues of grid having Electric Vehicles (EV): A review," *Journal of Energy Storage*, vol. 33, p. 102114, 2021.

[41] O. Sadeghian, A. Oshnoei, B. Mohammadi-Ivatloo, V. Vahidinasab, and A. Anvari-Moghaddam, "A comprehensive review on electric vehicles smart charging: Solutions, strategies, technologies, and challenges," *Journal of Energy Storage*, vol. 54, p. 105241, 2022.

[42] O. Ellabban, H. Abu-Rub, and F. Blaabjerg, "Renewable energy resources: Current status, future prospects and their enabling technology," *Renewable and sustainable energy reviews*, vol. 39, pp. 748–764, 2014.

[43] P. Barman, L. Dutta, S. Bordoloi, A. Kalita, P. Buragohain, S. Bharali, and B. Azzopardi, "Renewable energy integration with electric vehicle technology: A review of the existing smart charging approaches," *Renewable and Sustainable Energy Reviews*, vol. 183, p. 113518, 2023.

[44] K. Sevdari, L. Calearo, P. B. Andersen, and M. Marinelli, "Ancillary services and electric vehicles: An overview from charging clusters and chargers technology perspectives," *Renewable and Sustainable Energy Reviews*, vol. 167, p. 112666, 2022.

[45] B. Chatuanramtharnghaka, S. Deb, K. R. Singh, T. S. Ustun, and A. Kalam, "Reviewing demand response for energy management with consideration of renewable energy sources and electric vehicles," *World Electric Vehicle Journal*, vol. 15, no. 9, p. 412, 2024.

[46] S. Tirunagari, M. Gu, and L. Meegahapola, "Reaping the benefits of smart electric vehicle charging and vehicle-to-grid technologies: Regulatory, policy and technical aspects," *IEEE Access*, vol. 10, pp. 114 657–114 672, 2022.

[47] T. Yuvaraj, K. Devabalaji, J. A. Kumar, S. B. Thanikanti, and N. I. Nwulu, "A comprehensive review and analysis of the allocation of electric vehicle charging stations in distribution networks," *IEEE Access*, vol. 12, pp. 5404–5461, 2024.

[48] S. Deb, M. Pihlatie, and M. Al-Saadi, "Smart charging: A comprehensive review," *IEEE Access*, vol. 10, pp. 134 690–134 703, 2022.

[49] M. Taljegard, L. Göransson, M. Odenberger, and F. Johnsson, "Impacts of electric vehicles on the electricity generation portfolio–A Scandinavian-German case study," *Applied Energy*, vol. 235, pp. 1637–1650, 2019.

[50] C. F. Calvillo and K. Turner, "Analysing the impacts of a large-scale ev rollout in the uk–how can we better inform environmental and climate policy?" *Energy Strategy Reviews*, vol. 30, p. 100497, 2020.

[51] A. Arias-Londoño, O. D. Montoya, and L. F. Grisales-Noreña, "A chronological literature review of electric vehicle interactions with power distribution systems," *Energies*, vol. 13, no. 11, p. 3016, 2020.

[52] E. Mancini, M. Longo, W. Yaici, and D. Zaninelli, "Assessment of the impact of electric vehicles on the design and effectiveness of electric distribution grid with distributed generation," *Applied Sciences*, vol. 10, no. 15, p. 5125, 2020.

[53] A. Tavakoli, S. Saha, M. T. Arif, M. E. Haque, N. Mendis, and A. M. Oo, "Impacts of grid integration of solar pv and electric vehicle on grid stability, power quality and energy economics: A review," *IET Energy Systems Integration*, vol. 2, no. 3, pp. 243–260, 2020.

[54] M. Nour, J. P. Chaves-Ávila, G. Magdy, and Á. Sánchez-Miralles, "Review of positive and negative impacts of electric vehicles charging on electric power systems," *Energies*, vol. 13, no. 18, p. 4675, 2020.

[55] A. Al Zishan, M. M. Haji, and O. Ardakanian, "Adaptive congestion control for electric vehicle charging in the smart grid," *IEEE Transactions on Smart Grid*, vol. 12, no. 3, pp. 2439–2449, 2021.

[56] R. Jarvis and P. Moses, "Smart grid congestion caused by plug-in electric vehicle charging," in *2019 IEEE Texas Power and Energy Conference (TPEC)*. IEEE, 2019, pp. 1–5.

[57] J. Bollerslev, P. B. Andersen, T. V. Jensen, M. Marinelli, A. Thingvad, L. Calearo, and T. Weckesser, "Coincidence factors for domestic ev charging from driving and plug-in behavior," *IEEE Transactions on Transportation Electrification*, vol. 8, no. 1, pp. 808–819, 2021.

[58] Q. Wang, X. Liu, J. Du, and F. Kong, "Smart charging for electric vehicles: A survey from the algorithmic perspective," *IEEE Communications Surveys & Tutorials*, vol. 18, no. 2, pp. 1500–1517, 2016.

[59] A. Opstad, B. H. Bekken, H. S. Nygård, G. Doorman, and K. Sevdari, "Flexibility from electric vehicles-residential charging coincidence factors in Norway," in *CIGRE Paris Session*, 2024.

[60] A. R. Bhatti, Z. Salam, M. J. B. A. Aziz, and K. P. Yee, "A critical review of electric vehicle charging using solar photovoltaic," *International Journal of Energy Research*, vol. 40, no. 4, pp. 439–461, 2016.

[61] A. Verma, B. Singh, A. Chandra, and K. Al-Haddad, "An implementation of solar PV array based multifunctional EV charger," *IEEE Transactions on Industry Applications*, vol. 56, no. 4, pp. 4166–4178, 2020.

[62] K. Bell and S. Gill, "Delivering a highly distributed electricity system: Technical, regulatory and policy challenges," *Energy policy*, vol. 113, pp. 765–777, 2018.

[63] J. Merino, P. Mendoza-Araya, and C. Veganzones, "State of the art and future trends in grid codes applicable to isolated electrical systems," *Energies*, vol. 7, no. 12, pp. 7936–7954, 2014.

[64] A. Corsetti, R. Castro, C. Geyken, and A. Mohan, "Commercial ev fleet smart charging for cost reduction and renewables integration: a case study in germany," *Journal of Energy Storage*, vol. 100, p. 113765, 2024.

[65] M. Van Der Kam and W. Van Sark, "Smart charging of electric vehicles with photovoltaic power and vehicle-to-grid technology in a microgrid; a case study," *Applied energy*, vol. 152, pp. 20–30, 2015.

[66] S. Shao, M. Pipattanasomporn, and S. Rahman, "Demand response as a load shaping tool in an intelligent grid with electric vehicles," *IEEE Transactions on Smart Grid*, vol. 2, no. 4, pp. 624–631, 2011.

[67] S. Faddel and O. A. Mohammed, "Automated distributed electric vehicle controller for residential demand side management," *IEEE Transactions on Industry Applications*, vol. 55, no. 1, pp. 16–25, 2018.

[68] G. Deconinck, K. De Craemer, and B. Claessens, "Combining market-based control with distribution grid constraints when coordinating electric vehicle charging," *Engineering*, vol. 1, no. 4, pp. 453–465, 2015.

[69] L. Göke, J. Weibezahn, and M. Kendziorski, "How flexible electrification can integrate fluctuating renewables," *Energy*, vol. 278, p. 127832, 2023.

[70] W. Niewiadomski and A. Baczyńska, "Advanced flexibility market for system services based on tso–dso coordination and usage of distributed resources," *Energies*, vol. 14, no. 17, p. 5439, 2021.

[71] I. S. Bayram, G. Michailidis, M. Devetsikiotis, F. Granelli, and S. Bhattacharya, "Smart vehicles in the smart grid: Challenges, trends, and application to the design of charging stations," *Control and Optimization Methods for Electric Smart Grids*, pp. 133–145, 2012.

[72] International Renewable Energy Agency, "Innovation Outlook-Smart Charging for Electric Vehicles," IRENA, Tech. Rep., 2019.

[73] S. Chapaloglou, A. Nesiadis, P. Iliadis, K. Atsonios, N. Nikolopoulos, P. Grammelis, C. Yiakopoulos, I. Antoniadis, and E. Kakaras, "Smart energy management algorithm for load smoothing and peak shaving based on load forecasting of an island's power system," *Applied energy*, vol. 238, pp. 627–642, 2019.

[74] UK Government Electric vehicle smart charging. https://tinyurl.com/36p96eu9. Online; accessed June 25, 2025.

[75] Dutch grid operator wants to stop electric car charging during peak hours. https://tinyurl.com/3723zecd. Online; accessed June 25, 2025.

[76] Octopus Energy EV Tariffs. https://tinyurl.com/d7atn44v. Online; accessed June 25, 2025.

[77] National Grid ESO and Piclo to develop Local Constraint Market to limit Scottish wind curtailment. https://tinyurl.com/54x24h6h. Online; accessed June 25, 2025.

[78] Nuvve is the global market leader in providing grid services with electric vehicles to reduce total cost of ownership and support the clean energy transition. https://tinyurl.com/mupjvtvw. Online; accessed June 25, 2025.

[79] NESO Local Constraint Market. https://tinyurl.com/yfh8ynz3. Online; accessed June 25, 2025.

[80] AXLE Energy Local Network (DNO) Flexibility: Everything You Need to Know. https://tinyurl.com/ujztbjut. Online; accessed June 25, 2025.

[81] Tempo Zero tariff: Charge your electric car at no cost. https://tinyurl.com/2tdt8d9f. Online; accessed June 25, 2025.

[82] Best EV energy tariffs for electric vehicle owners. https://tinyurl.com/32er6hbv. Online; accessed June 25, 2025.

[83] A. R. Hansen, P. H. Hoelgaard, G. Trotta, and J. L. Andersen, "Demanding, distributing and selling energy flexibility: How dynamic tariffs entered the danish electricity market and what to do next," in *2021 ECEEE Summer Study on Energy Efficiency: A New Reality?* European Council for an Energy Efficient Economy, ECEEE, 2021, pp. 191–200.

[84] I. S. Bayram and A. Tajer, *Plug-in electric vehicle grid integration.* Artech House, 2017.

[85] D. Black, R. Yin, and B. Wang, *Smart Charging of Electric Vehicles and Driver Engagement for Demand Management and Participation in Electricity Markets: Final Project Report.* California Energy Commission, 2019.

[86] I. L. Brief, "Electric-vehicle smart charging," *International Renewable Energy Agency,(IRENA)*, 2019.

[87] V. Madaram, P. K. Biswas, C. Sain, S. B. Thanikanti, and S. Selvarajan, "Optimal electric vehicle charge scheduling algorithm using war strategy optimization approach," *Scientific Reports*, vol. 14, no. 1, p. 21795, 2024.

[88] S. Alyami, "Ensuring sustainable grid stability through effective ev charging management: A time and energy-based approach." *Sustainability (2071-1050)*, vol. 16, no. 14, 2024.

[89] Z. Ye, T. Li, and S. Low, "Towards balanced three-phase charging: Phase optimization in adaptive charging networks," *Electric Power Systems Research*, vol. 212, p. 108322, 2022.

[90] P. Lico, M. Marinelli, K. Knezović, and S. Grillo, "Phase balancing by means of electric vehicles single-phase connection shifting in a low voltage danish grid," in *2015 50th International Universities Power Engineering Conference (UPEC)*. IEEE, 2015, pp. 1–5.

[91] S. Rivera, S. Kouro, S. Vazquez, S. M. Goetz, R. Lizana, and E. Romero-Cadaval, "Electric vehicle charging infrastructure: From grid to battery," *IEEE Industrial Electronics Magazine*, vol. 15, no. 2, pp. 37–51, 2021.

[92] V. Monteiro, J. C. Ferreira, A. A. N. Melendez, J. A. Afonso, C. Couto, and J. L. Afonso, "Experimental validation of a bidirectional three-level dc-dc converter for on-board or off-board ev battery chargers," in *IECON 2019-45th Annual Conference of the IEEE Industrial Electronics Society*, vol. 1. IEEE, 2019, pp. 3468–3473.

[93] L. Lanz, B. Noll, T. S. Schmidt, and B. Steffen, "Comparing the levelized cost of electric vehicle charging options in Europe," *Nature Communications*, vol. 13, no. 1, p. 5277, 2022.

[94] N. Zhou, J. Wang, Q. Wang, and N. Wei, "Measurement-based harmonic modeling of an electric vehicle charging station using a three-phase uncontrolled rectifier," *IEEE Transactions on Smart Grid*, vol. 6, no. 3, pp. 1332–1340, 2014.

[95] M. S. Dahidah, G. Konstantinou, and V. G. Agelidis, "A review of multilevel selective harmonic elimination PWM: formulations, solving algorithms, implementation and applications," *IEEE Transactions on Power Electronics*, vol. 30, no. 8, pp. 4091–4106, 2014.

[96] Ł. Michalec, M. Jasiński, T. Sikorski, Z. Leonowicz, Ł. Jasiński, and V. Suresh, "Impact of harmonic currents of nonlinear loads on power quality of a low voltage network–review and case study," *Energies*, vol. 14, no. 12, p. 3665, 2021.

[97] R. Pogaki, "Western power distribution electric vehicle charging (pse0564001)," *Tech. Rep.*, 2018.

[98] A. Lucas, F. Bonavitacola, E. Kotsakis, and G. Fulli, "Grid harmonic impact of multiple electric vehicle fast charging," *Electric Power Systems Research*, vol. 127, pp. 13–21, 2015.

[99] M. Yilmaz and P. T. Krein, "Review of battery charger topologies, charging power levels, and infrastructure for plug-in electric and hybrid vehicles," *IEEE transactions on Power Electronics*, vol. 28, no. 5, pp. 2151–2169, 2012.

[100] R. K. Lenka, A. K. Panda, R. Patel, and J. M. Guerrero, "Pv integrated multifunctional off-board ev charger with improved grid power quality," *IEEE Transactions on Industry Applications*, vol. 58, no. 5, pp. 5520–5532, 2022.

[101] *SAE Electric Vehicle and Plug in Hybrid Electric Vehicle Conductive Charge Coupler (SAE J1772)*, SAE International Std., 2020.

[102] J. Dong, C. Liu, and Z. Lin, "Charging infrastructure planning for promoting battery electric vehicles: An activity-based approach using multiday travel data," *Transportation Research Part C: Emerging Technologies*, vol. 38, pp. 44–55, 2014.

[103] O. Elma, "A dynamic charging strategy with hybrid fast charging station for electric vehicles," *Energy*, vol. 202, p. 117680, 2020.

[104] K. L. López, C. Gagné, and M.-A. Gardner, "Demand-side management using deep learning for smart charging of electric vehicles," *IEEE Transactions on Smart Grid*, vol. 10, no. 3, pp. 2683–2691, 2018.

[105] Powering the future of mobility. https://tinyurl.com/mtcepw7e. Online; accessed June 25, 2025.

[106] M. R. Khalid, M. S. Alam, A. Sarwar, and M. J. Asghar, "A comprehensive review on electric vehicles charging infrastructures and their impacts on power-quality of the utility grid," *ETransportation*, vol. 1, p. 100006, 2019.

[107] S. A. A. Rizvi, A. Xin, A. Masood, S. Iqbal, M. U. Jan, and H. Rehman, "Electric vehicles and their impacts on integration into power grid: A review," in *2018 2nd IEEE Conference on Energy Internet and Energy System Integration (EI2)*. IEEE, 2018, pp. 1–6.

[108] C. Jiang, R. Torquato, D. Salles, and W. Xu, "Method to assess the power-quality impact of plug-in electric vehicles," *IEEE Transactions on Power Delivery*, vol. 29, no. 2, pp. 958–965, 2013.

[109] A. Ahmadi, A. Tavakoli, P. Jamborsalamati, N. Rezaei, M. R. Miveh, F. H. Gandoman, A. Heidari, and A. E. Nezhad, "Power quality improvement in smart grids using electric vehicles: A review," *IET Electrical Systems in Transportation*, vol. 9, no. 2, pp. 53–64, 2019.

[110] S. S. Letha, T. Busatto, and M. Bollen, "Interaction between charging infrastructure and the electricity grid," Lulea University of Technology, Tech. Rep., 2021.

[111] Y. Wang, H. Su, W. Wang, and Y. Zhu, "The impact of electric vehicle charging on grid reliability," in *IOP Conference Series: Earth and Environmental Science*, vol. 199, no. 5. IOP Publishing, 2018, p. 052033.

[112] S. Khan, B. Singh, and P. Makhija, "A review on power quality problems and its improvement techniques," *2017 Innovations in Power and Advanced Computing Technologies (i-PACT)*, pp. 1–7, 2017.

[113] F. Corti, S. D. Iacono, D. Astolfi, M. Pasetti, A. Vasile, A. Reatti, and A. Flammini, "A comprehensive review of charging infrastructure for electric micromobility vehicles: Technologies and challenges," *Energy Reports*, vol. 12, pp. 545–567, 2024.

[114] S. Chattopadhyay, M. Mitra, and S. Sengupta, "Electric power quality," in . Springer, 2011, pp. 5–12.

[115] K. Papailiou, *Springer Handbook of Power Systems*. Springer Nature, 01 2021.

[116] C. Edmunds, S. Galloway, J. Dixon, W. Bukhsh, and I. Elders, "Hosting capacity assessment of heat pumps and optimised electric vehicle charging on low voltage networks," *Applied Energy*, vol. 298, p. 117093, 2021.

[117] T. Bohn and H. Chaudhry, "Overview of SAE standards for plug-in electric vehicle," in *2012 IEEE PES Innovative Smart Grid Technologies (ISGT)*. IEEE, 2012, pp. 1–7.

[118] C. C. Chan and Y. Wong, "Electric vehicles charge forward," *IEEE Power and Energy Magazine*, vol. 2, no. 6, pp. 24–33, 2004.

[119] P. Papadopoulos, L. Cipcigan, N. Jenkins, and I. Grau, "Distribution networks with electric vehicles," in *2009 44th International Universities Power Engineering Conference (UPEC)*. IEEE, 2009, pp. 1–5.

[120] U. Rehman, D. Feng, H. Su, M. Numan, and F. Abbas, "Network overloading management by exploiting the in-system batteries of electric vehicles," *International Journal of Energy Research*, vol. 45, no. 4, pp. 5866–5880, 2021.

[121] S. Haider and P. Schegner, "Heuristic optimization of overloading due to electric vehicles in a low voltage grid," *Energies*, vol. 13, no. 22, p. 6069, 2020.

[122] J. Dixon, W. Bukhsh, C. Edmunds, and K. Bell, "Scheduling electric vehicle charging to minimise carbon emissions and wind curtailment," *Renewable Energy*, vol. 161, pp. 1072–1091, 2020.

[123] D. Dallinger and M. Wietschel, "Grid integration of intermittent renewable energy sources using price-responsive plug-in electric vehicles," *Renewable and Sustainable Energy Reviews*, vol. 16, no. 5, pp. 3370–3382, 2012.

[124] R.-C. Leou, C.-L. Su, and C.-N. Lu, "Stochastic analyses of electric vehicle charging impacts on distribution network," *IEEE Transactions on Power Systems*, vol. 29, no. 3, pp. 1055–1063, 2013.

[125] EN 50160, "CENELEC - EN 50160: Voltage characteristics of electricity supplied by public distribution systems," European Committee for Electrotechnical Standardization (CENELEC), Standard, 2010.

[126] J. Schlee, A. Mousseau, J. Eggebraaten, B. Johnson, H. Hess, and B. Johnson, "The effects of plug-in electric vehicles on a small distribution grid," in *41st North American Power Symposium*. IEEE, 2009, pp. 1–6.

[127] P. B. Evans, S. Kuloor, and B. Kroposki, "Impacts of plug-in vehicles and distributed storage on electric power delivery networks," in *2009 IEEE Vehicle Power and Propulsion Conference*. IEEE, 2009, pp. 838–846.

[128] J. P. Lopes, F. Soares, P. R. Almeida, P. C. Baptista, C. M. Silva, and T. L. Farias, "Quantification of technical impacts and environmental benefits of electric vehicles integration on electricity grids," in *2009 8th International Symposium on Advanced Electromechanical Motion Systems & Electric Drives Joint Symposium*. IEEE, 2009, pp. 1–6.

[129] X. Liu, A. Aichhorn, L. Liu, and H. Li, "Coordinated control of distributed energy storage system with tap changer transformers for voltage rise mitigation under high photovoltaic penetration," *IEEE Transactions on Smart Grid*, vol. 3, no. 2, pp. 897–906, 2012.

[130] F. Shahnia, A. Ghosh, G. Ledwich, and F. Zare, "Predicting voltage unbalance impacts of plug-in electric vehicles penetration in residential low-voltage distribution networks," *Electric Power Components and Systems*, vol. 41, no. 16, pp. 1594–1616, 2013.

[131] IEC 61000-2-5, "Electromagnetic compatibility (EMC) - Part 2-5: Environment - Description and classification of electromagnetic environments," International Electrotechnical Commission (IEC), Standard, 2017.

[132] A. Ul-Haq, C. Cecati, K. Strunz, and E. Abbasi, "Impact of electric vehicle charging on voltage unbalance in an urban distribution network," *Intelligent Industrial Systems*, vol. 1, no. 1, pp. 51–60, 2015.

[133] S. Weckx and J. Driesen, "Load balancing with EV chargers and PV inverters in unbalanced distribution grids," *IEEE Transactions on Sustainable Energy*, vol. 6, no. 2, pp. 635–643, 2015.

[134] Y. Zhang and A. Srivastava, "Voltage control strategy for energy storage system in sustainable distribution system operation," *Energies*, vol. 14, no. 4, p. 832, 2021.

[135] National Energy System Operator, "Future Energy Scenearios (FES)," NESO, Tech. Rep., 2024.

[136] J. Dixon, W. Bukhsh, K. Bell, and C. Brand, "Vehicle to grid: driver plug-in patterns, their impact on the cost and carbon of charging, and implications for system flexibility," *ETransportation*, vol. 13, p. 100180, 2022.

[137] S. Küfeoğlu and D. K. K. Hong, "Emissions performance of electric vehicles: A case study from the United Kingdom," *Applied Energy*, vol. 260, p. 114241, 2020.

[138] Worldwide roads on course for 31.1 million electric vehicle milestone by 2030. https://tinyurl.com/msfbaysn. Online; accessed June 25, 2025.

[139] M. K. Gerritsma, T. A. AlSkaif, H. A. Fidder, and W. G. van Sark, "Flexibility of electric vehicle demand: analysis of measured charging data and simulation for the future," *World Electric Vehicle Journal*, vol. 10, no. 1, p. 14, 2019.

[140] A. Brooks, E. Lu, D. Reicher, C. Spirakis, and B. Weihl, "Demand dispatch," *IEEE Power and Energy Magazine*, vol. 8, no. 3, pp. 20–29, 2010.

[141] A. Tavakoli, M. Negnevitsky, D. T. Nguyen, and K. M. Muttaqi, "Energy exchange between electric vehicle load and wind generating utilities," *IEEE Transactions on Power Systems*, vol. 31, no. 2, pp. 1248–1258, 2015.

[142] H. Liu, Z. Hu, Y. Song, and J. Lin, "Decentralized vehicle-to-grid control for primary frequency regulation considering charging demands," *IEEE Transactions on Power Systems*, vol. 28, no. 3, pp. 3480–3489, 2013.

[143] H. J. Jabir, J. Teh, D. Ishak, and H. Abunima, "Impacts of demand-side management on electrical power systems: A review," *Energies*, vol. 11, no. 5, p. 1050, 2018.

[144] S. Santoso, M. F. McGranaghan, R. C. Dugan, and H. W. Beaty, *Electrical power systems quality*. McGraw-Hill Education, 2012.

[145] IEC 61000-4-7, "Electromagnetic compatibility (EMC) - Part 4-7: Testing and measurement techniques - General guide on harmonics and interharmonics measurements and instrumentation, for power supply systems and equipment connected thereto," International Electrotechnical Commission (IEC), Standard, 2002.

[146] A. Lucas, G. Trentadue, H. Scholz, and M. Otura, "Power quality performance of fast-charging under extreme temperature conditions," *Energies*, vol. 11, no. 10, p. 2635, 2018.

[147] R. C. Dugan, M. F. McGranaghan, H. W. Beaty, and S. Santoso, *Electrical Power Systems quality*. McGraw-Hill New York, 1996.

[148] J. Arrillaga and N. R. Watson, *Power System Harmonics*. John Wiley & Sons Ltd, 2003.

[149] M. N. Iqbal, L. Kütt, B. Asad, T. Vaimann, A. Rassõlkin, and G. L. Demidova, "Time dependency of current harmonics for switch-mode power supplies," *Applied Sciences*, vol. 10, no. 21, p. 7806, 2020.

[150] M. P. Akter, S. Mekhilef, N. M. L. Tan, and H. Akagi, "Model predictive control of bidirectional ac-dc converter for energy storage system," *Journal of Electrical Engineering & Technology*, vol. 10, no. 1, pp. 165–175, 2015.

[151] I. Diahovchenko, V. Volokhin, V. Kurochkina, M. Špes, and M. Kosterec, "Effect of harmonic distortion on electric energy meters of different metrological principles," *Frontiers in Energy*, vol. 13, pp. 377–385, 2019.

[152] K. D. McBee, "Transformer aging due to high penetrations of PV, EV charging, and energy storage applications," in *2017 Ninth Annual IEEE Green Technologies Conference (GreenTech)*. IEEE, 2017, pp. 163–170.

[153] D. Ding, G. Zhang, G. Wang, Z. Ren, N. Mijatovic, T. Dragičević, and D. Xu, "Impedance reshaping for inherent harmonics in PMSM drives with small DC-link capacitor," *IEEE Transactions on Power Electronics*, vol. 37, no. 12, pp. 14 265–14 279, 2022.

[154] H. G. Beleiu, S. G. Pavel, I. M. Birou, A. Miron, P. C. Darab, and M. Sallah, "Effects of voltage unbalance and harmonics on drive systems with induction motor," *Journal of Taibah University for Science*, vol. 16, no. 1, pp. 381–391, 2022.

[155] I. Diahovchenko, B. Dolník, M. Kanálik, and J. Kurimskỳ, "Contemporary electric energy meters testing under simulated nonsinusoidal field conditions," *Electrical engineering*, pp. 1–16, 2022.

[156] N. Radwan-Pragłowska, D. Mamcarz, P. Albrechtowicz, and B. Rozegnał, "The current harmonic impact on active power losses and temperature distribution in power cables," *Energies*, vol. 17, no. 16, p. 4170, 2024.

[157] G. Foskolos, "Measurement-based current-harmonics modeling of aggregated electric-vehicle loads using power-exponential functions," *World Electric Vehicle Journal*, vol. 11, no. 3, p. 51, 2020.

[158] J. Gomez and M. Morcos, "Impact of EV battery chargers on the power quality of distribution systems," *IEEE Transactions on Power Delivery*, vol. 18, no. 3, pp. 975–981, 2003.

[159] A. K. Karmaker, S. Roy, and M. R. Ahmed, "Analysis of the impact of electric vehicle charging station on power quality issues," in *2019 international conference on electrical, computer and communication engineering (ECCE)*. IEEE, 2019, pp. 1–6.

[160] D. Contreras Ramírez and L.-G. Juan, "K-Factor Analysis to Increase the Actual Capacity of Electrical Distribution Transformers," in *Communication, Smart Technologies and Innovation for Society: Proceedings of CITIS 2021*. Springer, 2022, pp. 367–379.

[161] IEEE C57.91-2011, "IEEE Guide for Loading Mineral-Oil-Immersed Transformers and Step-Voltage Regulators," Institute of Electrical and Electronics Engineers (IEEE), Standard, 2011.

[162] N. R. Kalaskar and R. Holmukhe, "Report on power compensation and total harmonic distortion level analysis," *International Journal of Electrical and Computer Engineering*, vol. 6, no. 6, p. 2577, 2016.

[163] P. Mazurek and A. Chudy, "An analysis of electromagnetic disturbances from an electric vehicle charging station," *Energies*, vol. 15, no. 1, p. 244, 2021.

[164] S. S. G. Acharige, M. E. Haque, M. T. Arif, N. Hosseinzadeh, K. N. Hasan, and A. M. T. Oo, "Review of Electric Vehicle Charging Technologies, Standards, Architectures, and Converter Configurations," *IEEE Access*, vol. 11, pp. 41 218–41 255, 2023.

[165] X. Qu, H. Han, S.-C. Wong, K. T. Chi, and W. Chen, "Hybrid IPT topologies with constant current or constant voltage output for battery charging applications," *IEEE Transactions on Power Electronics*, vol. 30, no. 11, pp. 6329–6337, 2015.

[166] H. Shareef, M. M. Islam, and A. Mohamed, "A review of the stage-of-the-art charging technologies, placement methodologies, and impacts of electric vehicles," *Renewable and Sustainable Energy Reviews*, vol. 64, pp. 403–420, 2016.

[167] A. A.-H. Hussein and I. Batarseh, "A review of charging algorithms for nickel and lithium battery chargers," *IEEE Transactions on Vehicular Technology*, vol. 60, no. 3, pp. 830–838, 2011.

[168] K. Lorenzo, "Harmonics propagation and impact of electric vehicles on the electrical grid," 2014.

[169] Charging Device Testing, Idaho National Laboratory. https://tinyurl.com/9k2hyr9v. Online; accessed June 25, 2025.

[170] D. Andersson and D. Carlsson, "Measurement of ABB's prototype fast charging station for electric vehicles," Master's thesis, Chalmers University of Technology, 2012.

[171] IEC 61000-3-2, "Electromagnetic compatibility (EMC) - Part 3-2: Limits - Limits for harmonic current emissions (equipment input current $\leq$ 16 A per phase)," International Electrotechnical Commission (IEC), Standard, 2018.

[172] IEC 61000-3-12, "Electromagnetic compatibility (EMC) - Part 3-12: Limits - Limits for harmonic currents produced by equipment connected to public low-voltage systems with input current $>$ 16 A and $\leq$ 75 A per phase," International Electrotechnical Commission (IEC), Standard, 2021.

[173] IEC 61000-2-2, "Electromagnetic compatibility (EMC) - Part 2-2: Environment - Compatibility levels for low-frequency conducted disturbances and signalling in public low-voltage power supply systems," International Electrotechnical Commission (IEC), Standard, 2002.

[174] IEC 61000-2-4, "Electromagnetic compatibility (EMC) - Part 2-4: Environment - Compatibility levels in industrial plants for low-frequency conducted disturbances," International Electrotechnical Commission (IEC), Standard, 2002.

[175] IEC 61000-4-30, "Electromagnetic compatibility (EMC) - Part 4-30: Testing and measurement techniques - Power quality measurement methods," International Electrotechnical Commission (IEC), Standard, 2015.

[176] IEEE 519-2014, "IEEE Recommended Practice and Requirements for Harmonic Control in Electric Power Systems," Institute of Electrical and Electronics Engineers (IEEE), Standard, 2014.

[177] A. Collin, X. Xu, S. Djokic, F. Möller, J. Meyer, L. Kutt, and M. Lehtonen, "Survey of harmonic emission of electrical vehicle chargers in the European market," in *2016 International Symposium on Power Electronics, Electrical Drives, Automation and Motion (SPEEDAM)*. IEEE, 2016, pp. 1208–1213.

[178] S. Gugliotta, "Interaction between current harmonics produced by different electric vehicles DC chargers," Ph.D. dissertation, Politecnico di Torino, 2024.

[179] Ziyat, Isla and Gola, Alia and Palmer, Patrick R. and Makonin, Stephen and Popowich, Fred, "EV Charging Profiles and Waveforms Dataset (EV-CPW) and Associated Power Quality Analysis," *IEEE Access*, vol. 11, pp. 138 445–138 456, 2023.

[180] S. M. Miraftabzadeh, D. Pejovski, M. Longo, M. Brenna, and M. Pasetti, "Impact of Electric Vehicle Charging on Voltage and Current Harmonics at the Point of Common Coupling," in *2023 IEEE International Conference on Environment and Electrical Engineering and 2023 IEEE Industrial and Commercial Power Systems Europe (EEEIC/I&CPS Europe)*. IEEE, 2023, pp. 1–6.

[181] G. Ye, V. Cuk, and J. F. Cobben, "A study on harmonic current summation using field measurement data," in *2016 IEEE International Conference on Power System Technology (POWERCON)*. IEEE, 2016, pp. 1–6.

[182] IEC 61000-3-6, "Electromagnetic compatibility (EMC)–Part 3-6: Limits–Assessment of emission limits for the connection of distorting installations to MV, HV and EHV power systems," *HV and EHV power systems*, 2008.

[183] J. Wikston, "Harmonic summation for multiple arc furnaces," in *2002 IEEE Power Engineering Society Winter Meeting. Conference Proceedings (Cat. No. 02CH37309)*, vol. 2. IEEE, 2002, pp. 1072–1075.

[184] S. Xie, Q. Li, L. Zhao, and Y. Xu, "Study on summation exponents of harmonic of electrified railway," in *The Fifth International Conference on Power Electronics and Drive Systems, 2003. PEDS 2003.*, vol. 1. IEEE, 2003, pp. 816–820.

[185] F. Medeiros, D. C. Brasil, C. A. Marques, C. A. Duque, and P. F. Ribeiro, "Considerations on the aggregation of harmonics produced by large wind farms," in *2012 IEEE 15th International Conference on Harmonics and Quality of Power*. IEEE, 2012, pp. 364–369.

[186] K. Daniel, L. Kütt, M. N. Iqbal, N. Shabbir, A. U. Rehman, M. Shafiq, and H. Hamam, "Current harmonic aggregation cases for contemporary loads," *Energies*, vol. 15, no. 2, p. 437, 2022.

[187] L. Kütt, E. Saarijärvi, M. Lehtonen, H. Molder, and J. Niitsoo, "Estimating the harmonic distortions in a distribution network supplying EV charging load using practical source data—Case example," in *2014 IEEE PES General Meeting—Conference & Exposition*. IEEE, 2014, pp. 1–5.

[188] Energy System Integration Lab - SYSLAB. https://tinyurl.com/3cy6r8vt. Online; accessed June 25, 2025.

[189] K. Sevdari, "Control and clustering of electric vehicle chargers for the provision of grid services," Ph.D. dissertation, Technical University of Denmark, 2023.

[190] Fronius Wattpilot AC Smart Charger. https://tinyurl.com/4xp4rew3. Online; accessed June 25, 2025.

[191] Zaptec Pro AC Smart Charger. https://tinyurl.com/4uebhdvv. Online; accessed June 25, 2025.

[192] KeContact P30 x-series AC Smart Charger. https://tinyurl.com/4jkpntmx. Online; accessed June 25, 2025.

[193] Yokogawa WT500 Mid-Range Power Analyzer. https://tinyurl.com/3k896hkp. Online; accessed June 25, 2025.

[194] Users Manual for Fluke 434-II/435-II/437-II. https://tinyurl.com/3p58nu59. Online; accessed June 25, 2025.

[195] IEC 61851-1, "Electric vehicle conductive charging system - Part 1: General requirements," International Electrotechnical Commission (IEC), Standard, 2017.

[196] D. Shmilovitz, "On the definition of total harmonic distortion and its effect on measurement interpretation," *IEEE Transactions on Power delivery*, vol. 20, no. 1, pp. 526–528, 2005.

[197] A. G. Asuero, A. Sayago, and A. González, "The correlation coefficient: An overview," *Critical reviews in analytical chemistry*, vol. 36, no. 1, pp. 41–59, 2006.

[198] P. Berens, "CircStat: A MATLAB Toolbox for Circular Statistics," *Journal of Statistical Software*, vol. 31, no. 10, p. 1–21, 2009. [Online]. Available: https://tinyurl.com/ycxjj8aw

[199] L. M. A. Alsaqal, A. M. I. Alnaib, and O. T. Mahmood, "Comparison of multiple modulation techniques for various topologies of multilevel converters for single phase AC motor drive," *Int J Pow Elec & Dri Syst ISSN*, vol. 2088, no. 8694, p. 8694, 2019.

[200] V. Ćuk, J. F. Cobben, W. L. Kling, and P. F. Ribeiro, "Analysis of harmonic current summation based on field measurements," *IET Generation, Transmission & Distribution*, vol. 7, no. 12, pp. 1391–1400, 2013.

[201] C. Z. Mooney, *Monte carlo simulation*. Sage, 1997, no. 116.

[202] S. Raychaudhuri, "Introduction to monte carlo simulation," in *2008 Winter simulation conference*. IEEE, 2008, pp. 91–100.

[203] Ø. S. Laengen, "Application of monte carlo simulation to power system adequacy assessment," Master's thesis, NTNU, 2018.

[204] J. Cepeda, "Power system dynamic data generation based on monte carlo simulations for machine learning applications," *Engineering Proceedings*, vol. 47, no. 1, p. 6, 2023.

[205] F. Monforti, T. Huld, K. Bódis, L. Vitali, M. D'isidoro, and R. Lacal-Arántegui, "Assessing complementarity of wind and solar resources for energy production in Italy. A Monte Carlo approach," *Renewable Energy*, vol. 63, pp. 576–586, 2014.

[206] A. Alsharif, C. W. Tan, R. Ayop, A. Al Smin, A. Ali Ahmed, F. H. Kuwil, and M. M. Khaleel, "Impact of electric vehicle on residential power distribution considering energy management strategy and stochastic monte carlo algorithm," *Energies*, vol. 16, no. 3, p. 1358, 2023.

[207] S. Habib, M. M. Khan, F. Abbas, M. Numan, Y. Ali, H. Tang, and X. Yan, "A framework for stochastic estimation of electric vehicle charging behavior for risk assessment of distribution networks," *Frontiers in Energy*, vol. 14, pp. 298–317, 2020.

[208] IEEE C57.110-2018, "IEEE Recommended Practice for Establishing Liquid Immersed and Dry-Type Power and Distribution Transformer Capability when Supplying Nonsinusoidal Load Currents," Institute of Electrical and Electronics Engineers (IEEE), Standard, 2018.

[209] A. Visakh and M. P. Selvan, "Analysis and mitigation of the impact of electric vehicle charging on service disruption of distribution transformers," *Sustainable Energy, Grids and Networks*, vol. 35, p. 101096, 2023.

[210] E. Ediriweera, K. Wickramasinghe, K. Sithmini, E. Ekanayaka, R. Samarasinghe, and J. R. Lucas, "Localizing hotspot in an oil immersed distribution transformer using finite element analysis," in *2020 IEEE Electric Power and Energy Conference (EPEC)*. IEEE, 2020, pp. 1–6.

[211] G. Razeghi, L. Zhang, T. Brown, and S. Samuelsen, "Impacts of plug-in hybrid electric vehicles on a residential transformer using stochastic and empirical analysis," *Journal of Power Sources*, vol. 252, pp. 277–285, 2014.

[212] Low-cost Electric Car Charging with Fronius. https://tinyurl.com/wztv4mjw. Online; accessed June 25, 2025.

[213] M. Clerc, *Particle swarm optimization*. John Wiley & Sons, 2010, vol. 93.

[214] D. Wang, D. Tan, and L. Liu, "Particle swarm optimization algorithm: an overview," *Soft computing*, vol. 22, no. 2, pp. 387–408, 2018.

[215] F. Marini and B. Walczak, "Particle swarm optimization (PSO). A tutorial," *Chemometrics and Intelligent Laboratory Systems*, vol. 149, pp. 153–165, 2015.

[216] M. Clerc and J. Kennedy, "The particle swarm-explosion, stability, and convergence in a multidimensional complex space," *IEEE Transactions on Evolutionary Computation*, vol. 6, no. 1, pp. 58–73, 2002.

[217] J. Yang, L. He, and S. Fu, "An improved PSO-based charging strategy of electric vehicles in electrical distribution grid," *Applied Energy*, vol. 128, pp. 82–92, 2014.

[218] A. Rezaee Jordehi and J. Jasni, "Parameter selection in particle swarm optimisation: a survey," *Journal of Experimental & Theoretical Artificial Intelligence*, vol. 25, no. 4, pp. 527–542, 2013.